

**Towards the assessment of
human-relevant repeated dose toxicity
using an *in vitro* systems toxicological approach**

Dissertation

Zur Erlangung des Grades
des Doktors der Naturwissenschaften
der Naturwissenschaftlich-Technischen Fakultät
der Universität des Saarlandes

von
Sebastian Klein

Saarbrücken
2017

Tag des Kolloquiums:	04.12.2017
Dekan:	Prof. Dr. G. Kickelbick
Berichterstatter:	Prof. Dr. Ing. E. Heinzle Prof. Dr. G.-W. Kohring
Vorsitz:	Prof. Dr. U. Müller
Akad. Mitarbeiter:	Dr. B. Becker

“When I was a boy of fourteen, my father was so ignorant I could hardly stand to have the old man around. But when I got to be twenty-one, I was astonished at how much the old man had learned in seven years.”

Ambiguous source

“知之为知之 不知为不知 是知也。”

“Sei dir bewusst, was du weißt. Was du hingegen nicht weißt, das gib zu.
Das ist das richtige Verhältnis zum Wissen.”

Konfuzius (551 v. Chr. – 479 v. Chr.)

“As you think, so shall you become.”

Bruce Lee (1940 – 1973)

Table of content

	Zusammenfassung	7
	Abstract	7
Chapter 1	General introduction	9
Part I	Metabolic characterization of HepaRG cells	35
Chapter 2	Carbon metabolism in HepaRG cells and its alterations upon drug exposure in a comparative study with primary human hepatocytes and HepG2 cells	37
Part II	Optimization of HepaRG culture conditions for short- and long-term toxicity studies	59
Chapter 3	Hepatotoxicity assessment in 3D and 2D high-throughput systems using HepaRG cells	61
Chapter 4	Long-term maintenance of HepaRG cells in serum-free conditions and application in a repeated dose study	73
Part III	Application of HepaRG cells in repeated dose toxicity studies	87
Chapter 5	<i>In silico</i> modeling for the prediction of dose and pathway related adverse effects in human from in vitro repeated dose studies	89
Chapter 6	Systems toxicological evaluation of valproic acid-induced toxicity in HepaRG cells	105
Chapter 7	Summary, conclusion and outlook	133
	Supplementary material	139
	References	173
	Danksagung	195
	Contributions	196
	Curriculum vitae	198

Abstract

The aim of this thesis was to investigate the applicability of the human liver cell line HepaRG in toxicological long-term studies. For this purpose, cells were 1) characterized on metabolic level 2) optimized for long-term cultivation and 3) applied in relevant scenarios.

Metabolic characterization allows for comprehensive and meaningful phenotyping of cells. The HepaRG cell line was characterized in an untreated state, as well as upon treatment with drugs. Several commonalities with primary reference cells supported application of the cells in further toxicological studies. Next, optimization of HepaRG cells was investigated, using three-dimensional cultivation systems and adapting the composition of the culture medium. Increased activities in pivotal parameters and a 30-day duration were ensured with the tested approaches. In two concluding and comprehensive long-term studies, the potential hazard of drugs upon oral administration was estimated, and effects of drugs on the different cellular layers were assessed. The latter allowed for a holistic view and deep understanding of processes underlying drug-induced toxicity. Taken together, in this thesis, important steps and generally applicable techniques were illustrated that may help in reducing the number of animal testing in toxicological studies.

Zusammenfassung

Das Ziel der vorliegenden Arbeit bestand darin die Anwendbarkeit der humanen Leberzelllinie HepaRG in toxikologischen Langzeitstudien zu untersuchen. Für diesen Zweck wurden die Zellen 1) auf metabolischer Ebene charakterisiert 2) für die Langzeitkultivierung optimiert und 3) in praxisrelevanten Studien eingesetzt.

Die metabolische Charakterisierung erlaubt eine aussagekräftige Phänotypisierung von Zellen. Die HepaRG Zellen wurden hierfür sowohl unbehandelt, als auch unter Zugabe von Medikamenten untersucht. Zahlreiche Gemeinsamkeiten zu primären Referenzzellen unterstützten die Verwendung in weiteren toxikologischen Studien. Daraufhin wurde untersucht, inwieweit sich die Eigenschaften von HepaRG Zellen in 3D-Kultivierungssystemen und durch Anpassungen des Kulturmediums optimieren lassen. Mit den getesteten Verfahren konnten erhöhte Aktivitäten in zentralen Parametern sowie eine 30-tägige Studiendauer erzielt werden. In zwei abschließenden Langzeitstudien wurde die Gefährlichkeit von Medikamenten bei oraler Applikation abgeschätzt, und die Auswirkungen von Medikamenten auf den verschiedenen zellulären Ebenen untersucht. Letzteres ermöglichte eine ganzheitliche Abbildung und damit ein tiefgreifendes Verständnis der Prozesse die wirkstoffinduzierten toxischen Effekten zugrunde liegen. Insgesamt konnten in dieser Arbeit wichtige Schritte und generell anwendbare Techniken aufgezeigt werden, die mittelfristig zu einer Reduktion von Tierversuchen in Toxizitätsstudien führen können.

Chapter 1 General introduction

1.1 Drug development and the problem of drug discontinuation

Between 6 to 13% of all hospital admissions are related to adverse drug effects (Alexopoulou et al., 2008; Brvar et al., 2009; Pirmohamed et al., 2004) and even though in the past only 2.3% of these cases were lethal, the resulting costs are tremendous (Pirmohamed et al., 2004). Even more, further economic loss is caused by adverse drug reactions occurring while patients are treated in hospitals, resulting in prolongation of hospitalization (Bates et al., 1997; Classen, 1997; Moura et al., 2009).

Assessment of drug safety is an essential part of drug development in pharmaceutical companies to ensure a reasonable risk-benefit ratio. Safety assessment spans over the whole lifetime of a drug, starting with drug discovery and continuing in the preclinical, clinical and post-marketing phase. To understand why adverse drug effects still account for such a striking number of hospital admissions, the safety assessment process is critically examined in the following.

1.1.1 Overview on the drug development process

In the preclinical phase, drug candidates are tested for their therapeutic efficacy, as well as for their toxicological potential upon single and repeated dosing. Furthermore, the kinetics of the candidates are investigated, i.e. their absorption, distribution, metabolism and excretion (ADME) in the body (Dunne et al., 2013; Greaves et al., 2004). Additionally, data obtained in the preclinical phase is used to estimate a first-in-human dose. Low efficacy, intolerable toxicity and unfavorable ADME properties lead to discontinuation of the candidates (Kubinyi, 2003; Vuppala et al., 2013). Many of the experiments during the preclinical phase are conducted in animals, yet some parameters are estimated using *in vitro* test systems (figure 1.1) (Greaves et al., 2004). When drug candidates qualify for the clinical phase, first studies are performed in humans – initially only in few healthy individuals and eventually in several thousand patients in the third phase. Afterwards, promising drug candidates are subjected to evaluation and, if successful, approval by the regulating authorities (Dunne et al., 2013).

1.1.2 Discontinuation of drugs during drug development and beyond

In the USA, from originally 5,000 to 10,000 compounds in drug discovery only 1 to 2 drugs are eventually approved by the Food and Drug Administration (FDA), in a process that takes 10 to 15 years and costs 0.8 to 2 billion dollars (figure 1.1) (Dunne et al., 2013).

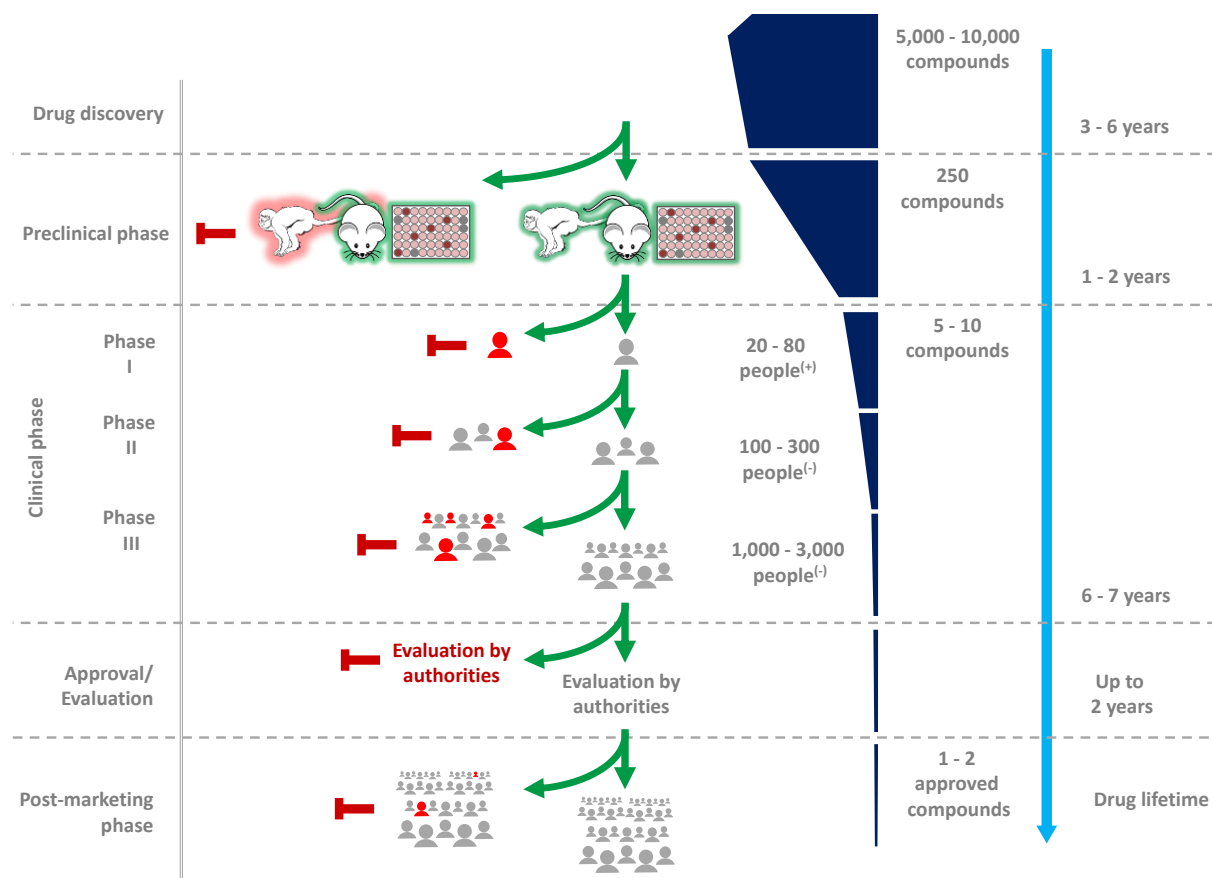


Figure 1.1 Overview on the drug development process in the USA. Current drug development procedure (adapted from Dunne et al, 2013), highlighting the number of drug candidates in the different phases and the type of test systems used. (+) and (-) indicate that tests are either conducted in healthy test subjects or in patients with target disease. Subjects highlighted in red are representative for adverse drug effects leading to discontinuation of drug development.

One third of failures in drug development result from adverse effects in humans or animals and around half the substances lack efficacy (Kubinyi, 2003) (figure 1.2). Cardiovascular and liver toxicity are the two main causes for adverse events with 27 and 15% of toxic events encountered respectively (Guengerich, 2011). But not all harmful substances are identified before entering the market. In some cases, severe adverse events, in particular those related to idiosyncratic drug hepatotoxicity, are not detected until the drug is available on the market. According to FDA reports, 32% of drugs withdrawn in the post-marketing phase were related to a hepatotoxic potential (Stevens and Baker, 2009). This not only causes unnecessary suffering of patients, but subsequent withdrawal of drugs additionally results in tremendous financial losses for the releasing companies. As each phase of the drug development involves expensive tools and manpower, early detection of toxicity is highly desired to avoid unnecessary expenses on hazardous compounds.

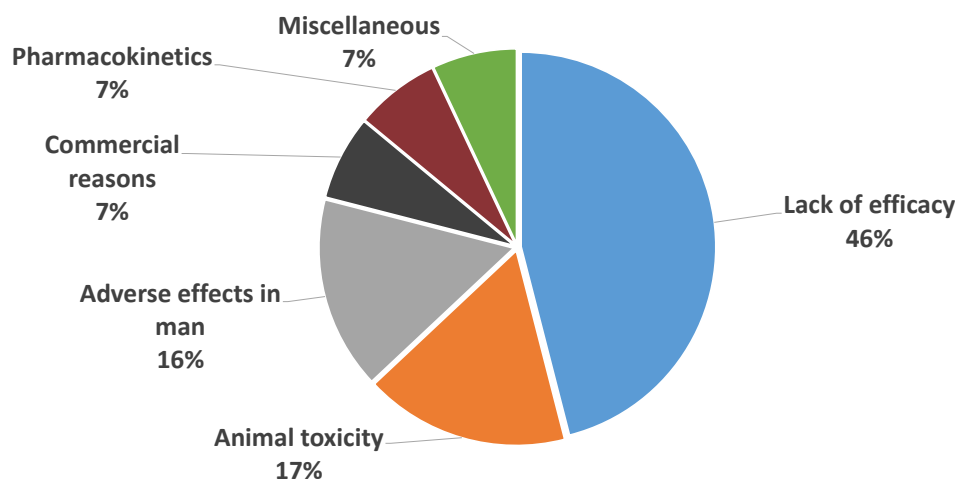


Figure 1.2 Reasons for drug candidate failure in drug development. Data is based on 121 new chemical entities taken from large UK companies between 1964 and 1985. Anti-infectives were excluded due to generally poor bioavailability. Redrawn from Kubinyi, 2003.

Reasons for late identification of hazardous properties of drug candidates will be discussed in the following paragraphs.

Idiosyncratic drug-induced liver injury

Despite its relevance in drug development, idiosyncratic drug-induced liver injury (iDILI) remains poorly understood. Per definition, iDILI only occurs in few individuals in a population, for which it is usually only discovered in large populations, resulting in being the most frequent cause of post-marketing warnings and withdrawals. It is generally suggested that formation of reactive metabolites resulting from bioactivation in the liver and the adaptive immune system may have major contribution to the development of iDILI (Gómez-Lechón et al., 2015; Kaplowitz, 2005).

Animal experiments in drug development

Additionally, almost all attempts to show idiosyncratic toxicity in animal models were doomed to failure. Yet, poor correlation of animal experiments to humans is not limited to iDILI, but is a general problem in toxicity assessment. Extensive reviewing of pharmacological studies has shown that sensitivity for the identification of toxic compounds during the preclinical phase is around 70% using a combination of rodent and non-rodent animal species. Looking at the prediction potential of the species individually, sensitivity is reduced to 43 and 63% respectively (Olson et al., 2000).

Apart from the low potential of reliably predicting human-relevant toxicity (Blaauboer and Andersen, 2007), and the ethical issue, which is inherent to experiments conducted in animals, animal studies are notably more costly, time consuming and throughput is low compared to *in vitro* studies (Shukla et al., 2010; Xia et al., 2008).

But what are the causes leading to poor animal/human concordance in toxicity studies? Firstly, animals and humans differ in cytochrome P450 (CYP450) enzyme concentrations, substrate specificity and the potential of the CYP450 enzymes for being induced or inhibited. The CYP450 superfamily contains a large set of enzymes responsible for metabolization of xenobiotics and endogenous molecules, making the substances more hydrophilic and facilitating their secretion (Martignoni et al., 2006). Therefore, the CYP450 superfamily plays a central role in detoxification and sometimes also

bioactivation of drugs. Secondly, concentrations of endogenous metabolites may differ drastically between species. For example, bile salt composition in humans and rats differ substantially from one another and as a result, only in humans toxicity elicited by the cholestasis-inducing compound bosentan is observed (Fattinger et al., 2001; Setchell et al., 1997). Thirdly, while animals used in these studies are healthy and handled under uniform conditions, e.g. in terms of housing and nutrition, the opposite is the case in humans (Olson et al., 2000).

Duration of studies and repeated dosing

Another aspect to consider is that it may take several weeks of treatment before manifestation of drug-induced injuries. Olson et al. reviewed that 94% of toxicity occurs within the first month; consequently 6% of adverse events develop not before at least one month of treatment. The time before manifestation also depends on the type of toxicity observed. E.g. in case of liver, toxicity was not observed after single doses, but always required repeated dosing (Olson et al., 2000). As a conclusion, it is obligatory to include repeated dosing and ensure sufficiently long experiments in the study design.

1.2 The human liver and its central role in the body

1.2.1 General liver functions

The liver plays a unique role within the human body in terms of metabolization of endogenous and exogenous metabolites, as well as regulation of metabolism. It is responsible for formation, degradation and storage of several endogenous metabolites, thereby maintaining homeostatic conditions in the system. One example is the storage of glucose as glycogen in the liver after a meal, and the process of glycogenolysis in fasting conditions to keep up constant glucose levels in blood and cells (figure 1.3). Another example is the synthesis of cholesterol. The liver is the main site of cholesterol synthesis, a molecule which is an integral part of all membranes in mammalian cells and precursor of steroid hormones, oxysterols and bile acids, central regulators of a multitude of essential functions in the human body. Bile acids recently moved back into focus of current research as they have been associated with various diseases such as Alzheimer's disease and diabetes (Quinn et al., 2014; Ramalho et al., 2008; Thomas et al., 2008) as well as due to the discovery of novel functions. Like their precursors, the majority of bile acids are synthesized in the liver from where they are transported into the gall bladder, which releases them when required. Historically, bile acids were described as mere solubilizing molecules, which aid in the digestion of lipid-rich diets. However, it was shown in recent studies that bile acids also act as hormones via the farnesoid X receptor (FXR) and G-protein coupled bile acid receptor 1 (GPBAR1, TGR5) (Makishima et al., 1999; Parks et al., 1999), exhibiting regulatory functions on cholesterol, glucose and triacylglyceride metabolism as well as on energy homeostasis and inflammation (Lefebvre et al., 2009; Staels and Fonseca, 2009).

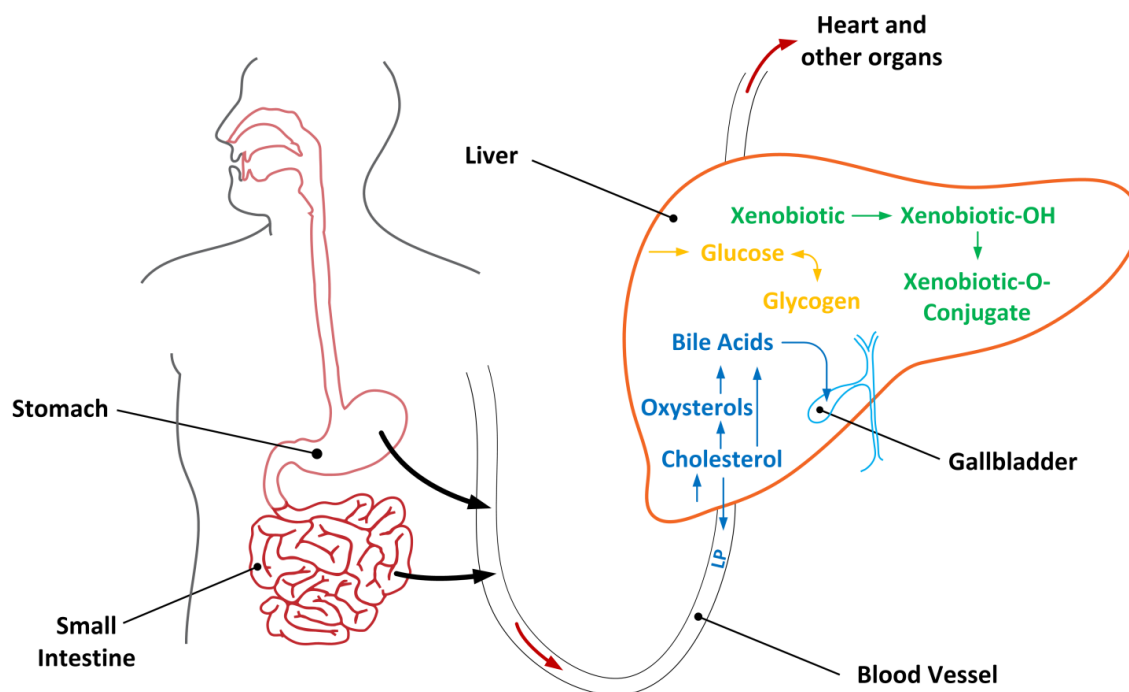


Figure 1.3 Metabolic functions of the liver. Nutrients and xenobiotics that are resorbed from the stomach and small intestine enter the liver via the blood stream. In the liver, nutrients and xenobiotics may undergo metabolism; such as postprandial glucose, which is stored inside the cells as glycogen and used when nutrients are limited (orange = pathway of gluconeogenesis, glycogenesis and glycogenolysis). Xenobiotics can be subject to phase I and phase II metabolism (green), which generally facilitates excretion of lipophilic compounds. Furthermore, the liver produces oxysterols and bile acids from cholesterol (blue). Bile acids are stored in the gallbladder and aid the digestion of lipophilic compounds. Lipoproteins (LP) are produced by the liver for transport of cholesterol and other lipids from and to the liver.

Even more, through production and secretion of lipoproteins of different density and the transport protein albumin, the liver is also involved in the transport of cholesterol and other lipids to different parts of the body and back to the liver (Nelson and Cox, 2008).

1.2.2 Metabolization of xenobiotics

The central role of the liver is further strengthened by the fact that stomach and intestine are connected to the blood stream via the hepatic portal vein which collects and transports blood to the liver before it is further distributed to the rest of the body (Abdel-Misih and Bloomston, 2010). I.e., nutrients from a meal and xenobiotics, resorbed in the stomach or intestine, first pass through the liver and may undergo metabolism, prior of being supplied to other organs. In case of drugs, this effect is called first-pass effect and depending on the compound may greatly reduce the amount of active drug reaching the organ of interest. Therefore, parenteral drug application is inevitable for certain compounds (Pond and Tozer, 1984). On the other hand, in case of so called prodrugs, the desired, pharmacologically active compound only emerges after the parent compound underwent metabolism (Grant, 1991). It is also worth mentioning that oral administration is not a prerequisite for metabolism in the liver, but compounds applied to the skin, e.g. cosmetics, or drugs that are administered intravenously eventually reach the liver via the blood stream (Sandanger et al., 2011). Therefore, not only orally administered compounds, but basically all compounds that man is exposed to, require investigation of potential toxicity upon metabolism in liver.

The liver, more precisely the parenchymal cells or hepatocytes are the main site of drug metabolism, however, other organs such as kidney and lungs also contribute (Lu and Kacew, 2002). Drug metabolism can be divided into different phases. Uptake of the compound into the cells sometimes is referred to as phase 0. Depending on the compound, uptake may occur either via passive diffusion or active transport – or both ways (Sugano et al., 2010). In phase I, non-polar and hydrophobic xenobiotics are modified by introduction of a polar group, most commonly in an oxidation reaction catalyzed by the CYP450 enzyme superfamily. Other modifications include reduction or hydrolysis of the compound. In phase II, xenobiotics are conjugated with hydrophilic molecules, such as sulfate, glucuronic acid or glutathione at the site where the first modification was introduced. The resulting molecules are more hydrophilic and excretion via the renal pathway is facilitated (Grant, 1991). Before xenobiotics can be excreted via urine, they first need to be secreted from the liver cells into the blood, also referred to as phase III of drug metabolism. Excretion from the liver cells is mainly dependent on two protein families, multidrug resistance-related proteins (MRP) and multidrug resistance proteins (MDR), both are members of ATP-binding cassette (ABC) transporters (Borst et al., 2000; Ferreira et al., 2015).

In many cases, drugs affect the cells such that their own metabolism, as well as metabolism of other compounds are either induced or repressed. This phenomenon is referred to as drug-drug interaction and is of high relevance when two or more drugs are applied in combination. These alterations can have unforeseeable consequences and may lead to detrimental responses, e.g. caused by increased production of reactive metabolites or impaired inactivation of the pharmacologically active drug. Due to its central role in clearance and metabolism of drugs, the liver is a particular target for drug-induced toxicity and it becomes evident that the liver has to be in the focus of toxicological and pharmacological testing (Kaplowitz, 2004; Soldatow et al., 2013).

1.3 Drug-induced liver injury

Given the multiple central functions of the liver, it is not surprising that imbalances in its regulation may result in severe and even fatal conditions. In the following, selected mechanisms will be discussed, by which drugs induce such imbalances and thereby exert toxic effects.

For further discussion, the term toxicity, though it may seem clear at first glance, will be briefly reflected. Already in the 16th century, Philippus Theophrastus Aureolus Bombastus von Hohenheim, also known as Paracelsus, stated that all substances were toxic and nothing was without toxicity, and only the dose would determine that a substance was not toxic (Borzelleca, 2000). Therefore, toxicity quantitatively describes the potency of a compound to exert harmful effects, but also the mechanism by which adverse events are triggered. As a consequence, no-observed-adverse-effect levels (NOAELs) or similar margins are commonly defined for each substance tested in the context of toxicology (Liebler and Guengerich, 2005).

1.3.1 Mechanisms of drug-induced toxicity

Drugs and drug metabolites binding to their target receptor may not only elicit the intended responses, but in some instances can be accompanied by a weak toxic reaction that only becomes evident upon overdosing or accumulation of the drug during repeated dosing (on-target or mechanism-based toxicity) (figure 1.4). For other drugs, binding properties may be insufficiently specific and binding to another than the intended target can lead to adverse events (off-target toxicity). The third mechanism

is based on the covalent-binding theory, which states that reactive metabolites formed during metabolism in the liver eventually impair cellular functions (Liebler and Guengerich, 2005).

These three initial events of adverse reactions are commonly associated with oxidative stress, mitochondrial dysfunction and endoplasmic reticulum (ER) stress as downstream effects (Foufelle and Fromenty, 2016). Oxidative stress is characterized by an imbalance in the formation of reactive oxygen species (ROS) and antioxidant defenses (Betteridge, 2000). As a result, ROS prevail and extensively form adducts with DNA and proteins, and produce lipoperoxides, such as 4-hydroxynonenal (HNE). HNE is considered a second messenger of oxidative stress and has been associated with the induction of apoptosis upon accumulation (Barrera, 2012). The mechanisms by which ROS cause cell damage are manifold and not yet fully elucidated. ROS binding to proteins may on the one side impair the function of important regulatory proteins, disturbing normal cell function and eventually causing necrotic or apoptotic cell death. Another theory is that binding of reactive species to proteins leads to formation of neoantigens, structures foreign to the body, with the potential of activating the immune system and triggering a cytotoxic immune response. When reacting with DNA, ROS may cause mutations in the DNA sequence, leading to carcinogenesis and genotoxicity (Gómez-Lechón et al., 2015; Guengerich, 2011).

Oxidative stress can be the source as well as one of the outcomes of mitochondrial dysfunction. Mitochondrial dysfunction is a collective term and comprises damage of mitochondrial components as well as changes in metabolic pathways related to mitochondria. Potential consequences of mitochondrial dysfunction comprise oxidative stress, energy shortage, accumulation of triacylglycerides, cell death as well as ER stress (Begrache et al., 2011). Lastly, ER stress describes a cellular state in which mis- or unfolded proteins accumulate within the cell, triggering the so called unfolded protein response (UPR). The UPR initiates processes to remove incorrectly folded proteins to reestablish fully functional folding. When a cell fails to restore normal conditions, pathways for programmed cell death are triggered (Sano and Reed, 2013).

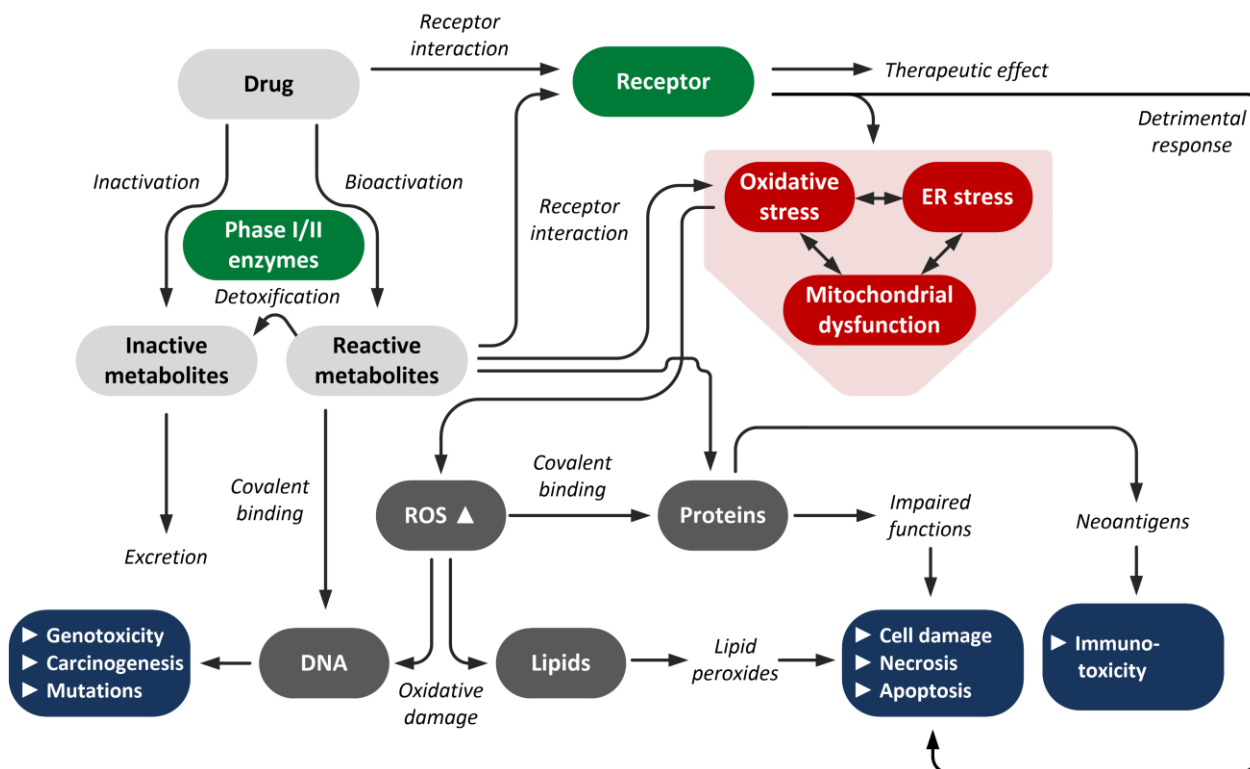


Figure 1.4 Scheme of mechanisms in drug-induced toxicity. In an ideal scenario, drugs or its metabolites (light grey boxes) bind selectively to the desired receptor and fulfil their purpose, while phase I and II enzymes lead to their inactivation over time (receptors and enzymes highlighted as green boxes). However, in case of overdose or drug accumulation, binding to the receptor may lead to a detrimental response. Alternatively, the parent compound or the metabolites may also bind to other receptors, which may likewise result in adverse effects. As a third mechanism, reactive metabolites may directly bind to DNA or proteins and cause cellular damage, or indirectly cause cellular damage by triggering oxidative stress. Oxidative stress, together with endoplasmic reticulum (ER) stress and mitochondrial dysfunction, are central events in the majority of drug-induced liver injuries (red boxes). Affected molecules and adverse outcomes are highlighted in dark grey and blue respectively. ROS = Reactive oxygen species. The figure is based on Liebler and Guengerich 2005 and Gómez-Lechón 2015.

Finally, there is iDILI, for which mechanisms leading to toxicity remain to be elucidated. According to current hypotheses, mechanisms in many cases are identical to those mentioned above, but only occur in few individuals due to the presence of one or more additional risk factors like inflammatory stress or genetic variability in the human leukocyte antigens (HLA), CYP450 enzymes or other proteins involved in drug biokinetics (figure 1.5) (Gómez-Lechón et al., 2015). The rare occurrence of detrimental mutations in these genes may explain the low incidence of iDILI of around 10^{-4} to 10^{-5} (Gómez-Lechón et al., 2015; Vinken, 2015).

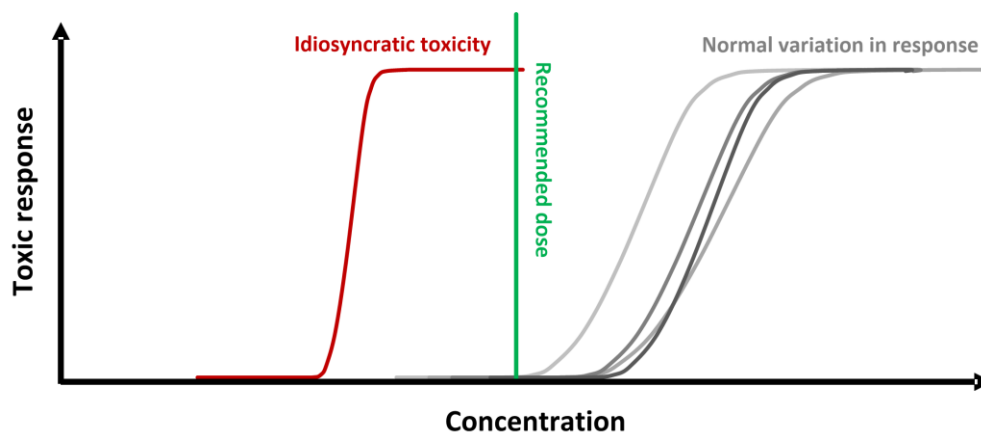


Figure 1.5 Scheme of response in idiosyncratic toxicity. Under normal conditions, application of a drug at its recommended dose does not evoke severe adverse reactions, if any at all. In a normal situation, response to the drug varies slightly between individuals, but remains in a safe range. In rare occasions, the dose response curve is shifted towards notably lower concentrations, eliciting toxicity at the recommended dose.

1.3.2 Patterns of drug-induced liver injury

While the mechanisms of drug-induced toxicity described above take place on molecular and cellular level, prolonged duration eventually affects organs and finally the whole organism, with several different outcomes depending on the initial perturbation. The 5 most common patterns of DILI are acute and chronic hepatitis, as well as acute and chronic cholestasis and a combination of the two patterns, cholestatic hepatitis. In total, these patterns make up for around 83% of observed DILI cases (Kleiner, 2014). Drug-induced hepatitis is characterized by the infiltration of inflammatory cells into the tissue together with the occurrence of hepatocellular necrosis (figure 1.6). The term cholestasis on the other hand describes the accumulation of bile acids within the liver due to intra- or extrahepatic obstruction of bile flow from the liver to the gall bladder. Beyond a certain threshold, bile acid accumulation leads to toxic reactions as a result of their detergent nature.

Another important pattern of DILI is the aberrant retention of lipids within hepatocytes, in particular triacylglycerides either in the form of small or large lipid droplets, referred to as micro- or macrovesicular steatosis respectively (Vinken, 2015). Steatosis results from mitochondrial dysfunction, leading to intrahepatic accumulation of fatty acids, which are partially converted into triacylglycerides to avoid toxicity caused by free fatty acids (Listenberger et al., 2003). Traditionally, steatosis is considered as the first step in the spectrum of the non-alcoholic fatty liver disease (NAFLD) and goes along with reversible enlargement of liver volume. In more severe cases of NAFLD, steatosis is accompanied by inflammation of the liver, an indication referred to as non-alcoholic steatohepatitis (NASH). Further progression of NAFLD causes fibrosis, i.e. scarring of the tissue and eventually hardening of the liver and permanent liver damage, called cirrhosis. In rare cases, drugs cause development of hepatocellular carcinoma (HCC) as the final stage of the NAFLD spectrum (Farrell and Larter, 2005; Yilmaz, 2012). However, fibrosis, cirrhosis and HCC not only occur in the context of NAFLD, but also as a result of other patterns, such as cholestasis (Bataller and Brenner, 2005).

Steatosis is a frequent disease in the general population (Browning et al., 2004), yet it is the predominant pattern in DILI in less than 2% of cases. However, it was also observed that around

27% of DILI showed at least some degree of steatosis (Kleiner et al., 2014; Rabinowich and Shibolet, 2015).

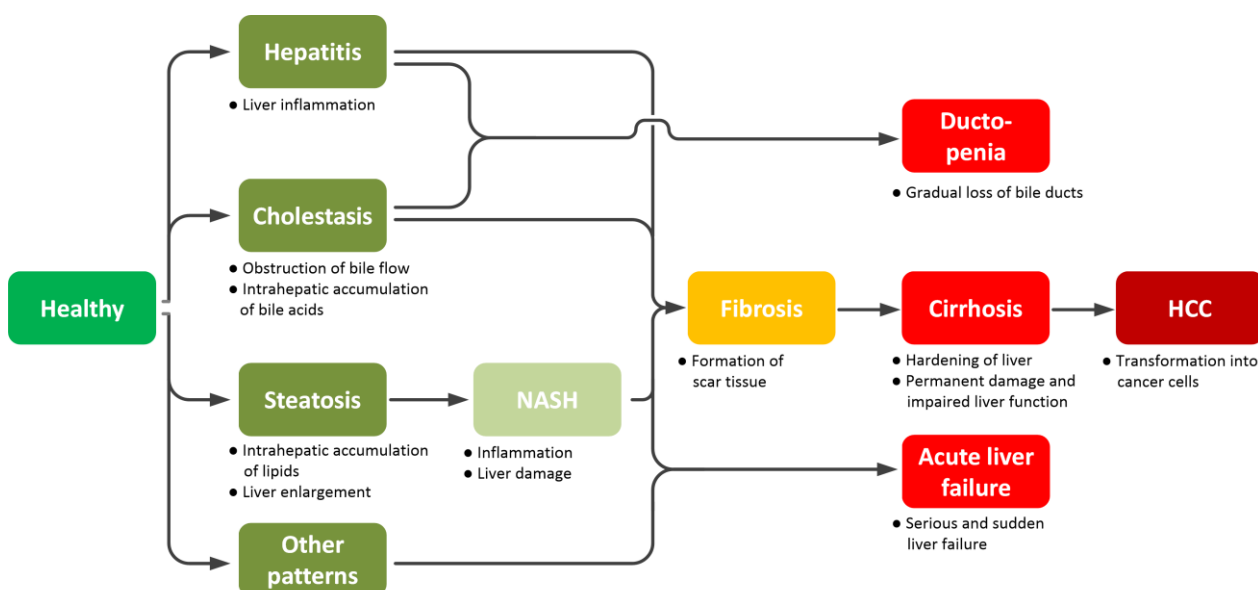


Figure 1.6 Patterns of drug-induced liver injury (DILI). The most relevant DILI patterns and progression towards severe liver damage including the characteristics of each step. NASH = Non-alcoholic steatohepatitis. HCC = Hepatocellular carcinoma.

Acute hepatic necrosis is yet another type of DILI pattern, which is usually caused by direct hepatotoxins such as acetaminophen.

In most of the cases of DILI, injuries eventually resolve completely. However, rare complications may occur during which the injury progresses towards acute liver failure, cirrhosis or ductopenia, i.e. the gradual loss of bile ducts. Due to their severity, these rare complications may be lethal and require liver transplantation (www.livertox.nih.gov, accessed 2016-03-26).

1.4 Test systems for the study of hepatotoxicity

1.4.1 Traditional test systems in *in vitro* toxicity assessment

For the study of liver functions and effects of compounds on these liver functions, several different test systems are available, ranging from simple enzyme expression systems and co-cultures of mammalian cells to xenograft animal models and eventually humans themselves. Depending on the question that is raised, simpler systems are sufficient or more complex systems may be required.

For the screening of drug- and chemical-induced hepatotoxicity and investigations on the underlying mechanisms, subcellular fractions, cell lines, primary hepatocytes, liver slices and perfused organs are the most commonly used *in vitro* systems (Guillouzo, 1998), with transgenic cell lines and stem cells slowly emerging into the field. These studies are traditionally complemented by *in vivo* experiments conducted in animals and ultimately, experiments directly conducted in humans during the clinical

phases. A summary of the different test systems used in toxicity assessment is given in table 1.1, highlighting their advantages and disadvantages.

Table 1.1 Overview on the different test systems for assessment of hepatotoxicity. The different test systems used in toxicity assessment are listed according to their complexity. Their characteristics are graded from non-existing (-) to optimal (+++). PHH = primary human hepatocytes; iPSC = induced pluripotent stem cells; hESC = human embryonic stem cells. Table was adapted from literature and expanded (Brandon et al., 2003; Fasinu et al., 2012).

Test system	Human <i>in vivo</i> correlation	Throughput	Technical Simplicity	Commercial availability	Viability period	Repro-ducibility	Ethical acceptance
Human	+++	-	-	-	+++	-	-
Xenograft animals	+++	+	-	-	+++	+	-
Animals	++	+	+	++	+++	+	-
Perfused liver	++	+	+	-	+	+	-
Liver slices	+++	+	+	-	+	+	++
PHH	+++	++	++	++	++	+	++
Stem cells							
iPSC	++	++	+	+++	+++	+	++
hESC	++	++	+	-	+++	+	-
Liver cell lines							
HepG2	+	+++	+++	+++	+++	++	+++
HepaRG	++	+++	+++	+++	++	++	+++
Subcellular fractions	+	+++	+++	+++	-	++ / +++	+++

Subcellular fractions

Subcellular fractions are the simplest systems applied in the study of hepatotoxicity. Different types of fractions are available, including recombinant enzymes, cytosolic fractions, microsomes and S9 fractions. Recombinant enzymes are used to study the activity of single enzymes related to the metabolism or transport of a given drug. Enzymes can be recombinantly expressed in transgenic cell lines, bacteria, yeast or insect cells. Depending on the system, this technique allows isozyme-specific drug biotransformation studies (Brandon et al., 2003). The cytosolic fraction only contains soluble phase II enzymes and is rarely used in drug biotransformation studies (Brandon et al., 2003). Liver microsomes on the other hand consist of ER vesicles and therefore are suitable to study drug metabolism via CYP450 enzymes and uridine diphosphoglucuronosyl transferases (UGT) in the context of drug metabolite profiling and for the comparison of metabolic activity in different groups, such as different species or effects based on the gender (Fasinu et al., 2012). S9 fractions combine cytosolic and microsomal fractions and allow assessing both, phase I and phase II metabolism of compounds. Compared to the cytosolic and microsomal fractions, enzyme levels are lower and consequently overall activity is lower. This may result in certain metabolic products being underrepresented and not being quantifiable or even detectable (Brandon et al., 2003).

Subcellular fractions are well established, affordable and easily applicable. Fractions from different origin are commonly pooled to overcome interindividual differences and increase reproducibility. Studying fractions originating from different individuals separately on the other hand offers the possibility to investigate differences in the xenobiotic metabolism within a population (Brandon et al., 2003).

Unlike whole cells, subcellular fractions do not possess all required cofactors and cofactor-regenerating systems necessary to perform all phase I and II reactions, even in case the enzymes are present. Thus, missing cofactors and enzymes need to be supplied depending on the reactions of interest, such as adenosine-3'-phosphate 5'-phosphosulfate (PAPS) in case of sulfotransferases (Fasinu et al., 2012). The limited set of reactions and the artificial conditions in these systems, e.g. the absence of drug transport, prevent a holistic and representative image of a drug's metabolism and lead to a poor correlation with *in vivo* (Brandon et al., 2003).

Hepatic cell lines

With cell lines, the complexity of the investigated systems increases notably. Several different human tumor-derived hepatic cell lines are used in toxicity studies. At least theoretically, cell lines are capable to conduct the complete set of drug metabolizing reactions as well as to provide all required non-essential cofactors. Most of them however lack a reasonable expression of major liver specific molecules, such as the CYP450 enzymes, phase II enzymes, membrane transporters and nuclear receptors. This also applies to the most widely used human hepatoma cell line, the HepG2 cell line (Donato et al., 2013; Soldatow et al., 2013). The HepG2 cell line was first established in 1979 by Barbara Knowles. It was derived from a male patient suffering from a hepatoblastoma (López-Terrada et al., 2009). Despite its shortcomings, the cell line may still yield accurate results when investigating parent compound toxicity or resistance to chemotherapy (Mueller et al., 2013; Niklas et al., 2009; Ong et al., 2008).

Another promising human hepatic cell line was established in 2002, where it was isolated from a female patient with hepatocarcinoma and hepatitis C infection (Gripon et al., 2002). Unlike other hepatic cell lines, the so called HepaRG cell line expresses liver specific enzymes in an amount that is comparable to that of primary human hepatocytes (PHH) (Lübberstedt et al., 2011). Furthermore, it is amenable to prolonged cultivation, while maintaining a differentiated state for several weeks (Josse et al., 2008). Contrary to other hepatic cell lines, it consists of two different cell types; hepatocyte-like (HLC) and biliary epithelial-like cells (BLC) (Cerec et al., 2007).

Hepatic cell lines generally allow well reproducible results, but on the other hand, they are not capable of representing a large population as each of the cell lines only has a single genotype (Soldatow et al., 2013). In this context, it is worth noting that polymorphisms, e.g. in the CYP450 enzymes may have a major impact on the fate of therapeutic compounds (Zhou et al., 2009). Contrary to subcellular fractions, cell lines allow induction studies, which necessitate functional transcription and translation of genes involved in drug metabolism (Castell et al., 2006).

Primary hepatocytes

The introduction of the collagenase perfusion method for isolation of hepatocytes from liver tissue paved way for the broad use of primary hepatocytes (Guillouzo, 1998; Howard et al., 1967). PHH are considered the gold standard in the assessment of hepatotoxicity as expression of liver specific enzymes is close to humans *in vivo*. Contrary to cell lines and primary rodent hepatocytes, the diversity of their origin yields a good representation of the human population and enables to assess

effects of genetic variation to a toxic response. This however goes along with sometimes poor reproducibility of results. Since the development of techniques for cryopreservation of hepatocytes (Diener et al., 1993), availability of PHH greatly improved. Still, PHH are often freshly isolated and used either in adherent cultures or in suspension. Compared to hepatic cell lines, cultivation of PHH generally requires more complex techniques to avoid dedifferentiation and maintain liver specific functions (Brandon et al., 2003). Under standard cultivation conditions, PHH retain liver specific activities for around 24 to 72 h (Godoy et al., 2009), and after 1 week, around 50% of the initial CYP450 amount still remains. The upkeep of functionality in PHH was found to be substantially better, compared to rodent-derived hepatocytes (Guillouzo, 1998; Guillouzo et al., 1985). With special media, viability and functionality of PHH can even be extended to several weeks (Mueller et al., 2012).

Liver slices

Liver slices resemble the *in vivo* situation even closer. They retain liver structure including periportal and pericentral zone specificity and functional bile canaliculi. Furthermore, they include all different cell types present in the liver. Studies involving liver slices usually run between few minutes and up to 120 h. Comparable with the previously mentioned systems, upkeep of liver functionality and viability is strictly limited. After 6 h to 72 h, CYP450 enzyme levels decrease quickly and cellular necrosis occurs after 48 h to 72 h (Soldatow et al., 2013), though in some studies viability was maintained until 96 h (Klassen et al., 2008).

Liver slices are usually prepared from animal liver, but can also be prepared from human liver, e.g. from liver biopsies. Standard slices have a thickness of approximately 250 μm (Guillouzo, 1998). Due to the dimensions, nutrient supply and exposure to xenobiotics is limited to a large extent to diffusion and gradients build up across the slices. Liver slices provide a good correlation to *in vivo* (Soldatow et al., 2013) and allow reducing the number of animals needed for an experiment as several slices can be prepared from a single animal.

Isolated perfused liver

Isolated perfused livers are the most complex *in vitro* tool for toxicity assessment and it is also the system closest to the *in vivo* situation. Its 3D architecture is preserved, including cell-cell contacts and intact bile canaliculi. Unlike for liver slices, not to mention more basic systems, bile can be collected and studied separately (Guillouzo, 1998). Despite its close resemblance to *in vivo*, the drawbacks of the system are overwhelming. The system is generally difficult to handle and only allows studies for few hours after which functional integrity is compromised. The complexity of the system brings along low throughput and limited reproducibility (Fasinu et al., 2012). Animals are the only source of perfused livers. From an ethical point of view, perfused livers do not harbor many advantages as each animal only yields a single liver (Brandon et al., 2003).

In summary, it is evident that the main advantage of more complex systems is the increased correlation to *in vivo*, while forfeiting throughput, technical simplicity, commercial availability, reproducibility and ethical acceptance. Thus, at least at the moment, the decision on one of the systems is always a compromise between these two sides.

1.4.2 Novel strategies and tools in toxicity assessment

To date, one of the biggest needs in toxicology is for methods to assess repeated dose toxicity in a human-relevant context. As *in vitro* systems either lack stable viability and functionality or human *in vivo* correlation, hopes rest on the improvement of current techniques or development of new

techniques, combining the advantages of both sides without hampering the one or the other. The ultimate goal is to provide a validated system that yields reliable data for prediction of adverse effects in humans (Soldatow et al., 2013).

The loss of functionality and induction of cell death that is observed during cultivation of primary hepatocytes, and to some extent in cell lines, is attributed to A) two-dimensional (2D) cultivation of cells, B) processes triggered during isolation and C) exogenous soluble factors (Guguen-Guillouzo, 2002; Guillouzo, 1998; Guillouzo et al., 1990)

Different strategies that have been applied to tackle these problems will be described in the following (figure 1.7).

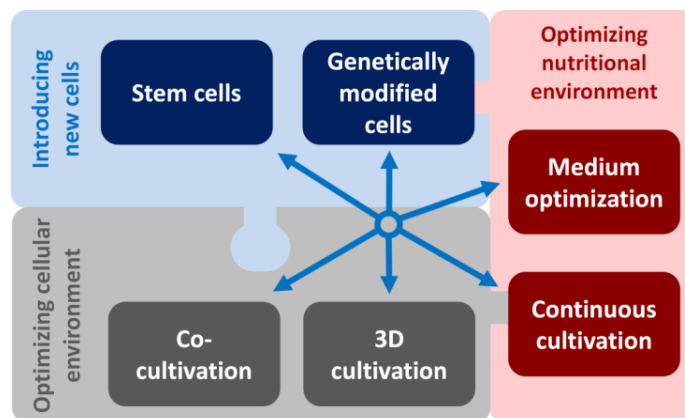


Figure 1.7 Summary on options available for improving *in vitro* cultivation. The approaches used to improve *in vitro* cultivations in order to allow them a more *in vivo*-like behavior were divided into three groups: 1) developing and introducing new cells, 2) optimizing cellular environment and 3) optimizing nutritional environment. The approaches can be used as a stand-alone version, but are readily combined in many studies for further improvement.

2D versus 3D cultivation

The first strategy aims at reestablishing an *in vivo*-like cellular morphology by cultivating cells in an environment that allows their three-dimensional (3D) spreading (3D cultivation). The idea to cultivate cells in a 3D environment has already been applied several decades ago, e.g. in producing spheroids of Chinese hamster V79 cells to develop an *in vitro* tumor model for investigation of effects of radiation (Sutherland et al., 1970). Differences between 2D and 3D cultivation are manifold. Baker and Chen summarized the dissimilarities that cells have to cope with in the traditional but artificial environment of a 2D cultivation, compared to 3D cultivation. Their main cues are depicted in figure 1.8. A major difference between cells in a 2D and 3D environment is their morphology. Cells in 2D monolayer cultures are flat and elongated and can freely spread on the surface they are growing on. Hepatocytes *in vivo* on the other hand have a cuboidal shape and their spreading is limited sterically. Also, *in vivo*, hepatocytes are mostly surrounded by other cells, whereas in 2D cultures, cells are almost exclusively in contact to the medium and the culture device. This has several implications. E.g., cellular nutrient or xenobiotic gradients are absent within 2D cultures. Furthermore, in a 2D environment adhesion is restricted to the surface of the culture device and therefore apical-basal polarity is forced upon the cells, whereas polarity is not prescribed in a 3D environment (Baker and Chen, 2012). This is

particularly of concern for hepatocytes, which have a special type of polarity. Unlike other epithelial cells, hepatocytes possess two basolateral surfaces as well as apical surfaces, which are connected to the lumen of bile canaliculi (Dunn et al., 1989).

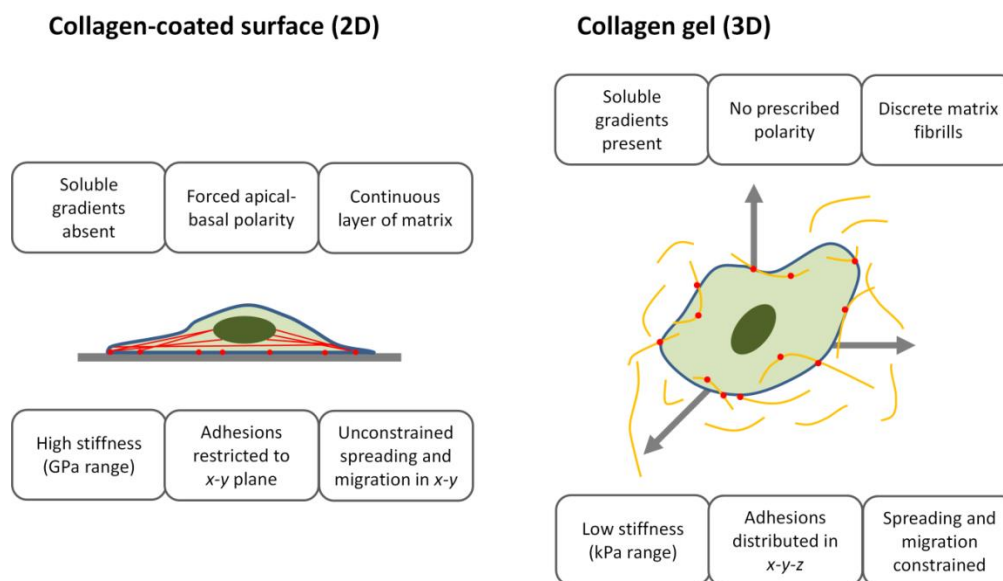


Figure 1.8 Differential factors in cell cultures in 2D and 3D environment influencing cellular behavior. A summary of the adhesive, topographical, mechanical and soluble factors that potentially determine cellular behavior in the two different cultivation setups. The figure was adapted from Baker and Chen, 2012.

3D cultivation systems

A variety of different systems for 3D cultivation is commercially available. Spheroid cultures for example are a scaffold-free system making use of the self-aggregation of cells upon establishing cell-cell contacts. There are various ways to form spheroids. Next to shaking cells in spinner flasks as in the example mentioned above (Sutherland et al., 1970), spheroids can also be formed in hanging drop cultures as well as on non-adhesive surfaces (Chen et al., 2012; Kelm and Fussenegger, 2004). To demonstrate the potential of spheroid cultures in toxicity assessment, our group has shown that the CYP450 activity as the crucial factor in studying toxicity, was significantly higher in HepaRG spheroids compared to 2D cultures (Mueller et al., 2014). Going along with elevated CYP450 activity, we were showing significant changes in the EC_{50} values upon exposure to 4 different compounds when HepaRG cells were cultivated as spheroids, compared to conventional 2D cultivation (Mueller et al., 2014).

CSW cultures are another type of 3D cultivation system where cells are embedded in between two layers of collagen matrix to favor formation of *in vivo*-like cellular geometry. Dunn et al. were the first to apply this technique to hepatic cells and could show that rat hepatocytes cultivated in a CSW retained morphology and albumin secretion for 6 weeks. 2D cultures on the other hand ceased albumin secretion completely within a week (Dunn et al., 1989). The CSW technique is applied in studies that essentially require *in vivo*-like polarity, e.g. in transporter studies (Liu et al., 1999), whereas application in toxicity studies (Hrach et al., 2011) is less common.

Continuous cultivation systems

More recently, systems have been developed combining 3D cultivation and a continuous media flow, mimicking *in vivo*-like morphology and blood flow. Unlike static cultures, this allows continuous supply of nutrients and removal of metabolic waste products resulting from metabolization of endo- and exogenous compounds, as well as establishing an extracellular steady state. Flow of medium also helps in preventing oxygen limitation, a major concern in 3D cultures (Dash et al., 2009). Realization of this principle was shown using different approaches, e.g. in the form of 3D hollow-fiber bioreactors (Mueller et al., 2011) and microfluidic hanging drop spheroid cultures (Frey et al., 2014). Cultivating PHH in hollow-fiber bioreactors allowed maintenance of the cells and upkeep of hepatic functions for at least two weeks, offering great improvement over 2D cultures of PHH (Mueller et al., 2011). Major drawbacks of this system are the tremendous amount of cells required (10^8 PHH per bioreactor) and incompatibility with high-throughput approaches. The afore-mentioned microfluidic hanging drop cultures are one solution to overcome these problems by reducing the number of cells per organotypic culture to around 10^3 and enabling the study of 16 cultures in parallel (Frey et al., 2014).

Medium supplements

In vivo, hepatocytes are not only embedded in an extracellular matrix (ECM) and engaged in cell-cell contacts with other hepatocytes, but they are also exposed to a multitude of molecules secreted by other cells that may potentially modulate their behavior, including hormones and growth factors (Guillouzo, 1998). To account for a lack of these exogenous factors, hepatocyte cultivation media are supplemented with various compounds with the goal to maintain and improve hepatic functions and longevity. Corticosteroids and insulin are traditional supplements in media for cultivation of hepatocytes, yet supplements are not limited to molecules of biological origin, but also include non-physiologic compounds such as dimethyl sulfoxide (DMSO), one of the most effective supplements to maintain hepatocytes in a differentiated state (Guillouzo, 1998; Isom et al., 1985). Optimization of media is a classical approach in bioprocessing to improve production yields (Subathra Devi et al., 2015), but is also applied in other fields of research, such as in the optimization of culture conditions for hepatic cell lines and primary hepatocytes (Dong et al., 2008).

Hepatocyte co-cultures

Another very effective way to improve maintenance of hepatic functionality in an *in vitro* setup is the co-cultivation of hepatocytes with other cell types, in many cases other liver cells (Begue et al., 1984; Krause et al., 2009). In animals, cells and organs fulfill specific functions and only their interactions eventually form a fully functional system. Therefore, *in vitro* models generally represent only a fraction of the processes that occur *in vivo*, which at the same time is the biggest drawback of *in vitro* systems. At least to some extent, co-cultivation allows cell-cell interaction as observed *in vivo*, yielding systems more reliably representing the *in vivo* situation (Kostadinova et al., 2013). Consequently, co-cultivation with primitive biliary cells extended survival of hepatocytes for several weeks while maintaining specific hepatic functions (Guguen-Gouillouzo et al., 1983). Superiority of the HepaRG cell line, which is an inherent co-culture of HLC and BLC is likely to be partially based on the same principles (Aninat et al., 2006).

In another study investigating the longevity and behavior of co-cultures upon exposure to several toxicants, it was shown that co-cultures of PHH with non-parenchymal cells, such as stellate and Kupffer cells, maintained liver-specific functions for up to 3 months. Furthermore, these cultures more accurately captured *in vivo* toxicity when exposed to drugs eliciting idiosyncratic toxicity, including trovafloxacin. The authors hypothesized that activation of Kupffer or stellate cells results in the release

of pro-inflammatory signaling molecules, eventually eliciting a toxic response (Kostadinova et al., 2013).

Another focus of current research deals with a more sophisticated version of co-cultivation where the different cell types are spatially separated and connected to each other only via channels in a microfluidic setup. These multi-organ-chip platforms, also referred to as body-on-a-chip or human-on-a-chip, allow co-cultivation of cells from different origins, e.g. hepatic, myocardial and skin cells combined with a blood stream-like medium flow to study their interactions in an *in vivo*-like environment (Maschmeyer et al., 2015). Several cellular functions and processes can be monitored using biosensors (Perestrelo et al., 2015) or simple sample collection and subsequent analysis. The body-on-a-chip approach currently is the best available way to close up to animal models in respect to their systemic nature.

Stem cells

Considered as promising alternatives to hepatic cell lines and primary hepatocytes, stem cells are slowly emerging as useful tools in drug development. Induced pluripotent stem cells (iPSC) and human embryonic stem cells (hESC) currently attract most attention, even though both systems still struggle with teething problems.

iPSC were originally derived from somatic cells using viral vectors for reprogramming by introduction of key transcription factors like OCT3/4 and C-MYC (Ko and Gelb, 2014; Takahashi et al., 2007; Takahashi and Yamanaka, 2006). Later on, an approach without the use of viral vectors was developed (Okita et al., 2008). While cells are in an embryonic-like state, they can be passaged indefinitely. After upscaling, iPSC can be differentiated into a wide range of different cell types, e.g. neurons, hepatocytes, cardiomyocytes, and hematopoietic cells (Ko and Gelb, 2014). Since iPSC are derived from somatic cells and still possess the genetic background of the individual they originate from, they may serve as an indispensable tool in personalized medicine in the future. iPSC can also be used to generate cell banks that can be used to study toxicity in a large *in vitro* population during early drug development. Even more, they allow predicting the effect of a compound in patients suffering from rare diseases (Knudsen et al., 2015; Ko and Gelb, 2014). One of the hurdles of this approach yet to overcome is the inconsistency and low efficacy of current protocols for reprogramming of cells. In case of protocols for iPSC differentiation into hepatocytes, populations of different liver cell types and different stages of hepatocyte-like maturity have been observed. Consequently, activity of liver specific enzymes was reported below activity in PHH (Baxter et al., 2010), and thus, protocols require further fine-tuning for the approach to be applied more broadly.

Sharing many advantages and disadvantages, few things differ between iPSC and hESC. For example, hESC are derived from blastocysts (Thomson et al., 1998) and unlike iPSC do not rely on previous reprogramming. Due to their origin, hESC are tainted with ethical concerns, which drastically limits their use. Furthermore, while iPSC are specific for patients and diseases as stated above, hESC are not (Ko and Gelb, 2014). Similar to iPSC, protocols for differentiation yield cell populations with highly variable and generally low functionality and additionally, both types of stem cells share one of the major disadvantages of primary hepatocytes, which is loss of functionality after few days in culture (Soldatow et al., 2013).

Genetically modified primary hepatocytes

Another very recent approach is based on the generation of proliferating hepatocytes from PHH by introduction of genetic modifications. The goal is to combine advantages of hepatic cell lines, i.e.

unlimited availability, easy handling and cost efficiency with the advantages of PHH, i.e. high, *in vivo*-like drug metabolizing capacity and the option to study interindividual differences using cells derived from different donors. Hepatocytes generated with this method are referred to as upcyte hepatocytes (Burkard et al., 2012). In a comparison with PHH and HepG2 cells, upcyte hepatocytes were found to be closer to PHH than the HepG2 cell line in terms of their gene expression profile. Furthermore, upcytes were shown to be readily applicable in toxicity studies with repeated dose regimen (Tolosa et al., 2016).

Chimeric animal models

At this point, an approach shall be briefly mentioned that takes another direction, which is the humanization of animal models, i.e. the production of chimeric animals. Unlike previously stated methods, the goal here is not to reduce the use of animal models, but to make use of the systemic view they provide and improving their reliability by introducing human-derived liver cells. For that purpose, immunodeficient animals, commonly mice, e.g. TK-NOG mice, undergo hepatectomy and human liver cells are transplanted into the animal (Nishimura et al., 2013). Interestingly, in a recent study, HepaRG cells have been used as a source of human liver cells (Higuchi et al., 2014). This approach generally allows the study of human xenobiotic metabolism in a systemic environment, but it also comes along with several disadvantages. One of them is the inherent immunodeficiency of these mice, which prevents them from being used in studies that involve immune-mediated adverse drug effects. Furthermore, chimeric mice harbor uncertainties in terms of extrahepatic influences and the degree of humanization of the biliary tract which is important, e.g. for hepatobiliary clearance (Nishimura et al., 2013). Additionally, inter-species differences in telomerase regulation and in cytokines put the approach on a shaky foundation (Griffith and Swartz, 2006).

1.5 *In silico* tools for risk assessment and implementation of *in vitro* methods

Considerable progress is made in providing more and more reliable *in vitro* tools. The question that now arises is how these tools can be implemented to assist the assessment of toxicity in a regulatory environment. One way these systems can be used is to replace animals in assessing parameters required for the evaluation of toxicity of a compound of interest, thereby reducing the number of animal tests and yielding results more relevant to the human organism. In another way, *in vitro* tools can be used to gain mechanistic understanding of toxicological processes, which may drastically help in prediction of DILI. The steps involved in risk assessment and how the *in vitro* tools can be employed will be discussed in more detail in the following.

1.5.1 Toxicological risk assessment

The risk of a substance to cause harmful effects is evaluated in a process called toxicological risk assessment, which comprises 4 steps (Kleijnans, 2003; Leeuwen and Vermeire, 2007):

1. Hazard identification
Identification of the inherent adverse effects of a substance.
2. Hazard characterization
Quantitative relation between dose and incidence and severity of an effect.

3. Exposure assessment
Specification of the population potentially exposed to the compound of interest and identification of exposure routes, magnitude and duration.
4. Risk characterization
Integration of the three previous steps, i.e. qualitative or quantitative estimation of the likelihood that hazards will be realized upon exposure.

In summary, the aim is to characterize the type, magnitude and probability of the hazard for a given substance and population (Kleinjans, 2003). The first two steps, hazard identification and characterization will be in the focus of the following discussion.

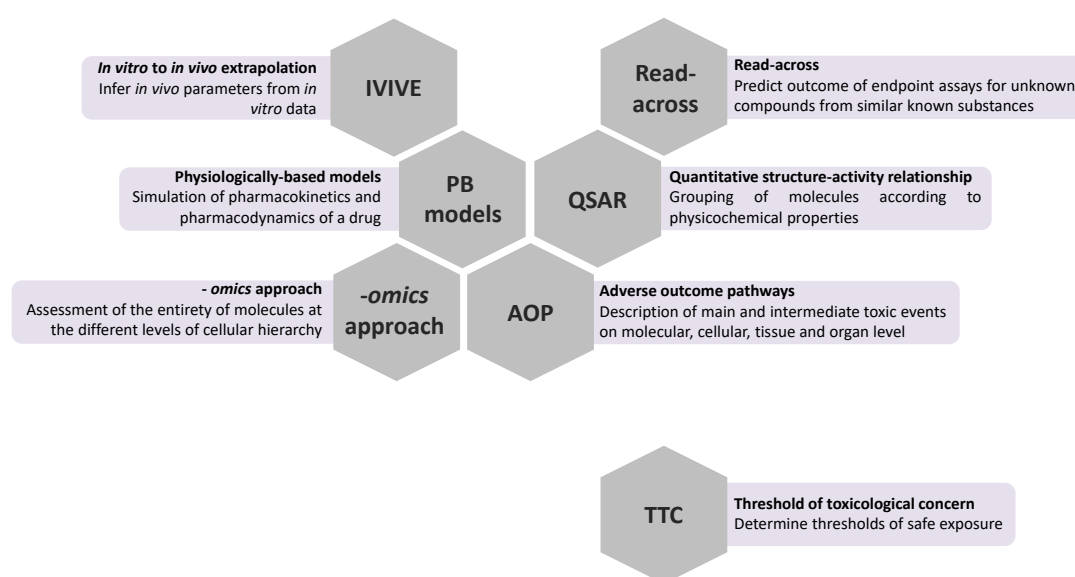


Figure 1.9 Overview on *in silico* tools and the –omics approach for risk assessment. Each tool is represented by a comb, and neighboring combs represent a potential interaction between the different tools. E.g., grouping of chemicals via quantitative structure-activity relationship can be used to find similar compounds to apply in the read-across approach.

1.5.2 Threshold of toxicological concern

An increasingly popular method applied in risk assessment of unknown substances is to determine the threshold of toxicological concern (TTC), i.e. the threshold below which the probability of harmful effects to human health is low (figure 1.9). The TTC is based on the distribution of the NOAEL of compounds with known toxicity. It further requires structural information on the unknown compound and reliable information on human exposure (EFSA, 2014). It is used as a screening method for less well-characterized compounds to prioritize toxicity testing (Felter et al., 2009)

1.5.3 Read-across and structure-activity relationships

The read-across approach is employed to predict results of an endpoint assay for the substance of interest, using one or more biologically or chemically similar compound(s) (source substance(s)) with

available endpoint information. Similarities can be of physicochemical nature or based on sharing a functional group related to adverse effects, or similarities in metabolism (EFSA, 2014; Low et al., 2013; Worth et al., 2011). Other *in silico* tools, such as the quantitative structure-activity relationship (QSAR) models can be used to automatically group substances according to predefined criteria, which can then be used as source substances for other compounds within the same group to estimate missing parameters. QSAR models relate molecular descriptors to biological activities via mathematical models. In general, molecular descriptors are the intrinsic physicochemical properties of the investigated substance, e.g. its atomic composition, structure, volume and hydrophobicity (EFSA, 2014). The approach implies that the biological activity of a chemical is based on these molecular descriptors and therefore, activity can be directly predicted from descriptors and further, that the activity for unknown substances can be inferred from compounds with similar traits and known activities.

Besides its use in grouping chemicals, the QSAR approach is also applied to quickly decide on the safety of a chemical when no toxicological data is present (Worth et al., 2011), as well as to predict physicochemical properties of a substance (Leeuwen and Vermeire, 2007)

Both, the QSAR and read-across method require considerable expert knowledge as reliability of the approaches heavily depends on the choice of analogue compounds as well on reliability of the underlying experimental data (EFSA, 2014; Leeuwen and Vermeire, 2007; Worth et al., 2011). Unlike QSAR, read-across is a non-formalized approach and therefore the data selection step is even more critical (EFSA, 2014). *In vitro* experiments are a viable source of data for such approaches, hence, to ensure reliability, appropriate *in vitro* tools have to be used for data generation.

1.5.4 *In vitro* to *in vivo* extrapolation and physiologically-based models

The approach of *in vitro* to *in vivo* extrapolation (IVIVE) refers to the use of *in vitro* data to infer *in vivo* parameters reflecting human physiology and metabolism. When variability in humans is considered, the approach is termed quantitative IVIVE (QIVIVE) (EFSA, 2014). To yield *in vivo* relevant parameters, adjustments need to be made, e.g. taking into account plastic binding in the *in vitro* scenario and differences in protein binding, as well as in drug metabolism compared to *in vivo* (Hamon et al., 2015).

IVIVE is commonly incorporated into physiologically-based pharmacokinetic (PBPK) or physiologically-based toxicokinetic (PBTK) models. The models describe the relation of external dose and the resulting internal organ-specific concentrations over time under consideration of ADME processes (EFSA, 2014). Though PBTK models are mostly applied to estimate the resulting internal concentration upon application of a drug (Bois et al., 2010), they can also be used in a reversed manner, i.e. to estimate the dose of a compound needed to be taken up orally, in order to achieve a steady-state blood concentration, equivalent to a given effective concentration (EC), e.g. EC₅₀ (Rotroff et al., 2010). PBTK models may also be applied to simulate and study inter- and intraindividual differences in a compound's kinetics (Bois et al., 2010), and even to predict pharmacokinetic parameters between different species (Sharma and McNeill, 2009). Missing information on physicochemical parameters are typically estimated from QSAR (EFSA, 2014).

PBTK models can furthermore be extended by their toxicodynamic counterpart, mathematically describing the tissue response to a biologically effective dose of a given substance. Such models are generally applicable to compounds with well-known toxicokinetic and toxicodynamic parameters and

allow estimation of internal levels of the parent compound and its metabolites and the resulting effects on the organism (EFSA, 2014).

Setting up a PBTK or even PBTK-TD model requires substantial knowledge and data, including drug-specific information, biochemical and physiological information and considerations on the ideal model structure (Bois et al., 2010); information which can be partially generated using *in vitro* models or taken from databases.

1.5.5 Adverse outcome pathways

The use of the adverse outcome pathway (AOP) framework is one approach to gain mechanistic understanding and compile knowledge on events occurring during toxicity. Thus, it facilitates the generation of models such as PBTK-TD by highlighting structures and pathways that are of crucial importance. AOP are characterized by a molecular initiating event (MIE) which is connected to an adverse outcome via a sequence of key events (KE), which may occur on different organism levels (Wittwehr et al., 2017). MIE can be processes such as inhibition of the bile salt export pump (BSEP) or activation of the liver X receptor (LXR), leading to cholestasis and steatosis respectively. Under the premise that compounds triggering the same MIE will cause the same adverse outcome, substances need to be grouped according to their MIE in order to predict toxic outcomes. Again, grouping can be conducted using approaches like QSAR (Vinken, 2015). Vinken has described the AOP for a number of toxicological endpoints related to DILI, such as liver fibrosis, steatosis and cholestasis (Vinken, 2015).

1.5.6 -omics approach

The -omics techniques are the predestined approach to gather the vast amount of information that is underlying an AOP. -omics is a collective term comprising various fields of study; in its traditional form representing the different levels of cellular hierarchy in a holistic manner, contrary to focusing on single genes, proteins or metabolites: The genome, epigenome, transcriptome, proteome, metabolome and fluxome (figure 1.10). The genome represents the genetic material of a cell, in case of mammalian cells including coding and non-coding regions of the DNA strands, as well as the genetic material inside of the organelles. The epigenome includes the whole set of modifications of histones and DNA with exception of mutations in the sequence. Epigenetic modifications serve the regulation of gene expression and are the cause for differential gene expression in distinct cell types in an organism despite identical genotype throughout the body. Methylation of DNA bases and histones and deacetylation of histones are classical examples for epigenetic modifications (Jaenisch and Bird, 2003). The next level of cellular hierarchy is represented by the entirety of DNA transcripts, i.e. mRNA, rRNA, tRNA and non-coding RNA molecules. mRNA is subsequently translated into proteins by the enzymatic activity of ribosomes. The complete set of proteins in or outside of a cell is termed proteome. Proteins, which have a multitude of different functions such as stabilization of cellular structure or regulation of transcription, may also catalyze biochemical reactions. Substrate and product of such biochemical reactions are usually molecules of low molecular weight also referred to as metabolites. The sum of all metabolites in or outside of a cell is called metabolome. The aim of metabolism is to gain energy and to form macromolecules, signaling or regulatory molecules as well as the temporary storage of molecules. On the apogee of cellular hierarchy is the fluxome which refers to reaction rates or fluxes as a whole, including rates for the conversion of one molecule into another, but also rates describing the transport of molecules across membranes. The fluxome integrates the effects of all hierarchical levels below and therefore, flux analysis is the best indicator for the actual cellular phenotype (Klein and Heinzle, 2012). Independent on the investigated cellular level, cells are

dynamic in nature, depending on environmental factors and therefore, -omics can only represent a snapshot of cellular status.

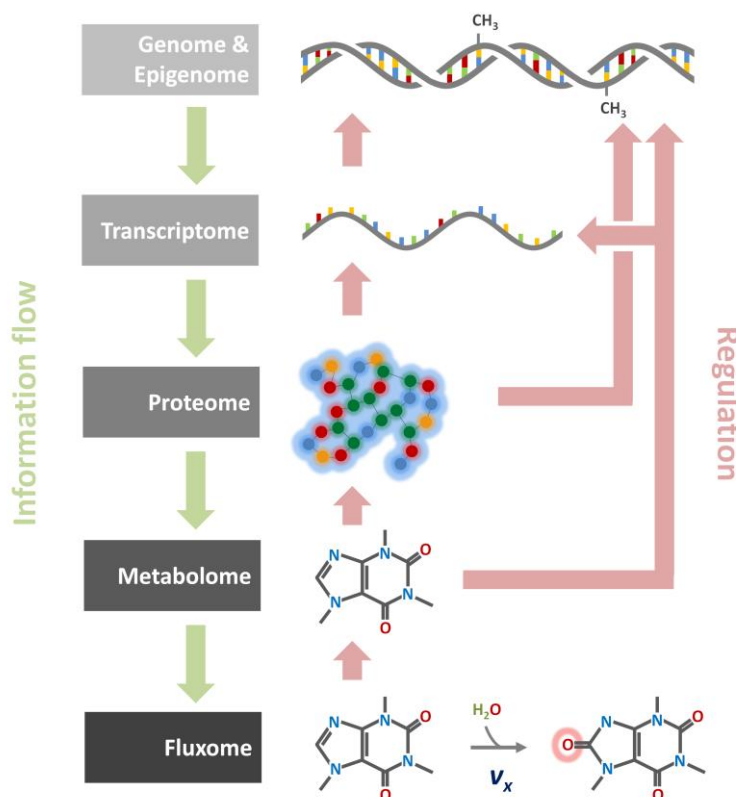


Figure 1.10 Overview on the different levels of cellular hierarchy and regulatory processes. The central dogma of molecular biology describes the flow of information from genes to proteins. Proteins in turn affect metabolite levels via enzymatically catalyzed reactions, while the concentrations of metabolites have an impact on the reaction and transport rates (fluxes). Possible regulatory actions are indicated by light red arrows.

In summary, the -omics approach yields information on all possible events occurring within a cell and therefore potentially allows full deciphering of DILI. Yet, this again emphasizes the need for an ideal model system, in detail reflecting the human *in vivo* situation.

In the light of current legislation, such as the European Union initiative on registration, evaluation, authorization and restriction of chemicals (REACH), the need for methods facilitating prediction of toxicity is more urgent than ever. The initiative requires safety assessment of chemicals in general, including cleaning products, cosmetic ingredients, dyes, and so on in order to minimize risks for human health and environment. In total, around 30,000 chemicals might require testing (Prieto et al., 2006). The overall goal of the tools described above is to avoid unnecessary toxicity testing either because human intake is appreciably below the TTC, or due to the fact that missing parameters can be estimated reliably from already existing data. Avoiding unnecessary experiments allows to focus limited resources on substances likely to be harmful and reducing the number of experiments performed on animals (Kroes et al., 2004). Besides their application in risk assessment, approaches

may also be used for estimation of ADME parameters during the screening of new drug candidates to aid in the selection of compounds with potentially favorable ADME properties (Rowland et al., 2004).

1.6 Metabolomics in detail

Metabolomics refers to the impartial analysis of the entirety of small molecules in a given compartment such as a cell, tissue or blood. Metabolites from different pathways may vary drastically in concentrations, size and a multitude of chemical properties such as lipophilicity and stability. As a result, covering the whole diversity of metabolites in an impartial or complete manner is currently restricted by technical limitations. To give an example, nitric oxide (NO), a signaling molecule in the human body, has a molar mass of 30 g/mol, is gaseous, hydrophilic and found in human blood in concentrations notably below 1 nM, whereas the liquid and lipophilic molecule docosahexaenoic acid, a source of anti-inflammatory eicosanoids, has a molar mass of 328.5 g/mol and is found in human blood in concentrations well above 1 μ M (www.hmdb.ca, accessed 2016-06-18).

1.6.1 Targeted versus untargeted metabolomics

Metabolomics is commonly divided into a targeted and an untargeted branch. In targeted metabolomics, extraction protocols and quantification methods are optimized for a predefined set of metabolites with known identity. The data is either of quantitative or semi-quantitative nature (Roberts et al., 2012). Owing to its focus on a subset of metabolites, targeted metabolomics is commonly considered as a hypothesis-driven approach (Sévin et al., 2015).

Untargeted metabolomics is also known as global metabolite profiling. It aims at maximum comprehensiveness and may include metabolites with known as well as unknown identity. Data is mostly reported as signal intensities and rarely yield absolute concentrations. The method is applicable in hypothesis-generating but also in hypothesis-driven studies, with a tendency towards the former. More than targeted metabolomics, it aims at the discovery of pathways previously not known to be affected by a certain disease, drug or other condition. Untargeted metabolomics commonly comes along with the generation of huge amounts of data which poses challenges in respect to data processing and management, as well as data interpretation (Sévin et al., 2015) The untargeted approach can be further divided into metabolic finger- and footprinting, referring to the global high-throughput analysis of intra- and extracellular samples respectively (Dunn et al., 2005).

1.6.2 Analytical tools in metabolomics

From an analytical point of view, metabolomics is particularly challenging due to the tremendous variety in the objects of investigation. In terms of popularity, two analytical approaches notably stand out within the field of metabolomics, namely mass spectrometry (MS) on the one hand, and nuclear magnetic resonance (NMR) spectroscopy on the other hand. Several factors have to be considered when selecting the best method for analysis, such as available sample volume, chemical nature of the metabolites of interest, budget, applicability to high-throughput and data output (Klein and Heinzle, 2012).

Mass spectrometers determine ion signals depending on mass-to-charge ratios, which can be specified for particular metabolites or metabolite classes. Mass spectrometers are usually coupled to a chromatographic system to compensate for the lack of separation in case of low resolution systems and to reduce so called matrix effects (Fuhrer and Zamboni, 2015). Depending on the compounds of interest, hyphenation to gas chromatography (GC) or liquid chromatography (LC) is used. In case of

high resolution systems, chromatographic separation can be omitted, which allows drastic reduction of the run time, and analysis of more than 1,000 samples per day. Flow injection is one approach for injection of liquid samples without prior chromatography, in which case samples are injected into a continuous eluent stream (Fuhrer and Zamboni, 2015).

NMR spectroscopy is a non-destructive method for identification and quantification of metabolites, which allows analysis in an unbiased manner with highly reproducible results. On the downside, the methodology is incompatible with high-throughput setups and acquisition costs of the equipment are high. Further, the sample volume requirements and limit of detection for NMR spectroscopy are notably above those of MS systems. Regarding the latter two points however, recent advances in technology led to an approximation of the two technologies (Cuperlović-Culf et al., 2010; Klein and Heinzle, 2012; Wishart, 2008).

1.6.3 Applications of metabolomics

Applications of metabolomics can be roughly divided into two sections. First, biomarker discovery and second, understanding of cellular processes, e.g. those underlying toxicological, pathological, and homeostatic responses, as well as the production of certain molecules. Both applications are intertwined but differ in focus. Biomarkers are quantifiable parameters, e.g. metabolites that can be used as indicators for a variety of biological processes. Such processes may include the assessment of drug efficacy or adverse reactions upon drug exposure during drug development. In a clinical environment, biomarkers may be used for diagnostic or prognostic purposes (Puchades-Carrasco and Pineda-Lucena, 2015). The newborn screening is a well-known example for the application of metabolic biomarkers. It allows screening of infants for a number of conditions related to inborn errors of metabolism such as phenylketonuria and severe combined immunodeficiency via the quantification of key metabolites.

Apart from the application in the context of biomarkers, metabolomics is used to gain better understanding of biological processes, both, as part of basic research as well as applied sciences. One example is a study on the interplay between lactic acid bacteria, acetic acid bacteria and yeast on a metabolic level during cocoa fermentation. Using ^{13}C labeled substrate, metabolomics was applied to derive the fluxes in different lactic acid bacteria strains and acetic acid bacteria. Comprehensive knowledge of the interaction of the metabolism of the different species allows selection of an ideal co-culture composition during fermentation for optimization of the ongoing reactions and eventually the taste of the resulting cocoa itself. Furthermore, it allows to veer the cocoa production away from an uncontrolled process towards a streamlined process including defined starter cultures (Adler et al., 2014, 2013).

One example related to drug discovery is the finding of the metabolite trimethylamine N-oxide (TMAO) and its association with the formation of atherosclerotic plaques (Wishart, 2016). In several studies, TMAO was shown to promote atherosclerotic plaques by a mechanism yet to be fully elucidated (Gregory et al., 2015; Organ et al., 2016). It is produced from trimethylamine (TMA) in the liver via the enzyme flavin monooxygenase 3 (FMO3). TMA in turn originates from several dietary sources such as choline, betaine or carnitine, i.e. largely from the consumption of meat. The formation of TMA is catalyzed by the TMA lyase, an enzyme found in the gut microbiota. This led to the hypothesis that the two enzymes FMO3 and TMA lyase may serve as targets for the prevention of atherosclerotic plaques (Wang et al., 2011; Wishart, 2016). FMO3 however is an important regulator of cholesterol metabolism and its knockdown was shown to promote hepatic inflammation and other adverse reactions (Warrier et al., 2015). Regarding the enzyme TMA lyase, 3,3-dimethyl-1-butanol,

which is a choline analogue and an ingredient in olive oil, was found to be an effective inhibitor of the enzyme and is currently tested for its use as a drug in atherosclerosis treatment (Wang et al., 2015, 2011; Wishart, 2016). Another molecule that was shown to reduce TMAO levels is resveratrol. Resveratrol is particularly abundant in red wine and is suggested to act via remodeling of the gut microbiota (Chen et al., 2016).

We described more applications related to metabolomics and fluxomics, technical considerations during the design of experiments and theoretical basics in a separate review in more detail (Klein and Heinzle, 2012). Yet, the theoretical background shall be briefly touched in the following.

1.6.4 Theoretical background on the calculation of metabolic fluxes

The aim of metabolic flux analysis (MFA) is to quantify intracellular reaction rates. In its simplest form, metabolic fluxes can be calculated using metabolite balancing. This requires quantitative information on uptake and secretion rates, biomass formation, as well as a stoichiometric network model of the organism of interest. Additionally, the presence of metabolic steady state or at least pseudo steady state is implied, i.e. intracellular metabolite concentrations are assumed to be constant over time. Though sufficient for less complex networks, metabolite balancing reaches its limits when cyclic pathways, reversible reactions or compartmentalization are to be considered. In case of underdetermined networks, additional constraints can be set to limit the space of possible solutions (Niklas and Heinzle, 2011).

One approach to increase the resolution and reliability of metabolite balancing is the addition of labeled substrates - in most cases ^{13}C -substrates. Therefore, this approach is also referred to as ^{13}C MFA. It uses the information residing in the pathway-specific rearrangement of the carbon atoms to gain deeper insight into the cellular metabolism (Niklas and Heinzle, 2011). Hence, this approach requires data on mass or positional isotopomers, which can be acquired using NMR or MS (Klein and Heinzle, 2012). Subsequently, data on isotopomers is combined with metabolite balancing, and iterative algorithms are applied to minimize the deviation between measured and simulated labeling patterns. This approach yields more accurate results compared to mere balancing approaches and allows to estimate fluxes in more complex pathways including split ratios between pathways (Niklas and Heinzle, 2011).

1.7 Objective of the thesis

The thesis was prepared in the context of the NOTOX project, a project funded by the European Union and cosmetics industry. The project in turn was part of the SEURAT (safety evaluation ultimately replacing animal testing) cluster which was brought into being to aid in the reduction, replacement and refinement of animal testing. The particular aim of NOTOX was to provide systems biological tools to predict toxic events; i.e. tools of experimental as well as computational nature. A particular focus was put on organotypic cultures, long-term toxicity and pathways related to toxicological outcomes.

In this work, the human hepatic cell line HepaRG will be put in context as to its applicability in single and repeated dose long-term *in vitro* toxicity setups, assisted by the use computational methods.

Reliable and human-relevant toxicity assessment and prediction incontrovertibly require a test system adequately reflecting the situation *in vivo*. Therefore, a first comparison was performed using HepG2 cells and PHH, the current gold standard in *in vitro* toxicity, as a benchmark for HepaRG cells (**chapter 2**). The focus of this comparison was two-fold. First, metabolic competence and basal carbon

metabolism was contrasted, and secondly, behavior upon drug exposure was investigated on in terms of viability as well as alterations in the central carbon metabolism.

Next, different cultivation techniques and medium compositions for HepaRG cells were investigated as to their potential to improve hepatic functionality and long-term stability of the cell line. The assessment of repeated dose toxicity is still one of the most pressing issues and alternative *in vitro* approaches allowing reliable assessment of toxicity are not available. Using a set of different 3D cultivation techniques as well as a 2D cultivation, we were investigating hepatic functionality in HepaRG cells by quantification of biokinetics parameters such as drug uptake, CYP450 activity and induction, as well as excretion of the glucuronidated drug (**chapter 3**). Additionally, we studied the effect of single and repeated dosing (three days) of bosentan, chlorpromazine and valproic acid on the viability of the cells, cultivated using different 3D and a 2D setup.

To further extend the cultivation period of HepaRG cells as well as to facilitate –omics analyses, we tested several different serum-free compositions for the cultivation medium (**chapter 4**). The study was conducted for 30 days, which is in accordance with the Organization for Economic Cooperation and Development (OECD) guideline 407 for long-term repeated dose toxicity studies. As an addition, we studied the differences in the metabolism of HepaRG cells maintained in the different media to gain better understanding of the processes occurring in the cells. Subsequently, as a proof of principle, we tested the medium in a repeated dose toxicity study using valproic acid as a hepatotoxic compound and investigated the toxic effects of two-week drug application.

Applying the previously obtained knowledge on long-term cultivation of HepaRG cells, we performed two in-depth repeated dose toxicity studies. In the first case, we exposed HepaRG cells to valproic acid and bosentan for one month and applied an IVIVE approach to estimate human-relevant toxicity and determined metabolic fluxes to obtain more information on the underlying pathways (**chapter 5**). In the second study, we exposed HepaRG cells to valproic acid for two weeks while collecting samples for a multi-omics analysis, including epigenetics, transcriptomics, proteomics, metabolomics and fluxomics (**chapter 6**). The focus will be on the analysis of the metabolomics data, but selected results obtained from other –omics technologies will also be briefly highlighted.

A final overall summary on the findings gathered during the work on this thesis, as well as a critical reflection of results in the context of current research is given in **chapter 7**. The chapter further provides an outlook with potential applications of the approaches elaborated in this thesis.

Part I
Metabolic characterization
of HepaRG cells

Chapter 2 Carbon metabolism in HepaRG cells and its alterations upon drug exposure in a comparative study with primary human hepatocytes and HepG2 cells

2.1 Abstract

Replacement of animal studies with *in vitro* tools in the field of toxicology is fueled by ethical, legal and monetary incentives, but essentially requires alternative approaches that are sufficiently reliable in predicting toxicity relevant for humans. Therefore, major effort is put into improving current *in vitro* technologies and developing new cell lines for better prediction of toxic events. Herein, we compare the recently introduced HepaRG cell line to the well-established HepG2 cells and primary human hepatocytes in terms of their central carbon metabolism as a representation of the overall cellular phenotype. In addition to the basal cellular metabolism, we investigated alterations therein when cells were exposed to the two hepatotoxic compounds acetaminophen and diclofenac, in order to compare the response in the different systems, using metabolomics as an easy-to-perform method for indirect quantification of the integrated underlying regulatory processes. We observed that for many metabolites, the HepaRG cell line closely resembled the metabolism in primary hepatocytes, whereas HepG2 cells were hallmarked by a typical cancer metabolism. When cells were exposed to the hepatotoxic compounds, both cell lines appropriately covered the majority of the metabolic features observed in primary hepatocytes. However, HepaRG cells more closely resembled the situation in primary cells, particularly in respect to glucose metabolism. As a conclusion, HepaRG cells are more suitable when studying the carbon metabolism and its alterations when exposed to external stimuli than HepG2 cells, and may play an important role in future *in vitro* toxicological studies.

This chapter is in preparation for submission as

Klein S, Beshr G, Shevchenko V, Mueller D, Noor F, Heinzle E. Carbon metabolism in HepaRG cells and its alterations upon drug exposure in a comparative study with primary human hepatocytes and HepG2 cells

2.2 Introduction

Strengthening the use of *in vitro* tools in pharmaceutical and cosmetic research and abandoning traditional animal studies is a major step towards modern toxicity assessment. Ethical issues associated with animal studies, high costs and poor transferability of results to humans in some cases (Blauboer and Andersen, 2007; Olson et al., 2000; Shukla et al., 2010), make this step inevitable.

Primary human hepatocytes (PHH) are the current gold standard in *in vitro* toxicity testing as they best mimic the human *in vivo* situation and therefore allow for most reliably predicting human toxicity. Dozens of alternative test systems have been tested and development of new cell lines and cultivation conditions is currently being pushed by the government and industry to overcome the shortcomings of PHH, which include scarce availability and a strictly limited lifespan.

The human liver cell line HepG2 is a well-established cell line for the application in toxicity studies (Donato et al., 1992; Niklas et al., 2009). However, HepG2 cells lack many liver specific functions and only possess a basal expression of most cytochrome P450 (CYP450) isoforms compared to PHH (Aninat et al., 2006; Sumida et al., 2000; Wilkening et al., 2003). Yet, activity of these enzymes is a decisive parameter for the outcome of toxicological studies, as they are involved in the detoxification of a vast amount of chemicals and in some cases produce reactive species causing cytotoxicity (Lammert et al., 2010; Leung et al., 2012). More recently, a human hepatic cell line with superior performance has been introduced (Gripon et al., 2002; Lübberstedt et al., 2011). The so called HepaRG cell line has been isolated from a female patient suffering from hepatocarcinoma and a hepatitis C infection (Gripon et al., 2002). Unlike in HepG2 cells, in HepaRG cells, expression levels of genes encoding for xenobiotics metabolizing enzymes and transporters were in a similar range as in PHH (Gerets et al., 2012) and, at the same time, HepaRG cells are available on demand without restrictions to cell number. Even more, in first studies the suitability of HepaRG cells in long-term studies has been demonstrated (Josse et al., 2008; Klein et al., 2014), making the cell line ideal for toxicity studies.

A multitude of drugs are known to elicit hepatotoxicity in humans and in many cases, poor concordance of animal and human toxicity contributed to its late discovery, not before the drugs entered the post-marketing phase. Many drugs have been withdrawn from the market due to their hepatotoxic potential, but in some cases, hepatotoxic drugs are still out on the markets. Two examples for such compounds are acetaminophen and diclofenac. Acetaminophen is one of the most commonly applied drugs worldwide, making use of its analgesic and anti-pyretic effects. At the same time, acetaminophen accounts for more than 50% of acute liver failure cases resulting from overdosing of the drug (Larson et al., 2005; Yoon et al., 2016). At therapeutic doses, acetaminophen is mainly metabolized by glucuronidation and sulfation, followed by its excretion from the body. Only few percent of the drug are oxidized via the CYP450 system, producing the reactive metabolite N-acetyl-p-benzoquinone imine (NAPQI), which is promptly detoxified by conjugation to glutathione (McGill et al., 2011; Nelson, 1990). However, upon overdosing glucuronidation and sulfation pathways are saturated and metabolization via the CYP450 system, in particular via the isoforms CYP2E1 and CYP3A4 (Laine et al., 2009; Snawder et al., 1994), becomes more prominent. NAPQI binds to mitochondrial proteins, leading to mitochondrial dysfunction, formation of reactive oxygen and nitrogen species (ROS and RNS) and ATP depletion (Burcham and Harman, 1990; Cohen et al., 1997; Jaeschke, 1990). This in turn results in fragmentation of DNA and eventually cell death via necrosis (Cover et al., 2005; Gujral et al., 2002). Only recently, acetaminophen has additionally been associated with endoplasmic reticulum (ER) stress, which was suggested to play a crucial role in acetaminophen-induced toxicity (Uzi et al., 2013).

Similar to acetaminophen, toxicity of the nonsteroidal anti-inflammatory drug (NSAID) diclofenac was shown to involve oxidative stress, ER stress and mitochondrial dysfunction (Begrache et al., 2011; Boelsterli, 2003; Gómez-Lechón et al., 2003; Kretzrommel and Boelsterli, 1993; Tsutsumi et al., 2004). Diclofenac is metabolized via the CYP450 system, with 4'-OH, 5'-OH and N,5-(OH)₂ diclofenac as the main metabolites, which can also potentially be oxidized to a p-benzoquinone imine, capable of binding to cellular structures (Boelsterli, 2003; Bort et al., 1999, 1998). Furthermore, reactive arene oxides of diclofenac have been detected after exposing human microsomes to diclofenac (Yan et al., 2005). Main CYP450 isoforms involved in the oxidation of diclofenac belong to the CYP2C family, however at high drug concentrations, CYP1A2, CYP2B6 and CYP3A4 can also contribute to its metabolization (Bort et al., 1999). In addition to reactive diclofenac metabolites disturbing metabolic homeostasis, severe immune mediated responses have been described upon diclofenac treatment (Boelsterli, 2003; Gutting et al., 2002; Jürgensen et al., 2001).

Besides its pivotal role in the metabolism of xenobiotics, the liver essentially contributes to various metabolic pathways and transport of molecules across the body. Examples include glucose, neutral lipid and cholesterol metabolism and the detoxification of ammonia via the urea cycle. Next to direct modulation of enzyme activity, nuclear receptors are a crucial factor in the regulation of metabolism. The terms metabolomics and fluxomics refer to approaches unbiasedly assessing the complete set of small molecules within a cell, tissue, organ and biological fluids, and their changes over time respectively. As metabolites and fluxes are situated downstream of genes, transcripts and proteins, they contain the integrated information of the processes occurring on these levels (Klein and Heinzle, 2012), and can be used as an easy-to-perform readout for regulatory processes, e.g. induced by drugs or diseases. In several studies, metabolomics and fluxomics have been applied to HepG2 cells to gain insight into the underlying mechanisms of drug-induced hepatotoxicity and to identify biomarkers for toxicological outcomes which will help in screening and classification of hepatotoxic compounds (García-Cañaveras et al., 2016, 2015; Niklas et al., 2009).

In this study, we address the question to which extent the hepatic cell line HepaRG is capable of replacing PHH in the context of *in vitro* toxicology, focusing on the central carbon metabolism and its perturbation upon exposure to the two hepatotoxic compounds, acetaminophen and diclofenac. Cancer cells, such as the hepatoblastoma-derived cell line HepG2, are well known to differ in carbon metabolism compared to normal tissue, as their environment *in situ* and demands differ considerably (Iyer et al., 2010; Zhou et al., 2012), arising the question whether they and other tumor-derived cell lines can be used for reliable predictions in toxicity studies.

2.3 Methods

2.3.1 Cell culture

HepG2 cells were obtained from DSMZ (Brunswick, Germany). HepaRG cells and cryopreserved PHH were supplied by Biopredic International (Saint-Grégoire, France). Detailed information on the donors is given in table S2.1.

For HepaRG and PHH cultures, before seeding, 96-well plates (Greiner Bio One, Frickenhausen, Germany) were coated with type I rat collagen (Roche Applied Sciences, Penzberg, Germany) by adding 100 µl of a solution of 50 µg collagen/ml in DMEM (AMIMED BioConcept, Allschwil, Switzerland), followed by a 1 h incubation at 37°C. Afterwards, wells were washed once with 100 µl phosphate buffered saline (PBS) (Gibco Invitrogen, Darmstadt, Germany) and equilibrated for 1 h

with Williams Medium E (Pan Biotec, Aidenbach, Germany) at room temperature. Medium was removed and cells were seeded into the 96-well plates ($n = 3$ for each condition and time point), suspended in 100 μl Williams Medium E supplemented with 10% fetal bovine serum (FBS) (PAA Laboratories, Pasching, Austria), 100 U/ml penicillin and 100 $\mu\text{g/ml}$ streptomycin (c.c. pro, Oberdorla, Germany). In case of PHH, seeding medium was additionally supplemented with 50 μM hydrocortisone 21-hemisuccinate and 5 $\mu\text{g/ml}$ human insulin. In addition to supplements for PHH, 1.8% DMSO (v/v) were added for HepaRG cells. Supplements, if not noted differently, were obtained from Sigma Aldrich, Steinheim, Germany. Numbers of seeded cells were 50,000 for PHH and HepG2 cells, and 72,000 for HepaRG cells. Seeding was done one day before beginning of analyses for PHH and HepG2 cells and a week before in case of HepaRG cells. Two days after seeding, medium for HepaRG cells was replaced by fresh medium with a reduced DMSO concentration of 0.5% (v/v). 12 h before beginning of analyses, medium was renewed using the same medium for all cells. The medium was supplemented with penicillin, streptomycin, hydrocortisone 21-hemisuccinate and insulin, without FBS and DMSO (hepatocyte culture medium). Cultivation was conducted in a cell culture incubator (Mettler, Schwabach, Germany) at 37°C with 95% relative humidity and 5% CO₂ supply.

2.3.2 Quantification of glucose, organic acids and urea

Glucose, pyruvate and lactate were quantified using a Kontron HPLC (Kontron Instruments, Neufahrn, Germany) as described previously in detail (Hans et al., 2003). Amino acids and urea were quantified in an Agilent 1100 HPLC system (Agilent, Waldbronn, Germany). Technicalities on the methods were elaborated on before (Clark et al., 2007; Klein et al., 2014; Krömer et al., 2005).

2.3.3 Calculation of secretion rates

From measured metabolite concentrations, secretion rates r_i were calculated using equation 2.1.

$$r_i = \frac{c_{i,t_1} - c_{i,t_2}}{(t_1 - t_0) \times X} \times V \quad [2.1]$$

C_i is the concentration of a metabolite i at time point 1 (t_1 , 24 h) or time point 0 (t_0 , 0 h). X represents the mean cell number during the 24 h cultivation and V is the culture volume.

2.3.4 Labeling studies for estimation of pathways contributing to formation of lactate

11.11 mM [1,2-¹³C] glucose (99%, Cambridge Isotope Laboratories, MA, USA) and 2 mM [U-¹³C] glutamine (99%, Cambridge Isotope Laboratories, MA, USA) were added to glucose- and glutamine-free Williams Medium E (Pan Biotec, Aidenbach, Germany) with otherwise identical composition as the hepatocyte culture medium. Cells were incubated with the tracers for 24 h and medium was collected after 2 h, 10 h, 18 h and 24 h from different wells.

2.3.5 Sample preparation for measurement of mass isotopomers in GC-MS

The procedure for sample preparation and measurement in a mass spectrometer coupled to a gas chromatograph (GC-MS) was adapted from literature (Strigun et al., 2011a) as follows. 25 μl of collected supernatants were frozen and lyophilized. Afterwards, 40 μl of N,N-dimethylformamide (Carl Roth, Karlsruhe, Germany) containing 0.1% pyridine (v/v) (Sigma Aldrich, Steinheim, Germany) and 40 μl N-methyl-N-tert-butyl-dimethylsilyl-trifluoroacetamide (MBDSTFA) (Machery-Nagel, Dueren, Germany) were added. Samples were then incubated for 30 min at 80°C, followed by centrifugation at 12,100 g for 5 min at 4°C. The supernatants were transferred into new glass vials with 0.2 ml inserts (Machery-Nagel, Dueren, Germany) for GC-MS analysis.

2.3.6 Measurement of mass isotopomers in GC-MS

For measurement of mass isotopomers, 1 μl of the derivatized sample was injected into a GC (HP 6890, Hewlett Packard, Palo Alto, CA, USA) equipped with a HP-5 MS column (5% phenyl-methylsiloxanediphenylpolysiloxane, 30 m \times 0.25 mm \times 0.25 μm , Agilent, Waldbronn, Germany) and coupled to a quadrupole MS (MS 5973, Agilent, Waldbronn, Germany). The flow rate for separation was 1.1 ml/min with helium as carrier gas, and the following temperature gradient was applied: 135°C for 7 min, 10°C/min increase until 160°C, 7°C/min until 170°C and 10 °C/min until 325°C which was held for 2.5 min. Ionization was done with electron ionization at 70 eV.

2.3.7 Processing of GC-MS spectra and estimation of pathways contributing to formation of lactate

From the mass spectra of MBDSTFA derivatized lactate, carbon mass isotopomer distributions were computed using a described method (Yang et al., 2009). Corrected mass isotopomer distributions were used for the estimation of the pathways contributing to the formation of lactate, using equations 2.2 to 2.5, with M_0 to M_3 representing the different carbon mass isotopomer fractions of lactate (figure S2.1). Pathways include glycolysis, pentose phosphate pathway (PPP), gluconeogenesis from glutamine, and other sources, which comprise glycogenolysis as well as gluconeogenesis from molecules other than glutamine. Degradation of [1,2- ^{13}C] glucose via glycolysis results in one lactate molecule labeled at two positions (M_2) and another one without labeling (M_0). M_2 is specific for this pathway, while M_0 is produced by two more sources. Hence, M_2 is used for the calculation of glycolytic contribution by doubling its value to account for the production of two molecules of lactate per molecule glucose (eq. 2.2). During degradation of [1,2- ^{13}C] glucose via PPP, the labeled C_1 atom is lost, resulting in a lactate molecule labeled only at one position (M_1) and one without labeling (M_0). In this case, M_1 is specific for the PPP and hence, it applied to estimate the pathway's contribution. The loss of the C_1 atom during the oxidative phase of the PPP was considered in the calculations by multiplying M_1 by 5/3 (instead of 2 as it is the case for glycolysis) (eq. 2.3). In case of lactate formation from [U- ^{13}C] glutamine, two carbon atoms are lost as CO_2 and the remaining labeled carbon atoms build the carbon backbone of lactate (M_3) (eq. 2.4). To calculate the contribution of other sources to the formation of lactate, unlabeled lactate molecules formed via the glycolytic pathway and PPP have to be subtracted from M_0 in the calculation (eq. 2.5). It was assumed that the interconversion of the different sources, e.g. glycogenesis from labeled glutamine, was negligible within the 24 h period.

$$\text{Glycolysis} = 2 \times M_2 \quad [2.2]$$

$$\text{PPP} = \frac{5}{3} M_1 \quad [2.3]$$

$$\text{Gluconeogenesis from glutamine} = M_3 \quad [2.4]$$

$$\text{Other sources} = M_0 - \frac{2}{3} M_1 - M_2 \quad [2.5]$$

2.3.8 Quantification of CYP450 activity

For determination of the CYP450 activity in the different hepatic cells, these were incubated with a substrate cocktail, and product formation was quantified using an LC-MS method. Incubation of the cells with the cocktail of CYP450 substrates was conducted in 100 μl hepatocyte culture medium for

1 h. In case of CYP2D6, CYP1A2, CYP2B6 and CYP3A4, further details on the substrates and the LC-MS method used for quantification of CYP450 products have been described previously (Klein et al., 2014). CYP2E1 activity was assessed using chlorzoxazone (Sigma Aldrich, St. Louis, MO, USA) as a substrate with a final concentration of 300 μ M in hepatocyte culture medium. Thorough information on the quantification of the CYP2E1 product OH-chlorzoxazone via LC-MS is given in literature (Gunness et al., 2013).

2.3.9 Dose response curves for acetaminophen and diclofenac in hepatic cells

First, acetaminophen (Sigma Aldrich, Steinheim, Germany) and diclofenac sodium salt (Sigma Aldrich, Steinheim, Germany) were dissolved in hepatocyte culture medium with concentrations of 80 mM and 5 mM respectively. From these stock solutions, drug concentrations ranging from 80 mM to 5×10^{-2} mM (acetaminophen) and 5 mM to 2.5×10^{-3} mM (diclofenac) were prepared in hepatocyte culture medium and subsequently applied to the cells in a volume of 100 μ l for 24 h.

2.3.10 Viability assessment

To determine the number of adhered cells after seeding, first a sulforhodamine B (SRB) assay was conducted as described in literature (Skehan et al., 1990) and results were compared to calibration curves for each cell type individually. To assess viability, a resazurin-based assay was applied (CellTiter-Blue® cell viability assay, Promega, Mannheim, Germany). The resazurin solution was mixed with medium in a ratio of 1:5. The mixture was prewarmed and a volume of 100 μ l was given to the cells which were then incubated for 3 h at 37°C. Fluorescence of the product resorufin was detected using a Fluoroskan Ascent CF fluorescence reader (Thermo Labsystems, Vantaa, Finland), measuring emission at 590 nm upon excitation at 540 nm. A mixture without cells served to assess the background signal. The fluorescence signals from treated samples were then normalized to the signal of the untreated control.

2.3.11 Curve fitting and calculation of confidence intervals

Boltzmann equation (eq. 2.6) was used for curve fitting to the experimental dose response data.

$$\hat{y} = y_{min} + \frac{y_{max} - y_{min}}{1 + e^{\frac{EC_{50} - x_c}{sl}}} \quad [2.6]$$

y_{min} and y_{max} are defined as the lowest and highest y-value in the data set, and x_c represents the applied drug concentration. An evolutionary algorithm within Excel 2010 (Microsoft, Redmond, WA, USA) was used to find the maximum value for the coefficient of determination (r^2), varying EC_{50} and the slope (sl) of the curve. The 90% Confidence interval (CI) at each concentration c was calculated according to equation 2.7,

$$CI_c = \hat{y}_c \pm t_{\alpha; n-2} \times \sigma_{est} \times \sqrt{\frac{1}{n} + \frac{x_c - \bar{x}}{SS_{XX}}} \quad [2.7]$$

where $t_{\alpha; n-2}$ is the critical t -value for degrees of freedom reduced by two and σ_{est} indicates the standard error of the estimate. The number of data points is given by n and SS_{XX} is the sum of squared deviations of x -values from the mean of x .

2.3.12 Detailed metabolic characterization of hepatic cells upon drug exposure

Three concentrations for each drug and hepatic system were chosen for in-depth investigation of the metabolism upon drug exposure. These concentrations included the EC_{10} and a subtoxic concentration, which were taken from the dose response curves and the c_{max} taken from literature (table 2.1). Untreated cells were added as a control. Drug preparation and exposure of the cells was identical to the procedure described above. Additionally, supernatants were collected for quantification of carbon metabolites.

Table 2.1 Drug concentrations applied to cell cultures. List of acetaminophen and diclofenac concentrations used during the detailed metabolic characterization of HepG2 and HepaRG cells, as well as primary human hepatocytes (PHH1, PHH2, PHH3) upon drug exposure.

Cell type	High drug concentration (EC_{10}) [mM]*		Medium drug concentration (subtoxic) [mM]*		Low drug concentration (C_{max}) [mM]**	
	Acetaminophen	Diclofenac	Acetaminophen	Diclofenac	Acetaminophen	Diclofenac
HepG2	6	0.05	1.25	0.008	0.125	0.002
HepaRG	3	0.2				
PHH1	2	0.3				
PHH2	3	0.3				
PHH3	1.5	0.3				

* Values were taken from dose response curves acquired prior to the metabolic characterization.

** Values were taken from literature (Hinz et al., 2005; Sevilla-Tirado et al., 2003).

2.3.13 Principal component analysis

All calculated secretion rates $r_{i,j}$ were Pareto-scaled, i.e. centered using the mean secretion rate for each metabolite and drug, and divided by the square rooted standard deviation, resulting in pretreated rates $\hat{r}_{i,j}$ (eq. 2.8) which were then subjected to a principal component analysis (PCA) to reduce the complexity of the data set and visualize results.

$$\hat{r}_{i,j} = \frac{r_{i,j} - \bar{r}_i}{\sqrt{s_i}} \quad [2.8]$$

Loading coefficients were determined to identify the relevance of the individual secretion rates for separation of the different clusters. PCA and 95% confidence intervals were calculated in MatLab 2007b (MathWorks, Nattick, MA, USA).

2.3.14 Hierarchical cluster analysis

Hierarchical cluster analysis (HCA) was applied to determine similarity of metabolic alterations in the different hepatic cells upon drug exposure. Before analysis, changes in the secretion rates r ($\Delta r_{i,j,d}$) upon drug exposure (index d) relative to the control (index ctrl) were calculated. To reduce the influence of rates with high absolute but low relative changes, and to correct for heteroscedasticity, data was normalized as following. The differences in rates from drug-treated to control conditions

were cube root transformed and subsequently scaled using the standard deviation as described in equation 2.9.

$$\Delta r_{i,j,d} = \frac{\sqrt[3]{r_{i,j,d} - r_{i,j,\text{ctrl}}}}{s_{i,d}} \quad [2.9]$$

Clustering and drawing of the heat map was done in MatLab 2007b using Euclidian distance as a measurement for similarity and Ward's minimum variance method clustering algorithm.

2.3.15 Student's *t*-test

Unpaired Student's *t*-tests were performed using MatLab 2007b. Differences in two measurements are considered significant at $p < 0.001$, $p < 0.01$ and $p < 0.05$.

2.4 Results

2.4.1 Central carbon metabolites in untreated human hepatic cell lines and PHH

A PCA on the secretion rates of untreated hepatic cells allowed their classification (figure 2.1) and identification of metabolites mostly contributing to their differences (figure S2.2). All hepatic cell systems were sorted into distinct clusters, while distances between the clusters within the different PHH were lowest, followed by the HepaRG cell cluster being close to PHH3 and PHH1. In addition, the HepaRG cell cluster was completely enclosed by the combined 95% confidence ellipse of the combined PHH cluster. Variance of the replicates was by lowest in HepaRG cells, and highest in PHH2.

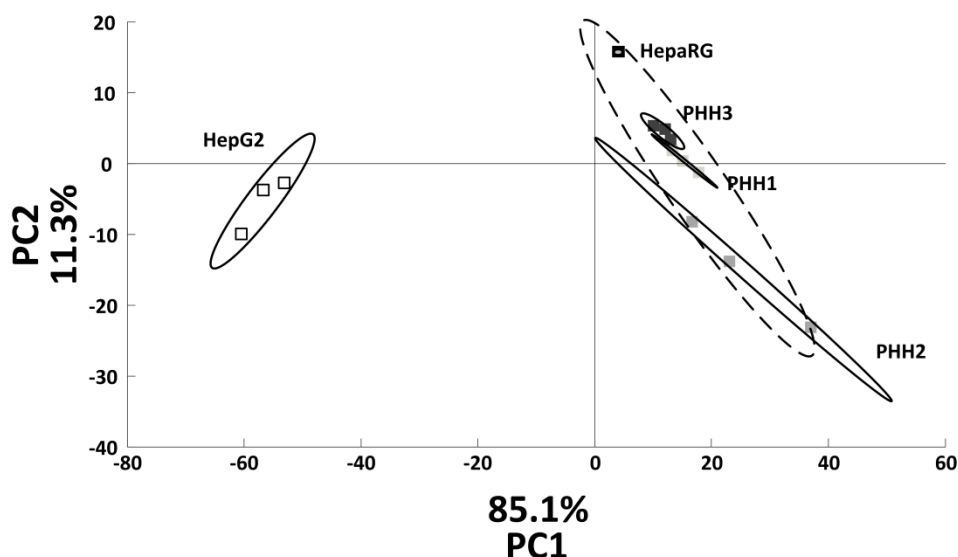


Figure 2.1 Principal component analysis on metabolic rates in untreated hepatic cells. Principal component analysis on Pareto-scaled secretion rates of untreated hepatic cells ($n = 3$). PHH1, PHH2 and PHH3 represent cells from 3 distinct donors. Principal components (PC) 1 and 2 are shown and their loadings are depicted in figure S2.2. Ellipses represent 95% confidence regions for each cell type individually (full lines) and additionally for all three donors of PHH combined (dashed line).

Metabolites with major impact on the separation of the clusters in the first principal component (PC1, mostly separation of HepG2 cells from other hepatic cells) and the second principal component (PC2, mostly separation of HepaRG and the different donors of PHH) were identical (figure S2.2), while separation along PC1 was clearly more pronounced than for PC2 (85% vs 11% contribution to total difference). Metabolites with highest relevance to cluster separation were glucose, lactate, urea, glutamine, glutamate, pyruvate and leucine. Based on the PCA, metabolites were selected and their secretion rates in untreated hepatic cells were compared (figure 2.2A). HepG2 cells had a strong uptake of glucose, which was 6 times higher than glucose uptake in HepaRG cells. PHH from all donors on the other hand secreted low (PHH1 and PHH3) to large quantities of glucose (PHH2). Similarly, HepG2 cells had a high demand in glutamine, whereas HepaRG cells only incorporated minor amounts. Consumption of glutamine in all PHH donors was slightly higher than in HepaRG cells, but notably lower than in HepG2 cells. Lactate secretion in HepG2 cells was more than 30 times higher than in HepaRG cultures and 12 to 60 times higher than in PHH. Ratios of lactate secretion to glucose uptake were 1.6 and 0.3 in HepG2 and HepaRG cells, respectively. In HepG2 cells, only traces of urea could be detected and the formation was around 1% of the average production found in PHH. Urea formation in HepaRG cultures was considerably higher compared to HepG2 cells with 4% of the average production in PHH. Pyruvate was secreted by both hepatic cell lines, whereas it was consumed in primary hepatocytes from all three donors. Alanine was taken up by all hepatic systems with a comparable level in HepaRG cells and PHH, and at a slightly lower rate in HepG2 cells. Leucine was taken up in the two hepatic cell lines at an identical rate, but secreted in low amounts in PHH from the three donors.

From the mass isotopomer fractional enrichment in lactate (figure S2.3), contributions of pathways to the formation of lactate were calculated (figure 2.2B). Mass isotopomer fractions reached steady state after around 10 h for all hepatic systems. For HepG2 cells, 79% of lactate formation was based on glycolytic pathway activity. The pentose phosphate pathway and other sources were contributing with 10 and 8%, respectively. In HepaRG cells only 18% of lactate formation was based on glycolysis and the major part was originating from other sources, which involve e.g. glycogenolysis. Likewise, in all PHH donors, other sources were the main contributors to lactate formation with percentages between 79% and 87%, and glycolysis only contributing 7 to 11%. For all hepatic systems, gluconeogenesis from glutamine only played a minor role (2 to 3%).

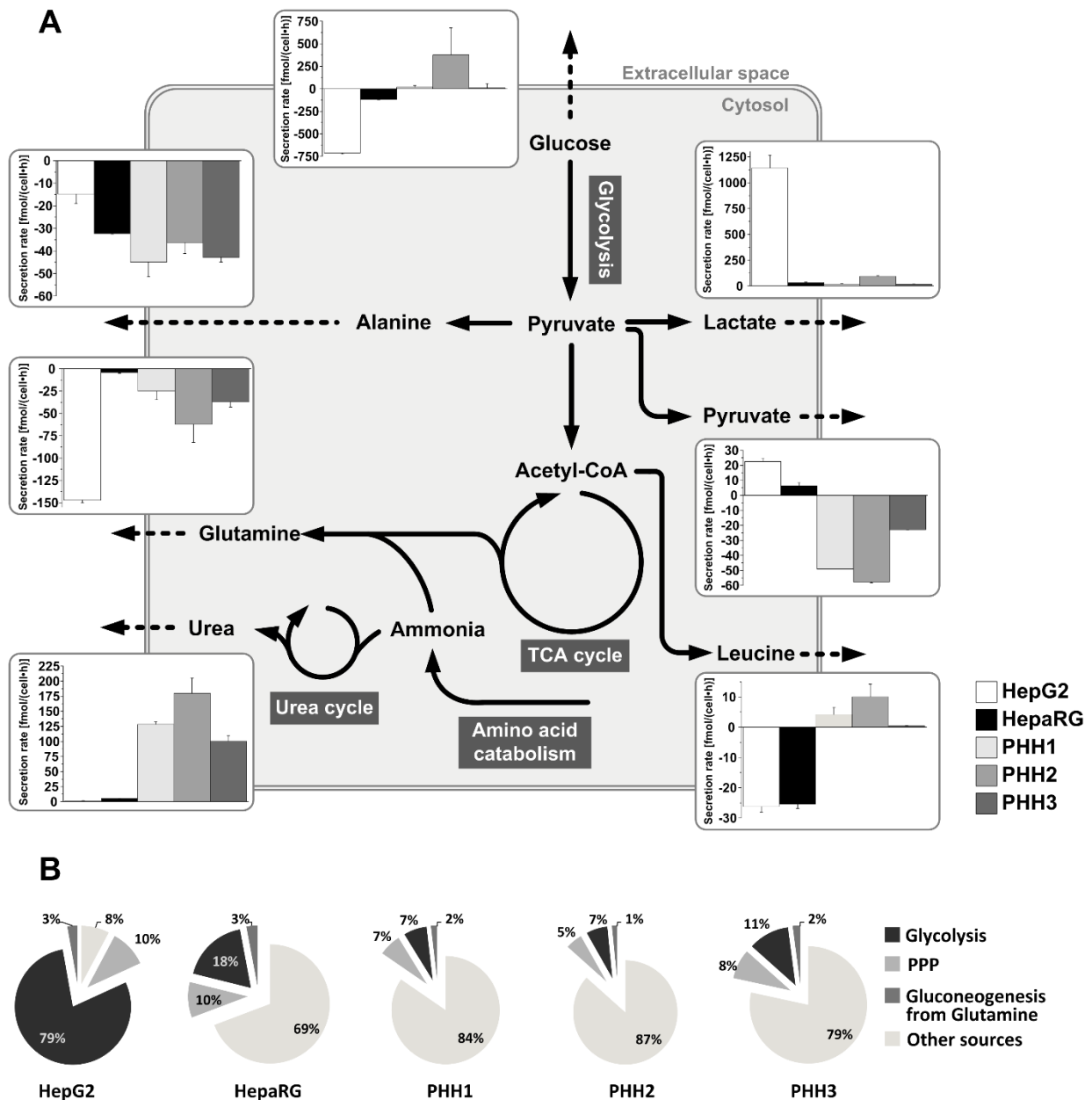


Figure 2.2 Secretion rates in untreated hepatic systems and pathway contributions to lactate formation. Mean secretion rates of selected central metabolites in the metabolism of untreated HepG2 and HepaRG cells, as well as for primary human hepatocytes from three different donors (PHH1, PHH2, PHH3). Selection of metabolites was based on the metabolites contributing to separation of the clusters in the principal component analysis in figure 2.1. Negative secretion is equivalent to uptake. Dashed arrows represent secretion, the interconnection between the different metabolites and their role in metabolism is signified by full arrows. Error bars indicate standard deviation ($n = 3$) (A). Percentages of pathways contributing to formation of lactate in the different cell types. Pathways include glycolysis, pentose phosphate pathway (PPP), gluconeogenesis from glutamine, and other sources, e.g. glycogenolysis and gluconeogenesis from molecules other than glutamine (B).

2.4.2 Metabolic competence in human hepatic cell lines and PHH

CYP450 activities were assessed in the two human hepatic cell lines HepG2 and HepaRG and in PHH from three different donors (figure 2.3). In case of HepG2 cells, no activity was found for any of the tested CYP450 isoforms. On the other hand, activity was found for all tested isoforms in HepaRG cells. For the isoforms CYP2D6, CYP2B6 and CYP2E1, activity in HepaRG cells was significantly

lower than in all the PHH (86%, 68% and 83% lower than average activity in PHH, respectively). In case of the isoforms CYP1A2 and CYP3A4, activity was on the same level or slightly higher than for donor 1 (PHH1), but significantly lower than for donors 2 and 3 (PHH2, 3).

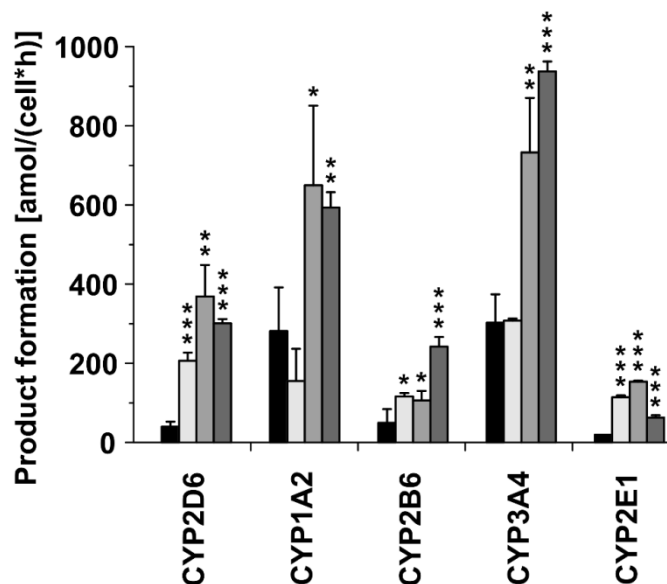


Figure 2.3 Activity of CYP450 enzymes in different hepatic systems. CYP450 activities in HepaRG cells (black bars) and primary human hepatocytes from three different donors (PHH1, PHH2, PHH3; light, medium and dark grey bars, respectively) for the isoforms CYP2D6, CYP1A2, CYP2B6, CYP3A4 and CYP2E1. In case of HepG2 cells, products were not detectable. Error bars indicate standard deviation ($n = 3$). An unpaired Student's *t*-test was performed for comparison of PHH to HepaRG cells. *, **, *** indicate a *p*-value of < 0.05, 0.01 and 0.001, respectively. Measurements have been performed by Valery Shevchenko at Biopredic International, Saint Grégoire.

2.4.3 Effects of acetaminophen and diclofenac treatment on viability of the different hepatic systems

The two human hepatic cell lines HepG2 and HepaRG, and PHH from three different donors were exposed to the two hepatotoxic compounds acetaminophen and diclofenac and their effects on viability were investigated (figure 2.4). In case of acetaminophen, HepG2 cells were least sensitive with an EC_{50} value of 23.2 mM, followed by HepaRG cells with an EC_{50} value of 18.4 mM. PHH from all three donors were more sensitive to acetaminophen exposure with EC_{50} values ranging from 6.8 to 12.7 mM and an average EC_{50} value of 9.2 mM. For diclofenac, HepG2 cells and PHH from donor 1 and 2 were affected similarly by the treatment. EC_{50} values were 0.5, 0.5 and 0.45 mM, respectively. HepaRG cells were least sensitive with an EC_{50} value of 0.73 mM, which was slightly higher than for PHH3 (EC_{50} value 0.63 mM). In average, the EC_{50} value in PHH upon diclofenac exposure was 0.53 mM.

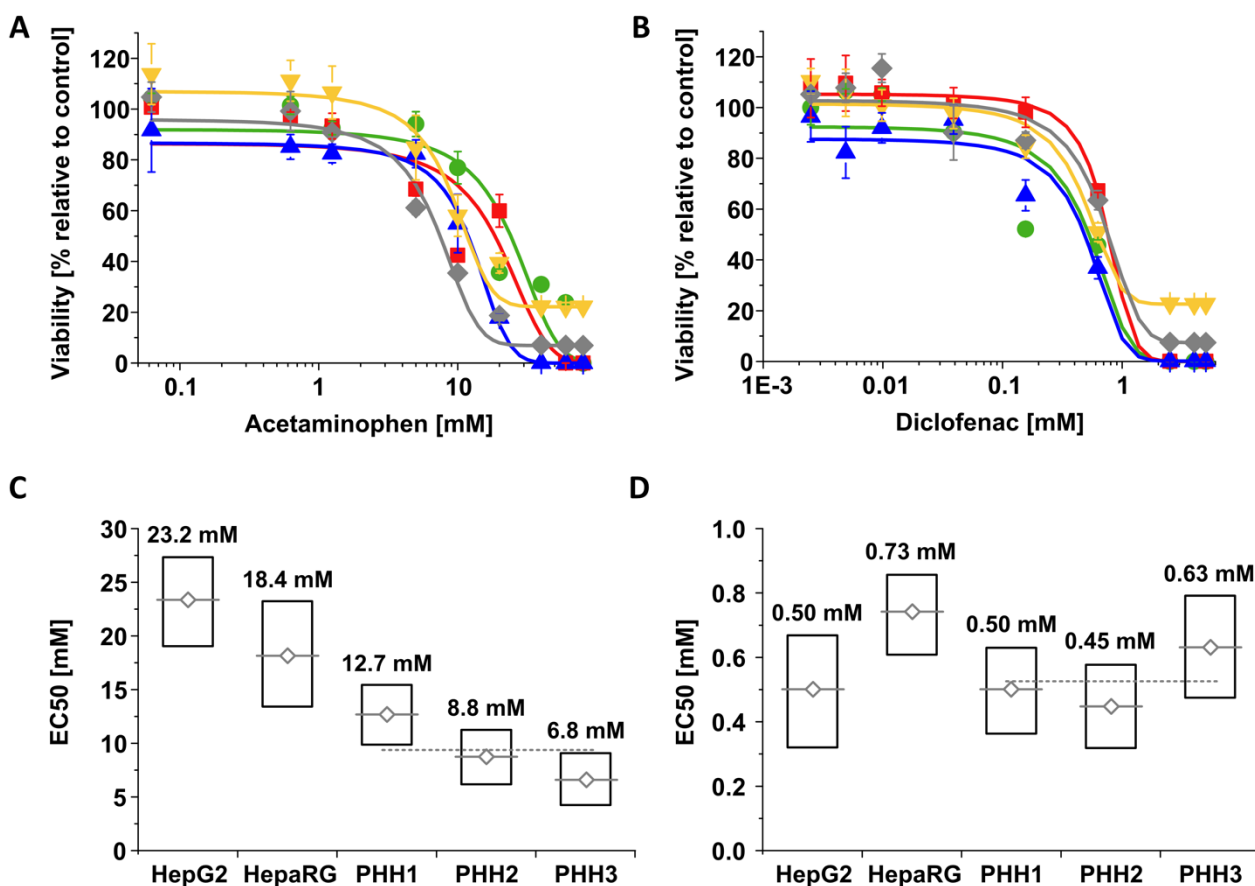


Figure 2.4 Dose response curves and EC₅₀ values in different hepatic systems upon exposure to acetaminophen and diclofenac. Dose response curves for HepG2 (●) and HepaRG cells (■), as well as for primary human hepatocytes from three different donors (PHH1 (▲), PHH2 (▼), PHH3 (◆)) exposed to acetaminophen (A) and diclofenac (B) for 24 h. Full lines represent curve fits using Boltzmann equation. Error bars indicate standard deviation ($n = 3$). EC₅₀ values in HepG2 and HepaRG cells, as well as PHH1, PHH2 and PHH3 upon exposure to acetaminophen (C) and diclofenac (D). EC₅₀ values are given and highlighted by grey diamonds. Upper and lower ends of the bars represent boundaries of the 90% confidence intervals. The mean EC₅₀ values of the primary hepatocytes from the three donors are indicated by grey dashed lines ($N = 3$). Viability was assessed using the resazurin-based CellTiter-Blue® cell viability assay.

2.4.4 Metabolic alterations in human hepatic cell lines and PHH upon drug exposure

PCA were performed on the secretion rates in the individual hepatic cell systems treated with acetaminophen and diclofenac; together with controls (figure 2.5, figure S2.4). In all systems, secretion rates upon acetaminophen and diclofenac treatment could be distinguished from each other using a PCA, indicated by non or slightly overlapping confidence ellipses for the respective EC₁₀ conditions and arrows pointing into different directions, with exception of HepG2 cells. On the other side, strongest alterations upon drug exposure were observed for HepG2 cells, while changes in PHH1, and particularly PHH2 were less pronounced.

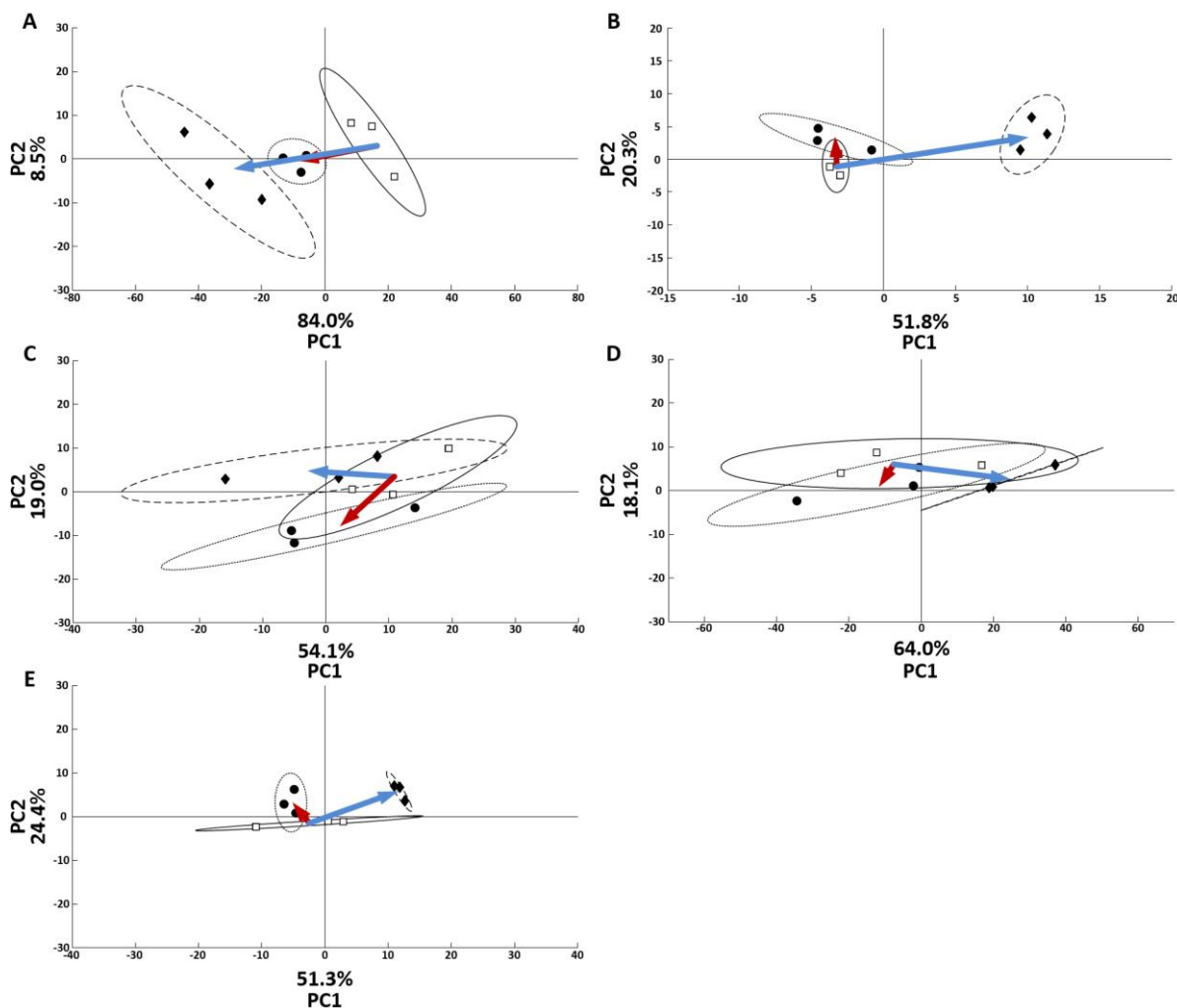


Figure 2.5 Principal component analysis on secretion rates in different drug-treated hepatic systems. Principal component analyses (PCA) representing all calculated secretion rates in treated (acetaminophen, diclofenac) and untreated hepatic cells ($n = 3$) for each system individually (HepG2 (A); HepaRG (B); PHH1 (C); PHH2 (D); PHH3 (E)). Data was Pareto-scaled prior to the PCA. Circles and diamonds represent secretion rates from cells treated with the highest concentration (EC_{10}) of acetaminophen and diclofenac, respectively. To increase clarity, data points for cells treated with lower concentrations are not depicted, but were part of the calculations (complete PCA plots in figure S2.3). White squares represent rates in control cells. Dotted, dashed and full lines indicate 95% confidence ellipses for acetaminophen-treated, diclofenac-treated and control cells, respectively. Red and blue arrows indicate the direction of the change from the control to cells treated with the highest concentration of acetaminophen or diclofenac.

To further classify the trends of metabolic alterations in the different hepatic cell systems upon drug treatment and visualize their direction, an HCA was carried out and results were plotted in a heat map (figure 2.6).

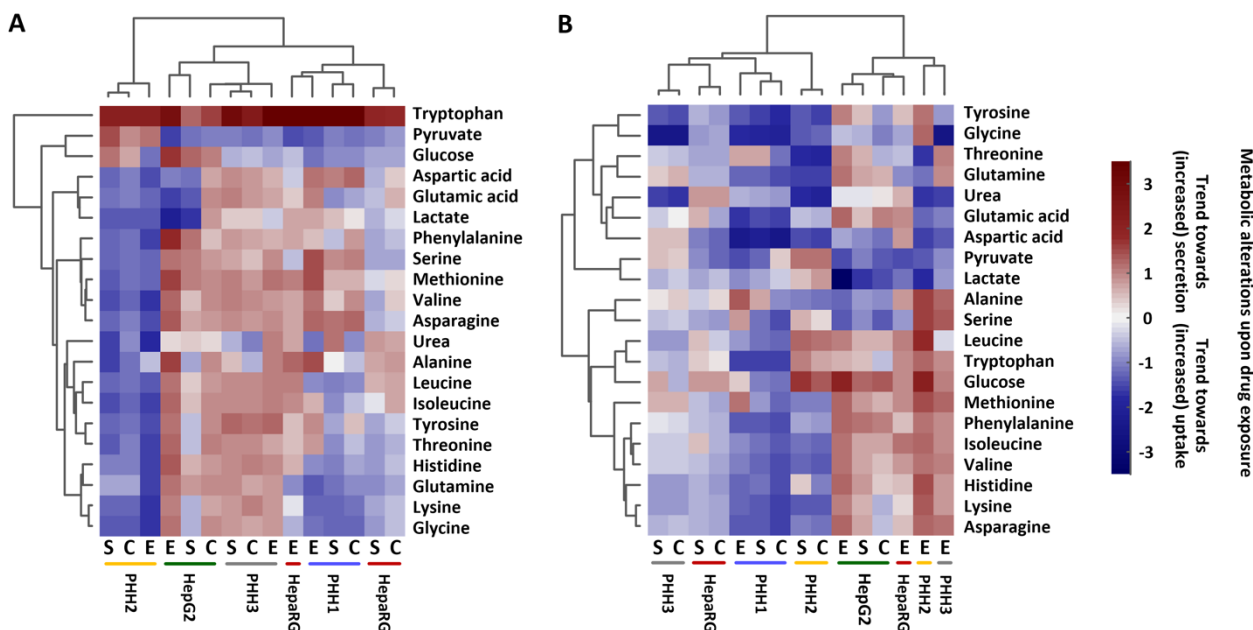


Figure 2.6 Hierarchical clustering of secretion rates in hepatic systems exposed to acetaminophen and diclofenac. Effects of exposure to acetaminophen (A) and diclofenac (B) on the secretion rates in HepG2 (green bars) and HepaRG (red bars) cells, as well as primary human hepatocytes from three different donors (PHH1, PHH2, PHH3 (blue, yellow and grey bars, respectively)). The hierarchical clustering analysis is based on drug-induced changes relative to the control. Drug-induced changes leading towards (increased) secretion or uptake are represented by red and blue colors, respectively. The different concentrations EC_{10} , subtoxic concentration and c_{max} are indicated by E, S and C, respectively.

Details on acetaminophen clustering

Cluster analysis on alterations in the secretion rates upon acetaminophen treatment resulted in two main clusters; PHH2 on the one hand, and all other cell systems on the other hand. The latter cluster was in turn divided into PHH3 and HepG2 on one side, and PHH1 and HepaRG on the other side. It is noteworthy that for PHH1 and PHH2 only 4 of the drug-induced alterations were significant, whereas the maximum number of significantly changed rates (a total of 18) was found for HepG2 cells (table S2.2). Generally, drug-induced alterations were weaker than differences between the systems and individuals. Hence, each system formed an individual cluster, with exception of the EC_{10} -treated HepaRG cells clustering together with the EC_{10} -treated PHH1.

There was a general trend towards (increased) glucose uptake upon high dose acetaminophen exposure; however not in case of HepG2 cells. The trend in lactate secretion was inconsistent between the different systems. There was a trend towards (increased) secretion for HepaRG cells and PHH1, while the opposite was the case for the other systems. Pyruvate metabolism was similarly affected in all cell systems with a trend towards (increased) uptake, except for PHH2. Upon treatment with the EC_{10} , a trend towards (increased) secretion was observed for 8 amino acids; except for PHH2 – amongst others alanine, the branched chain amino acids (BCAA) valine and isoleucine and two aromatic amino acids (AAA) tyrosine and phenylalanine. The third AAA tryptophan was the only metabolite for which the same trend was observed in all cell systems and under all conditions.

Details on diclofenac clustering

Cluster analysis on diclofenac-treated cells gave rise to two major clusters. HepG2 cells and the EC₁₀-treated HepaRG cells, PHH2 and PHH3 in one cluster, while their remaining conditions and PHH1 were grouped into the second cluster. In case of diclofenac treatment, only 9 rates were significantly affected for PHH1, while numbers ranged from 14 to 16 for the other cell systems.

For alanine, uptake was decreased in all systems upon exposure to the EC₁₀, except for HepG2 cells. BCAA (valine and isoleucine) and AAA (tryptophan and phenylalanine) uptake at EC₁₀ was lower in all systems, except for PHH1, where uptake was increased. For the metabolites glucose, methionine, lactate and pyruvate, trends in alterations at the EC₁₀ were identical in all systems. The former two metabolites were found to show a trend towards (increased) secretion, while for the latter two, there was a trend towards (increased) uptake.

2.5 Discussion

To draw conclusions from *in vitro* toxicity data, relevant for preclinical drug development and risk assessment in other industries, the experimental conditions, including the model cell system, have to reflect the *in vivo* situation as closely as possible. This implies that the model cell system reacts to stimuli as it happens *in vivo*. So far, PHH are the gold standard in toxicity assessment, but many studies have shown that HepaRG cells could be a suitable surrogate with unlimited availability and superior long-term stability. Yet, up to now, these studies had a strong focus on mRNA level and neglected other cellular levels (Aninat et al., 2006; Gerets et al., 2012; Hart et al., 2010; Jennen et al., 2010). In the present study, we first investigated key metabolites in the central carbon metabolism as well as metabolic competence in untreated hepatic cell lines HepG2 and HepaRG and compared it to PHH. Subsequently, the hepatic cell systems were exposed to two pharmaceutical compounds, acetaminophen and diclofenac, and their effects on viability and metabolism of the cells were evaluated.

2.5.1 Central carbon metabolites in untreated human hepatic cell lines and PHH

When investigating key metabolites of the central carbon metabolism in the different hepatic systems, we found that glucose uptake in HepG2 cells was significantly higher than in all other tested systems. The additional glucose molecules can be used for the generation of energy and for integration into cellular constituents, both of which is required as HepG2 cells were the only tested cells capable of proliferation. The majority of glucose (around 80%) was converted into lactate, which was mostly derived from glycolysis, and subsequently secreted into the medium. In previous studies, high glycolytic activity in cancer cells has been associated to compensate for the lower ATP formation due to reduced tricarboxylic acid (TCA) cycle activity (Kim et al., 2006), triggered by inherently increased ROS levels. ROS upregulate the hypoxia-inducible factor 1 α (HIF-1 α) (Jung et al., 2008; Shi et al., 2009) which leads to inactivation of the pyruvate dehydrogenase (Kim et al., 2006) and transcription of glucose transporters and the complete set of enzymes involved in glycolysis (Denko, 2008; Lee et al., 2004). To recover NAD⁺ from NADH, which is produced during glycolysis and normally reverted to NAD⁺ through oxidative phosphorylation, expression levels of L-lactate dehydrogenase B (LDH-B) are elevated likewise (Zhou et al., 2012, 2011), resulting in notably higher lactate secretion. This process of aerobic glycolysis is also known as the Warburg effect (Ferreira, 2010). We observed that relative contribution of the PPP to lactate formation in HepG2 cells was slightly higher than in the

other cell systems, which is likely to be related to the higher demand in nucleic acid building blocks as well as NADPH in proliferating cells.

Though the HepaRG cell line is also derived from a tumor, more precisely from a hepatocarcinoma (Gripon et al., 2002), glucose uptake was significantly lower compared to HepG2 cells and lactate secretion was in the range of PHH. We hypothesize that there are two main factors contributing to the differences in glucose metabolism in HepG2 and HepaRG cells. 1) Energy metabolism is more efficient, i.e. based on energy formation via oxidative phosphorylation instead of glycolysis. This hypothesis is supported by a notably lower lactate secretion to glucose uptake ratio in HepaRG cells (1.6 in HepG2 vs 0.3 in HepaRG cells), indicating that the majority of glycolytic products was channeled into the TCA cycle. This may be a result of lower HIF-1 α mRNA levels in HepaRG compared to HepG2 cells, shown by data from previous whole genome gene expression level studies (Hart et al., 2010; Jennen et al., 2010). 2) HepaRG cells are not proliferating and therefore require less energy for the production and upkeep of macromolecules.

Contrary to the cell lines and against our expectations, for all donors of PHH we observed secretion of glucose, which may partially also be related to HIF-1 α , for which mRNA levels in PHH are even lower than in HepaRG cells (Hart et al., 2010). Considering that the culture medium used in this study contains high concentrations of glucose and insulin, the medium may be compared to a postprandial situation *in vivo*. Both, glucose and insulin levels play a critical role in the regulation of glucose metabolism in healthy humans and high levels result in inhibition of gluconeogenesis and stimulation of glucose and amino acid uptake into the liver (Edgerton, 2006; Moore et al., 2012). For comparison, postprandial hyperglycemia starts at blood glucose levels of 2 g/l (Giugliano et al., 2008), which is the same concentration used in the culture medium. In addition, insulin levels in the culture medium are around 2,000 times higher than the maximum levels postprandially found in the blood of healthy individuals (Kelley et al., 1994). Winnike et al. have described similar observations in PHH in a previous study and related these to a stress response to injury and surgery, resulting in release of epinephrine, cortisol and glucagon leading to glucose intolerance, glycogenolysis and gluconeogenesis (Winnike et al., 2012). Further, we found very similar relative contributions to lactate formation in HepaRG cells and PHH, with a slightly higher contribution from glycolysis in HepaRG cells, which probably resulted from the net uptake of glucose, not observed in PHH.

Similar to glucose, we observed that pyruvate metabolism differed notably between cell lines and PHH. Contrary to the two cell lines secreting pyruvate, PHH ingested notable amounts of pyruvate which may serve as alternative fuel for the TCA cycle as PHH did not rely on extracellular glucose. Other than that, it was shown in previous studies that pyruvate does not only serve as a carbon source in central metabolism, but has also been related to maintenance of CYP450 (Tomita et al., 1995) and glutathione S-transferase (GST) activity in primary hepatocytes (Vanhaecke et al., 2001). As PHH readily dedifferentiate in 2D *in vitro* cultures (Godoy et al., 2009), increased uptake of pyruvate might act as a measure to counteract the dedifferentiation process.

Demand in glutamine in HepG2 cells was significantly higher than in the other systems. This could on the one hand again be attributed to the proliferating nature of the cell line and thus, a higher demand in nucleic acid and protein building blocks, but also to fulfilling some of the many additional biological functions previously described for glutamine. These functions include serving as a carbon source for *de novo* lipogenesis (Metallo et al., 2011), as source for pyruvate and TCA intermediates (Yang et al., 2014), as well as supporting glutathione synthesis (DeBerardinis and Cheng, 2010). Even more, studies have shown a regulatory role of amino acids, in particular glutamine and leucine, on the

mammalian target of rapamycin complex 1 (mTORC1). mTORC1 is a master regulator of protein translation and cell growth and plays an important role in cancer cells (Wise and Thompson, 2010).

Besides its role in regulation of mTORC1, leucine in the human liver is mainly used as a building block for macromolecules and not for production of energy. Redundant leucine is secreted by the liver and taken up by muscle tissue where it is used for both, protein synthesis and energy production (Brosnan and Brosnan, 2006). We found minor secretion of leucine in PHH, whereas it was taken up by both cell lines, which we expected for all our *in vitro* cultures based on the amino acid's essential nature. Though leucine secretion is a typical function of the liver *in vivo*, the question arises as to where it is originating from in *in vitro* cultures. One hypothesis is that secreted leucine is related to cell death and resulting proteolysis. As a first step, the rationality of the hypothesis can be checked by balancing the amount of secreted leucine against the amount of leucine within the cell, estimated from literature data. Accounting for more than 10% of the mole fraction of amino acids in human liver microsomes, leucine, together with glutamate, is the most abundant amino acid (Benga and Ferdinand, 1995). Using previously described data on the protein content in PHH (Richert et al., 2006) for an estimation, secretion of leucine is equivalent to less than 5% of the total protein mass. Thus, from a balancing point of view, proteolysis is a valid hypothesis for the secretion of leucine, however, looking at viability data (not shown), there is no evidence for major cell loss.

In vivo, alanine is secreted by muscle cells in exchange for glucose and taken up in the liver, where it can be converted into pyruvate in a one-step transamination reaction via the alanine aminotransferase, which then serves as a substrate for gluconeogenesis. This cycle, also referred to as Cahill cycle, on the one hand serves the purpose of carbohydrate regeneration, and on the other hand the transport of ammonia from muscles to liver for detoxification via the urea cycle. In tumor cells, secretion of alanine has been reported, resulting from a surplus in glycolysis and glutaminolysis pathways (DeBerardinis and Cheng, 2010). In our study, we observed alanine uptake for all tested hepatic systems, including HepG2 cells. Uptake rates were in a similar range with exception of HepG2 cells, for which the uptake was around half of the other systems. Based on these findings, uptake of alanine seems to be a well-conserved function in liver cells, however, in case of HepG2 cells uptake was reduced probably resulting from high glycolytic and glutaminolytic fluxes and the absence of gluconeogenesis. Consequently, the carbon backbone of alanine is unlikely to serve as a substrate in gluconeogenesis, instead its use in protein synthesis and substrate in the TCA cycle are more likely.

The urea cycle in HepG2 cells is known to be impaired due to the absence of two essential enzymes, ornithine transcarbamylase and arginase I (Mavri-Damelin et al., 2007). Minor production of urea, as also observed in our study, has been related to activity of the arginase II enzyme, which however does not aid in the detoxification of ammonia (Mavri-Damelin et al., 2008). It is not known how HepG2 cells dispose of redundant ammonia. It was suggested that tumor cells directly secrete ammonia involving protein transporters (DeBerardinis and Cheng, 2010). Though urea formation in HepaRG cells is significantly higher, it remains questionable whether this is sufficient for complete removal of redundant ammonia. On the contrary, urea cycle was intact and highly active in PHH, being in the range of *in vivo* rates (*in vitro* 6 - 10 $\mu\text{g}/(10^6 \text{ hepatocytes} \times \text{h})$; *in vivo* 5-8 $\mu\text{g}/(10^6 \text{ hepatocytes} \times \text{h})$, (Bhatia et al., 1999)).

Generally, secretion rates in HepaRG cells were more similar to PHH, than secretion rates in HepG2, as additionally confirmed in the multivariate analysis. Noteworthy, unlike HepG2 cells, carbon metabolism in HepaRG cells did not show notable tumor-like characteristics.

2.5.2 Metabolic competence in human hepatic cell lines and PHH

Activity of the investigated CYP450 enzymes in HepG2 cells was too low and therefore no products could be detected using our LC/MS-based approach. In contrast, products for all isoforms were detected in HepaRG cells, though in most cases at lower concentrations than in PHH. Generally, lower CYP450 enzyme activity in HepG2 cells has been attributed to lower transcription of CYP450 genes based on differential expression of key transcription factors (liver enriched transcription factors, LETFs), such as the hepatocyte nuclear factors (HNF) (Jover et al., 2001; Rodriguez-Antona et al., 2002).

Despite the fact that both hepatic cell lines are tumor derived, there were striking differences in their CYP450 activity and we hypothesize that one explanation could lie within their origin: The HepG2 cell line is derived from a hepatoblastoma (Dearfield et al., 1983), while HepaRG cells originate from a hepatocellular carcinoma (Gripon et al., 2002). The former has a higher prevalence of activation of β -catenin (Buendia, 2002), which is an antagonist for effects of activated peroxisome proliferator-activated receptor α (PPAR α). PPAR α has also been reported to regulate CYP450 enzyme expression together with other transcription factors, such as HNF (Thomas et al., 2015, 2013). Aninat et al. have further suggested that limited chromosomal rearrangements in HepaRG cells and their ability to differentiate into hepatocyte and biliary epithelial-like cells (HLC, BLC), which allows more *in vivo*-like cultivation, contribute to a phenotype that is closer to PHH than HepG2 cells (Aninat et al., 2006; Gripon et al., 2002).

Higher CYP450 activity in PHH was most obvious for donors 2 and 3, which were both male, while less distinct for donor 1, which was female. Sex differences in CYP450 expression were described previously, but were reported to be less pronounced in humans than in other animals, e.g. rats (Waxman and Holloway, 2009). Parkinson et al. investigated sex differences in CYP450 activity in cryopreserved human hepatocytes and only found significant differences for the isoform CYP3A4 (Parkinson et al., 2004). Inconsistent with our data, Parkinson reported a two-fold higher activity in female hepatocytes, compared to male, whereas in our study, activity for the female donor was around two-fold lower. However, variance in CYP450 activity within the population is high (Parkinson et al., 2004) and the sample size in our study is too little to allow drawing reliable conclusions on sex differences in PHH. Effects of CYP450 activity in the context of drug-induced toxicity will be discussed in the following.

2.5.3 Effects of acetaminophen and diclofenac treatment on viability of the different hepatic systems

In our study, EC₅₀ values upon acetaminophen exposure were lowest in PHH (9.4 mM in average), followed by HepaRG (18.4 mM) and HepG2 cells (23.2 mM). This is in accordance with the CYP450 enzyme activities found in these cell systems, decreasing from PHH to HepG2 cells, underlining previous findings, reporting that acetaminophen-induced hepatotoxicity is mainly mediated by the reactive metabolite NAPQI (Dahlin et al., 1984). In both cell lines toxicity upon acetaminophen exposure was underestimated eminently. In addition, for HepG2 cells it also has to be noted that toxicity does not occur via necrosis as it is the case *in vivo*, PHH and HepaRG cells (McGill et al., 2012; McGill et al., 2011; Xie et al., 2014), but via apoptosis (Manov et al., 2004), suggesting that the HepG2 cell line is a poor model cell system to study acetaminophen toxicity, at least in 2D cultures (Aritomi et al., 2014). The apparent discrepancy in the EC₅₀ values in HepaRG cells and PHH can likely be attributed to the two different cell types in HepaRG cultures – HLC capable of metabolizing

acetaminophen on the one hand, and BLC incapable of acetaminophen metabolization on the other hand.

Exposing the different hepatic systems to diclofenac, we found that the EC_{50} value of HepG2 cells was in line with the EC_{50} values obtained in PHH (0.5 mM vs 0.53 mM in average). HepaRG cells were least sensitive to diclofenac exposure (EC_{50} 0.73 mM). Hence, there was no apparent correlation between EC_{50} values and the activity of the tested CYP450 isoforms. However, we did not quantify activity of members of the CYP2C family, being the most relevant group in case of diclofenac metabolization (Bort et al., 1999). Comparing expression profiles of members of the CYP2C family (CYP2C9 and CYP2C18) in HepG2, HepaRG and PHH from previous studies (Aninat et al., 2006; Gerets et al., 2012), we find a similar picture as we have shown in our study for the other CYP450 isoforms (figure 2.3). Therefore, this would indicate that the parent compound is the major cause of toxicity in HepG2 cells. On the other hand, in literature EC_{50} values for HepG2 cells upon acute diclofenac exposure were around 0.8 mM (Bort et al., 1998; Choi et al., 2015), suggesting that the HepG2 EC_{50} value in our study was underestimated. Additionally, keeping in mind the two populations in HepaRG cultures, extent of toxicity may nevertheless correlate with CYP450 activities.

2.5.4 Metabolic alterations in human hepatic cell lines and PHH upon drug exposure

Next, we investigated the effects of the two drugs on the central carbon metabolism in all of the hepatic systems to study similarities and differences in cell lines compared to PHH. Since effects in PHH were partially inconsistent in themselves, we additionally reviewed other studies on acetaminophen- and diclofenac-induced metabolic alterations, as well as the drugs' interactions with metabolism-related transcription factors.

As demonstrated in the PCA on the metabolic alterations upon drug exposure, effects on metabolism were strongest in case of HepG2 cells and hence resulted in best separation from the control. At the same time and contrary to the other hepatic systems, the same metabolites were affected with an overall identical trend in HepG2 cells treated with either acetaminophen or diclofenac. Both observations may be related to an impaired regulation of carbon metabolism and a limited set of possible metabolic alterations in cells with a pronounced cancer phenotype, compared to cells with a healthy metabolic phenotype. One example is the assessment of mitochondrial toxicity in HepG2 cells. Since HepG2 cells largely depend on glycolysis for the generation of energy, they cannot be used for the identification of mitochondrial toxicity using standard cultivation conditions, but require special media compositions (Marroquin et al., 2007). Then again, recent studies have demonstrated the use of HepG2 cells for discriminating between different toxicological mechanisms upon drug treatment, including steatosis, oxidative stress and phospholipidosis (García-Cañaveras et al., 2016, 2015). Despite the presence of an additional cell type in HepaRG cells potentially masking metabolic alterations caused by HLC, separation of drug-treated conditions from controls was better than in PHH, except for PHH3, partially resulting from the low variance of the secretion rates within the replicates.

For both drugs, upon treatment with the EC_{10} , a trend towards decreased uptake/ increased secretion was observed for the vast majority of amino acids in all systems, except for PHH2 in case of acetaminophen and PHH1 in case of diclofenac. For the latter two conditions, behavior for most metabolites was contrary to all other systems as indicated in the cluster analysis, and metabolic alterations were statistically significant only for a small number of metabolites. For all other systems and conditions, the observed effects on amino acids may either originate from a lower demand in substrates for energy metabolism, or more likely from a lower protein synthesis and elevated

degradation of proteins. Based on previous findings that acetaminophen and diclofenac cause mitochondrial dysfunction (Bort et al., 1998; Burcham and Harman, 1990; Gómez-Lechón et al., 2003; McGill et al., 2014; Meyers et al., 1988), we expect treatment to trigger a metabolic switch towards less efficient energy formation and therefore it is unlikely that drug exposure leads to a decreased consumption of energy-rich substrates. Instead, the two drugs have also been associated with ER stress (Nagy et al., 2007; Tsutsumi et al., 2004), an indirect consequence of the mitochondrial dysfunction (Lim et al., 2009) and oxidative stress (Tse et al., 2016). ER stress leads to lysis of un- and misfolded proteins and reduced protein synthesis (Haynes et al., 2004; Ron and Walter, 2007), matching the observed changes in amino acid transport when cells were treated with acetaminophen and diclofenac.

Additionally, formation of reactive metabolites has been ascribed to both, acetaminophen and diclofenac (Kretzrommel and Boelsterli, 1993; Mitchell et al., 1973), suggesting the induction of HIF-1 α expression upon exposure. Based on this, as well as on the impairment of mitochondrial function, we expected elevated glucose uptake and lactate secretion for both drugs, resulting from an upregulation of glycolytic genes and compensation for a less efficient energy formation. Glucose uptake indeed was elevated for all systems at the EC₁₀ when treated with acetaminophen, except for HepG2 cells. Winnike et al. further related the increase in glucose uptake observed in acetaminophen-exposed PHH to the glucuronidation of acetaminophen, which requires a glucose derivative as substrate (Winnike et al., 2012). When exposed to the EC₁₀ of diclofenac, in none of the cases we observed an increased glucose uptake. Gottfried et al. recently reported a decrease in glucose transporter 1 (*GLUT1*), lactate dehydrogenase A (*LDHA*) and monocarboxylate transporter 1 (*MCT1*) gene expression in different diclofenac-treated tumor cell lines (Gottfried et al., 2013), an effect that seems to superimpose metabolic alterations originating from mitochondrial dysfunction and oxidative stress.

Regarding lactate secretion upon acetaminophen exposure, we did not find a common trend for the different systems, and only for HepaRG cells and PHH1 we observed the expected increase at the EC₁₀. For diclofenac at EC₁₀ on the other hand, we observed a decrease in lactate secretion for all tested systems, which contradicts expected results based on previous studies reporting mitochondrial dysfunction and oxidative stress, but is in accordance with the decrease in *GLUT1*, *LDHA* and *MCT1* gene expression.

For pyruvate, we found a trend towards (increased) uptake for both drugs at EC₁₀ for all systems, except for PHH2 upon acetaminophen exposure. Pyruvate has been shown to protect against ROS-induced cytotoxicity (Andrae et al., 1985; Kelts et al., 2015) and therefore, the observed trend in pyruvate uptake may serve as a general cellular response to protect cells from ROS generated upon drug treatment, and to compensate for pyruvate lost in the ROS quenching reaction.

Besides glucose, alanine was one of the few significantly altered metabolites for which we found changes to differ between HepG2 cells and the other hepatic systems. As HepG2 cells mostly rely on glucose as a carbon source, and diclofenac severely impaired its uptake, alanine might have served as an alternative source when HepG2 cells were exposed to the EC₁₀ of diclofenac. For the other systems, dependence on glycolysis was less prominent, and impairment of glucose metabolism was less severe, not requiring an alternative carbon source.

Other than that, surprisingly, the changes for the majority of significantly altered metabolites were the same in the different cells, even though they differed tremendously in the transport rates of central carbon metabolites in the basal state. We expected differences to be more pronounced as the

abundance of metabolic regulators and drug metabolizing enzymes for many cases are strikingly different between PHH and HepG2 cells, and to minor extent also to HepaRG cells.

In summary, HepaRG cells allowed to study alterations in central carbon metabolites upon drug exposure. Results were in accordance with changes found in PHH, as well as with literature data. HepG2 cells also allowed to study certain aspects of drug-induced metabolic alterations, but were not capable of adequately reflecting some pathways, due to intrinsic restrictions.

2.6 Conclusion

In conclusion, the basal carbon metabolism in HepaRG cells closely resembled the metabolism in PHH, but lacked, e.g. high urea cycle activity. On the other hand, they neither exhibited a cancer-like metabolic phenotype as in case of HepG2 cells, nor a metabolic phenotype dominated by a stress reaction as observed for certain metabolites in PHH. The metabolic response to drug exposure was similar in all systems including HepG2 cells, yet HepaRG cells more accurately reflected the metabolic alterations observed in PHH, particularly those directly or indirectly related to glucose metabolism. Results obtained in different donors of PHH varied greatly in some cases, likely resulting from interindividual differences, which cannot be mapped adequately using a single cell line. In this study, we illustrated that the HepaRG cell line is a promising alternative to PHH, when studying the metabolic phenotype of hepatocytes and its general alterations when exposed to drugs.

2.7 Acknowledgements

The presented research was carried out within the SEURAT-1 NOTOX project funded through the European Community's Seventh Framework Programme (FP7/2007-2013) under grant agreement N° 267038 and Cosmetics Europe. Further, we thank Michel Fritz for excellent technical assistance.

Part II

Optimization of HepaRG culture conditions for short- and long-term toxicity studies

Chapter 3 Hepatotoxicity assessment in 3D and in 2D high-throughput systems using HepaRG cells

3.1 Abstract

Many new systems for three-dimensional (3D) *in vitro* cultivation are entering the market and are focus of current research in different fields. With their help, cells are supported in forming structures to mimic *in vivo* complexity and maintain tissue specific activity, allowing more reliable physiological and toxicological studies. In combination with cell lines, such as the human hepatic HepaRG, 3D cultivation systems that are amenable to high-throughput screening (HTS) potentially allow for the testing of the vast number of compounds currently needed in risk assessment. In this study, we investigate drug uptake, phase I and phase II metabolism, as well as reduced and oxidized glutathione levels in HepaRG cells, cultivated in different three-dimensional and two-dimensional systems, all suitable for HTS. The systems comprise Alvetex® polystyrene scaffold (APS), collagen sandwich, spheroid and monolayer cultures. Additionally, we investigate the impact of the choice of cultivation setup on the outcome of toxicological studies by treating cells with single and repeated doses of three different hepatotoxic compounds. The tested parameters differ drastically between the different systems, even within the 3D-type systems. Notwithstanding, EC₅₀ values upon compound exposure were in the same range for the different test systems, with exception of APS cultures. In addition, in all systems, HepaRG cells were showing increased sensitivity upon repeated exposure to the compounds. Taken together, classical monolayer cultivation as well as spheroids of HepaRG cells are most promising candidates for application in an HTS setup, allowing for reliably testing large numbers of compounds.

This chapter is in preparation for submission as

Klein S, Maggioni S, Noor F, Heinzle E. Hepatotoxicity assessment in 3D and in 2D high-throughput systems using HepaRG cells

3.2 Introduction

Three-dimensional (3D) hepatocyte cultures are considered as one of the central tools in future *in vitro* toxicity assessment (Meng, 2010). Together with a high-throughput screening (HTS) approach, this allows effective and reliable assessment of potential toxicity for large numbers of compounds in an *in vivo*-like environment with corresponding functionality. Primary human hepatocytes (PHH) are the gold standard in *in vitro* toxicity assessment; however, their usefulness in an HTS setup suffers from their scarce availability and limited lifespan. Additionally, they often originate from heavily medicated patients, which may interfere with subsequent studies. Therefore, there is an urgent need for HTS systems that rely on the use of established cell lines (Kunz-Schughart et al., 2004).

In the recent years, the human HepaRG cell line drew more and more attention in the field of toxicology as it closely resembles primary human hepatocytes (PHH) in terms of drug metabolism and intact liver specific pathways without sharing the disadvantages mentioned above (Aninat et al., 2006; Josse et al., 2008; Lübberstedt et al., 2011). Though a 3D environment is not essential for long-term stability of HepaRG cells (Josse et al., 2008; Klein et al., 2014), it has been shown to improve metabolic competence of most cytochrome P450 (CYP450) isoforms (Bhattacharya et al., 2012; Gunness et al., 2013; Leite et al., 2012; Malinen et al., 2014; Mueller et al., 2014; Rebelo et al., 2014).

For our study, we chose four different cultivation systems that are amenable to an HTS setup: 2D, collagen sandwich (CSW), Alvetex® polystyrene scaffold (APS) and spheroid cultivation. While cells in 2D cultures are seeded on a single thin layer of collagen, cells in a CSW are entrapped between two thick collagen gels, allowing the cells to arrange in two to three layers and form an *in vivo*-like cuboidal geometry. Collagen-coated APS offer a highly porous and rigid environment, which supports formation of *in vivo*-like geometry and facilitated nutrient diffusion into deeper cell layers compared to other 3D setups. On the other hand, spheroid cultures are scaffold-free and thus, there are no interactions with an artificial surface but only to other cells. For better comparison, all experiments were performed in a 96-well format.

For adequate assessment of toxicity, it is insufficient to rely only on single dose toxicity, but it is essential to include repeated dosing in toxicological studies. Here, we applied three hepatotoxic compounds which cover different mechanisms and outcomes, using single and repeated dosing regimens. These drugs were chlorpromazine, bosentan and valproic acid. Chlorpromazine is a neuroleptic medication that elicits cholestasis *in vitro* and *in vivo* (Anthérieu et al., 2012a; Padda et al., 2011). Bosentan, an endothelin receptor antagonist, also causes cholestasis but unlike chlorpromazine does not depend on the formation of oxidative stress. Instead it inhibits the export of bile salts via the bile salt export pump (Fattinger et al., 2001). The effects of the anticonvulsant valproic acid are complex. It interferes with histone deacetylation as well as several enzymes of the central carbon metabolism and eventually causes microvesicular steatosis (Aires et al., 2011, 2010, 2008; Göttlicher et al., 2001; Luís et al., 2011, 2007)

We focused our research on phase I (CYP3A4 activity and induction) and phase II metabolism as well as drug uptake in the different cultivation systems. Furthermore, we investigated levels of the radical scavenger glutathione and the effects of the drugs on cellular viability. Finally, we simulated oxygen supply in the tested devices to investigate for potential shortages. The results obtained within the study aid in selection of an adequate cultivation setup depending on the desired properties of the system.

3.3 Methods

3.3.1 Cell culture

The human hepatoma cell line HepaRG was purchased from Biopredic International (St. Grégoire, France). Detailed seeding instructions are described individually below. Cells were cultured in a cell culture incubator (Mettler GmbH, Schwabach, Germany) at 37°C with 95% relative humidity and 5% CO₂ supply. The outer wells of the culture plates were not used for cultivation, but were filled with sterile distilled water (Gibco Invitrogen, Darmstadt, Germany) to avoid evaporation of medium. After seeding, cells were cultured for 4 days in 100 µl Williams Medium E (WME; Pan Biotec, Aidenbach, Germany), supplemented with serum-free supplement ADD650 (Biopredic International, St. Grégoire, France) and 0.5% dimethyl sulfoxide (DMSO; Sigma Aldrich, St. Louis, MO, USA) (Maintenance & treatment medium (MT medium)). On the 4th day of cultivation, experiments for drug uptake, phase I and II metabolism, glutathione quantification as well as toxicity were initialized. In the results and discussion section, beginning of experiments is referred to as day 0.

3.3.1.1 2D cultures

Before cell seeding, 96-well plates (Greiner Bio-One, Frickenhausen, Germany) were incubated for 1 h with 100 µl of 50 µg/ml type I rat collagen (Roche Applied Sciences, Penzberg, Germany) in Dulbecco's Modified Eagle Medium (DMEM; AMIMED BioConcept, Allschwil, Switzerland). Afterwards, wells were rinsed once with 100 µl sterile phosphate buffered saline (PBS; Gibco Invitrogen, Darmstadt, Germany) and equilibrated with WME overnight. Differentiated HepaRG cells were seeded in the collagen-coated 96-well plates 4 days prior to treatment with a density of 72,000 cells per well ($n = 3$) in 100 µl WME with supplement ADD670 (Biopredic International, St. Grégoire, France) and 0.5% DMSO (Thaw & seed medium (TS medium)).

3.3.1.2 3D cultures in Alvetex® polystyrene scaffold

Prior to cell seeding, the 96-well APS (Reinervate, Sedgfield, United Kingdom) were incubated with 100 µl 70% ethanol for 2 minutes and subsequently rinsed with 100 µl PBS. Afterwards collagen coating and seeding was performed as described for 2D cultures.

3.3.1.3 3D Collagen Sandwich cultures

For 3D CSW a collagen solution of 4.5 ml type I rat collagen in 0.2% acetic acid and 0.5 ml DMEM was prepared, resulting in a final concentration of 1 mg collagen/ml. A neutral pH was achieved using sterile 1 M NaOH.

70 µl of the freshly prepared collagen solution were added to 96-well plates to form the bottom collagen layer. After 1 h incubation at 37°C the collagen gel was washed once with 100 µl PBS and was then equilibrated with 100 µl WME for 30 minutes at 37°C. Afterwards, medium was removed and 72,000 cells per well in 100 µl TS medium were added. After 3 h adherence at 37°C, supernatants were removed and a top layer of collagen was added using a freshly prepared collagen solution as described above. After the collagen solidified, 100 µl of TS medium were added on top.

3.3.1.4 3D spheroid cultures

HepaRG cells were seeded in 96-well GravityPLUS™ culture plates (InSphero, Zurich, Switzerland) with 2,000 cells per well, suspended in 40 µl TS medium. After 4 days in culture, spheroids were harvested into GravityTRAP™ plates (InSphero, Zurich, Switzerland) using 80 µl TS medium.

3.3.2 CYP3A4 induction and activity assay

A 10 mM rifampicin (Sigma Aldrich, St. Louis, MO, USA) stock solution was prepared in DMSO for the induction of CYP3A4 expression. MT medium was used to perform the dilution steps. HepaRG cells were incubated for 24 h with rifampicin concentrations ranging from 5 nM to 5 μ M with an additional untreated control. For the CYP3A4 activity assay, supernatants were removed and CYP3A4 P450-Glo Assay with Luciferin-IPA (Promega, Madison, USA) was performed according to manufacturer's instructions with 45 minutes incubation at 37°C. Measured CYP3A4 activity was normalized to the seeded cell number.

3.3.3 Preparation of drug solutions and treatment

300 mM bosentan (Sequoia Research, Pangbourne, UK) and 50 mM chlorpromazine hydrochloride (Sigma Aldrich, St. Louis, MO, USA) stock solutions were prepared in DMSO. Sodium valproate stock solution (Sigma Aldrich, St. Louis, MO, USA) was prepared directly in MT medium in a concentration of 150 mM. First dilution of bosentan and chlorpromazine was performed in DMSO-free MT medium, while all further dilutions were prepared in standard MT medium to keep DMSO at 0.5% (v/v). Four days after seeding, HepaRG cells were treated with the compounds for either 24 h (single dose) or 72 h (three doses) with medium renewal every 24 h. Volumes were 100 μ l for 2D, APS and CSW cultures and 70 μ l for spheroid cultures. In case of CSW cultures, wells were briefly rinsed twice with medium containing the compound to reduce the effect of drug dilution, due to substantial volume of the collagen layers.

3.3.4 Quantification of ATP

To determine viability of the cells upon drug exposure, ATP was quantified using CellTiter Glo® Luminescent Cell Viability Assay (Promega, Mannheim, Germany) according to manufacturer's instructions. In case of CSW cultures, the suspension was mixed vigorously upon addition of the lysis and substrate reagents to ensure penetration into the collagen layers and allow immediate cell lysis as for the other cultivation systems.

3.3.5 Quantification of reduced and oxidized glutathione

Reduced and oxidized glutathione (GSH, GSSG) were quantified using the GSH/GSSG-Glo™ assay (Promega, Mannheim, Germany) according to manufacturer's instructions.

3.3.6 Quantification of valproic acid uptake and VPA glucuronide release

For the determination of the drug uptake and secretion of drug metabolites, the total drug parent compound concentration of valproic acid and its metabolite VPA glucuronide were quantified in medium supernatants. The compounds were extracted from 25 μ l of medium supernatants collected after 6 h of treatment as described in the following. As a reference, supernatants were additionally collected from cell-free incubations at 37°C.

First, the internal standard for valproic acid (Sigma Aldrich, Steinheim, Germany), valproic acid-d6 (Toronto Research Chemicals, Toronto, Canada) was added. Then, for extraction, 75 μ l acetonitrile, acidified with 0.1% formic acid (Sigma Aldrich, Steinheim, Germany), were added. Samples were vortexed for 30 s, followed by centrifugation at 12,100 g for 10 minutes. 25 μ l of the supernatants were collected and diluted with 50 μ l MilliQ water.

Quantification was performed with a Perkin Elmer series 200 HPLC connected to an Applied Biosystem-SCIEX API 3000 triple quadrupole mass spectrometer. An Ascentis Express-C18 column

150 × 2.1 mm i.d., 2.7 µm particle size (Supelco, USA), was used for chromatographic separation. The mobile phases were 0.05 % formic acid in MilliQ water for negative ionization (A) and acetonitrile (B) with a gradient set as follow: from 30 to 100 % B in 10 minutes, 100 % B for 2 minutes, 100 to 30 % B in 2 minutes, 30% B for 7 minutes, at 180 µl/minute. 10 µl sample were injected into the system. The turbo ion spray source temperature was 350 °C, the ion spray voltage was set at -4200 V, the nebulizer gas was set at 7 units and the curtain gas at 8. The analysis was done in the multiple reaction monitoring mode (MRM). The optimized transitions and parameters were: 143.0 - 143.0 m/z for valproic acid, with collision energy of -15 eV, declustering potential set at -40 V and focusing potential at -140 V; 149.0 - 149.0 m/z for valproic acid-d6 with collision energy of -5 eV, declustering potential set at -20 V and focusing potential at -120 V. Settings for VPA-beta-D-glucuronide (Toronto Research Chemicals, Toronto, Canada) were 319.0 - 175.0 m/z with collision energy -15 eV, declustering potential set at -40 V and focusing potential at -180 V.

3.3.7 Dose response curves

Sigmoidal curves were fitted to the dose response data using Boltzmann equation (eq. 3.1),

$$\hat{y}_i = y_{min} + \frac{y_{max} - y_{min}}{1 + e^{\frac{EC_{50} - x_i}{sl}}} \quad [3.1]$$

with y_{min} and y_{max} being defined as the lowest and highest y-value in the data set. Missing parameters (EC_{50} , slope (sl)) were estimated with least squares regression using an evolutionary algorithm within Excel 2010 (Microsoft, Redmond, WA, USA). Confidence intervals (CI) were drawn according to equation 3.2,

$$CI_i = y_i \pm t_{\alpha, n-2} \times \sigma_{est} \times \sqrt{\frac{1}{n} + \frac{x_i - \bar{x}}{SS_{xx}}} \quad [3.2]$$

where $t_{\alpha, n-2}$ is the critical t-value for the degrees of freedom reduced by two and σ_{est} indicates the standard error of the estimate. The number of data points is given by n and SS_{xx} is the sum of squared deviations of x-values from the mean of x.

3.3.8 Students *t*-test

Unpaired Student's *t*-tests were performed using MatLab 2007b. Differences in two measurements are considered significant at $p < 0.001$, $p < 0.01$ and $p < 0.05$.

3.3.9 Simulation of oxygen levels

Oxygen diffusion and consumption in the different culture devices were simulated with a cylinder diffusion model for 2D/APS and CSW cultures, and a conical model in case of spheroid cultures. The dimensions for the culture devices that were introduced into the simulation are depicted in figure 3.1. Berkeley Madonna 8.3.9 (Berkeley, CA, USA) was used to run the simulations. The differential equations and parameters are depicted in the supplementary material (figure S3.1 and S3.2). In brief, the medium component was divided into N segments (10 for the cylinder and 30 for the cone) and for each of them, oxygen in- and outflow was calculated. Additionally, in the bottom segment, cellular oxygen uptake was implemented with a Monod-type equation.

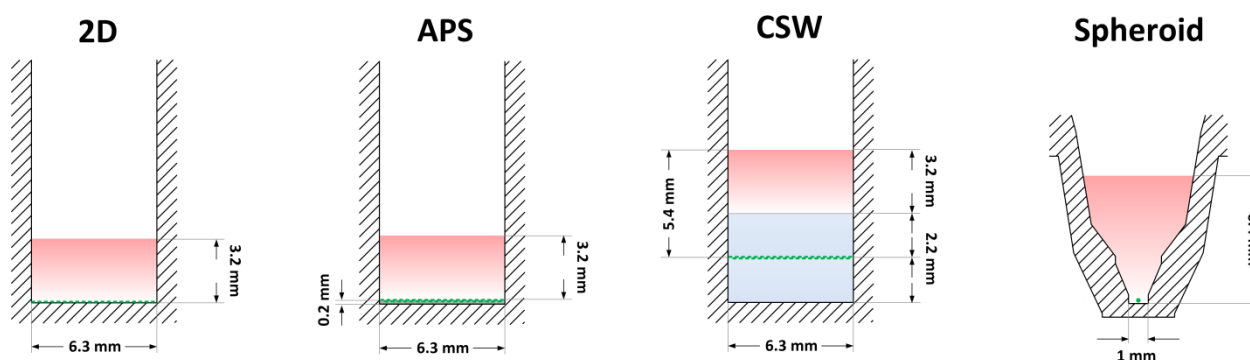


Figure 3.1 Overview on 2D, Alvetex® polystyrene scaffold (APS), collagen sandwich (CSW) and spheroid cultures. Dimensions of the plates that were used during experiments are given and barriers imposed by medium (red) and collagen layers (blue) are indicated. Cells are indicated in green.

3.4 Results

3.4.1 CYP3A4 activity and induction in HepaRG cells in 2D and 3D environment

Specific CYP3A4 activity in HepaRG cells cultured in 2D and 3D formats after 24 h and 72 h is shown in figure 3.2A. CYP3A4 activity in 2D HepaRG cultures after 24 h was around 3 times higher than in APS and CSW cultures. Spheroid cultures had the highest activity, which was 4 times higher than in 2D cultures. CYP3A4 activity remained stable in all tested culture conditions, with no significant loss at 72 h. Induction of CYP3A4 activity with rifampicin is displayed in figure 3.2B. Induction with 5 μ M rifampicin was highest in 2D, APS and spheroid cultures with around 3-fold increase in activity, while CSW cultures had a significantly lower induction (1.75-fold).

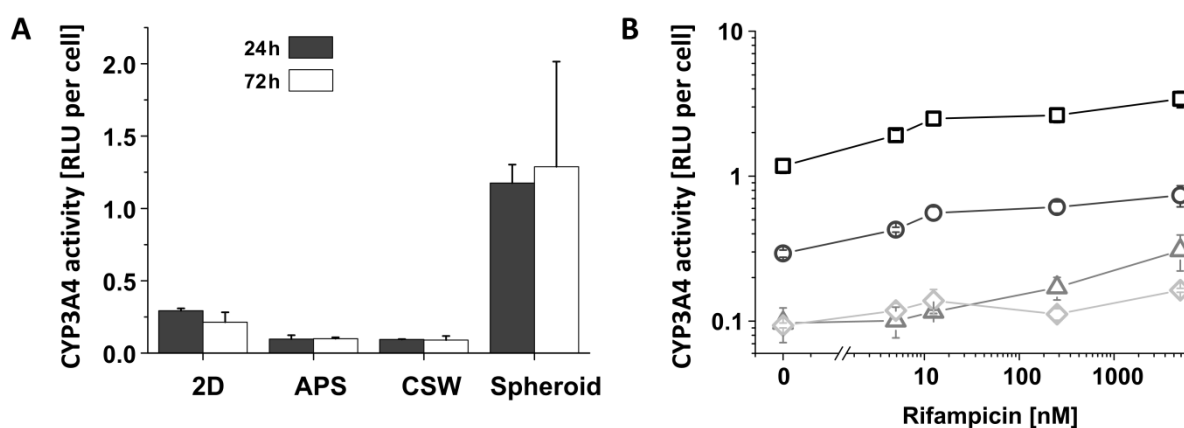


Figure 3.2 Specific CYP3A4 activity in HepaRG cells cultured in 2D and 3D formats as well as its induction using rifampicin. Specific CYP3A4 activity is given after 24 and 72 h (A). Induction of CYP3A4 activity in 2D (○), APS (△), CSW (◇) and spheroid (□) cultures by a range of rifampicin concentrations (B). Error bars indicate standard deviation ($n = 3$). APS, Alvetex® polystyrene scaffold; CSW, collagen sandwich; RLU, Relative luminescence units.

3.4.2 Drug uptake and phase II metabolism in HepaRG cells in 2D and 3D environment

Uptake of valproic acid and release of its metabolite VPA glucuronide by HepaRG cells in the different cultivation systems are summarized in table 3.1. By far highest uptake and metabolite release was found for spheroid cultures. Levels were 70-fold and 140-fold higher relative to the 2D cultures, respectively, for which we observed lowest activities among the different systems. Parent compound uptake and metabolite release in APS and CSW cultures were also notably lower compared to spheroids, but 1.3-fold and 1.9-fold higher regarding uptake and 3.7-fold and 2.2-fold higher in terms of VPA glucuronide release, respectively, compared to 2D cultures.

Table 3.1 Mean valproic acid uptake and VPA glucuronide release rates in 2D, Alvetex® polystyrene scaffold (APS), collagen sandwich (CSW) and spheroid cultures of HepaRG cells within 6 h, given in nmol/(cell × h) ± standard deviation for $n = 3$. Quantification of valproic acid and its product has been performed by S. Maggioni at the Mario Negri Institute, Italy.

Cultivation technique	Valproic acid uptake [nmol/(cell*h)]	VPA glucuronide release [nmol/(cell*h)]	Absorbed valproic acid released as VPA glucuronide in %
2D	0.28 ± 0.02	0.014 ± 0.002	4.8 ± 0.8
APS	0.35 ± 0.02	0.052 ± 0.004	15.1 ± 1.5
CSW	0.52 ± 0.02	0.031 ± 0.014	6.0 ± 2.8
Spheroid	19.6 ± 0.87	1.903 ± 0.015	9.7 ± 0.4

3.4.3 Reduced and oxidized glutathione in HepaRG cells in 2D and 3D environment

Intracellular levels of GSH and GSSG in HepaRG cells cultivated in the different systems are given in figure 3.3. HepaRG cells cultivated as spheroids had the highest concentration of GSH and GSSG, followed by 2D cultures (43% GSH, 32% GSSG compared to spheroids), both with a roughly 10 times surplus of the reduced form. APS cultures had slightly lower levels of GSH than 2D cultures, while CSW cultures had around 2% of the concentrations found in 2D. Only in CSW cultures GSSG levels were higher than GSH levels.

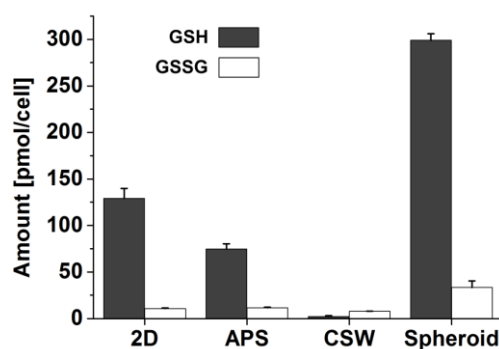


Figure 3.3 Levels of reduced (GSH) and oxidized glutathione (GSSG) in HepaRG cells cultured in 2D and 3D formats after 24 h, normalized to the seeded cell number. Error bars indicate standard deviation ($n = 3$). APS, Alvetex® polystyrene scaffold; CSW, collagen sandwich.

3.4.4 Toxicity assessment in HepaRG cells in 2D and 3D environment

EC₅₀ values resulting from exposure of HepaRG cells to the hepatotoxic compounds bosentan, chlorpromazine and valproic acid for 24 and 72 h are given in figure 3.4 and dose response curves are depicted in figure S3.3. After 24 h of exposure (single dose), EC₅₀ values from APS cultures differed notably from 2D and other 3D cultures, with cells being less sensitive to the drugs. After 72 h of exposure (three doses), values for all systems and drugs were in the same range, except for chlorpromazine-treated APS cultures. In accordance, fold changes in EC₅₀ values from 24 h to 72 h were highest in APS cultures for all tested compounds. Spheroid cultures were the most sensitive among the cultivations, having the lowest EC₅₀ values at both time points for bosentan and valproic acid. For chlorpromazine treatment, CSW (24 h) and 2D cultures (72 h) were more sensitive.

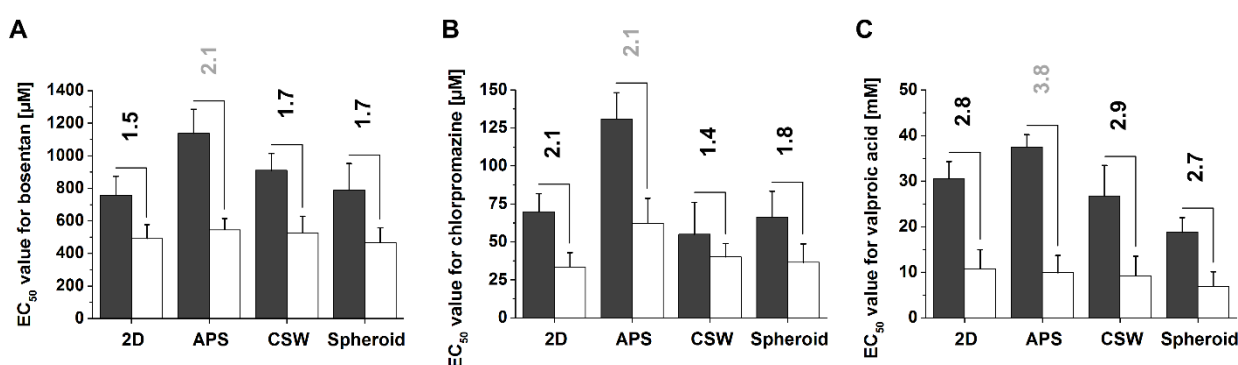


Figure 3.4 Summary of EC₅₀ values for HepaRG cells cultured in 2D and 3D formats after 24 h (1 dose, black bars) or 72 h (3 doses, white bars) exposure to bosentan (A), chlorpromazine (B) and valproic acid (C). 90% confidence intervals are given and fold change in EC₅₀ values from 24 h to 72 h is indicated for each drug and cultivation setup. Highest fold change for each drug is highlighted in grey. APS = Alvetex® polystyrene scaffold, CSW = Collagen sandwich.

3.4.5 Simulation of oxygen concentrations in 2D and 3D environment

Oxygen concentrations in the medium were simulated (figure 3.5) to investigate potential limitations in oxygen supply in the different culture devices. Steady state concentrations were reached after around 2 h. Surface oxygen levels were equal for all systems, yet, simulated oxygen concentrations in the middle and bottom region, differed greatly between the systems. For spheroids, the oxygen level dropped around 10% down to the middle segment, whereas it decreased by around 50% for 2D/APS and CSW cultures. At the bottom level, about 10% of the surface concentration was predicted to be left in case of spheroids, and 2.7% and 1.6% for APS/2D and CSW cultures respectively.

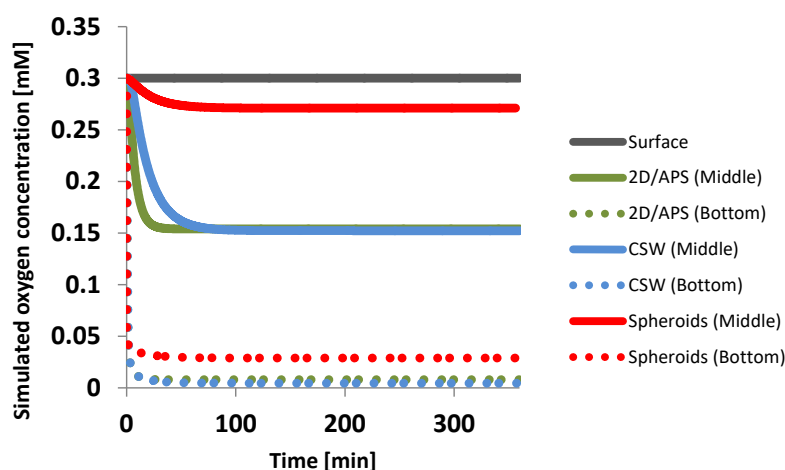


Figure 3.5 Simulated oxygen concentrations in the medium. Simulated concentrations are given for the four tested systems at different height: At the surface, in the middle (full lines) and at the bottom segment (dotted lines).

3.5 Discussion

For the prediction of human relevant toxicity, stable *in vitro* systems with *in vivo*-like behavior, amenable to an HTS setup, are strongly required. For this purpose, 3D cultures of human hepatocytes have been demonstrated to be an ideal basis. The objective of this study was to compare the human cell line HepaRG in different 3D cultivation systems and 2D cultivation, all suitable for HTS, in terms of physiological parameters and responses to drugs, to assess their potential role in toxicological studies.

3.5.1 CYP3A4 activity and induction in HepaRG cells in 2D and 3D environment

CYP3A4 is the major drug metabolizing enzyme and capable of metabolizing a wide variety of xenobiotic compounds. CYP3A4 activity in spheroid cultures was found to be drastically higher compared to 2D cultures in this study. Surprisingly, the other two tested 3D systems, namely APS and CSW cultures, had significantly lower activity when compared to 2D cultures. This suggests that certain environmental cues imposed by the culture system may drastically influence expression of CYP450 isoforms. For HepaRG spheroids and 2D cultures, similar findings have been described in a previous study, attributing the higher drug metabolizing capacity to two major factors: 1) higher expression of transcription factors controlling CYP450 expression, such as the pregnane X receptor (PXR) and 2) differential composition of HepaRG spheroid cultures regarding the two inherent cell types in HepaRG cultures, biliary epithelial-like cells (BLC) and hepatocyte-like cells (HLC) (Gunnesh et al., 2013; Rebelo et al., 2014). The latter phenomenon is one of the characteristics of HepaRG cells, which differentiate into HLC and BLC after seeding with a ratio of approximately 1:1 in 2D cultures (Cerec et al., 2007). Similar factors may influence CYP450 activity in APS and CSW cultures, yet in the opposite way, i.e. differentiation would occur in favor of the BLC.

For CSW cultures, an additional component is likely to contribute to poor metabolic competence. The top collagen layer acts as a second mass transfer barrier (MTB) (figure 3.1) and additionally limits oxygen supply as confirmed by our simulation (figure 3.5). The oxygen concentration in the bottom layer in CSW was about 40% lower than in 2D cultures. Available oxygen is an important factor in the regulation of CYP450 expression. In the *in vivo* liver, CYP450 activity is highest in the perivenous zone, a zone of low oxygen levels (Kietzmann, 2017). Camp and Capitano transferred these findings

into an *in vitro* setup with the human liver cell line HepG2 and investigated the dependence of CYP450 activity on medium height. In their study, highest CYP450 activity was achieved with a height of around 3 mm. An increase or decrease in height resulted in lower CYP450 activity (Camp and Capitano, 2007). To overcome this problem in CSW, more refined sandwich systems have been developed, using defined, synthetic layers (Du et al., 2008). Alternatively, CSW can be performed in wells with larger diameter, which allows reducing the thickness of the top collagen layer, therefore reducing the MTP, however also reducing its usefulness in a HTS setup. Schutte et al. reported lower gene expression for several CYP450 isoforms in primary rat hepatocytes cultured in the APS system, however still observed increased CYP450 enzyme activities, contrary to our observations (Schutte et al., 2011). This discrepancy might be related to primary hepatocytes generally greatly benefiting from a 3D culture environment, while the HepaRG cell line already has a stable phenotype in classical 2D cultivation with high expression of liver specific proteins.

At first glance, it might be expected that CYP450 activity in spheroids should be even more affected by restricted oxygen supply than CSW as the MTB is almost 20% higher (figure 3.1). However, next to the height of the medium layer, there are other decisive parameters, and it has to be considered that spheroids only contain around 2,000 cells, compared to 72,000 cells in the other setups. Consequently, the absolute oxygen consumption is lower and the available oxygen concentration can be expected to be higher than in the other setups. Indeed, our simulation predicts oxygen levels in the bottom layer of spheroid cultures that are 3.6 and 6.2 times higher relative to 2D/APS and CSW cultures respectively.

We found stable CYP3A4 activity in HepaRG cells under all tested culture conditions, suggesting that 3D cultures are not required for the upkeep of metabolic competence in this cell line. In accordance, we previously reported high stability of CYP450 activity in HepaRG cells under 2D culture conditions for 30 days (Klein et al., 2014).

Fold induction of CYP3A4 activity in HepaRG cells after rifampicin exposure was similar in all culture setups, except for CSW cultures. Lower fold induction in CSW cultures is probably related to dilution of the inducer in the collagen gel layers that constitute more than half of the volume in these cultures. Since the distribution of the inducer within the medium and the collagen layers, as well as cellular uptake are unknown, it is not possible to account for the difference in concentration. Nevertheless, studying CYP450 induction was possible in all systems, which is a critical part of drug discovery and development to ensure safe coadministration of compounds (Walsky and Boldt, 2008).

3.5.2 Drug uptake and phase II metabolism in HepaRG cells in 2D and 3D environment

Uptake of pharmaceuticals into the cells is in many cases essential for their beneficiary effect, but also for eliciting toxicity, as many targets are located within the cell. Valproic acid uptake into liver cells has not been fully elucidated yet and hypotheses range from diffusion based uptake (Booth et al., 1996) to uptake by a variety of transporters including monocarboxylate transporter 1 (MCT1) (Fischer et al., 2008), soluble carrier 4 (SLC4) family (Terbach et al., 2011) and organic anion-transporting polypeptide 2B1 (OATP2B1) (Thwaites and Anderson, 2007). In our experiment, uptake of valproic acid in spheroid cultures was considerably higher than in all other tested cultures, while uptake in 2D cultures was lowest, which is likely related to an increased expression of transporters in 3D cultures, in particular in spheroids. Ramaiahgari et al. found an increased gene expression for two major transporters of a variety of drug classes (OAT2 and OAT7) in HepG2 spheroids and a 95-fold higher OATP1B3 mRNA level, compared to classical 2D cultures (Ramaiahgari et al., 2014), which we assume is regulated similarly in HepaRG 2D and 3D cultures.

We observed that relative VPA glucuronide production was highest in APS cultures (15%), followed by spheroid cultures (10%) and CSW and 2D cultures (around 5%). *In vivo*, phase II metabolism of valproic acid mainly occurs via glucuronidation by UDP-glucuronosyltransferases (UGT) (Silva et al., 2008), whose contribution to the total valproic acid metabolization varies within a large range in patients and accounts for 7-89% (in average 30-50% (Silva et al., 2008)) of the total valproic acid metabolites (Gugler et al., 1977; Yoshida et al., 1999). Previous studies have shown that the expression of UGT1A6, one of the isoforms contributing to the formation of VPA glucuronide (Guo et al., 2012), is 10-fold higher in HepaRG cells compared to PHH (Darnell et al., 2012; Hart et al., 2010). Nevertheless, relative contribution of glucuronidation to valproic acid metabolization in our *in vitro* setup was at the lower end of what is known from *in vivo* data. Since glucuronidation of valproic acid does not require previous activation by a phase I reaction (Kiang et al., 2011), it can be excluded that prior steps are limiting the glucuronide conjugation in HepaRG cells. Instead, efflux of the conjugates might limit the extracellular availability of VPA glucuronide. However, there is no evidence that expression of multidrug resistance-associated proteins (MRP), which are responsible for transport of glucuronide and other conjugates (Jedlitschky et al., 1996), is impaired in the HepaRG cell line (Hart et al., 2010; Kanebratt and Andersson, 2008). Another possible explanation for the low concentration of VPA glucuronide in the supernatants is the cleavage of VPA glucuronide into its constituents by the VPA glucuronide hydrolase. Whereas *in vivo*, VPA glucuronide is readily removed from the liver via the blood stream, it remains in close vicinity to the liver cells in our *in vitro* batch setup and therefore remains a substrate to the VPA glucuronide hydrolase.

3.5.3 Reduced and oxidized glutathione in HepaRG cells in 2D and 3D environment

GSH is one of the major radical scavengers in mammalian cells and thus can have a major impact on the toxicity of certain compounds by preventing excessive cellular damage, e.g. as described for acetaminophen (McGill et al., 2011). Significantly higher GSH levels in spheroids than in other cultures as observed in our study might be related to upregulation of central enzymes of GSH metabolism in these cultures. However, data on GSH synthesis and its key enzyme glutamate cysteine ligase (GCL) in the context of 3D cultivation is scarce. Shimada et al. found increased gene expression for glutathione S-transferase (GST) in HepG2 spheroids (Shimada et al., 2007), which catalyzes the conjugation of GSH to a substrate. Both, GCL and GST are regulated by the nuclear erythroid factor-2-related factor 2 (Nrf2) (Jeyapaul and Jaiswal, 2000), so it can be assumed that GCL expression in a 3D environment is increased likewise. Low GSH and high GSSG levels, as we observed in CSW cultures can be caused by hypoxia, leading to production of reactive oxygen species in mitochondria and eventually depletion of cellular GSH (Lluis et al., 2005). For APS cultures on the other hand we determined similar GSH and GSSG levels as for 2D cultures, with the two systems having an almost identical mass transfer barrier.

3.5.4 Toxicity assessment in HepaRG cells in 2D and 3D environment

The uptake of a compound into the cytosol, its bioactivation or inactivation via phase I and II metabolism, as well as the levels of the radical scavenger GSH are decisive parameters on the outcome of drug exposure. Treating HepaRG cells in the different cultivation setups with drugs, we wanted to investigate the impact of the choice of cultivation format and of the accompanying differences in physiological parameters on the outcome of toxicity studies. In addition to valproic acid, we chose two more pharmaceutical compounds with a different mechanism of action, namely bosentan and chlorpromazine. Surprisingly, we barely observed differences in the EC₅₀ values of the three tested pharmaceutical compounds, but for HepaRG cells cultured in the APS system. This supports the idea that HepaRG cells cultured in APS system are more prone to differentiate into BLC. As a result, total

CYP450 activity would be lower, and consequently also the susceptibility to drugs that require transformation for toxicity or drugs that target liver specific proteins; as in the case of bosentan, which inhibits the bile salt export pump. Chlorpromazine is the only drug that we tested, for which cells rely on protection by GSH, due to cytotoxicity mediated by reactive metabolites (Anthérieu et al., 2012a; MacAllister et al., 2013). While GSH depletion may occur upon valproic acid treatment, it is considered only concomitant (Kiang et al., 2011). Consistent with poor GSH availability that we observed in CSW cultures, these were more susceptible to single dose chlorpromazine treatment than any of the other cultures. It is not clear why EC_{50} values in APS cultures drop drastically and approximate EC_{50} values of the other cultures at 72 h (3 doses), though they initially are rather distinct. However, further detailed investigation of this phenomenon might give in-depth knowledge about the exact mechanisms of repeated dose toxicity for each of the compounds.

Taken together, protective and potentially negative effects might counteract each other due to regulatory processes happening within the cells. E.g. high uptake of the hepatotoxic compound valproic acid on the one hand, and upregulated detoxification via phase I and II metabolism as well as subsequent secretion on the other hand, result in only minor differences in the EC_{50} values in the tested systems. In this context, determining the intracellular concentration of the drugs and their metabolites would be one of the most interesting parameters. However, this either requires very large cell numbers or very sensitive methods for quantification.

Since for all tested cultivation systems, EC_{50} values decreased when treated for 72 h instead of 24 h, and since all systems had a stable CYP3A4 activity, we state that all the tested systems are suitable for assessment of repeated dose toxicity in combination with HepaRG cells. Even more, since EC_{50} values were in the same range, it might be stated that a 3D environment is not required in repeated dose toxicity studies using this cell line. Yet, this strongly depends on the aim of each study.

3.6 Conclusion

We conclude that HepaRG cells are a valuable tool in toxicity studies, as they have stable physiological parameters, even in a 2D environment. Nevertheless, the cultivation system has to be chosen very carefully, as some systems might greatly affect the outcome of studies, as we observed for the APS cultures during single dose treatment. Additionally, each of the systems comes with its own advantages and disadvantages, which have to be traded off against. If studies go beyond simple assessment of a potential hazard of a compound via dose response curves, e.g. in-depth physiological studies, it is even more important that the cultivation system is chosen accordingly. As for standard toxicity studies, there is no compelling reason for the use of the CSW or APS cultures as their handling is more complex and prone to errors, while offering no visible benefits.

3.7 Acknowledgement

We thank Suellen Almeida Dragon for conducting first experiments supporting this study. The presented research was carried out within the SEURAT-1 NOTOX project funded through the European Community's Seventh Framework Programme (FP7/2007-2013) under grant agreement N° 267038 and Cosmetics Europe.

Chapter 4 Long-term maintenance of HepaRG cells in serum-free conditions and application in a repeated dose study

4.1 Abstract

Chronic repeated-dose toxicity studies are still carried out on animals and often do not correlate with the effects in human beings mainly due to species-specific differences in biotransformation. The human hepatoma cell line HepaRG has been used for human relevant toxicity assessment. However, HepaRG cells are commonly maintained in serum containing medium which limits their use in *-omics*-based toxicology. In this study, we compared the maintenance of HepaRG cells in standard serum-supplemented and serum-free conditions. Viability and cytochrome P450 (CYP450) activity during long-term cultivation were assessed. Liver-specific albumin and urea production was measured. The extracellular metabolome (amino acids, glucose, lactate and pyruvate) was analyzed to compare different cultivation conditions using metabolic flux analysis. Although metabolic flux analysis reveals differences in certain parts of the metabolism, e.g. production of urea, the overall metabolism of serum-free and serum-supplemented cultured HepaRG cells is similar. We conclude that HepaRG cells can be maintained in optimized serum-free conditions for 30 days without viability change and with high CYP450 activity. We also tested the acute (24 h) and long-term repeated-dose (7 doses, every second day) toxicity of valproic acid. We calculated an EC_{50} value of 1.4 mM after repeated exposure which is close to the c_{max} value for valproic acid. Maintenance of HepaRG cells in serum-free conditions opens up the opportunity for the use of these cells in human long-term repeated-dose hepatotoxicity studies and for application in systems toxicology.

This chapter has been published as

Klein S, Mueller D, Schevchenko V, Noor F (2014). Long-term maintenance of HepaRG cells in serum-free conditions and application in a repeated dose study. *Journal of Applied Toxicology*. *J Appl Toxicol*. 2014 Oct;34(10):1078-86. doi: 10.1002/jat.2929

4.2 Introduction

Long-term repeated-dose toxicity studies are still carried out on animals because of a lack of suitable *in vitro* alternatives. At the same time species-specific differences in hepatic biotransformation (Martignoni et al., 2006) often result in poor concordance of animal studies with human toxicity. Currently, primary human liver cells are used to assess human relevant metabolism-mediated acute toxicity. However, long-term maintenance of liver cells with high viability, liver-specific functions and cytochrome P450 (CYP450) activity still remains a challenge in easy-to-handle two-dimensional (2D) monolayer cultivation systems (Guillouzo et al., 2007). For reliable assessment of metabolism-induced toxicity, HepaRG cells have shown immense potential as they maintain metabolic competence for 4 weeks in 2D cultivation (Anthérieu et al., 2012b). This cell line consists of two cell types, biliary epithelial-like and hepatocyte-like cells (Cerec et al., 2007). Dimethyl sulfoxide (DMSO) is essential for the differentiation of HepaRG cells and induction of CYP450 expression (Gripon et al., 2002; Hoekstra et al., 2011). Studies that involve HepaRG cells are routinely carried out in medium containing high DMSO concentrations ($\approx 2\%$) and in the presence of fetal bovine serum (FBS) (Leite et al., 2012). As a result of undefined composition and batch-to-batch variations, the use of FBS poses a problem in reproducibility and standardization (Hahne and Reichl, 2011). In addition, the presence of FBS limits the application of *-omics* technologies in a systems toxicological setup. Proteins and peptides in the serum can serve as alternative carbon sources for the cultivated cells thereby challenging quantitative metabolome and flux analyses. These peptides and proteins also limit proteomics analyses where they usually mask the low abundant proteins/peptides which are produced by the cells. Furthermore, most drugs and other metabolites bind to serum albumin, thereby influencing the free-drug concentrations in *in vitro* toxicity studies (Broeders et al., 2013). However, other medium components, such as growth factors, also play a crucial role in the upkeep of hepatic functions. For example, hepatocyte growth factor (HGF) and epidermal growth factor (EGF) are important for the differentiation of hepatocytes and they can lead to improved liver-specific functions *in vitro* (Kim et al., 2010; Tan et al., 2012).

We investigated the maintenance of the HepaRG cells in serum-free medium (SFM) supplemented with growth factors and different concentrations of DMSO, in serum-free medium without growth factors as well as serum-supplemented medium (SSM), which is the current standard medium for HepaRG long-term cultivation. A period of 30 days was chosen in accordance with the Organization for Economic Cooperation and Development (OECD) guideline 407, requiring a minimum of 28 days for long-term repeated dose toxicity studies. We evaluated the activity of CYP450 enzymes and the secretion of albumin, urea and glutamine as markers for liver-specific functions. Furthermore, we determined viability and extracellular concentrations of amino acids, glucose, pyruvate and lactate. Potential bottlenecks caused by a lack of nutrients were identified. Moreover, we applied metabolic flux analysis to analyze metabolic changes over time and to investigate differences in metabolism between the different cultivation conditions. Metabolic flux analysis was shown to be a valuable tool for understanding the effects of experimental conditions and substrates as well as toxic compounds on cells (Guo et al., 2010; Mueller and Heinzle, 2013; Niklas and Heinzle, 2011; Orman et al., 2011). By applying stoichiometric constraints, reaction rates (fluxes) within the cells can be estimated (Jin and Jeffries, 2004). This allows a deeper insight into the cells' metabolism over various metabolic pathways. Finally, as a proof of principle, we assessed long-term (2 weeks, new dose every second day, 7 doses in total) toxic effects of the anticonvulsant drug valproic acid on HepaRG cells and compared them with acute effects (24 h) in SFM and SSM conditions. We conclude that the HepaRG cell line is suitable for repeated dose toxicity in serum-free conditions. This will allow an unbiased use of *-omics* technologies in systems toxicology.

4.3 Materials and Methods

4.3.1 Cell culture

The human hepatoma cell line HepaRG (differentiated cells, HPR116) was purchased from Biopredic International (St. Grégoire, France). The cells were maintained in Williams Medium E (Pan Biotech, Aidenbach, Germany) supplemented with $100 \text{ U} \times \text{ml}^{-1}$ penicillin, $100 \mu\text{g} \times \text{ml}^{-1}$ streptomycin (c.c.pro GmbH, Oberdorla, Germany), $50 \mu\text{M}$ hydrocortisone 21-hemisuccinate and $5 \mu\text{g} \times \text{ml}^{-1}$ human insulin (Sigma-Aldrich, St. Louis, MO, USA). Depending on the condition, 10% FBS (PAA Laboratories, Pasching, Austria, Germany), different concentrations of DMSO (Sigma-Aldrich) and $10 \text{ ng} \times \text{ml}^{-1}$ human hepatocyte growth factor (HGF) (Humanzyme, Chicago, IL, USA) as well as $2 \text{ ng} \times \text{ml}^{-1}$ mouse epidermal growth factor (EGF) (Sigma-Aldrich) were added to the medium. The different media compositions are summarized in figure 4.1 for seeding and adherence of the cells and in table 4.1 for the serum-free and serum-supplemented long-term cultivation.

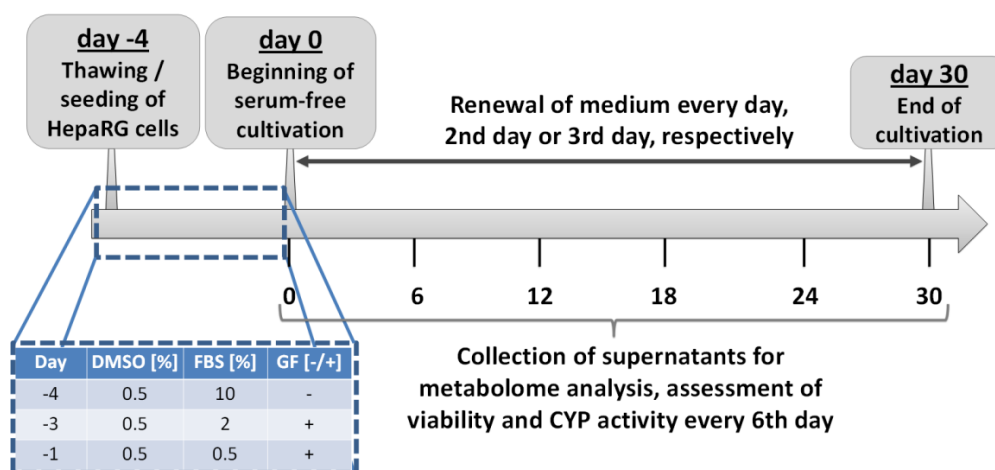


Figure 4.1. Experimental setup and media compositions used for seeding and adherence of the cells, before the start of the serum-free long-term cultivation. Media were changed every day, second or third day in respective culture plates – or + indicates the absence or presence of growth factors respectively. GF, growth factors (HGF and EGF).

HepaRG cells from 13 vials were pooled together and seeded (480,000 cells per well) in 24-well plates in triplicates (Greiner Bio-One, Frickenhausen, Germany) and kept in a cell culture incubator (Mettler GmbH, Schwabach, Germany) at $37 \text{ }^\circ\text{C}$ with 95% relative humidity and 5% CO_2 supply. Standard pre-cultivation of HepaRG cells results in a 1:1 ratio of hepatocytes and biliary epithelial-like cells. To reduce evaporation, the outer wells of the culture plate were filled with sterile distilled water (Gibco Invitrogen, Darmstadt, Germany).

Table 4.1 Composition of serum-free media (SFM) and serum-supplemented medium (SSM) used for the cultivation of HepaRG cells in the presence or absence of hepatocyte and epidermal growth factors (HGF/EGF), indicated by + and – respectively. FBS, fetal bovine serum.

Medium	DMSO concentration in			HGF and EGF
	10% FBS	% [v/v]		
SFM	SFM1	-	0	+
	SFM2	-	0.5	+
	SFM3	-	1.8	+
	SFM4	-	1.8	-
SSM		+	1.8	-

4.3.2 Quantification of metabolites in medium supernatants

Glucose, pyruvate and lactate

Glucose, pyruvate and lactate in the medium supernatants were quantified using high-performance liquid chromatography (HPLC) (Kontron Instruments, Neufahrn, Germany). After separation using an Aminex HPX 87H ion exchange column (300 × 7.8 mm, Bio- Rad, Hercules, CA, USA) at 60 °C with an isocratic flow rate of 0.8 ml × min⁻¹ of 7 mM H₂SO₄ as the mobile phase, compounds were detected via the refractive index (glucose) or UV absorption at 210 nm (lactate and pyruvate).

Amino acids

Quantification of amino acids was performed with an HPLC method as described previously (Krömer et al., 2005).

Urea

Urea was quantified using an HPLC method as described previously (Clark et al., 2007; Mueller et al., 2012).

Albumin

Human albumin was quantified with an indirect competitive enzyme-linked immunosorbent assay (ELISA) (Exocell, PA, USA). The assay was performed according to the manufacturer's instructions.

4.3.3 Viability Assessment

Cell viability was determined with the CellTiter-Blue® assay (Promega, Mannheim, Germany) on day 0 and afterwards every 6th day until day 30. The assay solution was mixed with medium in a ratio of 1:5. Next, 500 µl of the prewarmed mixture was added to the cells which were incubated for 2.5 h at 37 °C. Fluorescence was detected using a Fluoroskan Ascent CF fluorescence reader (Thermo Labsystems, Vantaa, Finland) at 590 nm (excitation 540 nm). Medium without cells served as a background control. The fluorescence signals were normalized to the signal on day 0 of the cultivation.

4.3.4 CYP450 activity assay

For the CYP450 activity assay, a cocktail of five substrates was used. The substrate cocktail mixture stock solution (1000×) was prepared in DMSO and consisted of 200 mM phenacetin, 100 mM bupropion, 100 mM dextromethorphan, 100 mM tolbutamide (Sigma-Aldrich) and 50 mM midazolam (Pharmacopée Européenne, Strasbourg, France). The stock was diluted in incubation medium to obtain final concentrations as follows: 200 μM phenacetin (CYP1A2), 100 μM bupropion (CYP2B6), 50 μM midazolam (CYP3A4), 100 μM dextromethorphan (CYP2D6) and 100 μM tolbutamide (CYP2C9). HepaRG cells were incubated in 325 μl of the medium per well in 24-well plates for 1 h, after which the supernatants were collected and immediately frozen. For analysis, samples were thawed at room temperature, diluted with a solution of stable-isotope labelled metabolites and subsequently analyzed by HPLC tandem mass spectrometry. The system consisted of an AB Sciex API3200 triple quadrupole mass spectrometer (Framingham, MA, USA) working in electrospray ionization mode, interfaced with an Agilent 1200SL HPLC (Santa Clara, CA, USA). Chromatography was performed at 70 °C with 10 μl injected into a Zorbax Eclipse XDB C18 column (50 × 4.6 mm, 1.8 μm particle size), at a flow rate of 1.5 ml × min⁻¹. The mobile phase was 0.1% formic acid in ultrapure water (A) and 0.3% formic acid in a mixture of methanol and acetonitrile (50% v/v) (B). The proportion of the mobile phase B was increased linearly from 0 to 98% in 3 min, and then the column was allowed to re-equilibrate at the initial conditions. The total run time was 4 min. The column eluent was split to an electrospray ionization interface, operating at 650 °C. Multiple reaction monitoring (MRM) mode in positive polarity was applied for detection.

4.3.5 Concentration response curves

HepaRG cells were seeded in 96-well plates with a density of 72,000 cells per well. For standard cultivation condition, cells were cultured according to the manufacturer's instructions for 1 week. Afterwards, these cells were tested in serum-free conditions for 24 h for acute toxicity of valproic acid (Sigma Aldrich). For SFM2 conditions the cells were precultivated according to figure 4.1 for 4 days. For acute toxicity, these cells were cultivated with a range (0.1-100 mM) of concentrations of valproic acid for 24 h in SFM2. For long-term repeated drug exposure in SFM2, cells were exposed to fresh medium containing the drug, every second day for 2 weeks (7 doses in total). All toxicity assays were carried out in the absence of serum. Viability was assessed using the CellTiter-Blue® assay in a volume of 120 μl per well and an incubation time of 3 h. Medium without cells served as background control. The fluorescence signals were normalized to the signal of the untreated control. EC₅₀ values were calculated using OriginLab 9.0 (OriginLab Corporation, Northampton, MA, USA).

4.3.6 Metabolic flux analysis

In this study, we adapted a previously described (Niklas et al., 2009) metabolic network model (table S4.1). The model consists of the glycolytic pathway, the tricarboxylic acid cycle (TCA) including anaplerotic reactions, the urea cycle and production of albumin, with a total of 55 reactions. 24 of those reactions are transportation reactions which were assessed by measuring metabolite concentrations in the culture supernatant before and after treatment. The remaining fluxes were assessed by applying the principles of flux balance analysis (Varma and Palsson, 1994a, 1994b), assuming pseudo steady-state as previously described (Niklas et al., 2009) with equation 4.1.

$$v_c = S_c^{-1} \times (-S_m \times v_m) \quad [4.1]$$

S_c and S_m are the matrices describing the stoichiometry of the metabolic network for which the rates are either calculated (c) or measured (m), and v_c and v_m represent the calculated and measured rates,

respectively. Solutions for fluxes and standard deviations were determined using Monte–Carlo simulation ($n = 100$) and afterwards calculating the mean outcome using MatLab 2007b (MathWorks, Natick, MA, USA).

4.3.7 Statistical analysis

An unpaired Student's t -test was performed using MatLab 2007b. Differences between two measurements are considered significant at $p < 0.001$, $p < 0.01$ and $p < 0.05$.

4.4 Results

4.4.1 Viability of HepaRG cells upon long-term cultivation

The viability of HepaRG cells upon maintenance in different media with daily medium renewal is depicted in figure 4.2. HepaRG cells remained viable (all values $> 83\%$) for the entire 30 day period when maintained in serum-free media supplemented with growth factors and a maximum of 0.5% DMSO (SFM1 and SFM2). In standard culture conditions (SSM), the viability of the HepaRG cells decreased between day 0 and 12 to around 72% and then remained constant. For the two serum-free conditions, SFM1 and SFM2, we observed a slight increase in the percentage of viable cells after day 18 of cultivation. Whereas, in case of HepaRG cells maintained in medium with 1.8% DMSO without FBS (SFM3 and SFM4), cell viability decreased to null after 18 days of cultivation with significant cell death already occurring in the first 6 days.

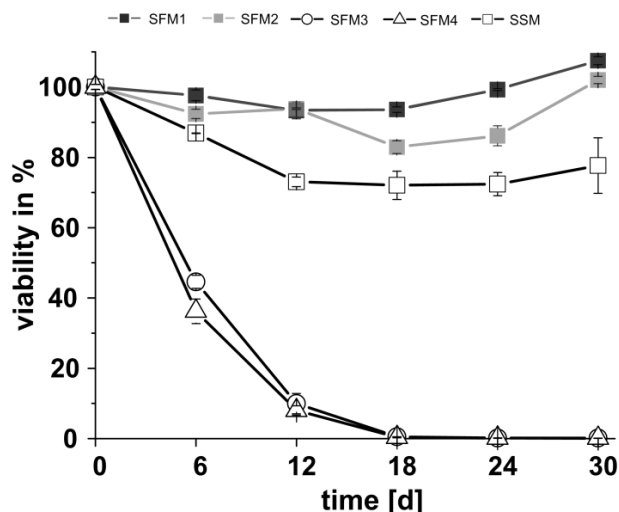


Figure 4.2. Viability of HepaRG cells during 30-day cultivation upon maintenance in different media with daily medium renewal. SFM1, 2 and 3 (serum-free medium with growth factors and 0%, 0.5% and 1.8% DMSO respectively), SFM4 (serum-free medium without growth factors and 1.8% DMSO), and SSM (serum-supplemented medium with 1.8% DMSO). Error bars indicate standard deviations ($n = 3$). Viability is given as percentage relative to HepaRG culture viability on day 0.

Regarding different medium renewal intervals (figure S4.1), cells maintained in SFM1 and 2 showed no differences in their viability when the medium was changed daily or every second day. With medium being renewed every third day, for both conditions (SFM1 and 2) HepaRG cells showed a

decrease in the viability after day 6 of cultivation. For all other conditions (SFM3, SFM4 and SSM) less frequent medium renewal assured a higher viability of the cells.

4.4.2 Assessment of CYP450 activity in HepaRG cells

The CYP450 activity for cultures in SFM1, SFM2 and SSM (figure 4.3) was determined. For CYP3A4, CYP2D6, CYP2C9 and CYP2B6, the activities between day 6 and 18 were higher when HepaRG cells were kept in higher DMSO concentrations. Activity of CYP1A2 was only slightly altered by the cultivation conditions investigated. Cells maintained in SSM showed high CYP450 activities until day 18, after which a significant loss of activities was detected. At day 30 of cultivation, the average remaining CYP450 activity for cells in SFM2 and SSM was in the same range (67% and 64% respectively), whereas for SFM1 only 38% of the remaining activity was detected. The activities of CYP3A4, CYP2B6, CYP3A4, CYP2C9 and CYP2D6 in HepaRG cells maintained in SFM were independent of the medium renewal interval (figure S4.2). However, for SSM longer intervals of medium change had a positive impact on the substrate conversion by the CYP450 enzymes.

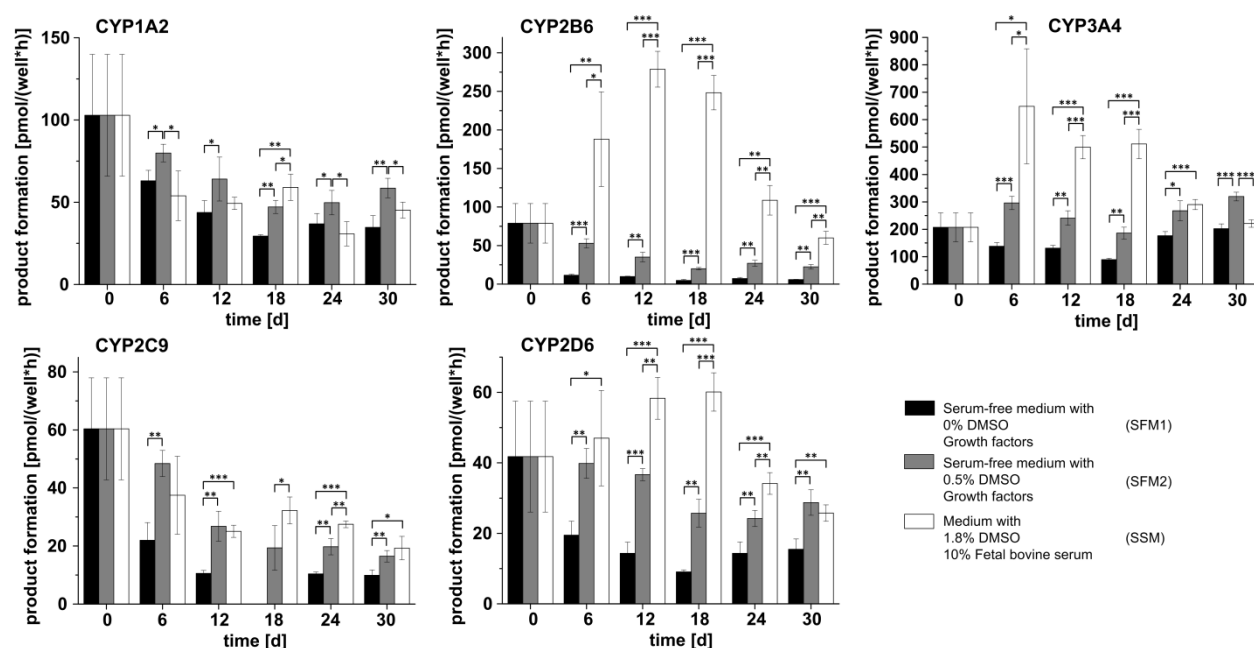


Figure 4.3 CYP450 activity during long-term cultivation. Activities of CYP1A2, CYP2B6, CYP3A4, CYP2C9 and CYP2D6 enzymes in HepaRG cells during long-term cultivation with daily medium renewal. Error bars indicate standard deviations ($n = 3$). *, **, *** indicate significance at $p < 0.05$, $p < 0.01$ and $p < 0.001$ respectively. Measurements have been performed by Valery Shevchenko at Biopredic International, Saint Grégoire.

4.4.3 Uptake and secretion rates of metabolites

Extracellular concentrations of organic acids, glucose, urea and albumin were quantified and uptake/secretion rates were calculated (figure S4.3). Amino acid concentrations in the supernatants were quantified and compared with concentrations in fresh medium (figure 4.4). In SFM, depletion of nutrients was observed upon renewal of medium every second day, whereas in SSM, depletion of nutrients only occurred when medium was renewed every third day. In terms of uptake of essential

amino acids, all HepaRG cultures exhibited very similar rates, except for the branched-chain amino acids (BCAA). Similarly, uptake and secretion rates of lactate, pyruvate and certain non-essential amino acids, e.g. glutamate, serine, arginine and alanine, were different. Secretion was only observed for serine, lactate, urea and albumin and in case of SSM cultivation additionally for alanine and pyruvate. Between day 18 and day 24, a significant change in metabolism was observed for all conditions. For lysine, histidine, phenylalanine, threonine, valine and glutamine, secretion was either reduced or uptake was increased. In some cases, there was a switch from secretion to uptake, e.g. for alanine and glycine. Concerning liver-specific functions, the production of albumin observed from day 18 onwards was lower when cells were cultivated in SSM conditions compared with SFM. On the other hand, SSM-maintained cells secreted significantly higher amounts of urea from day 6 of cultivation onwards, in comparison to cells maintained in SFM conditions. For all conditions, an increase in glucose consumption as well as lactate secretion over time was observed.

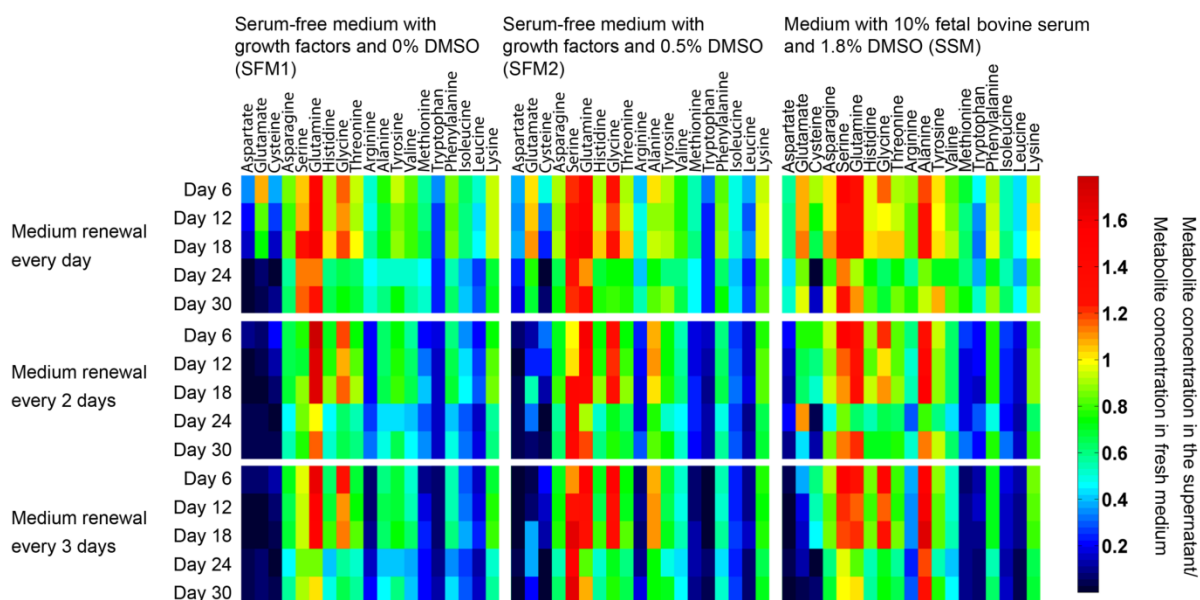


Figure 4.4 Heat map on amino acid production and consumption. A heat map showing the ratio of amino acid concentrations in the supernatants upon medium renewal every day, second or third day versus amino acid concentrations in the fresh medium, given for each investigated time point. An orange to red color indicates production of amino acids, a yellow color indicates that the amino acid was neither consumed nor produced. Green to blue color indicates increasing consumption.

4.4.4 Metabolic flux analysis

The effects of different cultivation conditions on the intracellular fluxes were determined by metabolic flux analysis. Several reaction and transportation rates are depicted in a flux distribution map (figure 4.5). Reaction rates in the glycolytic pathway of HepaRG cells were significantly lower in SSM as compared to SFM. In accordance, lactate secretion was lower for cells maintained in SSM. Generally, glycolytic activity increased for all conditions over time. For cells cultivated in medium without DMSO (SFM1), approximately 40% of the glycolytic pyruvate was converted to lactate; for cells kept in 0.5% and 1.8% DMSO respectively (SFM2 and SSM), about 50% to 55% of glycolytic pyruvate was metabolized to lactate. The lactate/glucose ratios on days 6 and 30 were identical for SSM, SFM1 and SFM2.

In case of SSM at day 6, a low amount of pyruvate was converted to acetyl-CoA as compared to SFM. Nevertheless, reaction rates in the TCA cycle (e.g. lumped reaction rates for conversion of succinyl-CoA to oxaloacetate) were in the same range for all conditions. Among the investigated conditions, HepaRG cells showed the highest TCA cycle activity when cultivated without DMSO (SFM1).

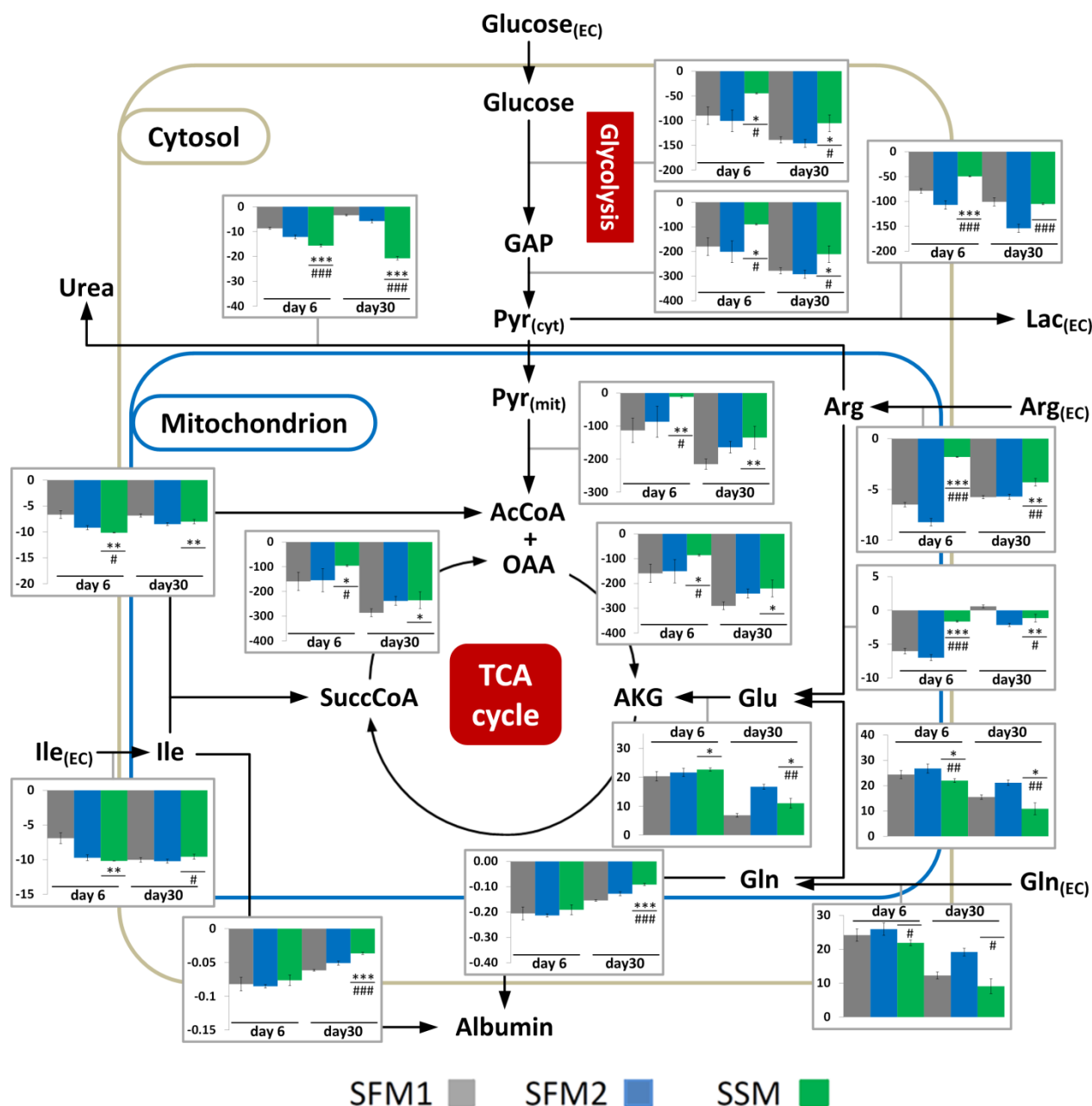


Figure 4.5. A flux distribution map of HepaRG cells upon long-term cultivation for days 6 and 30 for SFM1 and 2 (serum-free medium with growth factors and 0% or 0.5% DMSO, respectively) and SSM (serum-supplemented medium with 1.8% DMSO). Fluxes are given in fmol/(cell × h). Negative values indicate fluxes into the direction of the arrow and positive values in reversed direction. Error bars indicate standard deviations ($n = 3$). *, **, *** (comparison of SSM to SFM1) / #, ##, ### (comparison of SSM to SFM2) indicate significance at $p < 0.05$, $p < 0.01$ and $p < 0.001$, respectively. GAP, glyceraldehyde 3-phosphate; Pyr, pyruvate; AcCoA, acetyl coenzyme A; OAA, oxaloacetate; AKG, α -ketoglutarate; SuccCoA, succinyl coenzyme A; Lac, lactate; Glu, glutamate; Gln, glutamine; Arg, arginine; Ile, isoleucine; cyt, cytosolic; mit, mitochondrial; EC, extracellular; TCA, tricarboxylic acid.

Arginine uptake and its conversion to glutamate were significantly reduced for cells maintained in SSM. α -Ketoglutarate, derived from the TCA cycle, was probably metabolized to glutamine which was subsequently secreted. The highest rates for these reactions were found for cells kept in SFM2, whereas the lowest rates were found for the SSM-maintained cells.

Comparison of urea and albumin production after 30 days of cultivation shows that HepaRG cells exhibited high remaining activities for most conditions (table 4.2). At day 30, urea production was between 61% and 366% (SFM1 and SSM, respectively) and albumin production was between 45% to 75% (SSM and SFM1) relative to respective productions on day 0.

Table 4.2 Percentage remaining urea and albumin production after 30 days cultivation relative to day 0. SFM, serum-free medium; SSM, serum-supplemented medium.

Medium	Urea	Albumin
SFM1	61%	75%
SFM2	103%	65%
SSM	366%	45%

4.4.5 Drug response behavior

The 24 h EC_{50} values for valproic acid obtained by the concentration response curves (figure 4.6) were 21 (± 3.4) and 24 mM (± 3.6) upon precultivation either in SSM or SFM2 according to figure 4.1. After 2 weeks of repeated dose application (7 doses) in SFM2, the EC_{50} value decreased to 1.4 mM (± 0.2).

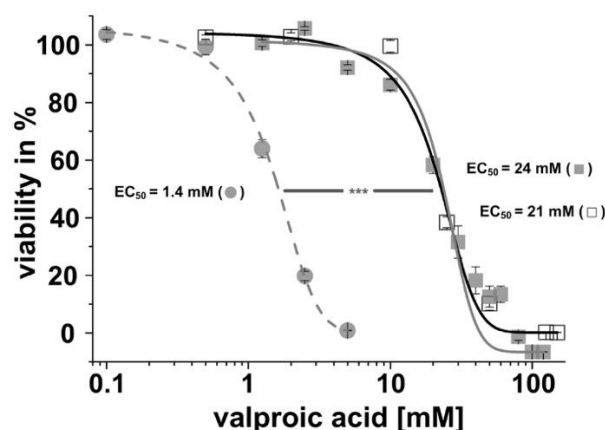


Figure 4.6 Concentration response curves upon valproic acid treatment for 24 h and 2 weeks (new dose every second day, 7 doses in total) under serum-free conditions. (□) shows dose response curve for HepaRG cells precultivated under standard cultivation conditions. (■) and (●) show dose response curves on HepaRG cells for 24 h and 2 weeks respectively, with precultivation of 4 days according to figure 4.1. All toxicity assays were carried out in the absence of serum. Error bars indicate standard deviations ($n = 3$). *** indicates significance at $p < 0.001$.

4.5 Discussion

Serum-free long-term cultivation is essential for reliable assessment of drug-induced effects in systems toxicological approaches. To the best of our knowledge, long-term studies on HepaRG cells, until now, were exclusively performed in serum-supplemented medium and usually these studies did not exceed 2 weeks of cultivation after the differentiation of the HepaRG cells (Anthérieu et al., 2011; Josse et al., 2012). Since HepaRG cells show stable CYP450 activity, they may be reliably applied in long-term repeated dose toxicity studies especially in the assessment of metabolism mediated adverse effects. In this study, we compared cultivation of HepaRG cells in SSM and different SFM for 30 days and the effects on cell viability, metabolic competence and exometabolome were investigated. Additionally, we show the application of this test system in a long-term repeated dose study on valproic acid.

We demonstrate that HepaRG cells can be maintained in growth factor supplemented medium without DMSO and with DMSO concentrations of 0.5% (SFM1 and 2, respectively) for 30 days. High DMSO concentrations (1.8%) in the absence of serum (SFM 3 and 4) led to cell death within 18 days of cultivation. Reports on the cytotoxic effects of DMSO on hepatic cells are ambiguous. For primary human hepatocytes (PHH), 2% DMSO is reported to be non-toxic upon 24 h of incubation, whereas in HepG2 cells 0.5% DMSO elicited cytotoxicity within 48 h (Niklas et al., 2009; Sumida et al., 2011). In SSM, the cytotoxic effects of DMSO were attenuated probably as a result of the membrane protective effects of FBS (Castro et al., 2011). Binding of DMSO to albumin might further contribute to its reduced toxicity in SSM.

In SFM conditions 1 and 2, we observed a decrease in viability ($\approx 20\%$) when the medium was renewed every 3 days, compared with every day and every 2 days. Upon metabolome analysis it could be shown that the essential amino acid tryptophan as well as aspartate and glutamate were completely depleted within a 3-day replenishment interval. Therefore, decreased cell viability is most probably due to starvation of the cells. Tryptophan contributes to the production of NAD^+ , which in turn is involved in signaling pathways, such as those regulating DNA repair and apoptosis (Chiarugi et al., 2012) as well as in energy metabolism. Considering that NADH is required in the reaction of the viability assay, the observed drop in viability may either come from a decrease in NAD^+ supply, or from an actual decrease in cell number. The slight increase in viability after 18 days of cultivation could be because of the regeneration of the hepatic cells, as occurring *in vivo* (Vodovotz et al., 2012). As the increase in viability is limited to serum-free conditions, it might be related to the presence of HGF, which is known to be a mitogen as well as for playing a role in liver regeneration (Forte et al., 2006; Tan et al., 2012).

For HepaRG cells cultivated in SFM2 with daily medium renewal, the average remaining CYP450 activity after 30 days was around 70%. For CYP2C9, CYP3A4 and CYP2D6, which are responsible for the metabolism of the majority of current drugs (Aninat et al., 2006), the mean remaining activity was approximately 85%, which was the highest among all the tested conditions.

HepaRG cultures consist of hepatocyte and biliary epithelial-like cells in a 1:1 ratio (Cerec et al., 2007). Hence, in the following comparison of liver specific functions (e.g. urea and albumin production) to hepatic *in vivo* rates, only hepatocyte-like cells were considered. In case of urea, we observed a production of around 40 fmol/(h \times hepatocyte) for HepaRG cells maintained in SSM. In SFM rates were about 6 and 10 fmol/(h \times hepatocyte) (SFM1 and SFM2, respectively). Although SSM cultivation shows a urea production that is closer to the one *in vivo* [80–130 fmol/(h \times hepatocyte)], the sum of the ammonia detoxifying reactions in all HepaRG cells catalyzed by glutamate

dehydrogenase (GDH), glutamine synthetase (GS) and carbamoyl phosphate synthetase 1 (CPS1) are identical for HepaRG cells maintained in SFM2 and SSM. For both conditions, detoxification occurs with rates of 60.5 fmol/(h × cell) on day 6 and 43 fmol/(h × cell) on day 30. Hoekstra *et al.* showed that DMSO increased urea production and omission of DMSO led to an increased expression of glutamine synthetase (Hoekstra *et al.*, 2011), which is in accordance with our findings on urea formation and the decrease in glutamine secretion when DMSO was supplemented. Interestingly, in the case of PHH in serum-free long-term cultivation, a significant decrease in urea production over time is reported (Mueller *et al.*, 2012).

Concerning albumin production, in SFM, production rates of 0.8 to 0.9 pg/(h × hepatocyte) and in SSM 0.5 pg/(h × hepatocyte) after 30 days of cultivation were measured. *In vivo* rates, with around 2 to 3 pg/(h × hepatocyte) (Bhatia *et al.*, 1999) are higher than the albumin production observed in any condition in our study. It was reported that DMSO had no effect on albumin production (Aninat *et al.*, 2006). We observed this for all conditions in the first 12 days. However, after 18 days of cultivation, albumin production in SSM was significantly decreased. Albumin secretion by PHH after 14 days of cultivation (Lübberstedt *et al.*, 2011) is roughly round 0.02 pg/(h × cell). In our system, the HepaRG cells, even after 30 days in SFM conditions, produced significantly higher amounts of albumin. Maintenance of albumin and urea production over a period of 30 days demonstrates that HepaRG cells under tested conditions are superior in retaining liver-specific functions as compared with PHH upon long-term cultivation.

Elevated lactate secretion is reported as a signal of stress (Limonciel *et al.*, 2011). In addition, it is a sign of wasteful metabolism, as further processing of glycolytic pyruvate through the TCA cycle instead of secretion as lactate, would yield more ATP per molecule of glucose. The ratio of glucose consumption and lactate secretion remained low and unchanged over time, indicating an efficient energy metabolism in SFM conditions. Moreover, the deprivation of FBS also did not elicit cellular stress, as indicated by identical lactate/glucose yields in SFM2 and SSM conditions. DMSO-free cultivation (SFM1) resulted in the lowest lactate/glucose yield, which further led to increased rates in the TCA cycle, compared with all other conditions. Therefore, we postulate that the presence of even low concentrations of DMSO imposes a burden on the HepaRG cells.

Increased uptake of nutrients and consequential increased TCA cycle fluxes at later time points of cultivation for all conditions may be associated with increased energy demand for general maintenance, e.g. repair of DNA damages. After 2 weeks of cultivation HepaRG cells show first indications of ageing (Pernelle *et al.*, 2011) which may explain increased energy demand. We observed an increased uptake of the BCAA isoleucine and leucine in SSM cultivation. These amino acids are mostly metabolized to acetyl-CoA. As reaction rates to acetyl-CoA coming from pyruvate are very low for SSM cultivation, feeding of the acetyl-CoA pool by other sources is essential to keep the TCA cycle running. Although we observed an increased uptake of BCAAs, we could not detect an increased uptake of other amino acids (such as threonine, tyrosine or lysine) which also produce acetyl-CoA when degraded.

Applying the optimized serum-free conditions we tested the acute (24 h) and repeated dose toxicity (2 weeks, new dose every second day, 7 doses in total) of valproic acid. Although acute toxicity of valproic acid is often due to overdosage, valproic acid may cause severe fulminating liver impairment within days after therapy start and microvesicular steatosis upon clinical use (Dreifuss *et al.*, 1987; Krähenbühl *et al.*, 2000). VPA substantially binds to serum proteins ($\geq 90\%$) (Silva *et al.*, 2008), hampering its use in serum-supplemented studies. The comparison of 24 h (acute) EC₅₀ values shows

that the HepaRG cells' response to VPA was not affected by the presence of growth factors. Furthermore, we found a significantly lower EC_{50} value (17 fold) after 2 weeks of repeated drug application than after a single 24 h exposure, demonstrating the usefulness of this test system in long-term repeated dose studies. The EC_{50} value upon long-term treatment (1.4 mM) is close to the c_{max} value which is around 714 μ M (Fisher and Broderick, 2003).

In this study, we show that the HepaRG cells can be maintained viable with constant CYP450 activities and liver-specific functions (urea and albumin production) for at least 30 days. The long-term viability and CYP450 activities in SFM conditions were superior to those reported for PHH. Metabolic flux analysis indicates that the central carbon metabolism in SFM conditions remains comparable to standard SSM conditions. It also indicated that there are slight adjustments in the central metabolism (e.g. urea production) of HepaRG cells to different cultivation conditions. This hints at the heterogeneity of HepaRG cells which probably allows them to adjust to the tested cultivation conditions with stable metabolic competence. The metabolome analysis indicated that depending on the medium replenishment interval, there may be nutrient limitations (e.g. some amino acids like tryptophan and BCAAs). Adaption of cultivation to avoid such nutrient limitations will allow optimal and standardized cultivation of HepaRG cells.

Metabolic flux analysis allowed the rational design of basal medium that does not cause major metabolic changes in the investigated cells. The HepaRG cells in this medium showed stable metabolic competence, thereby increasing the reliability of the test system. Although we tested the 2D cultivation system, this serum-free setup could be extended to 3D cultivation techniques such as organoids or bioartificial livers. Serum-free long-term cultivation of HepaRG will greatly facilitate the application of this system for repeated dose toxicity assessments on a high content *-omics* platform in systems toxicology.

4.6 Acknowledgments

The research leading to these results received funding from the European Community's Seventh Framework Programme (FP7/ 2007-2013) under grant agreement N° 267038 and Cosmetics Europe within the framework of the 'NOTOX' project of the SEURAT-1 (safety evaluation ultimately replacing animal testing) initiative. We thank the ToxBank project of SEURAT-1 for support in the selection of the test compound.

Part III

Application of HepaRG cells in repeated dose toxicity studies

Chapter 5 *In silico* modeling for the prediction of dose and pathway related adverse effects in humans from *in vitro* repeated-dose studies

5.1 Abstract

Long-term repeated-dose toxicity is mainly assessed in animals despite poor concordance of animal data with human toxicity. Advanced human *in vitro* systems e.g. with metabolically competent HepaRG cells, are used for toxicity screening. Extrapolation of *in vitro* toxicity to *in vivo* effects (IVIVE) is possible by reverse dosimetry using pharmacokinetic (PK) modeling. We assessed long-term repeated-dose toxicity of bosentan and valproic acid (VPA) in HepaRG cells under serum-free conditions. Upon 28-day exposure, the EC₅₀ values for bosentan and VPA decreased by 21 and 33 fold respectively. Using EC₁₀ as lowest threshold of toxicity *in vitro*, we estimated the oral equivalent doses for both test compounds using a simplified PK model for IVIVE. The model predicts that bosentan is safe at the considered dose under the assumed conditions upon 4-week exposure. For VPA, hepatotoxicity is predicted for 4 and 47% of the virtual population at the maximum recommended daily dose after 3 and 4 weeks of exposure respectively. We also investigated the changes in the central carbon metabolism of HepaRG cells exposed to orally bioavailable concentrations of both drugs. These concentrations are below the 28 day EC₁₀ and induce significant changes especially in glucose metabolism and urea production. These metabolic changes may have a pronounced impact in susceptible patients such as those with compromised liver function and urea cycle deficiency leading to idiosyncratic toxicity. The combination of modeling based on *in vitro* repeated-dose data and metabolic changes allows the prediction of human relevant *in vivo* toxicity with mechanistic insights.

This chapter has been published as

Klein S, Maggioni S, Bucher J, Mueller D, Niklas J, Shevchenko V, Mauch K, Heinzle E, Noor F (2016). *In silico* modeling for the prediction of dose and pathway related adverse effects in humans from *in vitro* repeated-dose studies. *Toxicol Sci.* 2016 Jan;149(1):55-66. doi: 10.1093/toxsci/kfv218

5.2 Introduction

Evaluation of long-term repeated-dose effects is still one of the most challenging areas in toxicity screening of compounds and risk assessment (Pfaller et al., 2001). Although for acute effects a variety of *in vitro* assays amenable to high throughput applications and multiplexing are available, long-term repeated-dose toxicity assessment is heavily dependent on animal studies. This is despite the fact that animal studies fail to predict human relevant toxicity mainly due to inter species variances (Baillie and Rettie, 2011; Collins, 2011; Greaves et al., 2004).

Modern toxicology is focusing on designing *in vitro* assays for the identification of early perturbations of biological pathways in human *in vitro* systems and the use of these for the prediction of adverse effects (Sheldon and Cohen Hubal, 2009). However, extrapolation of *in vitro* results to human *in vivo* is sometimes limited due to the fact that nominal concentrations in the *in vitro* assays are used without consideration of the exposure magnitude, timing and duration (Coecke et al., 2013). Other factors such as *in vivo* bioavailability, metabolic clearance and *in vitro* specific parameters such as plastic binding and evaporation (Groothuis et al., 2015) are often overlooked.

Reverse dosimetry is commonly used for the calculation of plausible exposure concentrations also called oral equivalent doses (OEDs). The OED represents the dose required to produce *in vivo* steady-state blood concentrations equivalent to a given *in vitro* effective concentration (Rotroff et al., 2010; Wetmore et al., 2012). This approach was used to compare acute effects of chemicals and drugs in humans by *in vitro* to *in vivo* extrapolation (IVIVE) using simple pharmacokinetic (PK) models (Chang et al., 2015; Rotroff et al., 2010; Wetmore et al., 2012; Yoon et al., 2014). The PK knowledge is needed to relate the *in vitro* exposure to the *in vivo* target tissue concentration. Metabolic clearance and dose-response data, both derived from *in vitro* uptake, metabolism and viability, can be used for the estimation of the OED by IVIVE.

Most compounds interfere with cellular carbon metabolism either directly or through effects at the transcriptional level. Determination of uptake and conversion rates of substrates (e.g. glucose) and cellular metabolites (amino acids, urea, lactate, etc.) gives insights into the pathways involved in central carbon metabolism and have been previously used to study drug effects (Niklas et al., 2009; Strigun et al., 2011b).

The human hepatic cell line HepaRG finds increasing application in toxicity studies (Jetten et al., 2013; Mueller et al., 2014) due to long-term functional stability and similarity to primary human hepatocytes in terms of drug metabolizing enzymes i.e. the cytochrome P450 (CYP450) system (Josse et al., 2008; Lübberstedt et al., 2011) and membrane transporters relevant for drug uptake and efflux (Kanebratt and Andersson, 2008).

In the present study, using HepaRG cells, we investigated the hepatotoxic potential of two drugs namely bosentan and valproic acid (VPA); upon acute and repeated-dose exposure for 28 days (14 doses). Viability, stability of CYP450 activity, metabolites of test drugs and drug efflux transporter activity were measured for the assessment of the quality of the test system. Using an IVIVE approach, we estimated the OED from our *in vitro* repeated-dose toxicity data taking EC₁₀ values (effective concentration in 10% of cell population) as lowest threshold of *in vitro* toxicity for the prediction of *in vivo* human toxicity. EC₁₀ values are considered as the lowest concentrations that cause statistically significant cytotoxic effects (Jover et al., 1992). For pathway relevant information, we investigated the alterations in the central carbon metabolism (uptake and secretion rates of selected metabolites) upon exposure to drug concentrations which are in the range of *in vivo* blood levels. The

study aimed at combining *in vitro* repeated-dose data and *in silico* tools for the prediction of OEDs and pathway relevant information for the assessment of repeated-dose toxicity in humans *in vivo*. Our approach is an important step towards replacing animal studies in long-term repeated-dose toxicity evaluations for which no adequate *in vitro* methods exist.

5.3 Methods

5.3.1 Cell culture

The human hepatoma cell line HepaRG was obtained from Biopredic International (St. Grégoire, France). Before seeding, 96-well and 6-well plates (Greiner Bio-One, Frickenhausen, Germany) were incubated for 1 h with 50 µg/mL type I rat collagen (Roche Applied Sciences, Penzberg, Germany) in Dulbecco's Modified Eagle Medium (DMEM, AMIMED BioConcept, Allschwil, Switzerland). Afterwards, wells were rinsed once with 0.1 or 2 mL sterile phosphate buffered saline (PBS) (Gibco Invitrogen, Darmstadt, Germany), respectively and equilibrated with the same volume of Williams Medium E (Pan Biotec, Aidenbach, Germany) overnight. Differentiated HepaRG cells were seeded in triplicates ($n = 3$) four days prior to treatment in collagen coated 96-well plates with a density of 72,000 cells per well for viability and CYP450 activity assay, as well as for the quantification of the drug parent compounds and selected metabolites of central carbon metabolism. For the study of transporter activity ($n = 1$) and quantification of drug metabolites ($n = 3$), cells were seeded in 6-well plates with a density of 2.4 million cells per well. Seeding and maintenance was conducted in Williams Medium E supplemented with 100 U/mL penicillin, 100 µg/mL streptomycin (c.c. pro, Oberdorla, Germany), 50 µM hydrocortisone 21-hemisuccinate, 5 µg/mL human insulin (Sigma Aldrich, St. Louis, MO, USA), 10% (v/v) fetal bovine serum (FBS, PAA Laboratories, Pasching, Austria) and 0.5% (v/v) dimethyl sulfoxide (DMSO, Sigma Aldrich, St. Louis, MO, USA). Medium was renewed one day after seeding as well as one day before treatment using serum-free seeding and maintenance medium, supplemented with 10 ng/mL human hepatocyte growth factor (HGF) (Humanzyme, Chicago, IL, USA) as well as 2 ng/mL mouse epidermal growth factor (EGF) (Sigma Aldrich, St. Louis, MO, USA). Cells were kept in a cell culture incubator (Memmert GmbH, Schwabach, Germany) at 37 °C with 95% relative humidity and 5% CO₂ supply. For reduction of evaporation, outer wells of the 96-well culture plates were filled with sterile distilled water (Gibco Invitrogen, Darmstadt, Germany). Culture medium was replaced with fresh medium (with and without drugs) every second day in the long-term cultures.

5.3.2 Viability assessment

Viability was assessed using the CellTiter-Blue® assay (Promega, Mannheim, Germany). The assay solution was mixed with medium in a ratio of 1:5. Pre-warmed mixture (120 µL) was added to the cells which were incubated for 3 h at 37°C. Fluorescence was detected using a Fluoroskan Ascent CF fluorescence reader (Thermo Labsystems, Vantaa, Finland), measuring emission at 590 nm (excitation 540 nm). Medium without cells served as background control. The fluorescence signals were normalized to the signal of the untreated control at each investigated time point. Sigmoidal curves were fitted to dose-response data using OriginLab 9.0 (OriginLab Corporation, Northampton, MA, USA) and determined parameters were used for the calculation of the EC₁₀ applying equation 5.1;

$$EC_{10} = EC_{50} \times \left(\frac{100 - 10}{10} \right)^{\frac{1}{p}} \quad [5.1]$$

where p represents the hill slope ($p < 0$). Contour graphs were plotted with OriginLab 9.0 to visualize time and dose dependency. From the acute and repeated-dose response curves, the viability at non-overlapping concentrations was estimated using equation 5.2;

$$Viability = BA + \frac{TA - BA}{1 + 10^{(\log x_0 - \log C) \times p}} \quad [5.2]$$

BA and TA are the bottom and top asymptote respectively. $\log x_0$ and $\log C$ represent the common logarithm of the EC_{50} and the drug concentration for which viability was to be calculated. All drug concentrations were corrected for the measured total concentration of the parent compound.

5.3.3 CYP450 activity assay

CYP1A2, CYP2B6, CYP3A4 and CYP2D6 activity was determined as described in a previous study (Klein et al., 2014). Additionally, the activity of CYP2E1 was assessed using chlorzoxazone (Sigma Aldrich, St. Louis, MO, USA) as a substrate with a final concentration of 300 μ M in medium. Cells in a 96-well plate were incubated with 100 μ L of the substrate cocktail for 1 h at 37°C, after which the supernatants were mixed with an equal volume of acetonitrile and frozen immediately. Details of the method are given in supplementary material.

5.3.4 Assessment of efflux transporter activity using fluorescence microscopy

For the comparison of efflux transporter activity in standard serum and serum-free cultivation, HepaRG cells were either cultivated for 4 days in serum as described by Kanebratt and Andersson (Kanebratt and Andersson, 2008) or in serum-free conditions as described before (cell culture). To assess activity of the multidrug resistance-associated protein 2 (MRP2), cells were incubated with 4 μ M of 5-chloromethylfluorescein diacetate (CMFDA, Thermo Fisher Scientific, MA, USA) in Williams Medium E. Additionally, nuclei were stained by the addition of 10 μ M Hoechst 33342 (Sigma Aldrich, Steinheim, Germany). After 15 minutes incubation at 37°C, cells were washed twice with 2.5 ml PBS and fluorescence was monitored using an Olympus IX70 fluorescence microscope (excitation at 494 nm for CMFDA and 555 nm for Hoechst 33342).

5.3.5 Preparation of drug solutions and exposure

For bosentan (Sequoia Research, Pangbourne, UK) a 200 mM stock solution in DMSO and for VPA (Sigma Aldrich, St. Louis, MO, USA) an 80 mM stock solution in serum-free seeding and maintenance medium were prepared. All dilutions were performed in serum-free seeding and maintenance medium. The end concentration of DMSO in all tested dilutions was kept at 0.5%. All drug concentrations and the exposure protocol are depicted in figure S5.1. A summary of the concentrations with the applied analyses is given in table 5.1. In case of the acute toxicity study, the concentrations were applied for 24 hours (1 dose). In the repeated-dose toxicity study, drug concentrations in fresh medium were applied every second day for 28 days (14 doses in total). Concentrations for the repeated-dose toxicity study were chosen from the results of the acute study. These concentrations ranged from 0.05% (lower limit) to 20% (upper limit) of the acute EC_{50} values of the respective drugs.

Table 5.1 List of concentrations used for quantification of drug clearance, central carbon metabolite analyses and drug metabolite quantification. The orally bioavailable concentrations (OBC) calculated from the recommended daily dose (Gabbay et al., 2007; Stefan and Fraunberger, 2005; Suzuki et al., 1991) and bioavailability (Perucca et al., 1978; Weber et al., 1999) are indicated.

	Bosentan [μM]			VPA [mM]		
	Acute	Repeated-dose	OBC	Acute	Repeated-dose	OBC
Drug clearance	38	32	19 to 38	11	0.13	0.5 to 4
Metabolome analysis (High dose)	-	65		-	1.6	
Metabolome analysis (Low dose)	-	32		-	0.13	
Drug metabolite quantification	1297 (EC ₁₀)	-	-	14.8 (EC ₁₀)	-	-

5.3.6 Quantification of drug metabolites

For the quantification of test drug metabolites in HepaRG cultures, cells were incubated with serum-free seeding and maintenance medium (control) or 5 μM rifampicin (Sigma Aldrich, Steinheim, Germany) in serum-free seeding and maintenance medium (induced) for 24 h. Subsequently, control and induced cells were treated with bosentan and VPA with acute (24 h) EC₁₀ (namely; 1.2 mM bosentan and 14.8 mM VPA) of each drug separately. Supernatants were collected after 3 h and 24 h incubation and stored at -80°C until quantification. The detailed method can be found in the supplementary material.

5.3.7 Extraction and quantification of total drug parent compound

For the determination of the *in vitro* drug removal, the total drug parent compound concentrations in medium supernatants were quantified at days 1, 6, 14, 20 and 28. Drugs were extracted from collected medium supernatants using 25 μL sample of cell medium. As reference, supernatants before and after incubation for 48 h at 37°C in cell-free collagen-coated 96-well plates at all sampling points were used.

Internal standards were used for the quantification. These were 15 ng bosentan-¹³C₂,²H₄ sodium salt (Alsachim, Illkirch-Graffenstaden, France) in case of bosentan and 5 μg benzoic acid (Sigma Aldrich, Steinheim, Germany) for VPA. Bosentan was extracted in 75 μL acetonitrile (Sigma Aldrich, Steinheim, Germany). For VPA extraction, acetonitrile was acidified with 0.1% formic acid (Sigma Aldrich, Steinheim, Germany). Samples were vortexed for 30 s, followed by centrifugation at 12,100 g for 10 minutes. 25 μL of the supernatant were collected and diluted with 50 μL MilliQ water.

Quantification was performed with a Perkin Elmer series 200 HPLC connected to an Applied Biosystem-SCIEX API 3000 triple quadrupole mass spectrometer. Details of the method are given in the supplementary material.

5.3.8 Reverse dosimetry for the estimation of the oral equivalent dose

Oral equivalent dose (OED) values were estimated following a published method based on the estimation of hepatic and renal clearance (Wetmore et al., 2012). We calculate OED values for

experimentally determined time-dependent EC_{10} values from the acute and repeated-dose experiment using equation 5.3. All calculations are based on the simplifying assumption of well mixed blood (supplementary figure S5.2).

$$OED = \frac{EC_{10} \times MW \times 24}{BW} \times (GFR \times fu_p + CL_{Hep}) \times \frac{1}{BA_{Oral}} \quad [5.3]$$

OED is the oral equivalent dose (mg/(kg BW \times day) necessary to produce a steady-state *in vivo* blood concentration equivalent to the measured *in vitro* EC_{10} . GFR is the glomerular filtration rate [L/h], fu_p the fraction of unbound compound in plasma [-], and MW and BW the molecular weight [g/mol] and body weight [kg], respectively. BA_{oral} is the *in vivo* oral bioavailability of the compound [-]. *In vivo* hepatic clearance CL_{Hep} was calculated following Poulin et al. (2012);

$$CL_{Hep} = \frac{Q_L \times R_{BP} \times CL_{int} \times \frac{fu_L}{fu_{invitro}}}{Q_L \times R_{BP} + CL_{int} \times \frac{fu_L}{fu_{invitro}}} \quad [5.4]$$

Q_L is the total blood flow in the liver (arterial and portal vein) [L/h], R_{BP} is the blood to plasma concentration ratio of the test compound, CL_{int} the intrinsic clearance rate [L/h] and fu_L the fraction of unbound compound in the liver [-]. $fu_{invitro}$ is the unbound fraction of the compound in the *in vitro* experiment [-] accounting for plastic and protein binding. Since we did not detect plastic binding for the two test compounds and due to the absence of serum proteins in our experiment, $fu_{invitro}$ was set to 1 (supplementary figure S5.3).

CL_{int} was calculated from the measured *in vitro* removal rate constant of the compound (Obach et al., 1997). The calculation took into account the different cellular volumes of HepaRG and primary human hepatocytes (PHH).

$$CL_{int} = k_{invitro} \times LW \times hc \times V_{invitro} \times \frac{V_{PHH}}{V_{HepaRG}} \quad [5.5]$$

$k_{invitro}$ is the *in vitro* first order rate constant calculated for a single cell [1/(cell \times h)] in the case of first order reaction, LW the liver weight [kg], hc the hepatocellularity [cells/(kg liver)], $V_{invitro}$ is the volume used in the *in vitro* incubation [L], V_{PHH} the average volume of a primary hepatocyte and V_{HepaRG} the average volume of a HepaRG cell. In the case of Michaelis-Menten kinetics, the corresponding value of $k_{invitro}$, depends on the compound concentration (supplementary material). The kinetics of removal of the compound in the *in vitro* experiment were determined at different time points of the acute and long-term *in vitro* experiment using a high and low concentration at each time point, including their values at the beginning and after incubation with HepaRG cells. Cell volumes (V_{PHH} and V_{HepaRG}) were estimated based on measured diameters of PHH and HepaRG cells using an automated cell counter (supplementary material and supplementary figure S5.4).

fu_L was calculated according to Poulin et al. (2012) as follows;

$$fu_L = \frac{PLR \times fu_{P,app}}{1 + (PLR - 1) \times fu_{P,app}} \quad [5.6]$$

with *PLR* as the plasma-to-whole-liver concentration ratio, taking into account the extracellular protein binding in plasma relative to liver. $f_{u_{P,app}}$ is the apparent unbound fraction in plasma, taking into account drug ionization, which is an important factor for ionizable compounds since extracellular and intracellular pH differs (7.4 vs. 7.0 respectively) (Poulin et al., 2012).

$$f_{u_{P,app}} = f_{u_P} \frac{1 + 10^{(pH_{Cytosol} - pK_a)}}{1 + 10^{(pH_{Plasma} - pK_a)}} \quad [5.7]$$

All values applied in the calculation of the OED are given in supplementary tables S5.1 and S5.2.

5.3.9 Quantification of the metabolites of the central carbon metabolism in medium

Glucose and lactate were quantified by high-performance liquid chromatography (HPLC) as described previously (Klein et al., 2014). Quantification of branched-chain amino acids (BCAA) valine, leucine and isoleucine was performed with an HPLC method as previously described in depth (Krömer et al., 2005). Urea concentrations were assessed using an HPLC method formerly reported in detail (Clark et al., 2007; Mueller et al., 2012).

5.3.10 Statistical analysis

Unpaired Student's *t*-tests were performed using MatLab 2007b. Differences in two measurements are considered significant at $p < 0.001$, $p < 0.01$ and $p < 0.05$.

5.4 Results

5.4.1 Characterization of the test system

Viability of HepaRG cells upon long-term cultivation

There was no loss of viability of untreated HepaRG cells upon long-term cultivation in serum-free condition (supplementary figure S5.5).

CYP450 activity in HepaRG cells

The CYP450 activity for untreated cultures over the course of 28 days remained stable for most isoforms (supplementary figure S5.6). However, at day 28, CYP3A4 (64% remaining) and CYP2B6 (62% remaining) activities were significantly lower relative to day 6. The other isoforms (CYP2D6, CYP1A2 and CYP2E1) had activities in the same range as on day 6.

Drug efflux transporter activity in serum and serum-free HepaRG cultivation

Microscopic analysis shows that CMFDA, a substrate for MRP2, was concentrated in the bile pockets in both cultivations of HepaRG cells (supplementary figure S5.7).

Quantification of drug metabolites

Drug metabolites were quantified to assess the system's capacity to form major metabolites upon incubation with the parent compounds. In the case of bosentan, all major metabolites described in literature were detected (supplementary figure S5.8A). As for Ro 64-1056, more than one peak was found, probably resulting from hydroxylation at different positions and the compound was therefore referred to as Ro 47-8634-OH. Pre-incubation of the HepaRG cells with rifampicin significantly increased the amount of bosentan metabolites found in the supernatants, except for bosentan

glucuronide. Between 3 and 24 h drug incubation, relative contribution of bosentan metabolites to the total drug molecules in the supernatant increased, while the proportion of the different bosentan metabolites was stable over time (supplementary table S5.3). The two primary metabolites Ro 48-5033 and Ro 47-8634 were the most abundant metabolites, with more than 98% contribution at both time points. In case of VPA, OH-VPA, ene-VPA and VPA glucuronide were detected (supplementary figure S5.8B). Contrary to bosentan, only the glucuronide conjugate concentration increased slightly, when cells were pre-incubated with rifampicin. From 3 to 24 h drug exposure, the amount of VPA glucuronide in the supernatant increased notably (supplementary table S5.4), whereas OH-VPA and ene-VPA metabolites remained below 2% of the drug metabolites. VPA-CoA, 2,4-diene-VPA and keto-VPA could not be detected in the supernatants.

Quantification of the total drug parent compound concentration in vitro

For the evaluation of the concentrations of the tested drugs to which the cells were exposed to in our *in vitro* setup, parent compound drug concentrations were measured before and after 48 h cell-free incubation in 96-well plates at 37°C (supplementary figure S5.3). No statistically significant differences in both bosentan and VPA concentrations upon incubation were observed.

Viability of HepaRG cells upon acute and repeated-dose drug treatment

Dynamic and dose-dependent viability of HepaRG cells upon acute and repeated-dose treatment with bosentan and VPA is depicted in figure 5.1. Additionally, for both drugs, EC₁₀ and EC₅₀ values at different time points are listed in table 5.2. For bosentan, EC₅₀ values ranged from 1,603 µM in case of acute toxicity to 75.9 µM after 4 weeks of repeated-dose application (14 doses in total), whereas the EC₁₀ dropped from 1,297 µM on day 1 to 45.3 µM after 4 weeks of treatment. EC₅₀ values for VPA ranged from 26.1 mM to 0.79 mM. The EC₁₀ after 4 weeks treatment was 0.42 mM as compared to 14.8mM at day 1.

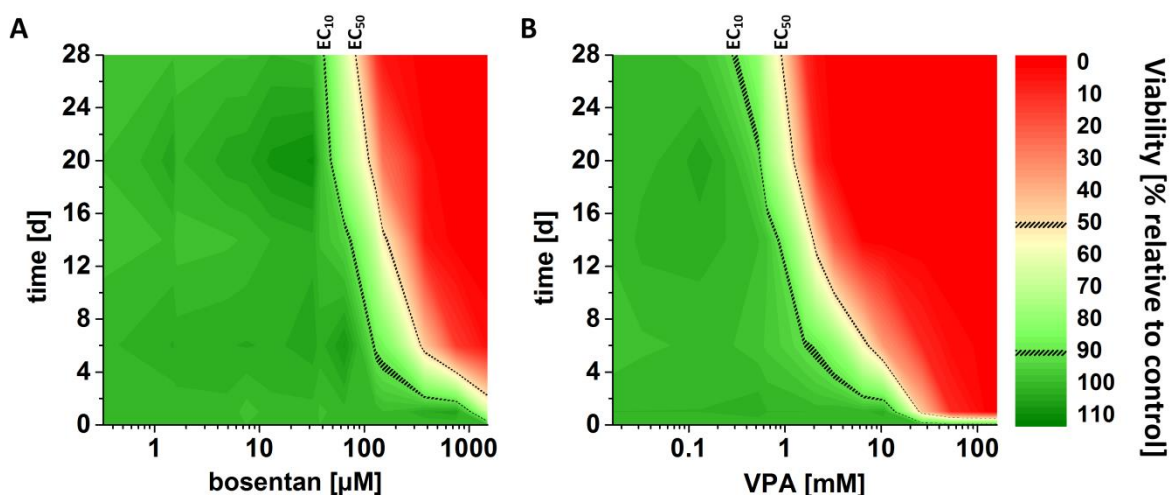


Figure 5.1 Dose-response dynamics upon long-term exposure. Dose-dependent viability of HepaRG cells upon exposure to bosentan (A) and VPA (B) for 28 days. Viability was assessed with an alamarBlue assay. Hashed lines indicate EC₁₀ and EC₅₀ values for all depicted time points. Color indicates viability of the HepaRG cells according to the scale on the right side (green represents high and red represents low viability).

For both drugs, EC₁₀ and EC₅₀ values decreased constantly over time. The highest drop in the EC was observed within the first 6 days of treatment. Upon application of 14 doses EC₅₀ values were reduced 21 fold for bosentan and 33 fold for VPA, compared to values for acute toxicity. Concentrations of 40 µM or lower in case of bosentan and 0.2 mM or lower for VPA did not elicit observable cell death after 4 weeks of treatment (14 doses).

Table 5.2 Summary of EC₁₀ and EC₅₀ values for bosentan and VPA during acute and repeated-dose exposure. Viability was assessed with alamarBlue assay.

time [d]	Bosentan [µM]		VPA [mM]	
	EC ₁₀	EC ₅₀	EC ₁₀	EC ₅₀
1	1,297	1,603	14.8	26.1
6	115.5	316.2	2.06	7.34
14	84.5	157.1	1.15	2.01
20	49.5	103.4	0.58	1.08
28	45.3	75.9	0.42	0.79

5.4.2 Estimation of drug hepatotoxicity potential in humans by using reverse dosimetry

For both drugs, the OEDs over the course of the study are depicted in figure 5.2. For bosentan (figure 5.2A), all individuals of the virtual population remained above the recommended daily dose ($\approx 3.8 \text{ mg}/(\text{kg BW} \times \text{day})$) at all time points. In the case of VPA (figure 5.2B), all estimated OEDs were above the maximum recommended daily dose of $60 \text{ mg}/(\text{kg BW} \times \text{day})$ for two weeks. At the third week, 4% of the population had an OED below that threshold followed by 47% during week 4. The average calculated whole body clearances (renal and hepatic clearance, for all time points and all individuals of the virtual population) were 4.9 ± 2.6 and $43.6 \pm 8.8 \text{ mL}/(\text{h} \times \text{kg BW})$ for bosentan and VPA respectively.

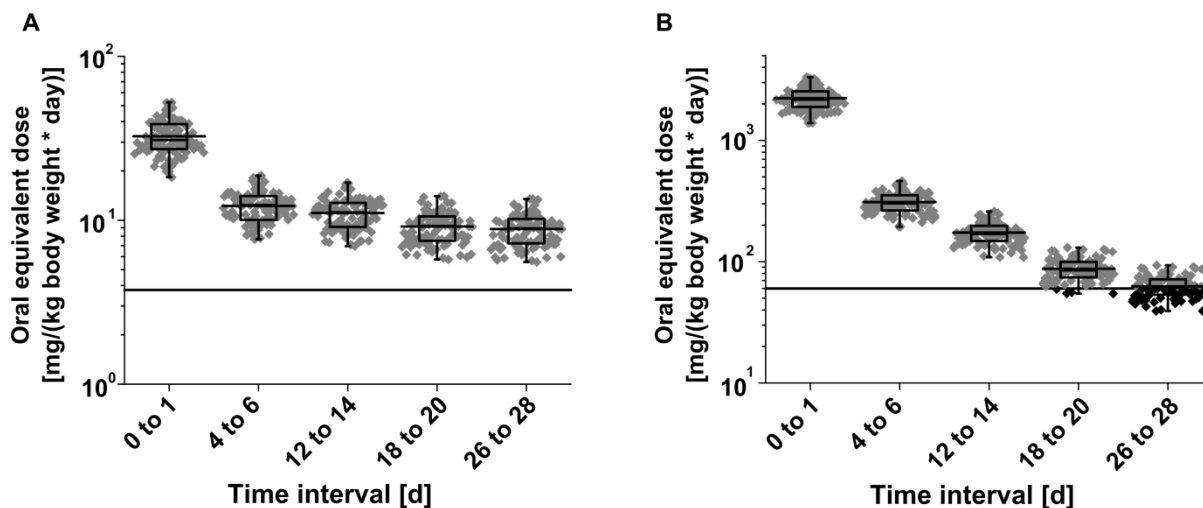


Figure 5.2 Reverse dosimetry. OEDs for bosentan (A) and VPA (B) over 28 days of exposure. OEDs were calculated using equation 5.3 and conditions for which calculations were performed are indicated in table 5.1. Depicted statistical evaluation includes the 25 and 75 percentiles, the median and mean as well as the maximum and minimum values. The straight lines refer to the recommended daily dosage. Individuals of the virtual population ($N=100$) are represented by diamonds and individuals with an OED overlapping the recommended daily dosage are highlighted as black diamonds.

5.4.3 Drug-induced metabolic alterations at orally bioavailable doses

Bosentan

Uptake and secretion rates for glucose, lactate, urea and BCAA in HepaRG cells upon repeated-dose exposure to bosentan are shown in figure 5.3. Viability and the lactate secretion to glucose uptake ratio are also depicted. During repeated-dose exposure to bosentan, glucose uptake was increased relative to the control except for the 4-week time point upon treatment with high dose (65 μ M). Lactate secretion increased upon treatment with high dose until day 20 after which it fell to the level at low dose (32 μ M) on day 28, both being significantly higher than the control. The ratio of lactate secretion and glucose uptake was affected only at the high dose (65 μ M), for which it increased over time to a value of almost 2 on day 28. Uptake of BCAA and secretion of urea were significantly decreased when cells were treated with bosentan. Urea production was decreased to similar levels irrespective of doses. Viability was only affected upon repeated high dose exposure from day 14 onwards dropping to 66% of the control on day 28.

VPA

The rates for metabolite transport in the cells upon exposure to VPA are illustrated in figure 5.4. Until day 14 of repeated high dose (1.6 mM) VPA treatment, glucose uptake was lower than in the control. After 3 weeks of treatment (10 doses) the uptake returned to the original level and eventually surpassed the uptake of glucose in the control. In case of the low dose (0.13 mM) there was a significant increase in glucose uptake at the last sampling point on day 28. Upon repeated high dose exposure, lactate secretion was decreased until day 14 and remained stable afterwards until day 28. However, at repeated low dose exposure, the lactate secretion was increased from day 14 onwards. BCAA uptake rates were significantly lower in the presence of VPA at high dose. Urea secretion was significantly lower as compared to the control irrespective of the dose. Viability was only affected at application of high dose whereby it dropped to roughly 15% after 4 weeks of repeated treatment

(14 doses). Lactate secretion in relation to the glucose consumption was lower upon repeated treatment with high dose than in the control.

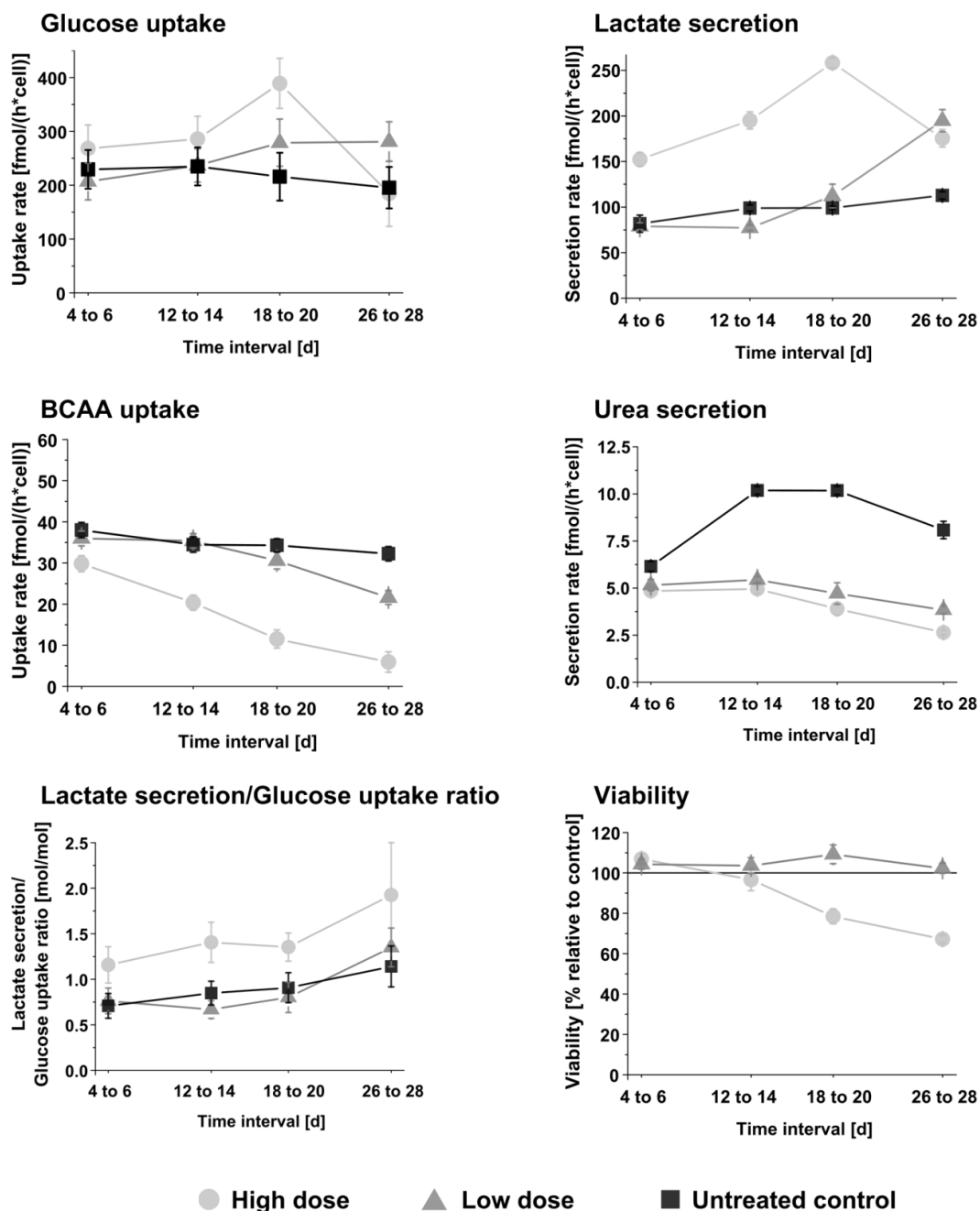


Figure 5.3 Metabolite profiles of HepaRG cells upon long-term bosentan exposure. Uptake and secretion rates for glucose, lactate, branched-chain amino acids (BCAA) and urea in HepaRG cells upon repeated-dose treatment with *in vivo* relevant concentrations of bosentan (65 μ M and 32 μ M corresponding to high and low dose respectively). Viability and the lactate secretion to glucose uptake ratio are also depicted. Error bars indicate standard deviations ($n=3$).

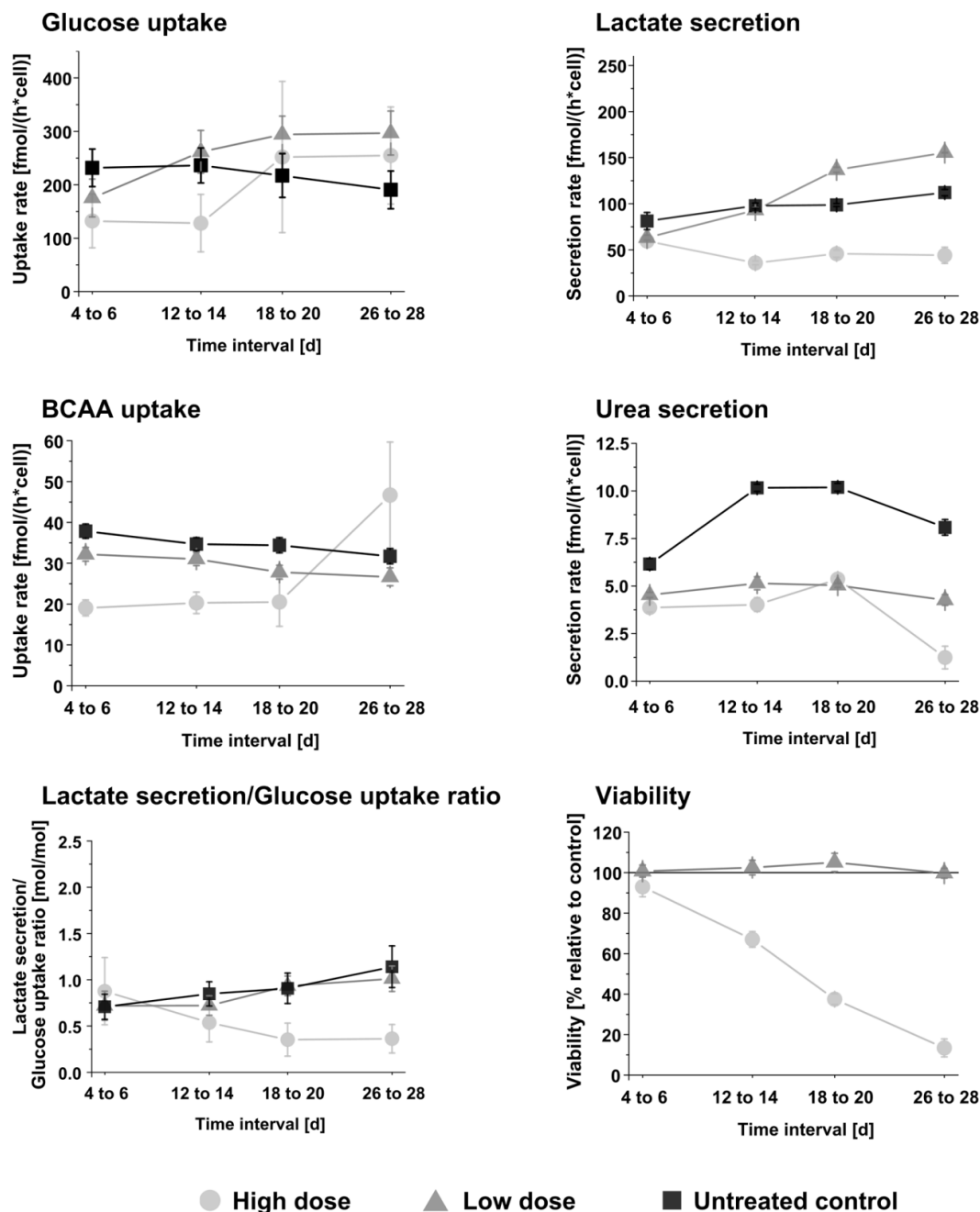


Figure 5.4 Metabolite profiles of HepaRG cells upon long-term VPA exposure. Uptake and secretion rates for glucose, lactate, branched-chain amino acids (BCAA) and urea in HepaRG cells upon repeated-dose treatment with *in vivo* relevant concentrations of VPA (1.6mM and 0.13mM corresponding to high and low dose respectively). Viability and the lactate secretion to glucose uptake ratio are also depicted. Error bars indicate standard deviations ($n=3$).

5.5 Discussion

Reliable prediction of human relevant repeated-dose toxicity using *in vitro* systems and tools is of major interest not only in preclinical drug development in pharmaceutical industry but also in prioritization and de-risking of chemicals in other industries. Recently, biokinetic/toxicodynamic (BK/TD) models were used to study the time course of test compound effects in HepaRG cultures upon acute and long-term exposure (Teng et al., 2015) emphasizing the necessity of long-term

exposure *in vitro* data for the recapitulation of chronic hepatotoxic effects. In the present study, we investigated the hepatotoxic potential of bosentan and VPA on HepaRG cells upon acute and repeated-dose exposure for 28 days and predicted their toxicity on humans *in vivo* by the estimation of the OEDs. At clinically relevant concentrations, changes in central carbon metabolism upon drug exposure *in vitro* provided mechanistic information that will help understand some of the effects observed *in vivo*.

5.5.1 Estimation of drug hepatotoxicity potential in humans by using reverse dosimetry

For bosentan and VPA several cases from mild to severe hepatotoxicity have been reported (Eriksson et al., 2011; Nanau and Neuman, 2013). However, their mechanisms of toxicity are only partially elucidated (Fattinger et al., 2001; Silva et al., 2008). In the case of bosentan, contradictory reports are available. Bosentan was reported to inhibit the bile salt export pump (BSEP) leading to hepatotoxicity (Fattinger et al., 2001). However, a recent study with patients showed that variants of the ABCB11 gene coding for the BSEP transporter are not associated with bosentan hepatotoxicity (Seyfarth et al., 2014). Another study linked the export of bosentan and its glucuronide conjugate to MRP2 rather than BSEP as clearance mechanism (Fahrmayr et al., 2012). CYP3A4 and CYP2C9 are involved in the metabolism of bosentan (Dingemans and Van Giersbergen, 2004; Treiber et al., 2007). Recently it was reported that besides metabolic bioactivation, the toxicity of bosentan is dose dependent (Kenna et al., 2014). As for VPA, complex and multiple effects are reported. Long-term VPA treatment is accompanied by intracellular accumulation of lipids occasionally resulting in microvesicular steatosis, which is not dose-dependent, leading to liver failure (Eadie et al., 1988; Fromenty and Pessayre, 1995). VPA causes elevation in liver transaminases in 5-10% of patients and in more than 100 fatal cases linked to hepatotoxicity have been reported (livertox.nih.gov/Valproate.htm, accessed on July 24th, 2015).

Bosentan causes mild hepatotoxicity in approximately 10 % of patients (Eriksson et al., 2011) necessitating withdrawal of therapy in about 3% of patients (Humbert et al., 2007). In susceptible patients there can be very severe consequences (Mulchey and Bshouty, 2009).

In our study, all members of the virtual population had an OED above the recommended daily dose predicting no adverse effects in these cases within 28-day treatment with bosentan. Comparing the whole body clearance of bosentan estimated from our *in vitro* experiment (4.9 ± 2.6 mL/(h \times kg BW)) to the clearance observed *in vivo* (116.6 ± 30.0 mL/(h \times kg BW)) (Ubeaud et al., 1995), the predicted clearance of bosentan in our study is almost 24-fold underestimated which had an impact on our calculated OEDs. Under- and overestimation of clearances is a major problem in *in vitro* pharmacokinetic studies and there are many attempts to overcome this obstacle by introducing further parameters into the estimation of clearances (Berezhkovskiy, 2011; Berezhkovskiy et al., 2009; Poulin et al., 2012). In the case of bosentan, underestimation of the hepatic clearance can be related to the absence of serum in our setup. A 14 times lower clearance for bosentan is reported when the incubation was performed in a serum-free instead of serum-supplemented environment (Blanchard et al., 2006). It is hypothesized that not only the unbound fraction of a compound can be taken up into the cells but compound-protein complexes can be similarly involved in uptake processes (Blanchard et al., 2004).

Regarding VPA, the incidence of liver failure is estimated to be below 0.02% (Nanau and Neuman, 2013). However mild hepatotoxicity (elevation of liver enzymes) is around 11% (Powell-Jackson et al., 1984). The doses upon which hepatotoxicity occurs range from 0.1 to 80 mg/(kg BW \times day). Infants and polymedicated patients are more susceptible to VPA hepatotoxicity (Nanau and Neuman,

2013). Moreover, inducers of CYP2E1 such as ethanol have been reported to increase hepatotoxicity of VPA (Neuman et al., 2001). In our study, after 4 weeks, 47% of the virtual population had an OED below the maximum recommended daily dose ($\approx 60 \text{ mg}/(\text{kg BW} \times \text{day})$) predicting hepatotoxic effects for these cases. VPA has a very wide therapeutic dose range. Thus, for better comparison, *in vitro* dosing should be adapted to specific recommended dosing in patients for patient-specific prediction. The whole body clearance for VPA *in vivo* was in the range of 17.0 ± 10.6 for men and $16.1 \pm 17.5 \text{ mL}/(\text{h} \times \text{kg BW})$ in women (Perucca et al., 1984). Our estimations were above these values with $43.6 \pm 8.9 \text{ mL}/(\text{h} \times \text{kg BW})$. In the case of VPA, the absence of serum had no major effects on the prediction of clearance.

Our *in silico* approach allows easy estimation of hepatic clearance and is amenable to high throughput setups. However, as a result of its simplicity there are some limitations and aspects like accumulation and distribution of compounds in tissues were not considered. In addition, many drugs show substantial serum binding and their uptake into the cells is complex. Therefore, it should be considered in the assessment and calculation of *in vitro* hepatic clearances. Moreover, incorporation of data on transport, permeability and metabolism is expected to improve predictions (Poulin, 2013).

5.5.2 Drug-induced metabolic alterations at orally bioavailable drug doses

Many drugs interfere with central carbon metabolism of cells disturbing metabolic homeostasis. These changes can provide important insights on the adverse outcome pathways. In this study, we investigated key metabolites in the central carbon metabolism of HepaRG cells upon exposure to *in vivo* relevant concentrations of bosentan and VPA. These selected concentrations were derived from dosing recommendations and oral bioavailability. Bosentan has not been reported to have any direct effects on enzymes involved in the central carbon metabolism. In our *in vitro* study we see an increased uptake of glucose with time. Collapse of glucose uptake (also lactate production) as observed after 4 weeks of treatment with a high dose could be the result of insulin resistance effected by repression of the GLUT4 gene, related to chronic PPAR α activation (Finck et al., 2005; Said et al., 2005). There was a steady increase in lactate production until day 20 of the experiment. Lactate is reported to be a marker for cellular stress (Limonciel et al., 2011). We observed an increase in the lactate to glucose ratio which may be due to increased expression of LDH which is involved in conversion of pyruvate to lactate. Increase in LDH is reported to be due to the activation of HIF-1 α (Kim et al., 2006) which is a known receptor for reactive oxygen species. Accumulation of bosentan and its metabolites probably results in oxidative stress in hepatocytes. These hypotheses must be confirmed by additional experiments. Furthermore, urea formation in hepatocytes was shown to be impaired upon exposure to bosentan (Chatterjee et al., 2013). However, in that study, it was not evident whether this effect was only due to loss of cells or due to effects of bosentan on cellular metabolism. We show that bosentan severely reduces urea formation and BCAA uptake.

Effects of VPA on the central carbon metabolism are manifold (Nanau and Neuman, 2013; Wang et al., 2012). Our observations support previous studies that show that VPA-CoA and other metabolites influence the carbon metabolism directly by inhibiting the dihydrolipoyl dehydrogenase, a subunit of the branched-chain α -ketoacid dehydrogenase complex (BCKDC) and pyruvate dehydrogenase complex (PDC) (Luís et al., 2007). VPA exposure resulted in a decrease in the lactate to glucose ratio although the formation of reactive oxygen species upon treatment is reported (Kiang et al., 2011). As VPA-CoA impairs the access of pyruvate to the TCA cycle by inhibiting the PDC, it is likely that pyruvate is converted into acetyl-CoA which then serves as a building block for fatty acid synthesis, contributing to the emergence of steatosis. Increasing concentrations of fatty acids are reported to up-regulate the glycolytic genes (Kota et al., 2005). Indeed, chronic VPA treatment is linked to metabolic

syndromes (Nanau and Neuman, 2013). In addition, we observed significantly decreased rates in urea secretion during repeated dosing. This is an indirect hint to urea cycle disruption upon long-term repeated-dose exposure to VPA. This effect may stem from the inhibition of N-acetylglutamate synthase which leads to hyperammonemia in certain patients (Aires et al., 2011). Again this hypothesis needs further investigation for verification. Nevertheless, patients with certain metabolic predispositions such as ornithine transcarbamylase deficiency resulting in hyperammonemia might be more susceptible to drug toxicity as a result of additional stress elicited by impaired ammonia removal.

5.6 Conclusion

Long-term repeated-dose *in vitro* toxicity data can be used for the prediction of human relevant toxicity using a simple *in silico* method of IVIVE. Metabolic changes upon drug exposure to *in vivo* relevant concentrations identify key players in cellular stress related to idiosyncratic toxicity. This knowledge can help in the adjustment of individual dosing regimens in a step towards personalized medicine. The methods can be adapted to compound screenings for long-term repeated-dose effects and could significantly contribute to animal-free assessment of toxicity.

5.7 Acknowledgements

This work was supported by the European Community's Seventh Framework Programme (FP7/2007-2013) under grant agreement N° 267038 and Cosmetics Europe within the SEURAT-1 NOTOX project. We thank Michel Fritz for technical assistance. The drug metabolites were measured at Pharmacelsus GmbH, Saarbrücken, Germany.

Chapter 6 Systems toxicological evaluation of valproic acid-induced toxicity in HepaRG cells

6.1 Abstract

Novel *in vitro* systems combined with state of the art –omics technologies yield unrivaled insights into the mechanisms underlying drug-induced toxicity. Here, we investigated VPA-induced toxicity in the human hepatic cell line HepaRG in a repeated dosing setup and combined functional assays with different –omics layers, i.e. transcriptomics, proteomics, metabolomics and fluxomics. HepaRG cells were exposed to VPA for 14 days, with a total of 7 doses in a serum-free setup. Measurements were performed for different time points throughout the exposure. Functional parameters were affected in a dose-dependent fashion, with an EC_{50} value of 0.85 ± 0.18 mM after 2-week exposure. Further, the composition of formed VPA metabolites was strictly dependent on the external dose. –Omics data revealed indications of endoplasmic reticulum stress, impaired urea cycle activity and early depletion of ATP. In conclusion, using this multi –omics approach it was possible to get a deeper insight into the underlying processes than with any of the –omics techniques alone and to reveal interesting aspects of VPA-induced toxicity. In the future, the wealth of the gained information gained with such an approach may not only help to improve current risk assessment approaches, but may eventually help in replacing animal studies.

The data used in this chapter is an excerpt of the data collected by several groups within the NOTOX project. The complete data set is used for the preparation of a separate manuscript including the following coauthors (list is subject to change; order is arbitrary):

Klein S, Tascher G, Plumel M, van Dorsselaer A, Bertile F, Mueller D, Heinzle E, Noor F, Kattler K, Luksic P, Tierling S, Walter J, Johannson I, Ingelman-Sundberg M, Sapony J, Tanay A, Bucher J, Mauch K, Shevchenko V, Guguen-Guillouzo C, Chesné C, Mitic-Potkrajac D, Apic G, Zamboni N, Fuhrer T, Maggioni S

6.2 Introduction

Assessment of potential hazards related to the exposure to a compound is an integral part not only in drug development, but also within several other industrial branches. Historically, *in vivo* animal studies were the method of choice to assess toxicity and even today they play a major role therein. Yet, ethical concerns, questionable correlation of results with the heterogeneous human population, high costs and not least legislative incentives cause industry to rethink, and consider to expand the application of alternative methods, i.e. *in vitro*- and *in silico*-based tools (Blaauboer and Andersen, 2007; Olson et al., 2000; Shukla et al., 2010; Westmoreland et al., 2010).

As such, tools like skin, hepatic or cardiac *in vitro* systems of human origin may provide similar or even superior reliability regarding the prediction of a compound's toxicity or pharmacokinetics in humans, compared to *in vivo* animal studies. Particularly when relevant properties differ largely from one species to another, human *in vitro* systems are beneficial (National Research Council, 2007; Zhang et al., 2012). Examples for such systems are primary human hepatocytes (PHH) and the human hepatic HepaRG cell line, which in several instances has been shown to be a suitable surrogate for PHH (Hart et al., 2010; Lübberstedt et al., 2011). Together with powerful analytical tools such as transcriptomics, proteomics or metabolomics, these systems allow to generate a wealth of reliable information that greatly contributes to a mechanistic understanding of the underlying processes and can be used to create predictive models or be applied within the adverse outcome pathway framework (Cui and Paules, 2010; Sturla et al., 2014; Vinken, 2015). Even more, the data obtained by such an approach may help in optimizing culture conditions for cells in general, and thereby further increase reliability of the output.

In the past few years, the number of publications combining several –omics layers, i.e. multi –omics approaches were growing exponentially, however, in the field of toxicology, multi –omics studies remain scarce. Yet, they allow even deeper understanding and provide useful information required in setting up holistic models (Kim et al., 2016; Wilmes et al., 2013). Besides the requirement of additional instruments, one potential reason for the reluctance in performing multi –omics studies may be related to the challenging integration and interpretation of the data originating from the different –omics layers, requiring experts from various fields. The integration of multi –omics data is a hurdle that is increasingly receiving attention in recent studies (Acharjee et al., 2016; Bersanelli et al., 2016; Schumacher et al., 2014; Shu et al., 2016).

One of the major challenges in today's risk assessment is the assessment of toxicity occurring upon repeated exposure to a compound. We have previously tackled this problem for two hepatotoxic compounds, bosentan and valproic acid (VPA), using the HepaRG cell line in a repeated dosing regimen in combination with a reverse dosimetry approach (Klein et al., 2016). VPA is a particularly interesting drug to study in a multi –omics setup as it interacts with a wide range of targets, broadly affecting cellular behavior. One example is the inhibitory effect of VPA on the histone deacetylase (HDAC), causing hyperacetylation of histones and thereby changing gene expression (Göttlicher et al., 2001). On the metabolic level, VPA interferes with amino acid metabolism, fatty acid beta-oxidation, urea cycle and other pathways, eventually resulting in microvesicular steatosis (Aires et al., 2011, 2010, 2008, Luís et al., 2011, 2007).

Here, we were using VPA as a model compound and investigated its effects in a repeated dosing regimen on several functional parameters in HepaRG cells, including viability, cytochrome P450 (CYP450) activity, triacylglyceride levels as well as drug uptake and metabolism. Further, we investigated the effects of the drug on transcript, protein, metabolite and flux levels, yielding a

comprehensive overall survey of the cellular state. In-depth characterization of the cell line upon drug exposure allows better understanding of the underlying mechanisms eliciting toxicity, and further, setting up extensive models for the prediction of toxicity, greatly aiding reliable hazard assessment.

6.3 Methods

6.3.1 Cell Culture

HepaRG cells were obtained from Biopredic International (Saint-Grégoire, France). For proteomics and transcriptomics analyses, cells were seeded in 6-well plates, intra- and extracellular metabolomics samples were taken from 24-well plates and all other measurements were conducted in 96-well plates (figure S6.1A). Before seeding, the well surfaces were coated with type I rat collagen applying a 50 µg/ml collagen solution in Dulbecco's Modified Eagle medium (DMEM; AMIMED BioConcept, Allschwil, Switzerland), followed by 1 h incubation at 37°C. Wells were then rinsed once with phosphate buffered saline (PBS; Gibco Invitrogen, Darmstadt, Germany). Next, the coating was equilibrated with Williams Medium E (WME; Pan Biotec, Aidenbach, Germany) for 1 h at room temperature, after which the medium was discarded. For seeding in 6- and 24-well plates, 2.4×10^6 and 4.8×10^5 cells were used respectively, with a concentration of 9.6×10^5 cells/ml. For 96-well plates, the cell number was 7.2×10^4 and the concentration was 7.2×10^5 cells/ml. Seeding and cultivation of cells prior to start of analyses, as well as medium composition are described in figure S6.1B. The basal medium was WME supplemented with 100 U/ml penicillin, 100 µg/ml streptomycin (c.c.pro GmbH, Oberdorla, Germany). In case growth factors (GF) were included, 10 ng/ml human hepatocyte growth factor (HGF) (Humanzyme, Chicago, IL, USA) and 2 ng/ml mouse epidermal growth factor (EGF) (Sigma-Aldrich) were added. The medium that was used throughout the experiment after precultivation will be referred to as cultivation medium subsequently. Cells were cultivated in a cell culture incubator (Memmert, Schwabach, Germany) at 37°C with 95% relative humidity and 5% CO₂ supply.

6.3.2 Viability assessment

Viability was assessed using a resazurin-based assay (CellTiter-Blue® Cell Viability Assay, Promega, Mannheim, Germany). To conduct the assay, supernatants were replaced with 100 µl of a 1:5 mixture of the resazurin solution in cultivation medium, previously heated to 37°C. The cells were then incubated in the cell culture incubator for 3 h. Afterwards, supernatants were transferred into new plates and fluorescence was detected using a Fluoroskan Ascent CF fluorescence reader (Thermo Labsystems, Vantaa, Finland). Excitation was performed at 540 nm and emission was quantified at 590 nm. A cell-free incubation served to assess the background signal. The fluorescence signals from treated samples were then normalized to the signal of the untreated control at the corresponding days.

6.3.3 Dose response curve

From a 100 mM VPA (Sigma Aldrich, St. Louis, MO, USA) stock solution in cultivation medium, drug concentrations ranging from 15 mM to 5×10^{-3} mM were prepared in cultivation medium. VPA was subsequently applied to the cells in a volume of 100 µl for 14 days, with medium renewal every second day (7 doses in total). Viability was assessed as described above.

6.3.4 ATP quantification

ATP was quantified from the same plates that were used for viability assessment by applying the CellTiter-Glo® Luminescent Cell Viability Assay (Promega, Mannheim, Germany) after supernatants

had been transferred to another plate. The assay was conducted according to manufacturer's instructions. Relative luminescence signals from treated samples were normalized to the signal of the untreated control at the corresponding days.

6.3.5 Oil Red staining

For quantification of neutral lipids, an Oil Red O staining was applied by first aspirating the culture medium. Afterwards, cells were washed twice with 110 μ l PBS. Cells were then fixed with 100 μ l of a 3.7% formaldehyde solution for 10 minutes. The formaldehyde solution was removed and cells were covered with 50 μ l fresh Oil Red O (Sigma Aldrich, St. Louis, MO, USA) working solution. The working solution was prepared by first dissolving Oil Red O in isopropanol (0.35% w/v), which was then mixed with H₂O_{dest} in a ratio of 3:2. After 15 minutes incubation, cells were washed 3 times with 130 μ l tap water to remove unbound dye. Water was removed and wells were left until remaining water evaporated completely. For extraction of the bound dye, 100 μ l isopropanol were added into each well, and plates were kept on a microplate mixer for 20 minutes. The solution was diluted 1:5 with isopropanol and 100 μ l of the dilution were transferred into new 96-well plates, followed by measuring the absorbance at 500 nm. Oil Red signals were normalized to the cell number calculated from the viability data.

6.3.6 Quantification of CYP450 activity

The activity of four CYP450 isoforms, namely CYP1A2, CYP2B6, CYP2D6 and CYP3A4 was quantified via a liquid chromatography-mass spectrometer (LC-MS) method at Biopredic International, France. The same method has been applied in previous studies and is described in detail in chapter 4.

6.3.7 Drug metabolite quantification

Drug metabolites were quantified at Mario Negri Institute, Italy. For the determination of VPA and VPA metabolite concentrations in the medium supernatants, compounds were extracted from collected medium using a volume of 25 μ l, to which an internal standard (valproic acid-d₆, Toronto Research Chemicals, Canada) was added. Then, 75 μ l acetonitrile, acidified with 0.1% formic acid (Sigma Aldrich, Steinheim, Germany) were added and samples were vortexed for 30 s, followed by centrifugation at 12,100 g for 10 minutes. 25 μ l of the supernatant were collected and diluted with 50 μ l MilliQ water.

The instrumental system is a Perkin Elmer series 200 HPLC connected to an Applied Biosystem-SCIEX API 3000 triple quadrupole mass spectrometer. An Ascentis Express-C18 column 150 \times 2.1 mm i.d., 2.7 μ m particle size (Supelco, Bellefonte, PA, USA), was used for chromatographic separation. The mobile phases were 0.05% formic acid in MilliQ water for negative ionization (A) and acetonitrile (B) with a gradient set as follow: from 30 to 100% B in 10 min, 100% B for 2 min, 100 to 30% B in 2 min, 30% B for 7 min, at 180 μ l/min. 10 μ l sample was injected into the system. The turbo ion spray source temperature was 350°C, the ion spray voltage was set at -4200 V, the nebulizer gas was set at 7 units and the curtain gas at 8. The optimized LC-MS/MS parameters for the selected compounds are summarized in the table S6.1.

6.3.8 Quantification of intracellular metabolites

Sample preparation

After collection of supernatants, cells were washed twice with 600 μ l of freshly prepared washing solution. Washing solution was 75 mM ammonium acetate in water, with a pH of 7.4, which was adjusted by addition of acetic acid. For extraction of metabolites, 150 μ l of a cold (-20°C) acetonitrile:methanol:water (40:40:20) mixture were added to the cells, which were then incubated for 10 minutes at -20°C . After incubation, supernatants were transferred into tubes and the extraction procedure was repeated once. Before transferring the supernatants into the tubes the second time, cells were scraped off using rubber-policemen (Sarstedt, Nuembrecht, Germany). Then, the suspension was transferred into its corresponding tube and tubes were centrifuged at 12,100 g for 2 minutes in a centrifuge cooled down to 4°C . 200 μ l of the supernatants were transferred into fresh vials and stored at -20°C until analysis.

Metabolite quantification

For quantification, samples were shipped to Nicola Zamboni at the Institute of Molecular Systems Biology at the ETH Zurich. Metabolites were quantified with flow injection Time-of-flight mass spectrometry as described in detail by Fuhrer et al. (Fuhrer et al., 2011).

Data processing

The first steps of data processing, i.e. ion annotation and matching, were performed by Nicola Zamboni as described in the publication highlighted above.

Next, all annotations were curated manually, i.e. metabolites were checked for potential occurrence in *in vitro* cultures of human liver cells. Metabolites not possible to occur in these cultures, e.g. those related to food or drug intake, or similar conditions, were considered unknown and labeled accordingly. Medium components including VPA and its metabolites were considered an exception and original names were kept. Afterwards, in case of duplicates, the metabolite with the higher score was kept and the other metabolite was considered unknown. In some instances, signal intensity was “1”, i.e. the metabolite could not be detected in that sample. Metabolites were removed from further analysis when more than 20% of the samples had a signal intensity of “1” for that metabolite. This led to removal of two metabolites. Remaining “1” were imputed a random number between 0 and the measured minimum signal intensity for the corresponding metabolite (excluding “1”) to prevent a negative impact on statistical evaluation. As a last step, cell numbers calculated from the viability determined with the CellTiter-Blue® Cell Viability Assay were included to receive signal intensities per 10^3 cells.

6.3.9 Quantification of intracellular proteins

Sample preparation

Samples were collected and analyzed by Georg Tascher from CNRS, Strasbourg. At each time point, cells were washed twice with warm (37°C) and twice with cold (4°C) PBS before lysis in the culture plates using lysis buffer containing 50 mM Tris, 150 mM NaCl, 1 mM EDTA, 0.1% (w/v) N-lauryl sarcosine and protease inhibitors (Sigma Aldrich, St. Louis, MO, USA). After 30 minutes at 4°C , cells were scraped off the plates using a rubber-policeman and cell debris was pelleted by centrifugation at $5,000 \times g$ for 10 minutes at 4°C . Supernatants were snap-frozen in liquid nitrogen and stored at -80°C before further analysis. Protein concentration in the cell extracts was estimated by a Bradford assay using BSA as standard (Bio-Rad, Hercules, CA, USA). 50 μ g of protein of each sample were

precipitated with 10% trichloroacetic acid overnight at 4°C. After centrifugation (10 minutes at 13,000 × g), protein pellets were washed with tetrahydrofuran (3 × 400 µL) to remove remaining salts and co-precipitated lauroyl sarcosinate. Proteins were solubilized in 200 µl of denaturation buffer (Urea 8 M, NH₄HCO₃ 0,1 M), disulfide bonds were reduced with 12 mM dithiothreitol (30 minutes at 37°C) and free sulfhydryl groups were alkylated using 40 mM iodoacetamide during one hour at room temperature in the dark. Afterwards, samples were diluted with digestion buffer (NH₄HCO₃ 0.1 mM) to reduce concentration of urea below 1 M, and proteins were digested with trypsin (Promega, Mannheim, Germany) at a trypsin-to-protein-ratio of 1:100 overnight at 37°C. Trypsin activity was quenched by the addition of formic acid to a final concentration of about 0.5% and peptides were cleaned-up using SPE cartridges (SEP-PAK tC18, 50 ccm; Waters, Milford, MA, USA). Sample volume and organic solvent concentration were reduced using a vacuum centrifuge (SpeedVac Savant, Thermo, St. Herblain, France) and samples were adjusted to 100 µl with 0.1% formic acid in water before MS-analysis.

Mass spectrometry analysis

Peptide mixtures were analyzed on a NanoACQUITY UPLC system (Waters, Milford, MA, USA) coupled to an Impact-HD Q-TOF mass spectrometer equipped with Captive Spray source and nano booster (Bruker Daltonics, Bremen, Germany). Both instruments were controlled by Hystar V3.2 and OtofControl Rev. 3.4 (Bruker Daltonics, Bremen, Germany). The solvent system consisted of 0.1% formic acid in water (solvent A) and 0.1% formic acid in acetonitrile (solvent B). 1 µg of sample was injected and first trapped on a precolumn (BEH C18, 180 µm × 20 mm, 5 µm; Waters, Milford, MA, USA) at 1% B at a flow rate of 5 µl/minute for 3 minutes and then eluted to a separation column (BEH C18, 250 mm × 75 µm, 1.7 µm; Waters, Milford, MA, USA) using a 180-minute gradient from 2 to 35% B at 450 nl/min. The Impact HD was operating in positive mode using the following settings: Source temperature was set to 150°C while dry gas flow was 3 l/minute and spray voltage was optimized to -1300 V. Acetonitrile was used as dopant in the nano booster and nebulizer pressure was set to 0.2 bar. Spectra were acquired by automatic switching between MS and MS/MS modes in the mass range of 100-2200 m/z with a fixed cycle time of 3 seconds. MS acquisition rate was set to 2.5 Hz and MS/MS acquisition rate ranged from 3 to 25 Hz depending on the precursor intensity. Preferably, ions with a charge of 2 to 5 were selected for CID fragmentation using nitrogen as collision gas. Ions were excluded from fragmentation after the acquisition of 1 MS/MS spectrum and exclusion was released after 1 minute, but only if precursor intensity did not exceed the value during the first selection by a factor of at least 3. If this was the case, the precursor was again fragmented to increase MS/MS spectra quality and excluded for 1 minute starting from this second fragmentation event. Online correction of TOF calibration was performed using hexakis(2,2,3,3,3-tetrafluoropropoxy)phosphazine ([M+H]⁺ 922.0098 m/z) as lock-mass which was spiked into the dopant solvent and thus continuously delivered together with the nebulizer gas.

Protein identification

Peak lists in mascot generic format were generated using Data Analysis (version 4.0; Bruker Daltonics, Bremen, Germany) and searched against a SwissProt-derived combined target-decoy database (created 2014-02-10, containing 20372 target sequences plus the same number of reversed decoy sequences) using Mascot (v2.3.02; Matrix Science, London, UK). The database contained sequences of human proteins including common contaminants and was created using an in-house database generation toolbox (Carapito et al., 2014). During database search, up to one missed cleavage by trypsin and two variable modifications (oxidation of methionine (+16 Da) and carbamidomethylation of cysteine (+57 Da)) were considered. The search window was set to 15 ppm

for precursor ions and 0.02 Da for fragment ions. Peptide and protein identifications were validated in Scaffold (v3.6.5; Proteome Software, Portland, OR, USA). Only peptides with a minimum ion score of 25 were considered and both protein and peptide false discovery rate was adjusted below 1% by adjusting the discriminant score (i.e. ion score minus identity score).

Protein quantification

Before quantification, peptides shared between proteins as well as peptides containing methionine(s) were removed from the dataset. Ion chromatograms were extracted using Skyline v2.1 (Schilling et al., 2012) using a window of 3 minutes around retention times of MS/MS identifications and a resolving power of 40,000. All extracted ion chromatograms were validated by visual inspection and area under curve of P, P+1 and P+2 ions were summed per peptide. After quantile normalization using Normalyzer v1.0 (Chawade et al., 2014), intraprotein-correlation of peptide abundance profiles across all experimental conditions was checked by comparing individual peptide intensities to a “model profile” (generated by averaging peptide signals for each protein and within each condition) using Pearson’s correlation. For proteins with only one peptide quantified, no correlation analysis could be performed. For proteins with two peptides, proteins were removed if both peptides exhibited a Pearson’s correlation coefficient below 0.8. For proteins with three peptides, if less than 3 peptides had a Pearson’s correlation coefficient above 0.8, the peptide with the lowest correlation coefficient was excluded from the dataset. For proteins with 4 peptides or more, the 25% of peptides with the lowest correlation coefficients were removed if their correlation coefficient was below 0.8. In total, less than 10% of all identified peptides were excluded due to low correlation.

6.3.10 Gene expression analysis

Total RNA extraction

The RNA for transcriptomic studies was extracted using the AllPrep DNA/RNA/Protein kit (Qiagen, Hilden, Germany) according to the manufacturer’s recommendation. The HepaRG cells were lysed directly in the culture dishes. RNA preparations from all samples maintained high quality and showed a mean RNA integrity number of 9.22 ± 0.14 .

Gene expression analysis

RNA samples were received by Inger Johannsson and submitted to the Bioinformatic and Expression Analysis (BEA) core facility (Karolinska Institutet, Huddinge, Sweden) for subsequent processing and gene expression analysis. Whole genome gene expression was determined using the Affymetrix® GeneChip Human Transcriptome Arrays 2.0 (Affymetrix, SantaClara, CA, USA) following the manufacturer’s instructions. The raw data (.cel files) was analyzed using the Signal Space Transformation-Robust Multichip Analysis (SST-RMA) sketch in Affymetrix® Expression Console™ software.

6.3.11 Quantification of extracellular metabolites and flux analysis

Metabolite quantification in supernatants

Glucose, pyruvate and lactate in the supernatant were quantified using a Kontron HPLC (Kontron Instruments, Neufahrn, Germany) as described previously in detail (Hans et al., 2003). Amino acids and urea were quantified in an Agilent 1100 HPLC system (Agilent, Waldbronn, Germany). Technicalities on the methods have been elaborated before (Clark et al., 2007; Klein et al., 2014; Krömer et al., 2005). Albumin was quantified using a reverse ELISA Kit (Albuwell II, Exocell, Philadelphia, PA, USA) as described by the manufacturer.

Secretion rates and metabolic flux analysis

From measured extracellular metabolite concentrations, secretion rates v_i were calculated using equation 6.1.

$$v_i = \frac{c_{i,t_1} - c_{i,t_0}}{(t_1 - t_0) \times X} \times V \quad [6.1]$$

C_i is the concentration of a metabolite i at a given time point ($t1$, $t0$). X represents the mean cell number during the cultivation and V is the culture volume.

For the calculation of intracellular fluxes, a stoichiometric model, consisting of several metabolic pathways was generated. The model includes the glycolytic pathway, the tricarboxylic acid (TCA) cycle including anaplerotic reactions, the urea cycle and production of albumin, with a total of 53 reactions (figure S6.2 and table S6.2). The rates of 23 of those reactions were assessed directly from the extracellular concentrations as described above. The remaining 30 fluxes (intracellular reaction rates) were assessed by applying the principles of metabolite balancing (Varma and Palsson, 1994a, 1994b), assuming pseudo steady-state as previously described (Niklas et al., 2009) with equation 6.2.

$$v_c = S_c^{-1} \times (-S_m \times v_m) \quad [6.2]$$

S_c and S_m are the matrices describing the stoichiometry of the metabolic network for calculated (c), or measured (m) conditions, with v_c and v_m representing the calculated and measured rates, respectively. Solutions for fluxes and standard deviations were determined using a Monte–Carlo simulation ($n = 100$) with standard deviations of the measured rates as input error using MatLab 2007b (MathWorks, Nattick, MA, USA). The resulting mean values are reported.

6.3.12 Statistics*Student's t-test*

Unpaired Student's t -tests were performed using Excel 2010 (Microsoft, Redmond, WA, USA). T -tests with subsequent multiple testing correction via the Benjamini-Hochberg procedure were performed within the MetaboAnalyst 3.0 Software (Xia et al., 2015).

Principal component analysis

The signal intensity for each metabolite i , SI_i was normalized to the cell number calculated from the resazurin-based viability data. Subsequently, data was \log_2 -transformed and Pareto-scaled and then subjected to a principal component analysis (PCA) to reduce the complexity of the data set. Loading coefficients were determined to identify the relevance of the individual metabolites to separation of the data points as well as potential outliers. The PCA was performed using MatLab 2007b (MathWorks, Nattick, MA, USA).

Fold changes

\log_2 fold changes were calculated by simple division as described in equation 6.3,

$$\log_2 fc = \log_2 \left(\frac{SI_1}{SI_0} \right) \quad [6.3]$$

where SI_t and SI_0 represent the signal intensities of two different conditions or time points, normalized to the cell number using the data obtained with the resazurin-based viability assay.

6.4 Results

6.4.1 Viability and ATP content upon repeated exposure to VPA

First, a dose response curve of HepaRG cells exposed to VPA for 14 days (in total 7 doses) was prepared (figure 6.1) to identify concentrations for further in-depth investigation. The EC_{50} value was $0.85 \text{ mM} \pm 0.18 \text{ mM}$.

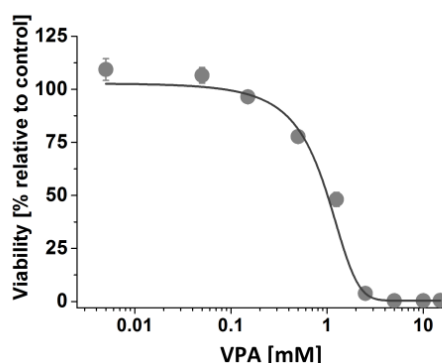


Figure 6.1 Dose response curve of HepaRG cells upon 14-day repeated valproic acid (VPA) exposure. Viability was assessed after 14 days of VPA treatment (7 doses) using a resazurin-based viability assay and normalizing results to the untreated control. Error bars indicate standard deviation ($n = 3$).

The following three concentrations of VPA below the 2-week EC_{50} value were selected for more comprehensive analyses: 0.05, 0.15 and 0.5 mM VPA. Viability and the cellular ATP content were assessed during a 14-day period (figure 6.2). Viability was significantly reduced to 87.8% on day 14, after exposure to 7 doses of 0.5 mM VPA. ATP levels on the other hand were decreased stepwise, with both time and concentration within 14-day treatment. Reduction in ATP content was significant from day 8 onwards for HepaRG cells exposed to 0.5 mM VPA. Levels were 77.9% and 58.4% relative to the control at day 8 and 14 respectively.

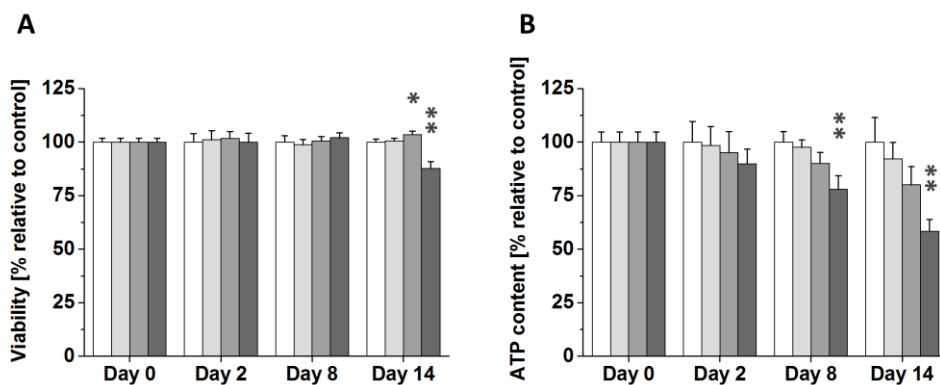


Figure 6.2 Viability (A) and ATP content (B) in HepaRG cells upon repeated valproic acid (VPA) exposure. HepaRG cells were exposed to VPA for 14 days with 7 doses in total. Parameters were assessed at indicated time points using a resazurin-based viability assay and a luminescence-based assay for ATP quantification. Results were normalized to the untreated control (white bars) at the corresponding time points. Results for the different concentrations of VPA, 0.05, 0.15 and 0.5 mM are represented by light, medium and dark grey bars. Error bars indicate standard deviation ($n = 3$). * and ** indicate p -values of < 0.05 and < 0.01 upon unpaired Student's t -test in comparison to the control respectively.

6.4.2 Morphological observations upon repeated VPA exposure

Effects of VPA treatment on cellular morphology were investigated using light microscopy (figure 6.3). On day 2, the morphology of HepaRG cells was indistinguishable between treated cells and the untreated control. On day 14, cell detachment was visible in case of the 0.5 mM condition. This was concluded from uncovered spots on the plate surface and spherically shaped cells floating in the medium. The latter effect could also be observed for the cells treated with lower concentrations, however to a notably less pronounced extent. There was no sign of major lipid accumulation, e.g. in the form of large lipid vacuoles or alterations in cellular shape, under any of the tested conditions.

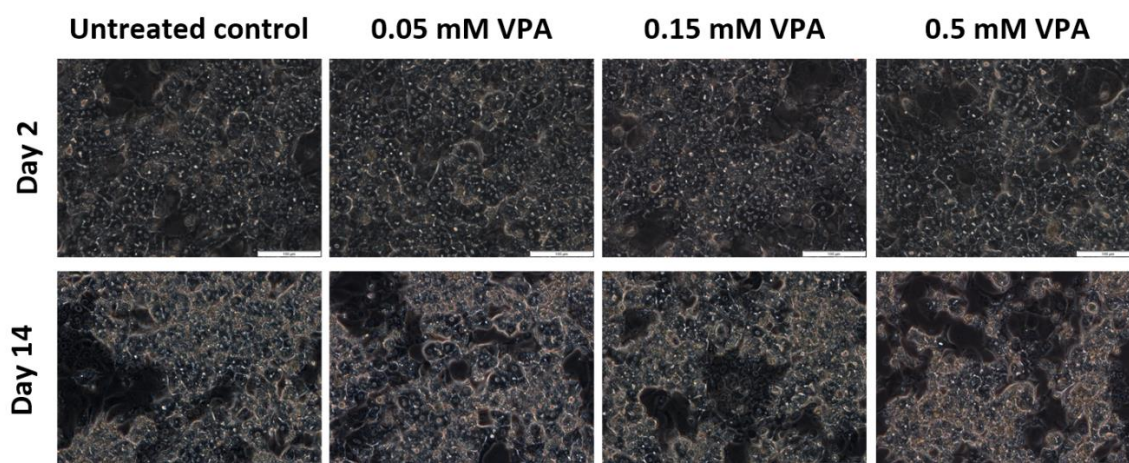


Figure 6.3 Light microscopic pictures of HepaRG cells during repeated valproic acid (VPA) exposure. Pictures were taken using a light microscope with phase contrast. Flattened cells represent biliary epithelial-like cells, and elevated and brighter cells represent hepatocyte-like cells. White bars represent 100 μm .

6.4.3 Triacylglyceride quantification upon repeated VPA exposure

The cellular content of triacylglycerides was assessed using an Oil Red staining (figure 6.4). On day 2, a dose-dependent effect was observed with the triacylglyceride content being significantly elevated in case of treatment with 0.15 and 0.5 mM VPA (128% and 139% relative to the control respectively). In the following days, triacylglycerides returned to normal levels, except for the 0.5 mM condition, for which levels remained significantly elevated on day 8 and 14 with 131% and 127% respectively.

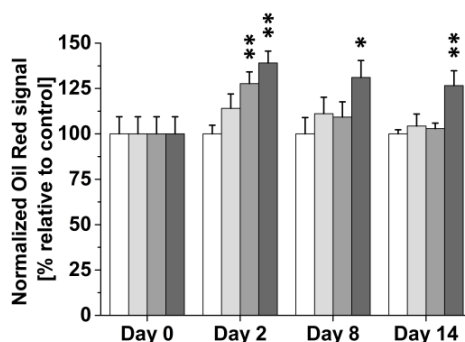


Figure 6.4 Quantification of cellular triglyceride content based on Oil Red staining. Signals were normalized to the cell number and to the untreated control (white bars) at each day. The different concentrations of valproic acid (VPA), 0.05, 0.15 and 0.5 mM are represented by light, medium and dark grey bars respectively. Error bars indicate standard deviation ($n = 3$). Significance of differences was tested for VPA treatment compared to the untreated control using an unpaired Student's *t*-test at each time point, with *p*-value thresholds of < 0.05 (*) and < 0.01 (**).

6.4.4 CYP450 activity in HepaRG cells repeatedly exposed to VPA

The activity of different CYP450 isoforms and effects of VPA on their activities were assessed during the 14-day period (figure 6.5, absolute values in table S6.3). For CYP1A2, significantly reduced activity was observed only on day 14, independent of the dose. CYP2B6 activity was generally independent of VPA treatment. For both, CYP2D6 and CYP3A4 on the other hand, activity was significantly reduced in a dose-dependent manner, starting on day 2 and 8 respectively. In both cases, the decrease was strongest on day 14 with exposure to the highest concentration of VPA, with a reduction to 32% for CYP2D6 and 35% in case of CYP3A4, relative to the initial activity.

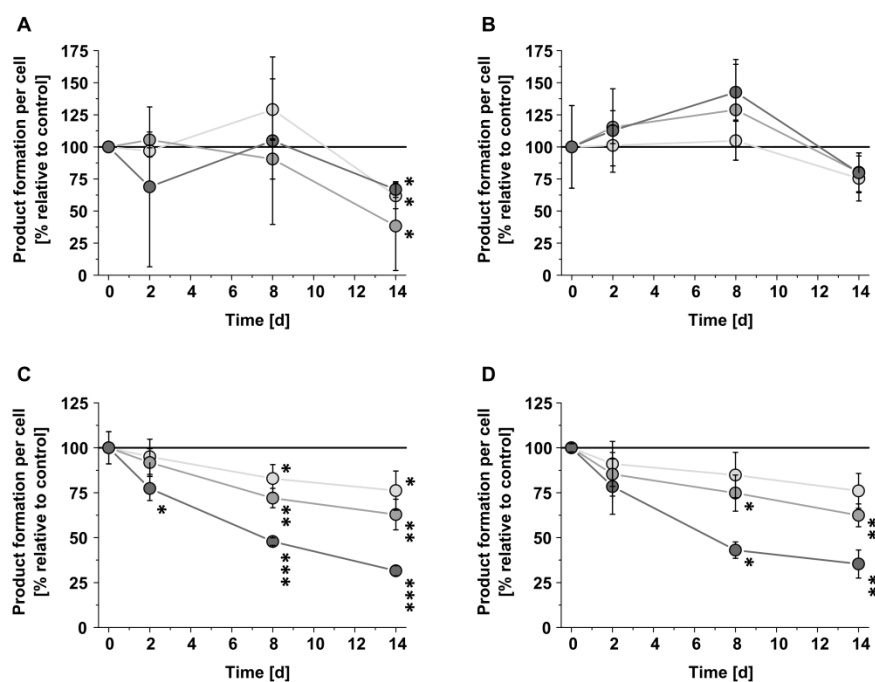


Figure 6.5 Dynamic CYP450 activities in HepaRG cultures upon repeated exposure to valproic acid (VPA) normalized to the untreated control at each day. CYP1A2 (A), CYP2B6 (B), CYP2D6 (C) and CYP3A4 (D) activities are given. The different concentrations of VPA are represented by light, medium and dark grey colors (0.05, 0.15 and 0.5 mM VPA respectively). The horizontal line at 100% indicates activity of the control and error bars indicate standard deviation ($n = 3$). To test for differences between VPA-treated cells and the untreated control, an unpaired Student's *t*-test was performed at each time point, with *p*-value thresholds of < 0.05 , < 0.01 and < 0.001 (*, ** and *** respectively). Measurements have been performed by Valery Shevchenko at Biopredic International, Saint Grégoire.

6.4.5 Time profile of VPA removal and metabolism

Specific removal of VPA and secretion of VPA metabolites were quantified using an LC-MS approach (figure 6.6). Removal of VPA increased significantly from day 2 to day 8 from 3.1 to 7.7 fmol/(cell \times day) in case of 0.05 mM VPA treatment, while no increase was observed from day 8 to day 14. In case of treatment with 0.15 mM VPA, removal was constant over all investigated time points, with an average removal of 14.5 fmol/(cell \times day). When HepaRG cells were treated with 0.5 mM VPA, removal on day 2 was 87.5 fmol/(cell \times day), which then declined significantly to 70.4 and 56.7 fmol/(cell \times day) on day 8 and 14 respectively.

The secretion of VPA metabolites was monitored over time: VPA-beta-D-glucuronide (VPA-glucuronide), 3-keto-VPA, 3-OH- and 4-OH-VPA (figure 6.6.B). In case of HepaRG cells treated with 0.05 mM VPA, the major metabolite was 3-keto-VPA with 82% on day 2, decreasing to 75% of the measured released metabolites on day 8 and 14. The metabolite with the second highest prevalence was VPA-glucuronide with 15% on day 2, increasing stepwise to 23% on day 14. Both metabolites of VPA also play the major role when HepaRG cells were treated with 0.15 and 0.5 mM VPA, but VPA-glucuronide became the metabolite with the highest abundance in the extracellular compartment. For 0.15 mM VPA treatment, levels ranged from 60 to 66%, and in case of 0.5 mM VPA treatment, percentages were 77 to 87%. Also for the minor metabolites, i.e. 3-OH- and 4-OH-VPA a trend upon exposure to different concentrations of VPA could be observed. The percentage of 3-OH-VPA decreased with exposure to higher concentrations of VPA, with a trend towards increase over time in

all conditions. In case of 4-OH-VPA, the trend was less clear, but levels seemed to decrease with increasing VPA concentrations. Overall, the effect of different VPA concentrations was more pronounced than effects of treatment duration.

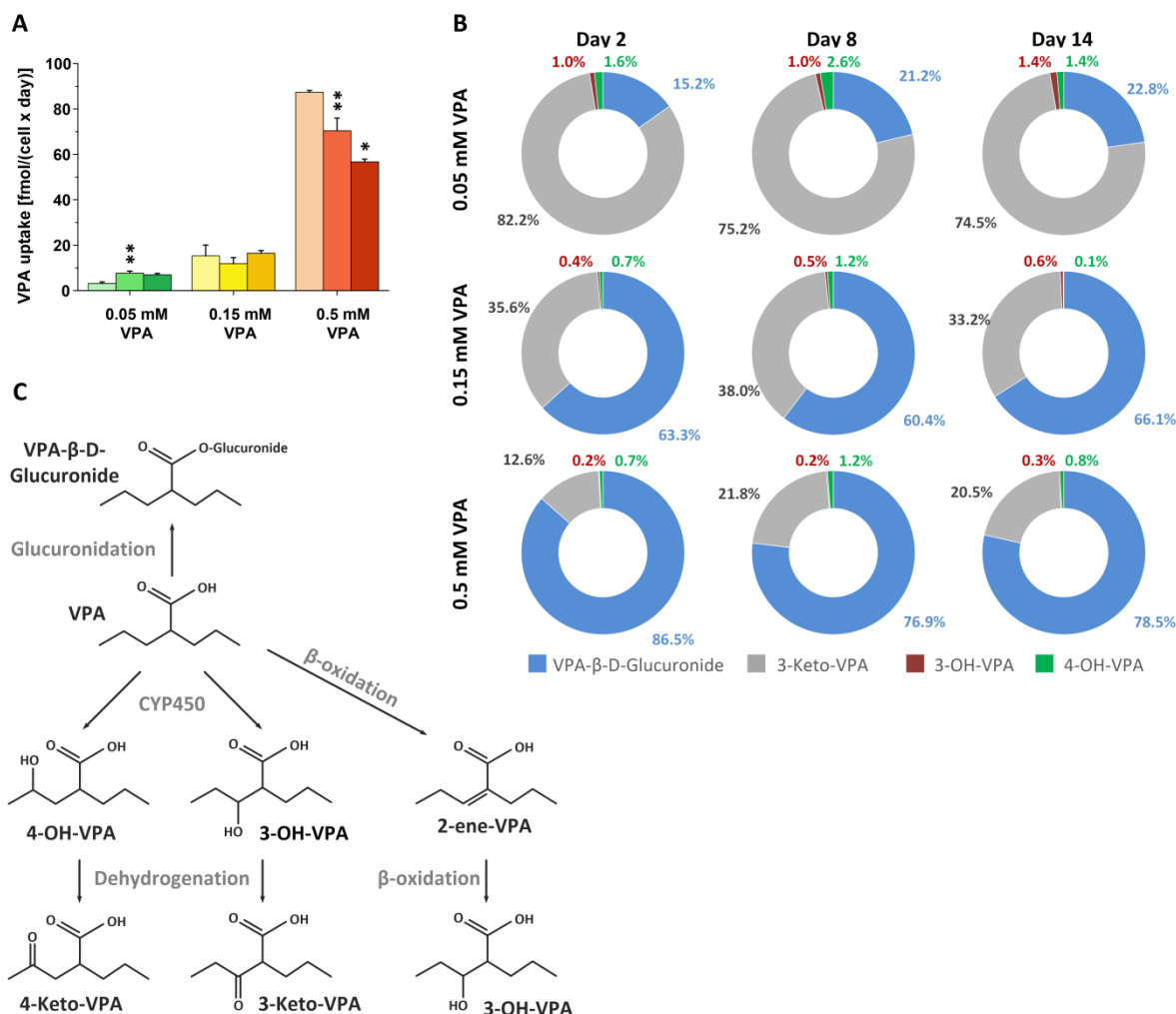


Figure 6.6 Specific valproic acid (VPA) removal and metabolite formation in HepaRG cells during repeated dose long-term exposure. VPA removal at different time points is indicated by light, medium and dark colors for day 2, 8 and 14 respectively (A). Error bars indicate standard deviation ($n = 3$). Significance of differences to the preceding time point within one condition was tested using an unpaired Student's t -test. * and ** indicate p -values of < 0.05 and < 0.01 respectively. Dynamic relative composition of the secreted VPA metabolites upon treatment with different concentrations is represented by ring plots (B). Percentage is given relative to the sum of the four metabolites quantified within the study. Associated pathways for the metabolization of VPA (C). The Graph was adapted from Kiang et al. 2011. Measurements have been performed by Silvia Maggioni at the Mario Negri Institute, Milan.

6.4.6 Metabolic alterations upon repeated VPA exposure

A PCA was performed on the signal intensities of the intracellular metabolites, normalized to the cell number (figure 6.7). Along PC1, there is a clear formation of two clusters - on the one hand, all conditions on day 0 and day 2, and on the other hand all conditions on day 8 and day 14. Along PC2,

there is a trend, separating the control and treatment with low concentrations from treatment with 0.5 mM VPA. With progression of time, the cluster of HepaRG cells treated with 0.5 mM VPA more clearly separates from the other conditions. As for the loadings plot (figure S6.3), metabolites were homogeneously distributed and there was no sign of outlying metabolites.

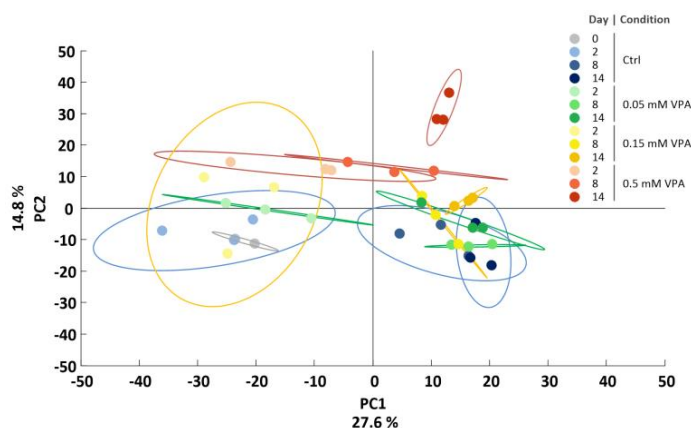


Figure 6.7 Principal component (PC) analysis on the intracellular metabolome data. The PCA was performed on the normalized intracellular metabolome data obtained at all time points and drug concentrations including the control ($n = 3$). The first two PC are depicted and ellipses correspond to the 95% confidence intervals. The loadings plot is depicted in figure S6.3. Measurement of the underlying data has been performed by Nicola Zamboni at ETH Zurich.

Volcano plots comparing treatment with different concentrations (figure 6.8, list of highlighted metabolites in table S6.3) and comparing changes within one condition over time (figure S6.4) were prepared to identify critical time points and concentrations, as well as pathways most affected by VPA exposure. Similar to the PCA, it is seen in the volcano plots that alterations in metabolite levels induced by cultivation alone are more pronounced than effects induced by drug exposure. The number of metabolites exceeding the thresholds set for fold change and p -value increase with both, time and concentration (figure 6.8). When treated with 0.05 and 0.15 mM VPA, elevated metabolite levels are predominant among the significant metabolites, while for treatment with 0.5 mM, decreased levels prevail for the metabolites of interest. Even more, on day 8 and 14, the number of metabolites with significantly decreased levels ($|\log_2 \text{fold change}| > 1$) is higher in the controls, than in treated HepaRG cells. On the other hand, metabolites with significantly increased levels are notably higher in treated cells, compared to the control at the corresponding time points. While for HepaRG cells treated with 0.5 mM VPA 72 metabolites are significantly altered already on day 2 ($|\log_2 \text{fold change}| > 1$), major changes do not occur until day 8 for HepaRG cells exposed to 0.05 and 0.15 mM VPA. However, as the same findings apply to the control, it is not clear whether effects originate from cultivation or drug exposure.

Using the volcano plots, pathways of highest relevance upon VPA exposure were identified. Most hits were related to nucleotide metabolism, amino acid metabolism including dipeptides and fatty acid metabolism including acylglycines. To a lesser extent, changes in glycolytic intermediates as well as TCA cycle metabolites and metabolites involved in drug metabolism were observed.

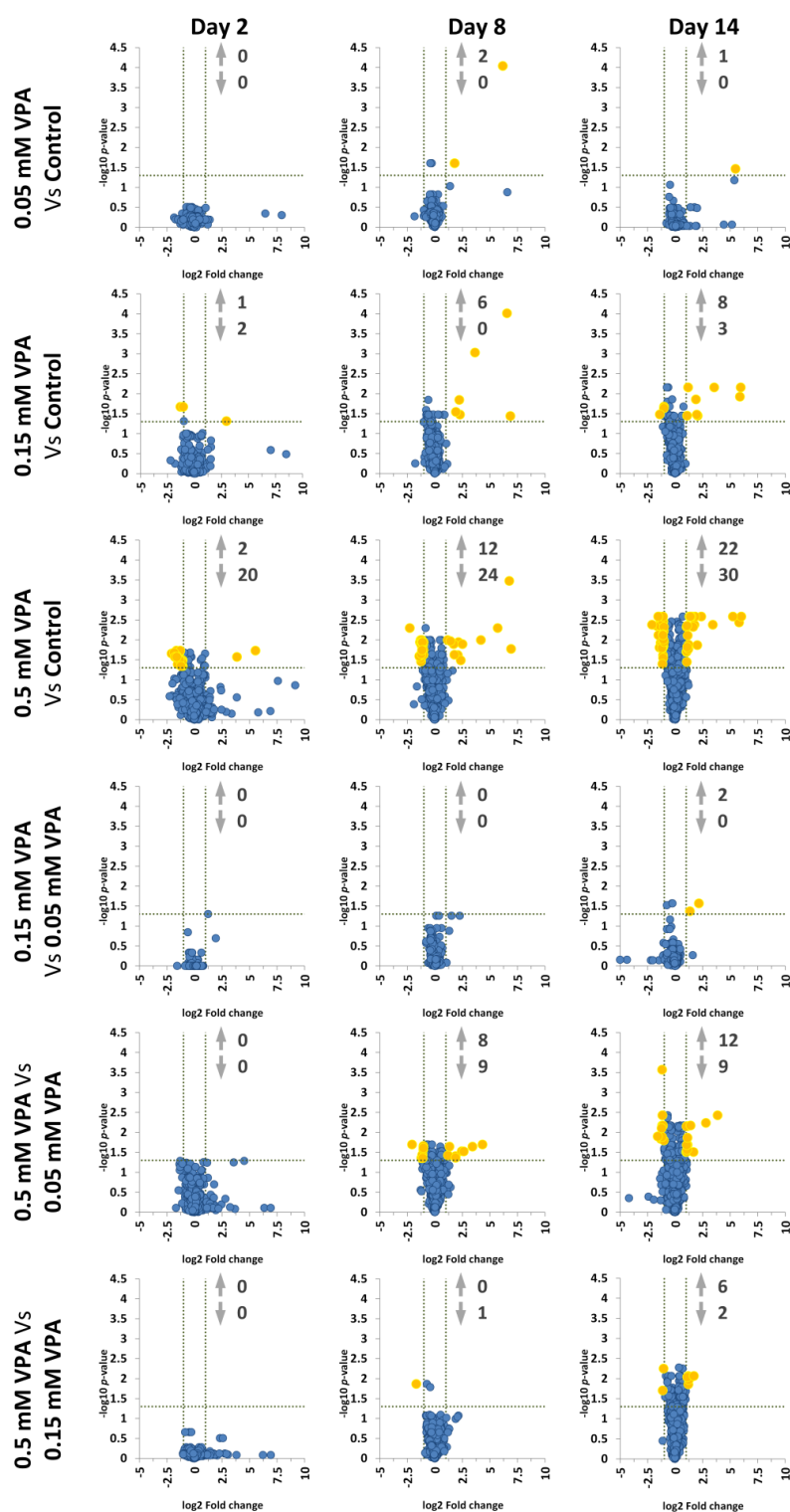


Figure 6.8 Volcano plot comparing the intracellular metabolome in HepaRG cells upon exposure to different concentrations of valproic acid (VPA). A p -value of 0.05 and an absolute \log_2 fold change of 1 were selected as thresholds which are indicated by dotted lines. Metabolites exceeding both thresholds are highlighted as yellow circles, while all other metabolites are depicted as blue circles. For the former, metabolites are further distinguished according to whether levels are decreasing or increasing, with corresponding numbers indicated. The p -values are based on a t -test with subsequent Benjamini-Hochberg correction for multiple testing. Measurement of the underlying data has been performed by Nicola Zamboni at ETH Zurich.

6.4.7 Effects of repeated VPA treatment on different cellular levels

An overview on intracellular metabolites (M) and enzymes (P) in the previously identified pathways has been plotted with indication of changes upon VPA exposure (figure 6.9). Detailed time courses and data on transcripts and fluxes (F) are given in the supplementary (figures S6.5 to S6.9)

Fatty acid metabolism

Metabolites related to fatty acid metabolism were significantly increased in HepaRG cells upon treatment with VPA (figure 6.9, figure S6.5). These metabolites include octanoyl-CoA, an intermediate of fatty acid β -oxidation, derivatives of β -oxidation intermediates, such as (R)-3-hydroxyoctadecanoic acid and octanoic acid, as well as acylglycines. Likewise, enzymes involved in β -oxidation were found to be upregulated in HepaRG cells upon VPA treatment (figure 6.9, figure S6.5 P1 to P8). On the other hand, levels of enzymes related to fatty acid synthesis (FASN, P9), triacylglycerol synthesis (glycerol-3-phosphate dehydrogenase, P10) and activation of fatty acids (acyl-coenzyme A synthetases, P11, 12) were decreased, with exception of the long-chain fatty acid CoA ligase 1 (P13) (figure S6.5, figure 6.9). The trend observed for the enzymes likewise was found for the corresponding transcripts.

Nucleotide metabolism

Regarding nucleotide metabolism, with increasing VPA concentration, levels of metabolites either decreased from the beginning of the study (5-phosphoribosyl-N-formylglycineamide, aminoimidazoleribotide, adenosine, guanosine, thymine, (R)-5,6-dihydrothymine, 5,6-dihydrouracil, 3-ureidopropionate, CDP, CTP, ADP, UTP) or remained unaltered initially but then decreased at a later time point (1-(5'-phosphoribosyl)-5-formamido-4-imidazolecarboxamide, orotidylate, inosine, urate, β -alanine), independent of the anabolic or catabolic nature of the pathways (figure 6.9 and figure S6.6). There were few notable exceptions to this observation. Only in case of dADP (M41), a significant increase in concentration was observed. Interestingly, levels of nucleoside monophosphates increased initially (not significantly), but eventually declined as shown for uridine, inosine and guanosine monophosphate (UMP, IMP, GMP; M35, M15, M38), as well as xanthine (M20). In respect to the enzymes involved in pyrimidine catabolism, dihydropyrimidine dehydrogenase levels (P15) decreased upon VPA exposure, while there was no trend on transcript level. Contrary, a subunit of the ribonucleotide reductase (RRM2, P16) was found to be upregulated with treatment. The enzyme is responsible for the formation of deoxyribonucleotides from ribonucleotides.

Amino acid metabolism

Intracellular levels of L-glutamate, L-glutamine and glycine were generally lower when HepaRG cells were exposed to VPA (figure 6.9 and figure S6.7). Alterations in metabolic fluxes were observed for the conversion of 2-oxoglutarate into L-glutamate (F4), being reduced when cells were treated with VPA. The uptake of L-glutamine and its subsequent conversion into L-glutamate on the other hand were increased in case of treatment (F2, F5). Uptake of glycine and L-glutamate were generally low and effects of VPA on cellular intake were minor (F1, F3).

Intracellular levels of the branched-chain amino acid (BCAA) L-isoleucine were significantly elevated with treatment, and concentrations of propanoate (figure 6.9, figure S6.7 M54), a late metabolite of L-valine degradation, were lower upon treatment. The uptake of the three BCAA was reduced in a dose-dependent manner when HepaRG cells were exposed to VPA (figure S6.7 F6 to F8). Expression of the enzyme catalyzing the first step in the catabolism of BCAA, the BCAA aminotransferase (figure 6.9, figure S6.7 P17), was not affected by VPA treatment, neither on the level of transcripts nor on protein

level. Protein concentrations and to a lesser extent transcript levels of the methylcrotonyl-CoA carboxylase (P18), which is involved in L-leucine catabolism, were elevated with VPA treatment. Further, there was a slight trend towards upregulation of the short/branched-chain specific acyl-CoA dehydrogenase (P19). The enzyme catalyzes a step in the catabolism of L-isoleucine, but may also use valproyl-CoA as a substrate.

Levels of metabolites closely related to L-serine and L-cysteine, i.e. L-homocysteine and L-cystathionine (figure 6.9, figure S6.7 M57, M58) were elevated with treatment.

With exposure to VPA, intracellular concentrations of metabolites of the urea cycle, i.e. L-arginine and L-ornithine significantly increased and decreased, respectively. Levels of guanidinoacetate (M65), which marks the first step in the formation of creatine, were slightly elevated, whereas concentrations of the two subsequent metabolites creatine and phosphocreatine (figure 6.9 M66, M67) were lower with VPA treatment. The carbamoyl-phosphate synthase (P20), which catalyzes the first committed step in the urea cycle, and the arginase 1 (P21), decreased in a dose-dependent fashion on protein and transcript level upon VPA treatment. For the glycine amidinotransferase (P22), the trend was towards increasing protein concentrations when exposed to VPA.

Several dipeptides were quantified and in many cases concentrations significantly declined with exposure as shown exemplarily for asparaginyl-proline (figure S6.7 M75). For two dipeptidyl peptidases, DPP3 and CTSC (figure S6.7 P23, P24), we found interesting but opposing trends, i.e. decreasing and increasing levels respectively

Carbohydrate metabolism

Trends for the intermediates of the glycolytic pathway were mixed, e.g. with levels of 3-phospho-D-glyceroyl phosphate decreasing and phosphoenolpyruvate increasing upon exposure to VPA (figure 6.9 M78, M80). Other quantified intermediates did not change significantly (M77, M79 and M81). Uptake of D-glucose, secretion of lactate as well glycolytic fluxes (figure S6.8 F10 to F13) declined with treatment. The ratio of secretion of lactate relative to glucose intake initially dropped from 1.26 on day 0, to 0.84 on day 4, and eventually rose to 1.45 on day 14. Similar to effects on glycolytic fluxes, VPA caused downregulation of several of the corresponding enzymes and transcripts (ALDOB (P25), PKLR (P26), LDHA (P28), PFKL (P30); figure 6.9, figure S6.8).

Concentrations of all quantified TCA cycle intermediates (cis-aconitate, citrate, fumarate, (S)-malate) decreased with treatment, with exception of 2-oxoglutarate (figure 6.9, figure S6.8). Likewise, the fluxes of the corresponding reactions decreased with VPA exposure (figure S6.8 F14, F15). In case of the pentose phosphate pathway, transcripts and protein levels of glucose-6-phosphate 1-dehydrogenase (P31) increased upon VPA exposure.

Miscellaneous pathways

Generally, identified proteins in the context of oxidative phosphorylation were observed to be upregulated on protein level upon exposure to VPA (figure S6.9 P33 to P39).

Concentrations of 3-hydroxybutyryl-carnitine were significantly increased when cells were exposed to VPA (figure S6.9 M104). Levels of (R)-mevalonate on the other hand were lower in treated cells compared to the control (figure 6.9, figure S6.9 M105). Two enzymes, hydroxymethylglutaryl-CoA synthase 2 (mitochondrial) and 1 (cytosolic) are responsible for the formation of ketone bodies and the first step of the cholesterol synthesis via the mevalonate pathway respectively. While the

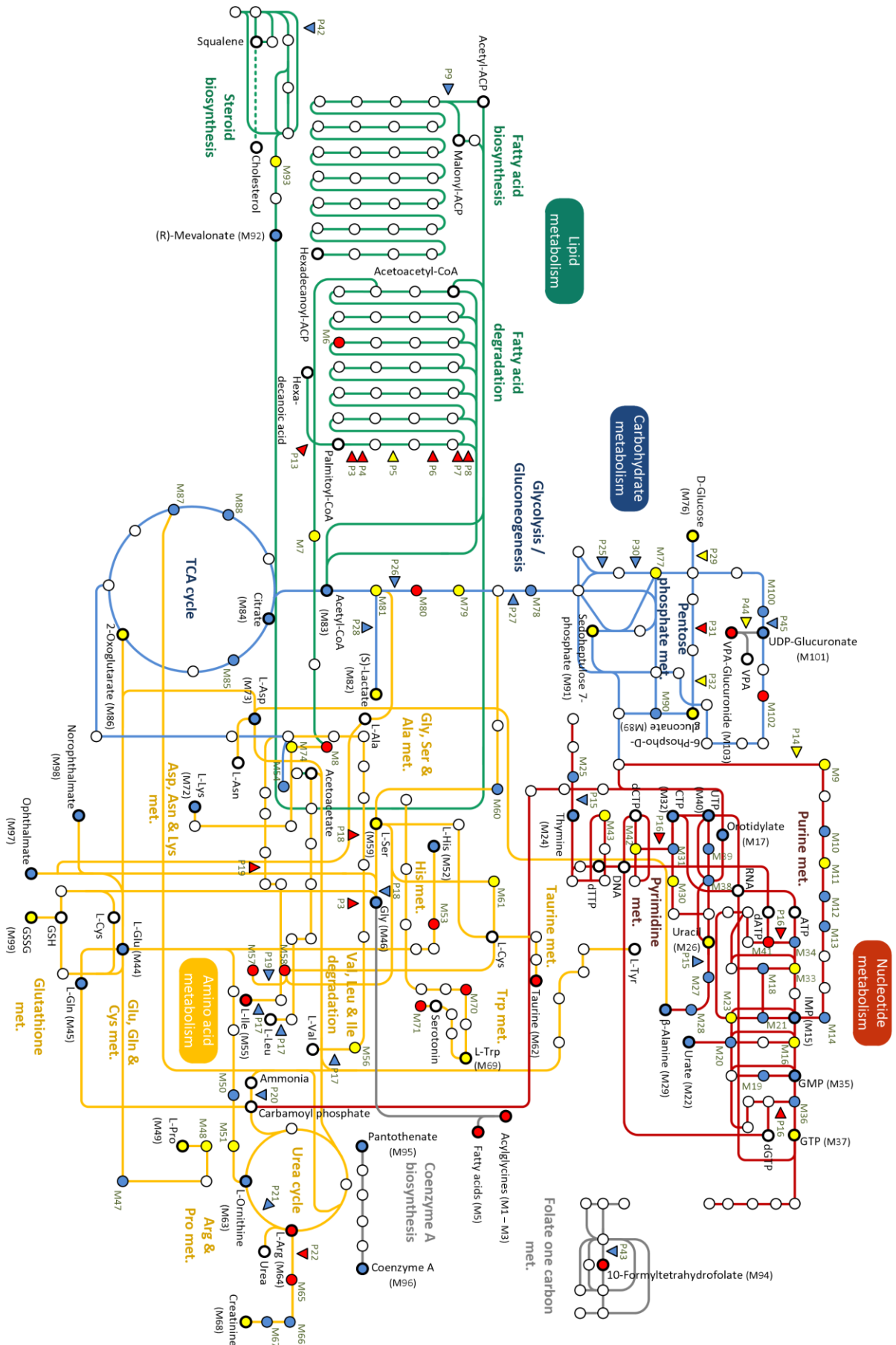


Figure 6.9 (Continued on the following page)

Figure 6.9 Metabolic pathway map for HepaRG cells treated with valproic acid (VPA). The map shows pathways that were identified to be particularly affected by 2-week treatment with VPA. Metabolites are represented by circles, while the enzymes catalyzing the adjacent reactions are shown as triangles. Key metabolites are labeled with their full name and highlighted by circles with bold lines. Names are in accordance with the Kyoto Encyclopedia of Genes and Genomes. Different major pathways are indicated by colored lines – blue, carbohydrate metabolism; orange, amino acid metabolism; red, nucleotide metabolism; green, lipid metabolism; grey, miscellaneous pathways. For metabolites that were quantified, circles are filled with either yellow, blue or red, depending on whether there was no significant alteration, a significant decrease or a significant increase upon drug exposure after Benjamini-Hochberg correction, respectively. Triangles were colored in the same way, when there was a trend upon exposure to VPA. Time courses for selected metabolites, reaction rates, proteins and transcripts are depicted in figures S6.5 to S6.9. Abbreviations for metabolites (M) and proteins (P): **M1**, N-heptanoylglycine; **M2**, capryloylglycine; **M3**, nonanoylglycine; **M5**, octanoic acid; **M6**, ictanoyl-CoA; **M7**, glutaryl-CoA; **M8**, 2-oxoadipate; **M9**, 5-phosphoribosylamine; **M10**, 5'-phosphoribosyl-N-formylglycineamide; **M11**, 2-(formamido)-N1-(5'-phosphoribosyl)acetamidine; **M12**, aminoimidazoleribotide; **M13**, 1-(5-phospho-D-ribose)-5-amino-4-imidazolecarboxylate; **M14**, 1-(5'-phosphoribosyl)-3-formamido-4-imidazolecarboxamide; **M16**, xanthosine 5'-phosphate; **M18**, adenosine; **M19**, guanosine; **M20**, xanthine; **M21**, inosine; **M23**, hypoxanthine; **M25**, (R)-5,6-dihydrothymine; **M27**, 5,6-dihydrouracil; **M28**, 3-ureidopropionate; **M30**, CMP; **M31**, CDP; **M33**, AMP; **M34**, ADP; **M36**, GDP; **M38**, UMP; **M39**, UDP; **M41**, dADP; **M42**, dCDP; **M43**, dUTP; **M47**, L-glutamyl 5-phosphate; **M48**, (S)-1-pyrroline-5-carboxylate; **M50**, N-acetyl-L-glutamate-5-semialdehyde; **M51**, N-acetylmethionine; **M53**, urocanate; **M54**, propanoate; **M56**, 3-methyl-2-oxobutanoic acid; **M57**, L-homocysteine; **M58**, L-cystathionine; **M60**, O-phosphoserine; **M61**, mercaptopyruvate; **M62**, taurine; **M65**, guanidinoacetate; **M66**, creatine; **M67**, phosphocreatine; **M70**, L-kynurenine; **M71**, 5-hydroxyindoleacetate; **M73**, L-2-aminoadipate; **M77**, beta-D-fructose 6-phosphate; **M78**, 3-phospho-D-glyceroylphosphate; **M79**, 2-phospho-D-glycerate; **M80**, phosphoenolpyruvate; **M81**, pyruvate; **M82**, (S)-lactate; **M85**, cis-aconitate; **M87**, fumarate; **M88**, (S)-malate; **M90**, D-ribulose-5-phosphate; **M93**, (R)-5-diphosphomevalonate; **M100**, UDP-glucose; **M102**, D-glucuronate; **P3**, medium-chain specific acyl-CoA dehydrogenase, mitochondrial (ACADM); **P4**, very long-chain specific acyl-CoA dehydrogenase, mitochondrial (ACADVL); **P5**, enoyl-CoA hydratase, short chain 1 (ECHS1); **P6**, long-chain 3-hydroxyacyl-CoA dehydrogenase (HADHA); **P7**, 3-ketoacyl-CoA thiolase (HADHB); **P8**, 3-ketoacyl-CoA thiolase, mitochondrial (ACAA2); **P9**, fatty acid synthase (FASN); **P13**, long-chain fatty acid CoA ligase 1 (ACSL1); **P14**, amidophosphoribosyltransferase (PPAT); **P15**, dihydropyrimidine dehydrogenase [NADP+] (DPYP); **P16**, ribonucleotide-diphosphate reductase subunit M2 (RRM2); **P17**, branched-chain amino acid amino-transferase, mitochondrial (BCAT2); **P18**, methylcrotonyl-CoA carboxylase beta chain, mitochondrial (MCCC2); **P19**, short/branched-chain specific acyl-CoA dehydrogenase (ACADSB); **P20**, carbamoyl-phosphate synthase ammonia, mitochondrial (CPS1); **P21**, arginase 1 (ARG1); **P22**, glycine amidinotransferase, mitochondrial (GATM); **P25**, fructose-bisphosphate aldolase B (ADOLB); **P26**, pyruvate kinase (PKLR); **P27**, phosphoglycerate kinase 1 (PGK1); **P28**, L-lactate dehydrogenase A Chain (LDHA); **P29**, putative hexokinase (HKDC1); **P30**, 6-phosphofructokinase, liver type (PFKL); **P31**, glucose-6-phosphate dehydrogenase (G6PD); **P32**, 6-phosphogluconolactonase (PGLS); **P42**, farnesyl pyrophosphate synthase (FDPS) (FDPS); **P43**, cytosolic 10-formyltetrahydrofolate dehydrogenase (ALDH1L1); **P44**, UDP-glucuronosyl-transferase 1A6 (UGT1A6); **P45**, UDP-glucose 6-dehydrogenase (UGDH). The measurement of the metabolome data was performed by Nicola Zamboni, ETH Zurich. Proteome data originates from Georg Tascher, CNRS Strasbourg.

mitochondrial form was upregulated on transcript and protein level, the opposite was observed for the cytosolic form with VPA treatment (figure S6.9 P40, P41). Another enzyme within the synthesis of cholesterol, namely the farnesyl pyrophosphate synthase, was likewise downregulated (P42).

The formyl-group donor 10-formyltetrahydrofolate was significantly increased by treatment, while particularly the protein levels of the corresponding enzyme 10-formyltetrahydrofolate dehydrogenase were found to be decreased (figure 6.9, figure S6.9 M94, P43). Concentrations of a set of metabolites

directly or indirectly involved in drug detoxification were significantly decreased compared to the control, including ophthalmate, norophthalmate and UDP-glucuronate, whereas there was no significant change for the oxidized form of glutathione (GSSG). On the level of transcripts, a slight increase was observed for the UDP-glucuronosyl-transferase 1A6 (UGT1A6, P44), catalyzing the conjugation of VPA to glucuronate. CYP2C9 levels on the other hand decreased with treatment. Protein levels of the enzyme that is responsible for the conjugation of reduced glutathione to xenobiotics, i.e. the microsomal glutathione S-transferase were notably elevated upon VPA exposure (figure S6.9).

6.4.8 Transcriptional alterations in stress-related and lipid pathways

ER stress, Nrf2 oxidative stress response, the p53 pathway, protein degradation as well as lipid regulators upon VPA exposure were investigated on transcriptional level (figure 6.10). ER stress elicits a so called unfolded protein response (UPR), resulting in the activation of the three branches, PERK/ATF4, IRE1/XBP1 and ATF6. On day 2 and day 8, there was a strong downregulation of several transcripts related to the PERK/ATF4 branch of the UPR, which includes transcripts associated with amino acid uptake and translation, i.e. members of the solute carrier family and tRNA synthetases. Only on day 14, there was a switch towards upregulation for several transcripts, including ASNS, ATF3 and certain isoforms of solute carriers, particularly SLC7A11. In case of the IRE1/XBP1 branch, MYC was particularly interesting, with dose-dependent downregulation upon treatment, with exception of the 14-day time point and treatment with the two highest concentrations.

Like MYC, FOS and JUN, part of the Nrf2 oxidative stress response, were initially downregulated, but upregulated after 14-day treatment with 0.15 and 0.5 mM VPA. While most transcripts related to glutathione were independent of VPA exposure, glutathione peroxidase 2 (GPX2), also part of the Nrf2 response, decreased notably with treatment.

Two isoforms of growth arrest and DNA-damage-inducible (GADD45A and GADD45B) and PMAIP1 which are all associated with the p53 pathway were upregulated when HepaRG cells were exposed to 0.15 and 0.5 mM VPA for 14 days. Upon treatment, moderate upregulation of transcripts related to protein degradation was observed throughout the duration of the treatment, including several proteasomes, heat shock and ubiquitin-related proteins.

For transcripts of lipid regulators, there was a clear downregulation for NFKB1, MLXIPL (ChREBP) and the associated MLX. For transcripts regulated by the ChREBP/MLX heterodimer, namely SLC2A2 (GLUT2), PKLR and FASN, a dose-dependent downregulation was observed.

Transcripts related to the peroxisome proliferator-activated receptor α (PPAR α)/RXR heterodimer, were found to be upregulated in case of CYP450 isoforms, but mildly downregulated in case of the acyl-coenzyme A thioesterase 1 (ACOT1). However, transcripts of the hepatocyte nuclear factor 4 α (HNF4 α), which is also involved in the regulation of ACOT1 expression, were not altered by VPA treatment.

Liver X receptor α (LXR α (NR1H3)) was slightly downregulated with treatment, while LXR β (NR1H2) mRNA levels were independent of VPA treatment. Downstream elements such as ATP-binding cassettes, CYP7A1 and the sterol regulatory element-binding protein-1 (SREBP1) were moderately downregulated.

Transcript levels of elements regulated by SREBP1 and SREBP2, e.g. fatty acid elongation and desaturation, as well as cholesterol synthesis (HMGCR) respectively, were found in lower levels when HepaRG cells were exposed to VPA.

6.5 Discussion

Multi-omics studies are an essential approach in promoting *in vitro* and *in silico* tools in the field of toxicology. They not only allow access to a tremendous amount of information that is pivotal in the generation of holistic models, but also allow to challenge *in vitro* cultures and, when needed aid in their optimization. In a previous study, Wilmes and coworkers demonstrated the relevance of an integrated-omics approach in a repeated dose toxicity environment using renal epithelial cell culture (Wilmes et al., 2013). Here, we investigated the effects of a repeated VPA dosing regimen in the human hepatic cell line HepaRG on the different layers of cellular hierarchy, as well as on its functionality with the aim of better understanding VPA-induced toxicity.

6.5.1 Functional and morphological analyses in HepaRG cells exposed to VPA in a repeated dosing setup

In previous studies, we identified that drug-mediated toxicity in HepaRG cells occurs at lower drug concentrations when the drug was applied over a prolonged period with repeated dosing (Klein et al., 2016, 2014; Mueller et al., 2014). To assess the extent of toxicity after a 14-day repeated VPA treatment, we assessed viability of HepaRG cells in an initial run, for selection of ideal treatment concentrations in a second in-depth investigation. After 2-week exposure, corresponding to a total of 7 doses, the EC₅₀ value was 0.85 mM +/- 0.18 mM (figure 6.1), compared to a 24 h EC₅₀ value of 24 to 26 mM (Klein et al., 2016, 2014). Based on this result, three concentrations were selected: 0.05 mM VPA as a concentration in the subtoxic range, 0.15 mM being on the verge of overt adverse reactions, and 0.5 mM eliciting mild toxic effects.

Consequently, in the subsequent in-depth study, viability was only affected upon 14-day treatment with 0.5 mM VPA. ATP levels on the other hand decreased significantly already after 8 days of treatment and the trend could already be denoted on day 2 (figure 6.2). This strongly indicates that VPA interferes with energy metabolism and that a decline in ATP precedes overt toxicity. This is even likely to contribute to the adverse drug reaction as the upkeep of processes strongly depending on energy may no longer be assured. Studies from the group of Silva, stated a VPA-induced inhibition of mitochondrial pyruvate uptake and inhibition of the dihydrolipoyldehydrogenase (DLDH), part of the pyruvate dehydrogenase complex (Aires et al., 2008; Luís et al., 2007). In another study, the authors reported the inhibition of the carnitine palmitoyltransferase I (CPT1) by VPA (Aires et al., 2010), which normally aids in the transfer of fatty acids into the mitochondria for subsequent β -oxidation.

Severe impairment of mitochondrial fatty acid β -oxidation often goes along with accumulation of lipids inside the liver (Wajner and Amaral, 2016), causing a microvesicular steatotic phenotype in case of VPA treatment (Tang et al., 1995). However, investigation of the cellular phenotype using light microscopy did not allow us to reveal the presence microvesicular steatosis. Instead, in addition to the quantitative description of viability above, it can be stated that control cells maintain a healthy phenotype throughout the period of treatment, while the occurrence of cell death can be observed when HepaRG cells were exposed to VPA, particularly in case of treatment with 0.5 mM VPA (figure 6.3). Yet it is also worth mentioning, that light microscopy without additional staining is not particularly suitable for assessing microvesicular steatosis, as appendant lipid vesicles are less than

1 μm in diameter. Neither can other characteristics of microvesicular steatosis, such as distended hepatocytes (Tandra et al., 2011), clearly be stated in our experiment. Therefore, Oil Red O staining with subsequent quantification was chosen as another approach to investigate the accumulation of lipids inside the HepaRG cells (figure 6.4). Using the Oil Red O staining, slight but significant accumulation of neutral lipids was observed in HepaRG cells upon VPA exposure. Surprisingly however, accumulation was largest on day 2, and accumulation partially regressed within the following days. Unlike *in vivo*, in our setup, fatty acids are not supplied externally, but originate solely from internal sources such as *de novo* synthesis or membrane decomposition. Hence, accumulation of fatty acids might be limited compared to a setup with external supply of fatty acids. Further supporting this hypothesis, the finding that accumulation was highest on day 2 of treatment could be related to remnant fatty acids from initial cultivation in serum-supplemented medium. On the other hand, at least under physiological conditions, around 90% of fatty acids in mammalian cells come from the *de novo* synthesis (Kopf et al., 2012). Consequently, the absence of external fatty acid supply should not drastically impair triacylglyceride accumulation upon VPA treatment.

VPA metabolism involves several potential pathways (partly depicted in figure 6.6), including hydroxylation and desaturation, which are both mediated by CYP450 enzymes. The main CYP450 isoform contributing to metabolism is CYP2C9, yet CYP2B6 and CYP2A6 are also capable of metabolizing VPA (Kiang et al., 2011, 2006). In our study, CYP450 activity was reduced significantly and in a dose-dependent fashion in case of CYP1A2, CYP2D6 and CYP3A4, while CYP2B6 activity remained stable (figure 6.5). The observed decrease in activity for CYP1A2, CYP2D6 and CYP3A4 may originate from VPA entering and blocking the active site of the enzyme without being metabolized or only at a very low rate. Indeed, it was shown in a previous study that VPA *in vitro* competitively inhibits activity of certain CYP450 isoforms including CYP2C9 ($K_i = 600 \mu\text{M}$) and to a lesser extent CYP3A4 ($K_i = 8 \text{ mM}$) (Wen et al., 2001). Yet, based on the K_i values and the magnitude of the observed decrease in CYP450 activities in our study, the effect is more likely to be based on the transcriptional level. This is strongly supported by the observation that both transcript and protein levels of CYP2C9 were downregulated dose-dependently with VPA treatment (figure S6.9). Previous results on the effect of VPA on CYP450 activity are contradictory. In a study from 2007, it was reported that VPA results in upregulation of CYP3A4 activity via the main regulators of CYP450 expression, i.e. pregnane X receptor (PXR) and constitutive androgen receptor (CAR) (Cervený et al., 2007). Since that study has been performed in the poorly metabolizing cell line HepG2, secondary effects originating from metabolites of VPA as well as other indirect effects, may have been missed. Consequently, another study performed in epilepsy patients supports our findings on the downregulation of CYP2C9 (Gunes et al., 2007). Nevertheless, further in-depth studies are required to clarify effects of VPA on drug metabolizing enzymes.

Interestingly, VPA uptake was enhanced with duration of the treatment in case of exposure to 0.05 mM VPA, but declined when cells were exposed to 0.5 mM VPA (figure 6.6A). Uptake of VPA into the liver has been studied in few instances and as a result, several transporters have been suggested to be involved in its uptake into cells (Booth et al., 1996; Fischer et al., 2008; Terbach et al., 2011; Thwaites and Anderson, 2007). Up to now, however, there is no unambiguous study on the uptake of VPA into liver cells. Hence we may only speculate that VPA is taken up by an ATP-dependent transporter, which is induced when exposed to low levels of VPA. In case of treatment with higher concentrations of VPA, ATP might therefore strictly limit its uptake.

There were two major VPA metabolites in the supernatant, namely VPA-glucuronide and 3-keto-VPA (figure 6.6B). While 3-keto-VPA was predominant upon exposure to 0.05 mM VPA, there was major

trend towards VPA-glucuronide with exposure to higher VPA concentrations. Even though the absolute amount of 3-keto-VPA in the supernatant increased when HepaRG cells were exposed to higher concentrations of VPA, the increase in case of VPA-glucuronide was drastically more pronounced. This phenomenon may be explained by the decrease in the protein levels of CYP2C9, the main CYP450 isoform contributing to the formation of 3-keto-VPA, with exposure to higher VPA concentrations. The decrease in CYP2C9 level goes along with a decrease in the capacity of the pathway and may therefore result in a saturation of the hydroxylation and dehydrogenation step. Levels of UGT1A6, one of the UDP-glucuronosyltransferases responsible for the glucuronidation of VPA (Guo et al., 2012), on the other hand remained stable throughout the treatment (figure S6.9). The differences in metabolite formation are particularly interesting as the VPA metabolites may differ in target molecules as well as in their potential to deplete radical scavengers and eventually in eliciting toxicity (Kiang et al., 2011; Luís et al., 2007). Hence, different dosing may drastically change effects elicited in patients.

6.5.2 –Omics analyses on HepaRG cells treated with VPA in a repeated dosing setup

Levels of metabolites, proteins and transcripts changed notably when HepaRG cells were exposed to VPA, but also as a result of mere cultivation. In both instances, affected metabolites were similar, broadly related to the major central pathways, i.e. lipid, nucleotide, amino acid and carbohydrate metabolism, but also metabolites associated with drug and one carbon metabolism. Despite having the medium adapted to the final composition two days prior to the start of treatment to reduce the effects resulting from changes in medium composition on cellular behavior, effects in several cases were greater than those induced by VPA. To a certain extent, changes might be related to aging of the cells, though in previous studies, putative aging effects were only mild, despite a 30-day study period (Klein et al., 2014). Yet this overlap between drug and cultivation effects does not impair subsequent analyses, and effects originating from cultivation alone were not considered in the following.

One of the most interesting pathways in our study in terms of the number of affected metabolites by VPA treatment was the metabolism of lipids, with a focus on fatty acid metabolism (figure 6.9, figure S6.5). Levels of metabolites related to fatty acid metabolism were generally elevated and included intermediates as well as derivatives of β -oxidation. Several of these metabolites belong to the group of acylglycines, which have previously been associated with disturbances in mitochondrial β -oxidation and oxidative damage (Derks et al., 2014; Wajner and Amaral, 2016). The enzyme glycine N-acyltransferase, responsible for the formation of acylglycines, normally serves the detoxification of xenobiotics like salicylic acid (Matsuo et al., 2012) but in this case might help to prevent accumulation of free fatty acids. To further investigate the observed increase in fatty acids and metabolites, we examined levels of enzymes involved in fatty acid metabolism and major regulators thereof. Enzymes in the context of fatty acid degradation (P1 to P8) were found to be upregulated, while enzymes related to fatty acid and triacylglycerol synthesis (P9, P10) were partially downregulated (figure 6.9, figure S6.5). Upregulation of fatty acid degradation and downregulation of their synthesis may help to counteract increasing levels of fatty acids, yet, downregulation of triacylglycerol synthesis is contradictory. The upregulated ACSL1 (P13) might help in degradation of fatty acids via their activation. There are several major regulators of lipid metabolism, including the nuclear receptors PPAR α , SREBP1, LXR and ChREBP. While PPAR α regulates genes associated with β -oxidation, the latter three were shown to be involved in the regulation of lipogenic genes such as FASN (Joseph et al., 2002; Rakhshandehroo et al., 2010; Sae-Lee et al., 2016). Using the gene expression data (figure 6.10) we could show activation for PPAR α and repression of the other nuclear receptors, in accordance with our protein and other transcript data on downstream targets. In case of PPAR α ,

saturated and unsaturated fatty acids serve as ligands, explaining the increase in activation of PPAR α when HepaRG cells were exposed to VPA. In previous studies, the question on the mechanistic background for the impairment of β -oxidation was addressed. Though mechanisms are not yet fully understood, impairment is thought to be caused by sequestration of CoA and carnitine, as well as direct inhibition of enzymes involved in fatty acid oxidation (Aires et al., 2010; Silva et al., 2008), while these regulators only received minor attention. In case of CoA, we indeed observed decreased intracellular levels (figure 6.9, figure S6.9), which may contribute to impairment of β -oxidation in our setup.

Another central pathway greatly affected by VPA treatment in HepaRG cells, was the metabolism of nucleotides (figure 6.9, figure S6.6). There was a general trend towards lower concentrations in nucleotides as well as their catabolic end products. It is not possible to conclude from these observations that the observed decrease results from either an increased demand and consequently consumption of nucleotides, or a decrease in the demand and a subsequently lower production. However, there are few hints, suggesting a generally lower production of nucleotides. 1) Transcripts of MYC, a critical transcription factor in the regulation of nucleotide synthesis were downregulated throughout the period of exposure, with exception of day 14 and exposure to 0.15 and 0.5 mM VPA (figure 6.10), 2) elevated concentrations found for 10-formyltetrahydrofolate (figure 6.9, figure S6.9), which is an essential cofactor required in two steps in the synthesis of purines, might come from a lower demand due to reduced nucleotide synthesis, 3) catabolic products like thymine, β -alanine and urate decreased together with nucleotides (figure 6.9, figure S6.6), yet we would expect an increase in case of a higher metabolic turnover of nucleotides, 4) levels of the catabolizing enzyme dihydropyrimidine dehydrogenase (P15, figure 6.9, figure S6.6) were found to be decreased with treatment.

What might be the reason behind the potential downregulation of nucleotide synthesis? With exposure to VPA, HepaRG cells show strong signs of ER stress, such as transcriptional upregulation of proteasomes and downregulation of tRNAs and amino acid transporters (figure 6.10). ER stress is a condition triggered by mitochondrial dysfunction and oxidative stress, during which protein folding is impaired and mis- or unfolded proteins accumulate. To restore normal conditions, cellular protein synthesis is reduced and chaperone levels are increased in the context of the UPR (Begrache et al., 2011; Sano and Reed, 2013). Since in non-proliferating cells, the majority of nucleotides is required for the synthesis of RNA (mRNA, rRNA and tRNA) (Lane and Fan, 2015), downregulation of nucleotide synthesis via MYC, which is also regulated within the UPR, might be a mechanism to adapt nucleotide synthesis to reduced requirements in ER stress conditions.

Interestingly, activation of MYC on day 14, goes along with a renunciation from the UPR, i.e. elevated transcript levels for tRNA synthetases as well as amino acid transporters, but also with notably upregulated levels of GADD45A, GADD45B, PMAIP1, FOS and JUN (figure 6.10). The latter molecules are involved in regulation of apoptosis (Oda et al., 2000; Shaulian and Karin, 2002; Takekawa and Saito, 1998) and coincide with the observed decrease in viability (figure 6.2). The initiation of apoptotic pathways is a common fate of cells that fail to recover from ER stress (Sano and Reed, 2013) and suggests that ER stress could be a major contributor to cell death in HepaRG cells exposed to VPA.

The initial increase in nucleoside monophosphates (UMP, IMP and GMP; M38, M15 and M35) as well as xanthine (M20) upon treatment (figure 6.9, figure S6.6) is particularly interesting, as the trend for other purine and pyrimidine intermediates was clearly towards the opposite direction. Nucleoside

monophosphates result either from *de novo* synthesis, or by cleaving of a pyrophosphate from a nucleoside triphosphate. Further conversion of nucleoside monophosphates into di- and triphosphates might be hampered in case of critical ATP levels, as the phosphate groups required in these reactions commonly originate from ATP. The slight decrease in ATP levels already observed on day 2 might have slowed down the conversion of nucleoside mono- into diphosphates and hence led to an accumulation of UMP, IMP and GMP. At later time points, the impairment of nucleotide synthesis suggested above would lead to a drop in nucleoside monophosphate levels, which in turn would result in the fading of the initial dose-dependent increase as observed in our experiment.

The effects of VPA on amino acid metabolism in HepaRG cells were very diverse. E.g., intracellular L-glutamate levels decreased in a dose-dependent manner, despite being increasingly fed from the L-glutamine pool as well as extracellular L-glutamate in the first 8 days (figure S6.7 F5, F2). Yet, on the other hand, feeding from 2-oxoglutarate was reduced with increasing VPA concentration (figure S6.7 F4). Since protein synthesis is expected to be reduced based on the ER stress stated above, it is more likely that the reduction of L-glutamate levels is a result of increased formation of the radical scavenger glutathione than due to an increase in synthesis of proteins or nucleotides. Supporting this hypothesis, glycine, which is also part of the tripeptide glutathione was found to be reduced in a similar fashion when HepaRG cells were exposed to VPA, despite a minor increase in its uptake (figure S6.7 M46, F3). Though levels of several enzymes involved in glutathione metabolism were not affected by exposure to VPA, protein concentration of the microsomal glutathione S-transferase 1 increased up to around 2.5-fold with VPA (figure S6.9 P47). The enzyme catalyzes the conjugation of reduced glutathione to a wide range of exogenous and endogenous electrophiles. However, GPX2, which detoxifies organic hydroperoxides and hydrogen peroxide was the most prominently downregulated enzyme within the Nrf2 response, when cells were exposed to VPA (figure 6.10). This suggests that transcription of the molecule was either directly or indirectly impaired by VPA. VPA and particularly its dehydrogenated metabolites are well known to be capable of depleting cellular glutathione (Kiang et al., 2011). In another study on mouse liver treated with acetaminophen, similar findings were observed with reduced levels for L-glutamine, L-glutamate and glycine, relative to untreated cells (Soga et al., 2006).

In case of BCAA, the effect of VPA on their metabolism was consistent. Uptake of all three BCAA was reduced with treatment (F6 to F8), while intracellular L-isoleucine (M55) accumulated and levels of propanoate (M54) as a product of L-valine catabolism declined (figure 6.9, figure S6.7). Thus, it can be concluded that catabolism of BCAA is impaired by VPA, with subsequent intracellular accumulation of the amino acids. Though transcriptional regulation of the associated enzymes is poorly studied, it is likely that accumulation of the amino acids triggers an upregulation of the associated enzymes as we observed for the methylcrotonyl-CoA carboxylase (P18) and short/branched-chain specific acyl-CoA dehydrogenase (P19). Consistently, Luis et al., who previously studied the effects of VPA and its metabolites on BCAA metabolism, found inhibitory effects on the activity of the branched-chain alpha-keto acid dehydrogenase complex as well as the short/branched-chain specific acyl-CoA dehydrogenase (Luís et al., 2011, 2007). Since VPA did not cause an effect on the protein and transcript level of the BCAA aminotransferase (P17), any impairment would have to be based on the level of direct or indirect inhibition of its activity (figure S6.7).

The results obtained for downstream products of L-serine and L-methionine catabolism are partly in contrast to the hypothesis on elevated glutathione synthesis upon VPA exposure. L-homocysteine and L-cystathionine were found in significantly higher concentrations (figure 6.9, figure S6.7 M57, M58),

despite being a potential source for L-cysteine, which commonly is the bottleneck in the synthesis of glutathione. Yet, in our *in vitro* setup, supply of L-cysteine might not be limiting. Supporting this idea, we even observed a decrease in the concentrations of ophthalmate and norophthalmate (figure 6.9, figure S6.9 M97, M98), which are increasingly produced as a substitute of glutathione in case L-cysteine supply is running low (Soga et al., 2006).

Further, detoxification of ammonia via the urea cycle was impaired by VPA in a dose-dependent manner (figure S6.7 F9). At the branching point towards urea and guanidinoacetate formation, there seems to be a trend towards the latter, with the corresponding enzyme being upregulated, while arginase 1 levels decreased with VPA (figure 6.9, figure S6.7 P21, P22). As the carbamoyl-phosphate synthetase I (P20), the key enzyme of the urea cycle, was also downregulated at protein and transcript level, the urea cycle is likely to be downregulated in general. Impairment of the urea cycle may have severe consequences such as hyperammonemia. We and others have previously described effects of VPA on the urea cycle (Aires et al., 2011; Klein et al., 2016), but up to now the impairment was thought to reside in a decrease in the formation of the activator of the carbamoyl-phosphate synthetase I, N-acetylglutamate. These results suggest a more complex mechanism underlying the inhibition of the urea cycle activity.

Eventually, we found a significant decrease for several dipeptides in HepaRG cells exposed to VPA (figure S6.7). Being formed by the action of dipeptidyl peptidases, which cleave dipeptides from polypeptides, they are an intermediate product in protein catabolism. As such, alterations found in dipeptides may well be associated with ER stress mentioned above.

Besides lipid, nucleotide and amino acid metabolism, VPA likewise affected carbohydrate metabolism, including the glycolytic pathway, the TCA cycle and the pentose phosphate pathway (figure 6.9, figure S6.8). Though there was no clear trend for metabolite levels in case of glycolysis, metabolic fluxes were markedly reduced in HepaRG cells exposed to VPA (figure S6.8 F10 to F13). As already stated in the context of fatty acid metabolism, we found a strong indication for downregulation of ChREBP. ChREBP not only regulates lipid metabolism, but is also the key responsible for activation of several enzymes of the glycolytic pathway, like pyruvate kinase, liver type (Iizuka, 2013) and thus, might play a pivotal role in the decrease in glycolytic reaction rates observed in our study. The activation process of ChREBP is not fully understood, but suggested to involve xylulose-5-phosphate, glucose-6-phosphate and/or fructose-1,6-bisphosphate as ligands (Filhoulaud et al., 2013). The secretion of lactate (Limonciel et al., 2011), or the ratio of secreted lactate to ingested D-glucose may be used as an indicator of cellular stress, and in our study, indicates an initially stressed phenotype, which might be related remnant stress in the context of seeding and alterations in the medium composition. After an interim recovery, said ratio steadily increased from day 8 onwards, suggesting an increase in cellular stress in HepaRG cells.

As a result of the decline in substrate supply via the glycolytic pathway, reaction rates in the TCA cycle dropped in a similar fashion as observed for glycolytic fluxes (figure S6.8 F14, F15). Additionally, other reactions such as degradation of BCAA, which might normally help supplying carbon sources and thus, maintaining normal TCA cycle activity, were also decreased by treatment with VPA. These observations are in accordance with the early drop in ATP levels described above (figure 6.2).

The key enzyme of the pentose phosphate pathway (glucose-6-phosphate 1-dehydrogenase, P31) was upregulated with VPA treatment (figure 6.9, figure S6.8), which probably results from an increased demand in NADPH for the recovery of reduced glutathione. Though NADPH may also be used for *de*

novo lipogenesis and the pentose phosphate pathway may as well serve for the production of ribose 5-phosphate, these scenarios are unlikely in the light of already elevated fatty acid levels and low nucleotide formation as speculated before.

Upregulation of proteins involved in oxidative phosphorylation was consistent throughout the different molecules (figure S6.9 P33 to P39), suggesting a common regulation. Regulation of these genes is not fully elucidated, but might involve PPAR α and the PPAR γ coactivator-1 α (Misu et al., 2007; Rakhshandehroo et al., 2010), indicating regulation at least partially via fatty acids. Despite upregulation of enzymes of the oxidative phosphorylation, cells were not able to maintain ATP levels when exposed to 0.5 mM VPA for two weeks (figure 6.2), likely as a result of diminished supply of reducing equivalents from upstream pathways.

Besides these major pathways, VPA also interfered with minor pathways, such as the formation of ketone bodies (figure S6.9). 3-hydroxybutyryl-carnitine for example was found to be notably elevated with treatment. The metabolite is a carnitine conjugate of 3-hydroxybutyrate, which is formed from acetoacetate. In agreement with increased levels of 3-hydroxybutyryl-carnitine, the mitochondrial hydroxymethylglutaryl-CoA synthase was found upregulated, while its cytosolic isoform and (R)-mevalonate were downregulated. Whereas the former enzyme is responsible for the formation of ketone bodies, the latter is involved in the synthesis of cholesterol, suggesting a prioritization of ketone bodies under VPA exposure. Additional downregulation of the farnesyl pyrophosphate synthase strengthens the subordination of cholesterol formation. The potential increase in ketone body formation however is surprising, as they are formed in mitochondria, whose function is assumed to be impaired by VPA. Further, their physiological meaning is mainly related to extrahepatic tissue. Yet, the increase might simply be a consequence of PPAR α activation, which also controls the expression of the mitochondrial hydroxymethylglutaryl-CoA synthase (Rakhshandehroo et al., 2010). Interestingly, in addition to the inhibition of HDAC via VPA, 3-hydroxybutyrate is capable of inhibiting HDAC2 and HDAC3 (Sleiman et al., 2016).

6.6 Conclusion

Taken together, VPA affected a multitude of pathways in HepaRG cells. ER stress, depletion of ATP and the impairment of the urea cycle are probably the most critical steps in VPA-induced toxicity. Despite expecting to see major accumulation of lipids, we only found a minor increase triacylglycerides. This may either indicate that microvesicular steatosis only plays a minor role in the course of toxicity of VPA, or that the cultivation setup needs to be further optimized, e.g. by supplying fatty acids with the cultivation medium. In a next step, the -omics data may be used in setting up a model for the prediction of adverse events induced by VPA. For that purpose, targeted and absolute quantification of metabolites of the pathways of interest would provide more reliable parameters and confirm annotation within the untargeted analysis.

6.7 Acknowledgements

The presented research was carried out within the SEURAT-1 NOTOX project funded through the European Community's Seventh Framework Programme (FP7/2007-2013) under grant agreement N° 267038 and Cosmetics Europe. Further, we thank Michel Fritz for excellent technical assistance.

Chapter 7 Summary, conclusion and outlook

In the context of this thesis, the suitability of the human hepatic HepaRG cell line for its application in toxicological studies and eventually in risk assessment was elaborated. The aim of this study was to provide tools and knowledge that help to ultimately replace *in vivo* animal studies in pharmaceutical and cosmetics industry. The initial studies were limited to short-term acute toxicity, but in later studies, the focus shifted towards long-term repeated dose toxicity. The approach that was taken can be divided into three major parts. In the first part, the performance of the HepaRG cell line was compared to well-established systems in the context of toxicological studies (chapter 2), while in the second part, the cells were optimized in respect to their culture environment (chapter 3 & 4). In the third and last part, the knowledge gained from previous studies was used to apply the HepaRG cells in in-depth characterization with relevance for risk assessment (chapter 5 & 6). The individual chapters will be summarized in more detail in the following.

Part I Metabolic characterization of HepaRG cells

In **chapter 2**, HepaRG cells were compared to the well-established human hepatic cell line HepG2 and to the gold standard in *in vitro* toxicological studies, primary human hepatocytes (PHH). The central carbon metabolism of each of these hepatic systems was in the focus of this study. For that purpose, we investigated the basal carbon metabolism, but also alterations in metabolism when cells were exposed to two hepatotoxic compounds, acetaminophen and diclofenac. The comparison was rounded off by including functional analyses, such as cytochrome P450 (CYP450) activity as well as viability assessment. We could show that basal carbon metabolism in HepaRG cells closely resembled metabolism in PHH, whereas metabolism in HepG2 cells was dictated by its hepatoblastoma origin. Further, we found that CYP450 activity in HepaRG cells was clearly superior to HepG2 cells, and in a similar range to one of the tested PHH batches, yet slightly lower than in PHH from the other two donors. Surprisingly, even though HepaRG cells performed slightly better than HepG2 cells, we found effects of the hepatotoxic compounds acetaminophen and diclofenac on viability and metabolism to be similar in all tested systems. With these results, we were able to demonstrate from a metabolic point of view that HepaRG cells may well serve as a surrogate for PHH in toxicological studies.

To predict adverse events that are relevant for humans, it is essential that the model system used to assess required parameters correctly depicts the *in vivo* situation in humans. By performing a comparison of HepaRG cells to PHH on metabolic level, we revealed major overlaps between the two hepatic *in vitro* models. This is of particular importance for two reasons. First, among the different cellular levels, the metabolome best reflects the cellular phenotype as well as changes therein. Second, PHH are currently the closest system available to the *in vivo* situation and therefore, are considered as the gold standard in *in vitro* toxicology.

Unlike for PHH, availability of HepaRG cells is unlimited. Also, they are easier to handle than their primary counterpart and cells are more suitable for long-term studies. However, it is not possible to adequately represent the heterogeneity of the human population using only the HepaRG cell line. Though in some instances, the variance caused by inter-donor differences is unwanted, it is necessary to consider for prediction of toxicity in a population. At least to some extent, variance may be included in *in silico* approaches as we did for the estimation of the oral equivalent dose in chapter 5.

Based on our results, as well as results obtained in previous studies, HepaRG cells are well suitable as a surrogate for PHH. With current research focusing on the improvement of stem cells and genetically

modified primary hepatocytes, these systems might eventually replace HepaRG cells and PHH in toxicological studies. Particularly in the context of personalized medicine, stem cells and modified PHH would be beneficial, but they both currently still struggle with teething problems and their success depends on researchers managing to overcome these problems.

Part II Optimization of HepaRG cell culture conditions for short and long-term studies

Next, in **chapter 3**, we investigated the effects of the culture environment on functional parameters and on the outcome of toxicity studies in HepaRG cells. Four different setups suitable for application in high-throughput screening were used for the cultivation of HepaRG cells: 1) Traditional 2D cultivation, 2) collagen sandwich cultivation, 3) cultivation in an Alvetex® polystyrene scaffold and 4) spheroid cultivation. Investigated parameters included drug uptake, drug metabolization via phase I and II enzymes and levels of the radical scavenger glutathione. Subsequently, short-term toxicity upon single and repeated dosing was assessed using bosentan, chlorpromazine and valproic acid as test compounds. We found that the individual functional parameters differed to a great extent between the different cultivation systems, with spheroid cultures being the most active among the systems. In collagen sandwich cultures on the other hand, we observed lowest CYP450 activity and induction, as well as a critical ratio of reduced to oxidized glutathione. Interestingly, despite in some instances major differences in decisive functional parameters, EC₅₀ values obtained in the context of the toxicological studies were in the same range with exception of those in the Alvetex® polystyrene scaffold after single dosing. In total, we demonstrated that collagen sandwich HepaRG cultures require further optimization for application in toxicity-related studies, and we could show that Alvetex® polystyrene scaffold cultures did not provide superior results compared to the cheaper and easier to handle 2D cultures. Spheroid and 2D cultures on the other hand were shown to be overall most promising for future application in high-throughput screening approaches.

In **chapter 4**, we went about long-term cultivation of HepaRG cells for later application of the cells in a long-term repeated dose setup. Different compositions and renewal intervals for the cultivation medium were tested for providing best functionality and longevity to the HepaRG cell line. To avoid interference of medium components with subsequent analyses like proteomics and metabolomics, medium was kept serum-free, and serum-supplemented medium served as a reference. In accordance with the Organization for Economic Cooperation and Development (OECD) guideline 407, a duration of 30 days was chosen to investigate the performance of the different media. Over that period, stability of functional parameters, i.e. viability and CYP450 activity was assessed. Additionally, we quantified extracellular metabolites to identify potential bottlenecks in nutrients, as well as to perform metabolic flux analysis to better understand differences in cultivation with the different media. In order to maintain cells viable for 30 days, we found that in serum-free medium a maximum concentration of 0.5% dimethyl sulfoxide (DMSO) could be used, while HepaRG cells were able to cope with 1.8% DMSO in classical serum-supplemented medium. As DMSO induces the expression of several CYP450 isoforms, high DMSO concentrations offer an advantage in respect to the metabolization of xenobiotics. Yet, we observed a more stable CYP450 activity over the 30-day period in HepaRG cells cultivated in serum-free medium with 0.5% DMSO. Further, we identified the essential amino acid tryptophan and other non-essential amino acids as potential bottlenecks in nutrient supply, even when fresh medium was added every day. Therefore, the addition of tryptophan might further improve results obtained in the long-term cultivation of HepaRG. As a prove of principle, we could further show that HepaRG cells were susceptible to repeated dosing of valproic acid, with a 17-fold decrease in the EC₅₀ value after 2-week treatment, compared to a 24-h exposure.

In these two studies, we have shown the potential in optimizing media and the culture system environment to improve functionality of the HepaRG cell line as well as its potential application in long-term repeated dose toxicity studies. The latter is essential for reliable predictions of adverse events, as in many cases, toxicity does not occur before several weeks of exposure. Generally, there are three major points to improve current and future *in vitro* systems, which are described in the following. Particularly the first two points are intensively studied within the field of toxicology.

First, including additional cell types, i.e. co-cultivation of cells, often improves functionality of the hepatic system, but in some cases may also be indispensable to correctly predict adverse events. E.g. when the adverse reaction involves inflammatory responses, cells of the immune system will be necessary to fully depict the toxic processes. Combining different cell types is also part of the body-on-a-chip concept, which connects organotypic cultures or other types of cultures with a constant medium flow. This additionally allows studying processes like cardiotoxicity mediated by drug metabolites originating from drug metabolization in liver cells. Also, this approach eventually enables *in vitro* models to catch up with *in vivo* animal studies in terms of their systemic nature, which currently is likely to be the most striking reason for the use of animals in toxicology.

Second, improvement of *in vitro* cultures may be accomplished by cultivating cells in a 3D environment. As we have shown in our study on cultivation of HepaRG cells in a 3D environment, effects on cellular parameters may be tremendous and may help in adapting cellular activity to levels as observed *in vivo*. The 3D environment enables the cells to spread with *in vivo*-like cell-cell interaction and geometry, thereby triggering cellular responses that improve cells' functionality. Probably the most promising system among the plethora of available 3D cultivation tools is spheroid cultivation. Next to improved functionality, they offer other advantages, such as compatibility with microfluidic devices and high-throughput setups, as well as minimal cell number requirements. The latter however may become a problem in case analyses require large amounts of cell material, as it is the case for proteome analyses, but the problem can be overcome by pooling the necessary amount of spheroids. It is also worth mentioning that HepaRG spheroids have already been successfully applied to the body-on-a-chip concept (Maschmeyer et al., 2015).

Third, systems may be improved by optimizing the composition of the cultivation medium, as shown in chapter 4 of this thesis. Here, the goal is to provide nutrients and external stimuli required for optimal functionality of the cultures. For co-cultures as described before, the optimization process may become difficult, as the medium needs to be adapted for all involved cell types simultaneously and some essential supplements might be incompatible between different cell types. At the same time, the medium should be kept as close as possible to the *in vivo* situation.

In face of these challenges, it becomes clear that alternative systems for the study of toxicity will further require several years of intensive research to yield truly reliable data for the prediction of toxicity in humans.

Part III Application of HepaRG cells in repeated dose toxicity studies

Following the metabolic characterization and optimization of culture conditions for the HepaRG cell line, its applicability in risk assessment was investigated in a 4-week study in **chapter 5**. For that purpose, HepaRG cells were exposed to the two compounds bosentan and valproic acid, and viability was monitored throughout the treatment. Additionally, drug clearance was quantified and results were combined with viability data to estimate the oral equivalent dose using a reverse dosimetry approach. The oral equivalent dose is the amount of a compound that is needed to be taken up by an individual to

reach a steady state blood concentration of interest, such as the EC₁₀ for a given compound. In addition to the oral equivalent dose, we assessed alterations in metabolism in HepaRG cells upon repeated exposure to clinically relevant concentrations of the two compounds to better understand the underlying mechanisms inducing adverse events. Using the reverse dosimetry approach, we were able to estimate the risk that the compounds exert on a virtual human population, but also highlighted possible improvements to the technique. Based on alterations in concentrations of key metabolites, we could further demonstrate the influence of the compounds on metabolism and relate the effects to direct modulation of enzymatic activity or indirect effects via nuclear receptors. Verification of these hypotheses on the origin of metabolic alterations will be required in upcoming studies.

In a second application study, described in **chapter 6**, effects of valproic acid on HepaRG cells were assessed in a multi –omics approach to gain in-depth knowledge on the key mechanisms preceding an overt toxic response. In the context of this study, HepaRG cells were treated with valproic acid for 2 weeks in a repeated dosing regimen, and samples for functional assays, transcriptomics, proteomics, metabolomics and fluxomics analyses were collected on 4 different time points. We observed mild depletion of ATP already after 2 days of treatment, while viability was not affected until 14 days of exposure. Despite previous studies stating microvesicular steatosis as an adverse outcome upon valproic acid treatment, accumulation of triacylglycerides was only minor in our study. Instead, using transcriptomics, proteomics and metabolomics data, we found strong indications for endoplasmic reticulum stress on day 2 and day 8, turning into an apoptotic response by day 14. Further, fluxomics data provided information on an impaired ammonia detoxification via the urea cycle. Together, these three mechanisms are likely to be major contributors to the adverse response induced by valproic acid. In summary, we could demonstrate that the integration of several layers of –omics yields notably more comprehensive and more reliable information than any of the individual –omics tools could provide.

In these two chapters, we have applied two approaches, on the one hand reverse dosimetry to estimate the oral equivalent dose, supported by metabolic data, and on the other hand a multi –omics approach. Noteworthy, both approaches are independent of the cell system and may likewise be applied to genetically modified PHH or other cells.

Simple *in vitro* to *in vivo* extrapolation as we used in the reverse dosimetry approach gives first information on the risk associated with the compound of interest. The method is generally applicable and also compatible with high-throughput setups. Eventually, more sophisticated models will be required to predict adverse events. For example, the accumulation of a compound is not considered in with reverse dosimetry and requires more comprehensive pharmacokinetic models.

Multi –omics approaches as used in the second of these studies, are primarily applied to gain a better understanding of the mechanisms underlying adverse reactions. This may then be used to create *in silico* models, or to fill in gaps in already existing ones, thereby improving prediction of toxicity. The new insight in the corresponding processes may however also be used for improvements of the test system in the initial phase, in case needed. Even more, better understanding of the mechanisms of toxicity but also disease mechanisms may assist in relabeling of chemicals, i.e. the reallocation of known drugs to other indications, which further helps in reducing tests on animals.

Generally, *in silico* tools become more and more powerful and together with advances in *in vitro* approaches, they are a major driving force in replacing animals in the context of risk assessment. Moreover, not only may these approaches help in reducing animal experiments, but also in saving drug candidates from unnecessarily being sorted out during preclinical animal tests, despite being harmless to the human being. Using cell systems of human origin, false positive indications for

adverse events can be avoided. Therefore, it may be concluded, that upcoming methods are not meant to only replace animal studies, but to serve as an even better tool in the assessment of toxicity.

Supplementary material

Table of content

Supplementary material of chapter 2	140
Supplementary material of chapter 3	144
Supplementary material of chapter 4	145
Supplementary material of chapter 5	148
Supplementary material of chapter 6	161

Supplementary material of chapter 2

Supplementary figures

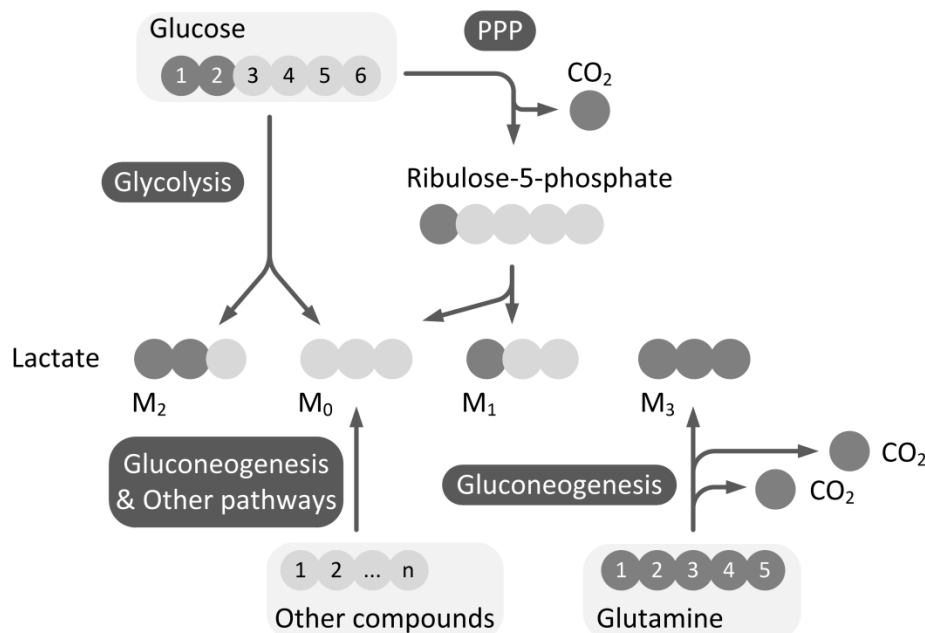


Figure S2.1 Scheme of the connection of the carbon atoms of [1,2- ^{13}C] glucose, [U- ^{13}C] glutamine and other compounds to lactate via different pathways. The connection of labeled and unlabeled sources for the formation of lactate applied in our study is highlighted. Carbon atoms of relevant compounds are represented as grey circles, with light grey circles representing unlabeled carbon atoms, and dark grey circles representing labeled, i.e. ^{13}C carbon atoms. The resulting mass isotopomers of lactate and their dependence on the source is highlighted.

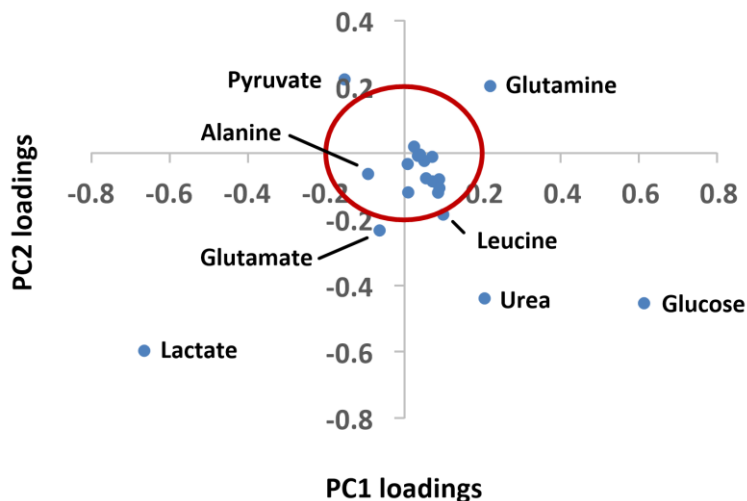


Figure S2.2 Loading coefficients of the secretion rates in untreated hepatic cells used for the first two principal components (PC) of the PCA shown in figure 2.1. A distance of greater 0.2 from the origin was used as a threshold (red circle) for metabolites particularly contributing to the differences in the hepatic cells. Metabolites with major contribution to the separation, as well as alanine, are labeled.

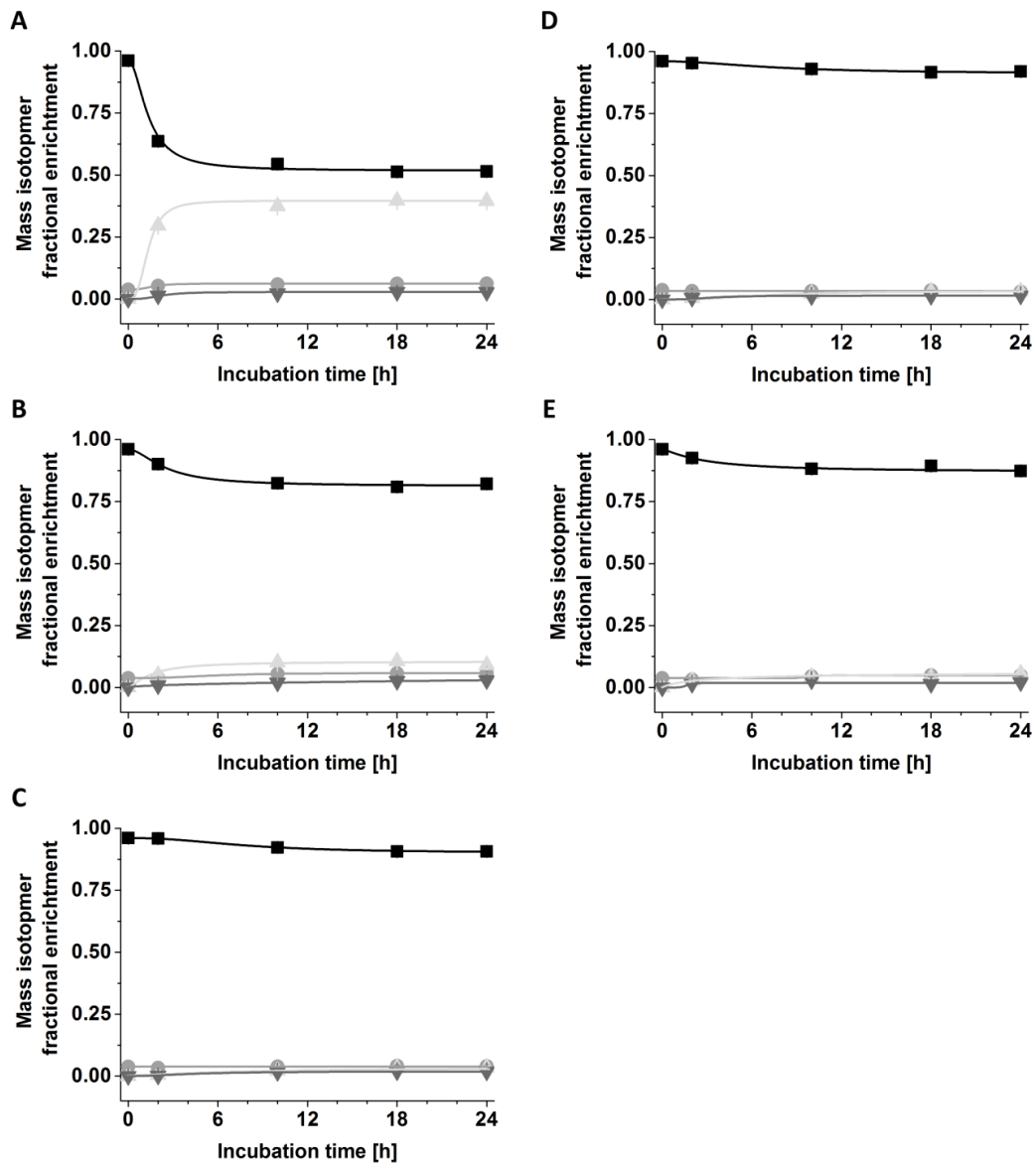


Figure S2.3 Mass isotopomer fractional enrichment in extracellular lactate over the course of 24 h in untreated HepG2 (A) and HepaRG cells (B), as well as for primary human hepatocytes from three different donors (PHH1 (C), PHH2 (D), PHH3 (E)). Mass isotopomers M_0 , M_1 , M_2 and M_3 are indicated by ■, ●, ▲ and ▼ respectively. Curve fits to the time course for the individual mass isotopomers are represented by lines in the respective color. Error bars indicate standard deviation ($n = 3$).

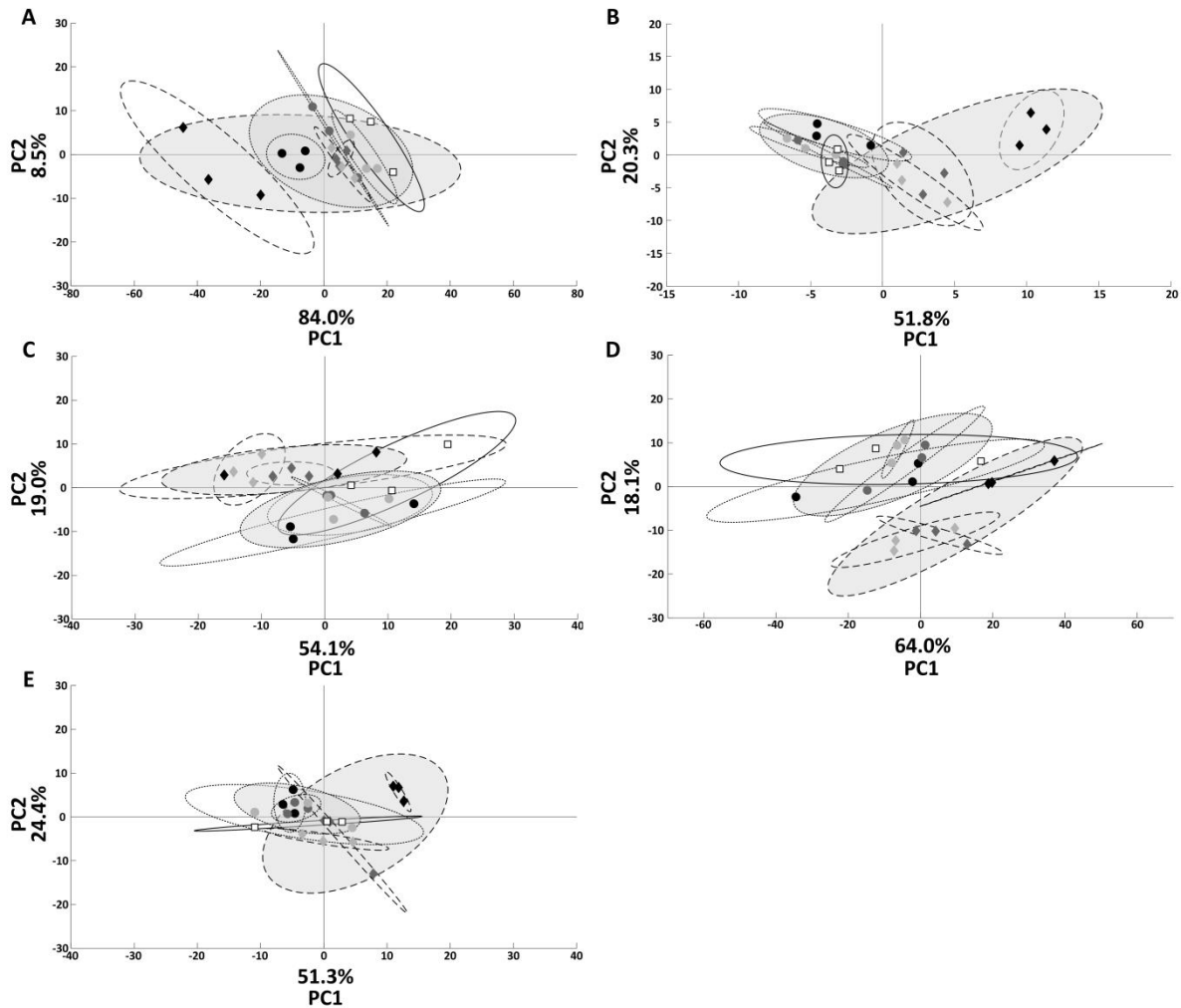


Figure S2.4 Principal component analyses representing all calculated secretion rates in treated (acetaminophen, diclofenac) and untreated hepatic cells ($n = 3$), for each system individually (HepG2 (A); HepaRG (B); PHH1 (C); PHH2 (D); PHH3 (E)). Circles and diamonds represent secretion rates from cells treated with acetaminophen and diclofenac, respectively. The different conditions are color-coded with light grey, dark grey and black representing c_{max} , subtoxic concentration and EC_{10} , respectively. White squares represent control cells. Dotted, dashed and full lines indicate 95% confidence ellipses for acetaminophen-treated, diclofenac-treated and control cells, respectively. Filled ellipses represent confidence regions for all tested concentrations combined (c_{max} , subtoxic concentration and EC_{10}).

Supplementary tables

Table S2.1 Donor characteristics of primary human hepatocytes (PHH1, PHH2, PHH3).

Donor	Sex	Age	Liver pathology	Diabetes	Smoking	Alcoholism	Batch number
PHH1	f	64	Hepatic synovialosarcom	No	No	No	HEP187225
PHH2	m	76	Cirrhosis	No	No	Not available	HEP187156
PHH3	m	25	Liver metastasis from colorectal cancer	No	No	No	HEP187103

Table S2.2 Summary of significantly altered secretion rates in the different hepatic cell systems upon exposure to the EC₁₀ for each drug relative to the control. *, ** and *** indicate a *p*-value lower than 0.05, 0.01 and 0.001 respectively.

	Acetaminophen					Diclofenac				
	HepG2	HepaRG	PHH1	PHH2	PHH3	HepG2	HepaRG	PHH1	PHH2	PHH3
Alanine	**	**			*	***	*	**	***	***
Asparagine	**				*	**			*	***
Aspartic Acid								*		**
Glucose	***	**				***	***			
Glutamic Acid	*						**	**	*	*
Glutamine	**	*				***	***	*	**	**
Glycine	*						*	**		***
Histidine	**				*	**			*	
Isoleucine	**	*			*	**	**		*	**
Lactate	*		**	***		*	**	**	***	**
Leucine	**	*			**	**	**		***	
Lysine				*					*	
Methionine	***	*			**	***	*		**	***
Phenylalanine	***					***		*	*	***
Pyruvate	*	*	***	*	***	**	**	***	***	***
Serine	**				**	**	**		**	***
Threonine	*					*			**	*
Tryptophan	*	***	**		**	*	*	*	***	**
Tyrosine					**					
Urea	*	*	**	*			*			**
Valine	*					**	*			**
Significantly altered metabolites	18	9	4	4	10	15	14	9	15	16

Supplementary material of chapter 3

Supplementary figures

```

[Values with no further indication were taken from Dunn et al., 2005, Biological Reaction Engineering, doi: 10.1002/3527603050]

DT=10
STOPTIME=21600 ;[s]
method stiff
dtmax=10

{Constants}
R =0.00315 ;Radius of single well in 96-well plate [m]
L =0.0032 ;height of MTP filling [m] / (in case of CSW cultures, value was 0.0054)
DO =3.1E-9 ;Diffusion coeff. for Oxygen in biofilm [m^2/s] (compost.css.cornell.edu/oxygen/oxygen.diff.water.html)
C_OS =0.3 ;Saturation conc. for oxygen at 35°C mM=[mol/m^3]
C_OG =C_OS
vmax =1.65E-15 ;[mol/(s x cell)] (estimated from doi: 10.1016/j.biomaterials.2015.11.026)
nCells =72E3 ;Number of cells in the bottom layer
KO =0.1 ;Saturation constant for Oxygen, mM=[mol/m^3]
N =10 ;Number of finite differences
Z =L/N ;Thickness of a biofilm segment [m]
V_N =3.14*Z*R^2 ;Volume of one segment [m^3]

{Initial concentration, mol/m^3}
init C_O[0..N] =C_OG

{For graphing purposes}
Nmid =round(N/2)
Osurface =C_O[0]
Omid =C_O[Nmid]
Obot =C_O[N]

{BALANCES FOR BIOFILM IN N SEGMENTS}
d/dt(C_O[0]) =0
d/dt(C_O[1..N-1]) =DO*(C_O[i-1]-2*C_O[i]+C_O[i+1])/(Z^2)
d/dt(C_O[N]) =DO*(C_O[i-1]-C_O[i])/(Z^2)+r_O/V_N

{Reaction rates in the biofilm segments, [mol/(m^3 x s)]}
r_O =-vmax*nCells*C_O[N]/(KO+C_O[N])

```

Figure S3.1 Differential equations for the calculation of oxygen diffusion in 2D/APS and CSW cultures.

```

METHOD stiff ;[s]
STOPTIME=21600
DT=10
DTMAX=10
DTOUT=10

{geometry}
d0 = 0.001 ; [m]
d1 = 0.0045 ; [m]
d2 = 0.0055 ; [m]
h1 = 0.004 ; [m]
h2 = 0.0024 ; [m]
hfill=h1+h2
r0 =d0/2
r1 =d1/2
r2 =d2/2
h1tot =h1*r1/(r1-r0)
h2tot =h2*r2/(r2-r1)
Nelements =30 ;Number of difference elements
Nupper=ROUND(Nelements*h2/hfill) ;Element at the transition upper_lower
delta2=h2/Nupper
delta1=h1/(Nelements-Nupper)
h[0..Nupper]=hfill-i*delta2
r[0..Nupper]=(h[i]-h1)*r2/h2tot+r1
h[Nupper+1..Nelements]=h1-(i-Nupper)*delta1
r[Nupper+1..Nelements]=h[i]/h1tot*r1+r0
A[0..Nelements]=r[i]^2*PI
V[0]=0
V[1..Nelements]=PI/3*(r[i-1]^2*h[i-1]-r[i]^2*h[i])
Vtot=ARRAYSUM(V[*]) ;Total volume [m^3]
VtotmL=Vtot*1e6 ;Total volume [µL]

{Constants}
DO =3.1E-09
C_OS =0.3
vmax =1.65E-15
nCells =72E3
KO =0.1

{Initial Conditions}
INIT C_O[0..Nelements] =C_OS

{SUBSTRATE OXYGEN BALANCES FOR EACH DELTA R ELEMENT}
dcdt[0]=0
{upper cone}
dcdt[1..(Nelements-1)]=DO*(A[i-1]*(C_O[i-1]-C_O[i])/(h[i-1]-h[i]) - A[i]*(C_O[i]-C_O[i+1])/(h[i]-h[i+1]))/V[i]

{Bottom layer}
dcdt[Nelements]=DO*A[i-1]*(C_O[i-1]-C_O[i])/(h[i-1]-h[i])/V[i] +r_O/V[Nelements]
d/dt(C_O[0..Nelements])=dcdt[i]
limit C_O>=0

Osurface =C_OS
Omid =C_O[Nupper]
Obot =C_O[Nelements]

{RATE EQUATION}
r_O=-vmax*nCells*C_O[Nelements]/(KO+C_O[Nelements])
timeh=Time/3600

```

Figure S3.2 Differential equations for the calculation of oxygen diffusion in spheroid cultures.

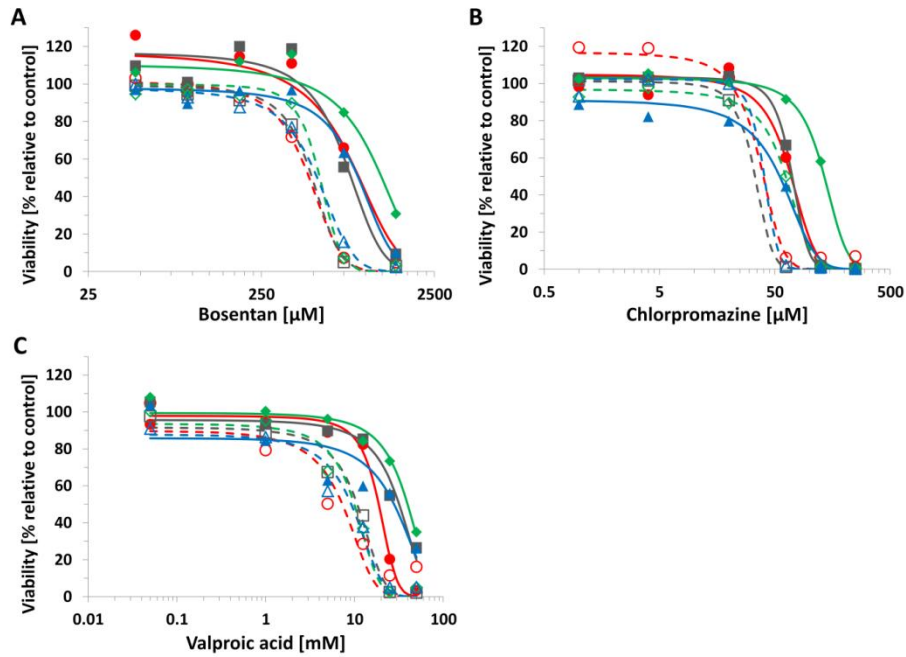


Figure S3.3 Dose response curves of HepaRG cells in different cultivation systems exposed to bosentan (A), chlorpromazine (B) and valproic acid (C) for either 24 h (single dose, closed symbols, full lines) or 72 h (three doses, open symbols, dashed lines). Symbols indicate 2D (■), Alvetex® polystyrene scaffold (◆), collagen sandwich (▲) and spheroid (●) cultures. Viability was assessed by quantification of ATP.

Supplementary material of chapter 4

Supplementary figures

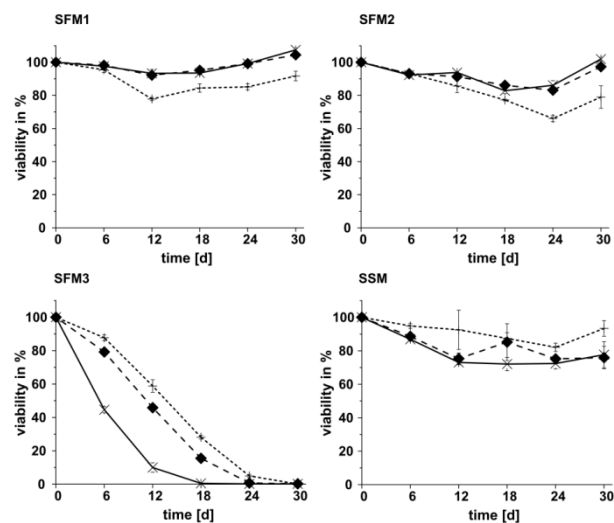


Figure S4.1 Effect of different medium renewal intervals on the viability of HepaRG cells when kept in different media. Medium renewal was performed daily (X), every second day (♦) or every third day (+) in SFM1 / 2 / 3 [serum-free medium with growth factors and 0% / 0.5% and 1.8% dimethylsulfoxide (DMSO),

respectively] and SSM (serum-supplemented medium with 1.8% DMSO). Error bars indicate standard deviation ($n = 3$). Viability is given in percentage relative to HepaRG culture viability on day 0.

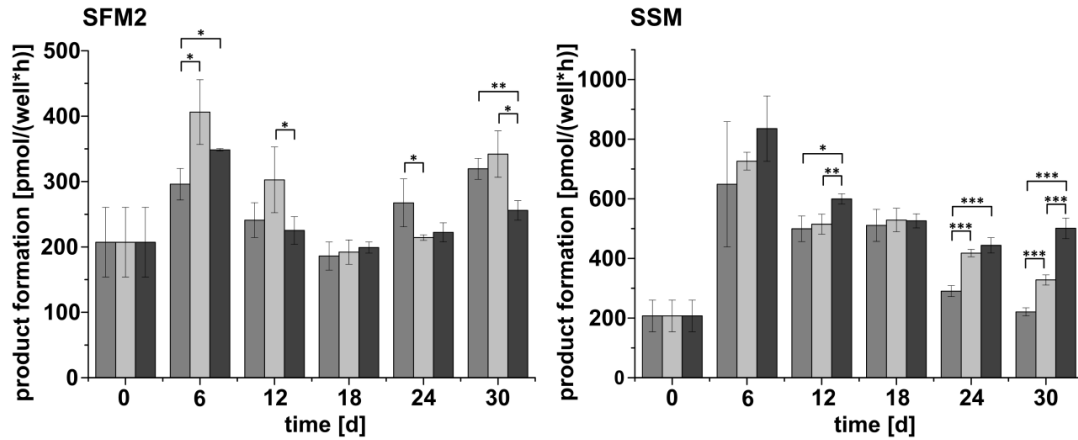


Figure S4.2 Effect of different medium renewal intervals on the activity of CYP3A4 for HepaRG maintained in SFM2 [serum-free medium with growth factors and 0.5% dimethylsulfoxide (DMSO)] and SSM (serum-supplemented medium with 1.8% DMSO). Dark grey histograms represent every day, light grey histograms show every second day and black histograms every third day renewal interval. Error bars indicate standard deviation ($n = 3$). *, **, *** indicate $p < 0.05$, $p < 0.01$ and $p < 0.001$, respectively.

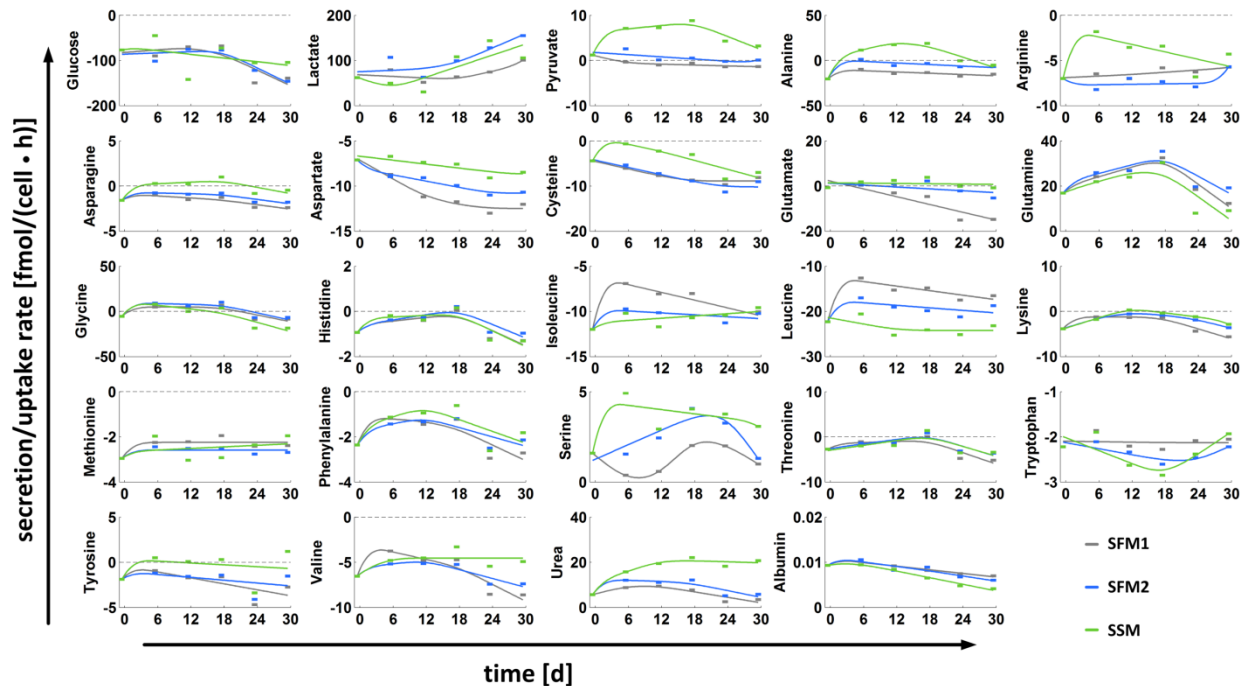


Figure S4.3 Secretion and uptake rates of organic acids, glucose, urea and albumin for HepaRG cells during 30-day cultivation. SFM1 / 2 [serum-free medium with growth factors and 0% or 0.5% dimethylsulfoxide (DMSO), respectively] and SSM (serum-supplemented medium with 1.8% DMSO). Negative values mean uptake, positive values correspond to secretion. Splines were fitted to the extracellular rates using MatLab 2007b and SLM spline toolbox.

Supplementary material of chapter 5

Supplementary figures

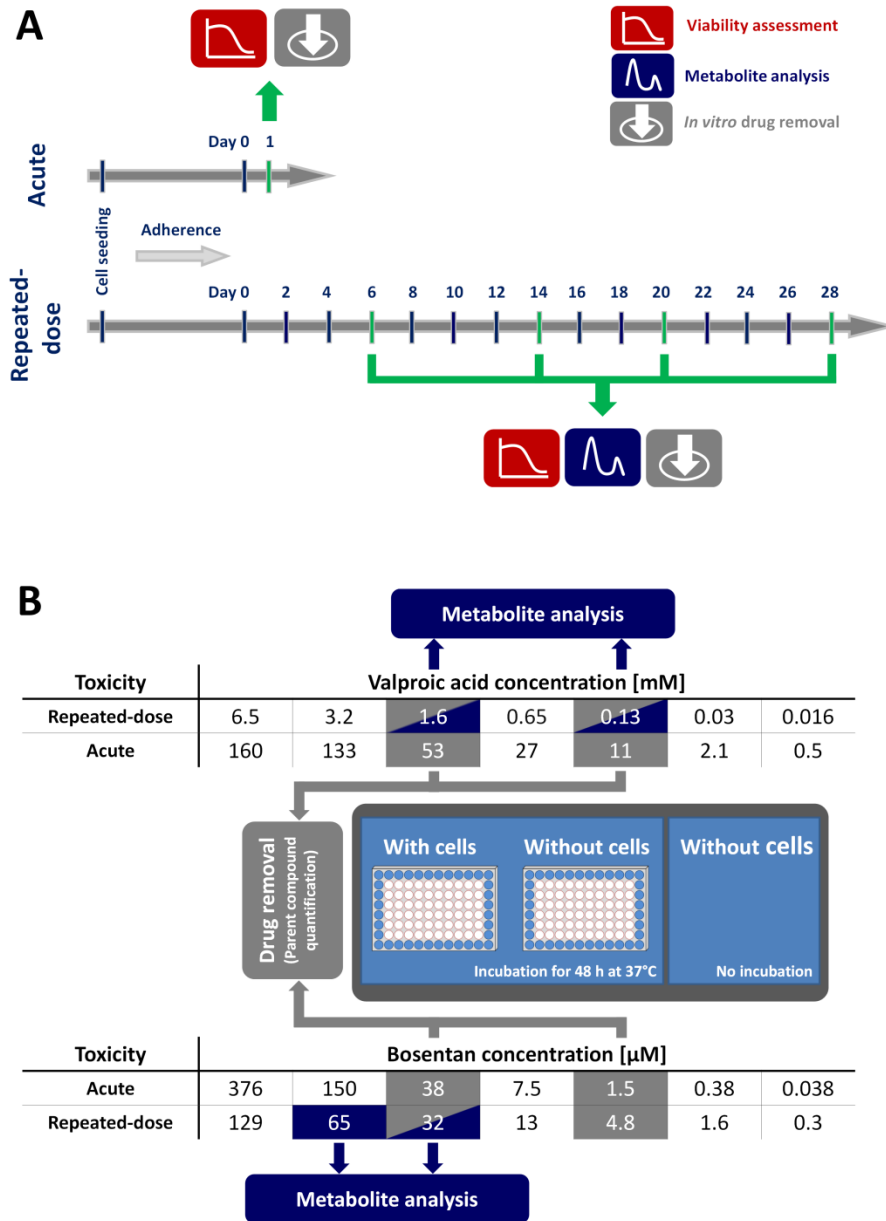


Figure S5.1 Experimental design. Protocol for acute and repeated-dose exposure to bosentan and VPA. Time schedule and performed analyses are given (A). Vertical lines indicate medium renewal (blue) or medium renewal plus analyses (green). Sampling points are highlighted by green arrows. Exposure concentrations for both bosentan and VPA including experimental setup for drug clearance (parent compound quantification) is depicted (B). Conditions investigated in detail are highlighted in dark blue (metabolites analyses) and grey (*in vitro* drug removal).

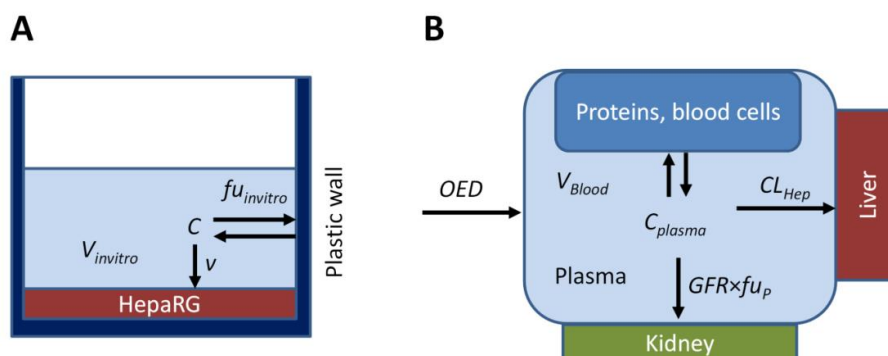


Figure S5.2 Graphical representation of *in vitro* and *in vivo* balances for drug clearance. Schemes of experimental *in vitro* system (A) and of the human body (B) PK model used for the calculation of OED. The *in vitro* system uses 2D cultures of HepaRG cells attached to the bottom of a microtiter plate well. Since there are no free cells and no plasma in the system, only binding of the compound to the walls of the microwell has to be considered. The removal by the HepaRG cells is quantified by the reaction velocity v (A). The human body model consists of the blood containing plasma, plasma proteins and blood cells. The test compound is introduced with a rate characterized by the oral equivalent dose (OED). It may bind to blood cells and serum proteins as characterized by f_{u_p} , the fraction of unbound compound in plasma. The compound is removed by the liver, characterized by hepatic clearance, CL_{Hep} and by the kidney, characterized by GFR , the glomerular filtration rate [L/h] (B).

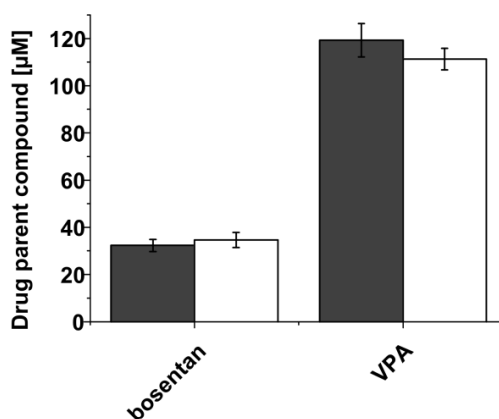


Figure S5.3 Parent compound concentration in the *in vitro* setup. Mean drug parent compound concentrations in medium before (white bars) and after (grey bars) 48 h cell-free incubation at 37°C. Error bars indicate standard deviations from measurements taken at different sampling time points during repeated-dose study (N=4, total n=12 for samples after incubation, N=4 for samples before incubation). Unpaired Student's t -test was performed for comparison of parent drug concentrations in medium with and without cell-free incubation. Bosentan concentration changed from 34.6 μM to 32.3 μM after incubation. VPA was found in concentrations of 111 μM before and 119 μM after incubation. The differences were not statistically significant.

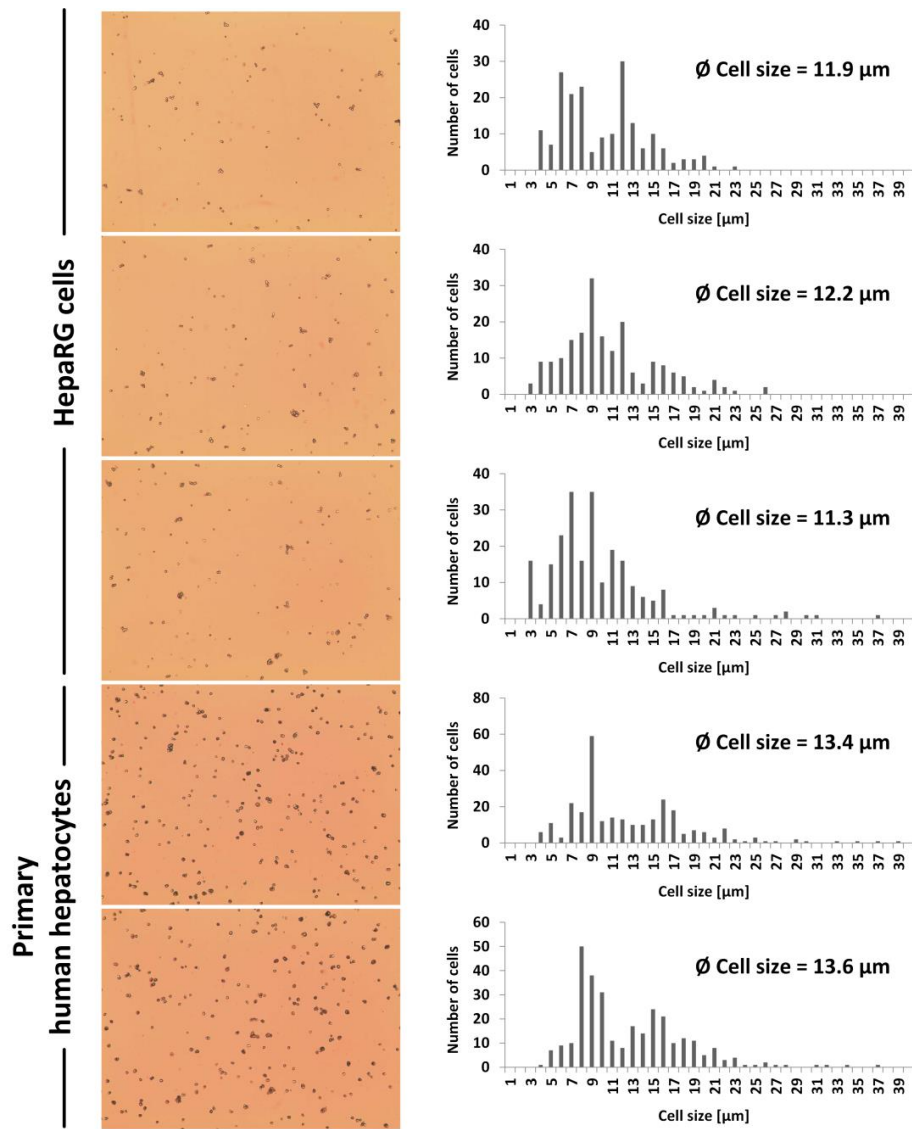


Figure S5.4 Cell size. Cell diameters of HepaRG cells and primary human hepatocytes in suspension. Cell size was determined using a Countess™ Automated Cell Counter giving the average cell diameter of living cells. Pictures and histograms are given for HepaRG ($n=3$) and primary human hepatocytes ($n=2$).

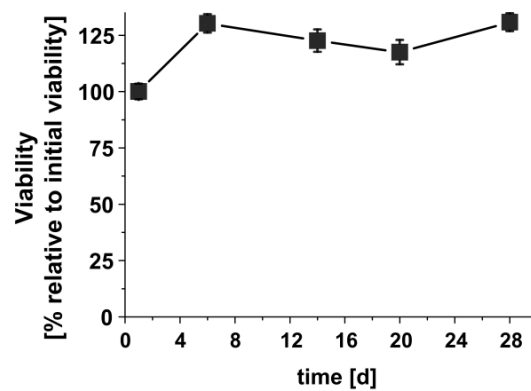


Figure S5.5 Long-term viability. Viability of HepaRG cultures assessed with CellTiter-Blue® assay over a period of 28 days. Viability was calculated by normalizing fluorescence signals to the initial signal assessed on day 0. Error bars indicate standard deviations ($n=3$).

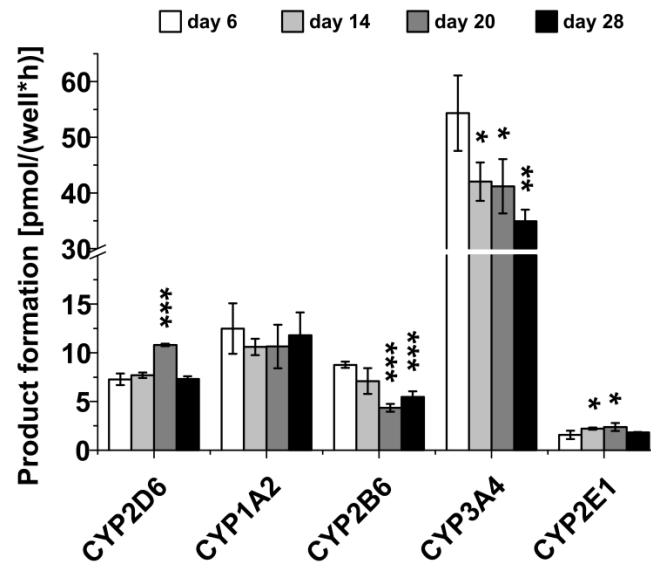


Figure S5.6 Metabolic competence. CYP450 activities for CYP2D6, CYP1A2, CYP2B6, CYP3A4 and CYP2E1 in untreated HepaRG cells over time. Error bars indicate standard deviations ($n=3$). Unpaired Student's t -test was performed for comparison of each CYP450 activity to its activity on day 6. Significance is indicated by *, **, *** corresponding to $p < 0.05$, $p < 0.01$ and $p < 0.001$ respectively.

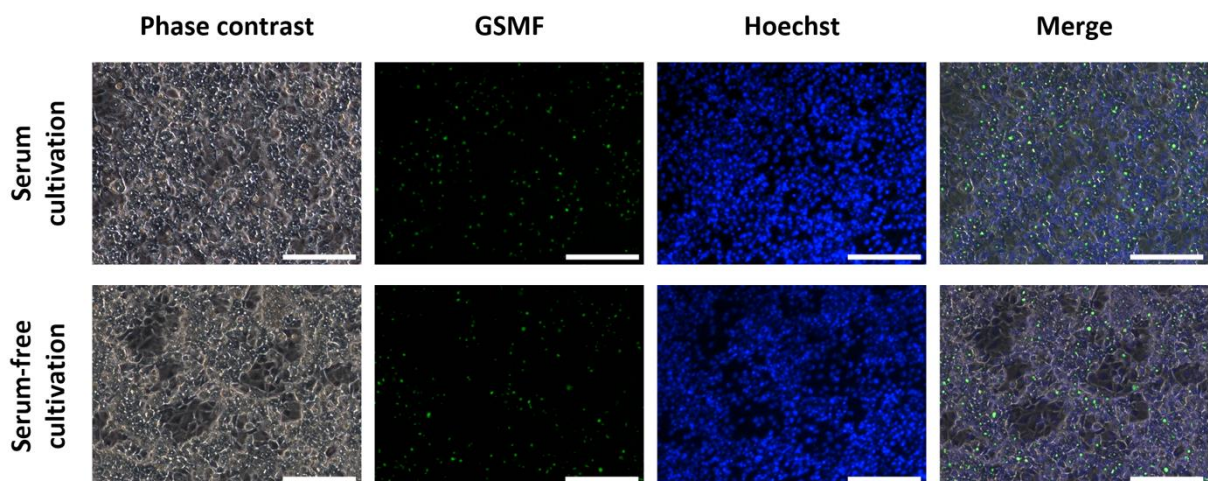


Figure S5.7 Drug efflux transporter activity. Light and fluorescence microscopy for the localization of CMFDA in the assessment of MRP2 activity. HepaRG cells were either incubated with serum-free or serum-supplemented medium for 4 days prior to microscopy. Nuclei were stained using Hoechst dye. White bars represent 200 μm .

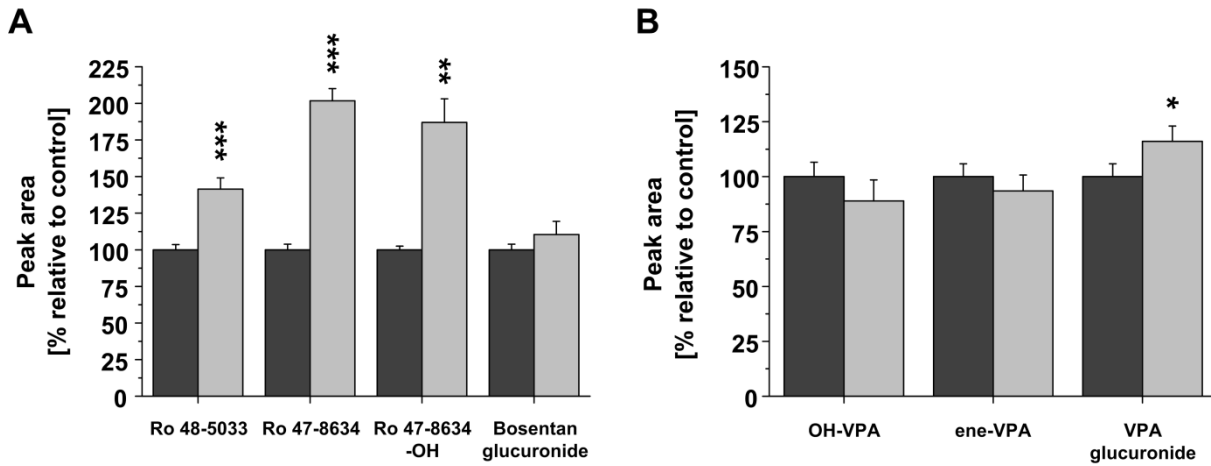


Figure S5.8 Drug metabolism. Drug metabolite formation in HepaRG cells. Relative peak area of bosentan (A) and VPA (B) drug metabolites found in the supernatants after 24 h incubation with the parent compound. Peak areas upon induction of HepaRG cells with rifampicin (light grey) are normalized to the peak areas found in the un-induced control (dark grey). Error bars indicate standard deviations ($n = 3$). Significance is indicated by *, **, *** corresponding to $p < 0.05$, $p < 0.01$ and $p < 0.001$ respectively.

Supplementary tables

Table S5.1 Physiological parameter ranges used for the virtual population. Values were taken from (ICRP, 2002).

	Mean	Lower limit	Upper limit
<i>GFR</i> [L/h]	7.5	3.75	11.25
<i>Q_L</i> [L/h]	97.8	78	114
<i>LW</i> [kg]	1.6	1.1	2.1
<i>BW</i> [kg]	66.5	50	90

Q_L = Liver blood flow, *LW* = Liver weight, *BW* = Body weight

Table S5.2 Summary of parameters used during the calculation of the OED and their sources.

	Value	Source
R_{BP} (bosentan)	0.55	(Poulin, 2013)
R_{BP} (VPA)	0.2	(Shirkey et al., 1985)
pH (cytosol)	7.0	(Poulin et al., 2012)
pH (plasma)	7.4	(Poulin et al., 2012)
pK_a (bosentan)	5.2	(Poulin, 2013)
pK_a (VPA)	4.8	http://www.drugbank.ca/drugs/DB00313 accessed on July 10, 2015
PLR	13.3	(Poulin et al., 2012)
fu_p (bosentan)	0.0053	(Poulin, 2013)
fu_p (VPA)	0.1425	Average value calculated from data available on http://www.drugbank.ca/drugs/DB00313 accessed on July 10, 2015
BA_{Oral} (bosentan)	0.5	(Weber et al., 1996)
BA_{Oral} (VPA)	1	(Perucca et al., 1978)
Hepatocellularity (hc)	1.39×10^{11} cells per kg liver	(Sohlenius-Sternbeck, 2006)
$V_{invitro}$	100×10^{-6} L	Experimental parameter
V_{HepaRG}	0.86×10^{-12} L	Experimentally determined
V_{PHH}	1.29×10^{-12} L	Experimentally determined
$k_{invitro}$ (bosentan) day 1	$2.73 \times 10^{-12} \text{ h}^{-1}$	Calculated
$k_{invitro}$ (bosentan) day 6	$2.57 \times 10^{-11} \text{ h}^{-1}$	Calculated
$k_{invitro}$ (bosentan) day 14	$3.30 \times 10^{-11} \text{ h}^{-1}$	Calculated
$k_{invitro}$ (bosentan) day 20	$4.84 \times 10^{-11} \text{ h}^{-1}$	Calculated
$k_{invitro}$ (bosentan) day 28	$5.13 \times 10^{-11} \text{ h}^{-1}$	Calculated
$k_{invitro}$ (VPA)	$1.44 \times 10^{-11} \text{ h}^{-1}$	Calculated

Table S5.3 Relative distribution of bosentan and its metabolites in the supernatant after 3 and 24 h incubation with HepaRG cells. Relative distributions are given for the drug and its metabolites (total), and separately only for the metabolites (metabolites).

Incubation period (h)	Percentage of	Bosentan	Ro 48-5033	Ro 47-8634	Ro 47-8634-OH	Bosentan glucuronide
		Total	96.6	1.5	1.9	0.04
3	Metabolites	-	42.5	56.2	1.2	0.2
	Total	95.0	2.6	2.3	0.07	0.01
24	Metabolites	-	51.3	47.0	1.4	0.3

Table S5.4 Relative distribution of VPA and its metabolites in the supernatant after 3 and 24 h incubation with HepaRG cells. Relative distributions are given for the drug and its metabolites (total), and separately only for the metabolites (metabolites).

Incubation period (h)	Percentage of	VPA	OH-VPA	ene-VPA	VPA glucuronide	VPA-CoA	2,4-diene-VPA	Keto-VPA
		Total	96.8	0.01	0.04	3.1	<i>n.d.</i>	<i>n.d.</i>
Metabolites	-	0.4	1.2	98.4				
24	Total	88.5	0.03	0.03	11.5			
	Metabolites	-	0.2	0.3	99.5			

n.d. = not detected.

Supplementary methods

CYP450 activity assay

Frozen samples were thawed at room temperature and diluted with 0.1% formic acid in ultrapure water. OH-chlorzoxazone was quantified by HPLC tandem mass spectrometry. The system consisted of an AB Sciex API3200 triple quadrupole mass spectrometer (Framingham, USA) interfaced with an Agilent 1200SL HPLC (Santa Clara, USA). Chromatography was performed at 70°C with 20 µL injected into a Zorbax Eclipse XDB C18 column (50 mm × 4.6 mm, 1.8 µm particle size) at a flow rate of 1.5 mL/min. The column eluent was split to an electrospray ionization interface, operating at 650°C in multiple reaction monitoring mode (183.9 to 119.9) in negative polarity. The mobile phase was 0.01% formic acid in ultrapure water (A) and acetonitrile (B). The proportion of the mobile phase B was increased linearly from 10 to 50% in 1.2 min and then the column was flushed with 95% of the mobile phase B and then allowed to re-equilibrate at initial conditions.

Quantification of drug metabolites

Samples for drug metabolite quantification were precipitated by the addition of acetonitrile. After centrifugation, the supernatants (containing 90% acetonitrile) were analyzed by LC/MS. A high performance LC system consisting of an Accela U-HPLC pump and an Accela auto sampler (Thermo Fisher Scientific, USA) was used. The LC was performed in the gradient mode using acetonitrile with 0.2% acetic acid as organic phase (A), and aqueous 0.2 % acetic acid (B); the pump flow rate was set to 420 µl/min (% A (t (min), 0(0-0.1)-97(1.2-2.5)-0(2.6–5.0)). LC was performed using a Kinetex Phenyl-Hexyl, 2.6 µm, 50 × 2.1 mm (Phenomenex, Germany) analytical column with a pre-column (UHPLC Phenyl for 2.1 mm ID columns, Phenomenex, Germany). Mass spectrometry was performed on a Q-Exactive or an Exactive mass spectrometer (Orbitrap® technology with accurate mass) for valproic acid and bosentan respectively, equipped with a heated electrospray interface (Thermo Fisher Scientific, USA) connected to a PC running the standard software Xcalibur 2.1.

As MS tune file, a generic tune file was used, applying the negative or positive ion mode for valproic acid or bosentan respectively. As lock mass for internal mass calibration the $[M+H]^+$ ion of the Diisooctyl phthalate (m/z 391.28429), which is ubiquitously present in the solvent system, was used. The analytes were acquired by scanning ± 1 Thomson around the expected mass of the monoisotopic $[M+H]^+$. High-resolution mass measurement was performed in Orbitrap® mode with a resolution of 50,000. The accurate mass of each metabolite was used for peak integration. Further instrument settings were as follows: high-energy collisional dissociation 20 eV, automatic gain control high dynamic range, max. trap injection time 100 ms, sheath gas 30, aux gas 8, sweep gas 2, spray voltage 4 kV, capillary temperature 250°C, electrospray ionization 2 heater temperature 250°C. The data acquisition was performed on a Thermo Fisher Scientific mass spectrometer, consisting of a standalone Orbitrap® mass analyser (Exactive).

For the analysis of VPA metabolites, the accurate masses of VPA and the following metabolites were used ($[M+H]^+$, theoretical exact mass): VPA (143.1078), monohydrated valproic acid (159.1027, OH-VPA), dehydrogenated valproic acid (141.0921, ene-VPA) and valproic acid glucuronide conjugate (319.1398, VPA glucuronide).

For the analysis of bosentan metabolites, the accurate masses of bosentan and the following metabolites were used ($[M-H]^-$, theoretical exact mass): bosentan (552.1911), monohydrated bosentan (568.1861, Ro 48-5033), demethylated bosentan (538.1754, Ro 47-8634), monohydrated

and demethylated bosentan (554.1704, Ro 47-8634-OH) and bosentan glucuronide conjugate (727.7382, bosentan glucuronide).

Extraction and quantification of total drug parent compound

Quantification was performed with a Perkin Elmer series 200 HPLC connected to an Applied Biosystem-SCIEX API 3000 triple quadrupole mass spectrometer. A Kinetex XB-C18 column 50×2 mm i.d., 5 μ m particle size (Phenomenex, USA), was used for chromatographic separation. The mobile phases were 0.1 % formic acid in MilliQ water for positive ionization and 0.05 % acetic acid in MilliQ water for negative ionization (A) and acetonitrile (B) with a gradient set as follow: from 30 to 100 % B in 6 min, 100 % B for 2 min, 100 to 30 % B in 2 min, 30 % B for 7 min, at 200 μ L/min. The injection volume was 10 μ L of the sample. The turbo ion spray source temperature was 350 $^{\circ}$ C. Ion spray voltage was set to 5000 V for bosentan and -4200 V for VPA. The nebulizer and the curtain gas were set at 7 and 8 units respectively. The analysis was done in the multiple reaction monitoring mode (MRM). The optimized transitions and parameters were: 552.2-202.2 and 552.2-280.2 m/z for bosentan, with collision energy of 47 and 57 eV respectively, declustering potential set at 60 V and focusing potential at 220 V; 558.3-202.3 and 558.3-280.1 m/z for Bosentan- $^{13}\text{C}_2, ^2\text{H}_4$, with collision energy of 45 and 55 eV respectively, declustering potential set at 55 V and focusing potential at 200 V; 143.0-143.0 m/z for VPA, with collision energy of -5 eV, declustering potential set at -40 V and focusing potential at -140 V; 121.0-77.0 m/z for benzoic acid with collision energy of -17 eV, declustering potential set at -10 V and focusing potential at -70 V.

Reverse dosimetry for the estimation of the oral equivalent dose

Reverse dosimetry was used for the estimation of the oral equivalent dose (OED). These calculations are based on simplified balances of the *in vitro* in *in vivo* model systems as depicted in supplementary figure S5.2.

Kinetics estimation

Most common kinetics used for the description of drug metabolism are first order and to a lesser extent Michaelis-Menten-type kinetics (MM kinetics). A common procedure to identify first order kinetics it to check for constant half-life time of the reaction. In our experiment, we obtained data for one high concentration and one low concentration at each time point of the repeated-dose experiments, i.e. at days 1, 6, 14, 20, 28. We measured the conversion over a period of 24 h or 48 h. Apparent first-order rate constants were determined by

$$k = -\frac{\ln C_0 - \ln C_1}{t_0 - t_1} \quad [\text{S5.1}]$$

C is the drug concentration (mol/L). If the estimated k values [1/h] were identical at high and low initial concentrations, first order kinetics were assumed. This was the case for valproic acid (VPA) but not for bosentan. Dividing by the viable cell number yields the rate constant per cell that is used in equation 5.5 of the main text.

$$k_{\text{invitro}} = \frac{k}{N_{\text{invitro}}} \quad [\text{S5.2}]$$

We found that k_{invitro} remained nearly constant throughout the 28 days of experiment. This was the case for valproic acid (VPA) but not for bosentan. Therefore, we decided to estimate one constant (k) value

for the whole dataset in the case of VPA. In the case of bosentan MM kinetics were applied and one single set of constants (k_{MM} and K_M) was determined for the whole set of bosentan experimental data using a numerical procedure. MM kinetics were defined as

$$v = k_{MM} \times N_{invitro} \times \frac{C}{K_M + C} \quad [S5.3]$$

k_{MM} is the rate constant [mol/(L × h × cell)] and K_M the Michaelis-Menten constant (mol/L). The resulting differential equation

$$\frac{dC}{dt} = -v \quad [S5.4]$$

was solved numerically using the function *ode15s* of MATLAB. Simultaneously, all experimentally determined concentrations were compared with concentrations calculated by the model. A suitable objective function, i.e. weighted least squares, was used to find optimal parameter values. Weighting was done by division of model deviation by the model value at that time point. Parameter estimation was accomplished by using the function *fmincon* of MATLAB. In the case of VPA, k_{MM} and K_M were highly correlated and only the ratio could be determined

$$k_{invitro} = \frac{k_{MM}}{K_M} \quad [S5.5]$$

In the case of MM kinetics, $k_{invitro}$ used in equation 5.5 of the main text depends on the test compound concentration C as can be derived from the following equation;

$$k_{invitro} = \frac{k_{MM}}{K_M + C} \quad [S5.6]$$

Bosentan *in vitro* kinetics

The parameter estimation progress is depicted in figure SM1 showing the objective function, k_{MM} and K_M .

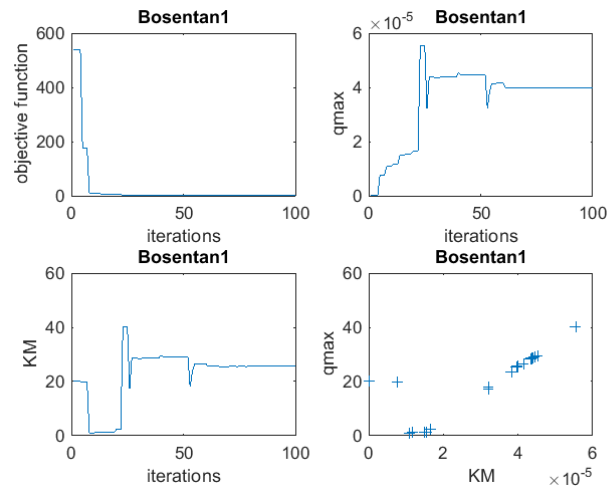


Figure SM1 Parameter estimation progress using MM kinetics. q_{max} is k_{MM} of equation S5.3.

Table SM1 lists the resulting experimental and model data of the kinetic experiment. A graphical comparison is shown in figure SM2

Table SM1. Experimental and model data of Bosentan removal by HepaRG cells in 96-well plates.

Day	C_0	C_{exp}	C_{model}	$C_{model} - C_{exp}$
	$\mu\text{mol/L}$	$\mu\text{mol/L}$	$\mu\text{mol/L}$	$\mu\text{mol/L}$
1	37.56	26.68	22.94	-3.74
6	30.73	3.77	7.27	3.50
6	7.65	0.43	0.71	0.28
14	32.09	7.15	8.02	0.87
14	4.94	0.46	0.43	-0.03
20	31.21	8.22	6.83	-1.39
20	4.56	0.59	0.35	-0.24
28	5.25	0.63	0.46	-0.17

The determined kinetic parameters are:

$$k_{MM} = 3.62 \times 10^{-5} \text{ mol}/(\text{L} \times \text{h} \times \text{cell})$$

$$K_M = 25.2 \text{ mol/L}$$

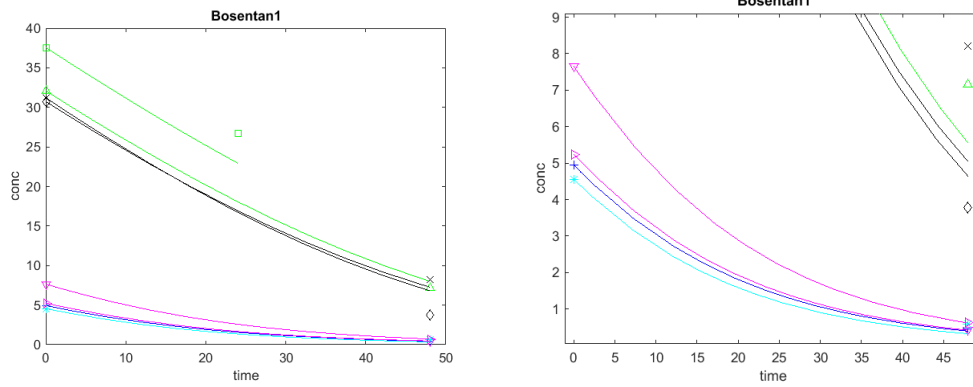


Figure SM2 Bosentan removal by HepaRG cells following MM kinetics. The right-hand part shows data with a magnified concentration scale.

VPA in vitro kinetics

The parameter estimation progress is depicted in figure SM3 showing the objective function, k_{MM} and K_M .

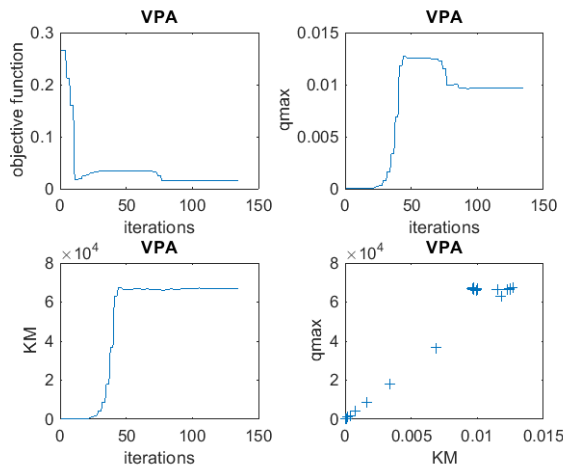


Figure SM3 Parameter estimation progress using MM kinetics. qmax is k_{MM} of equation 3.

Table SM2 lists the resulting experimental and model data of the kinetic experiment. A graphical comparison is shown in figure SM4.

Table SM2 Experimental and model data of VPA removal by HepaRG cells in 96-well plates.

Day	C_0	C_{exp}	C_{model}	$C_{model} - C_{exp}$
	mmol/L	mmol/L	mmol/L	mmol/L
1	53.105	47.154	49.594	2.440
1	10.991	10.448	9.686	-0.762
6	1.655	1.288	1.313	0.026
6	0.115	0.087	0.090	0.002
14	1.558	1.373	1.319	-0.054
14	0.117	0.096	0.091	-0.005
20	1.553	1.318	1.415	0.097
20	0.117	0.089	0.090	0.001
28	1.692	1.641	1.636	-0.005
28	0.127	0.096	0.099	0.003

The determined kinetic parameters are:

$$k_{MM} = 9.66 \times 10^{-3} \text{ mmol}/(\text{L h cell})$$

$$K_M = 66920 \text{ mmol/L}$$

The very high estimated K_M value indicates first order kinetics that are described by

$$k_{MM}/K_M = 1.4429 \times 10^{-7} \text{ (1/h)}$$

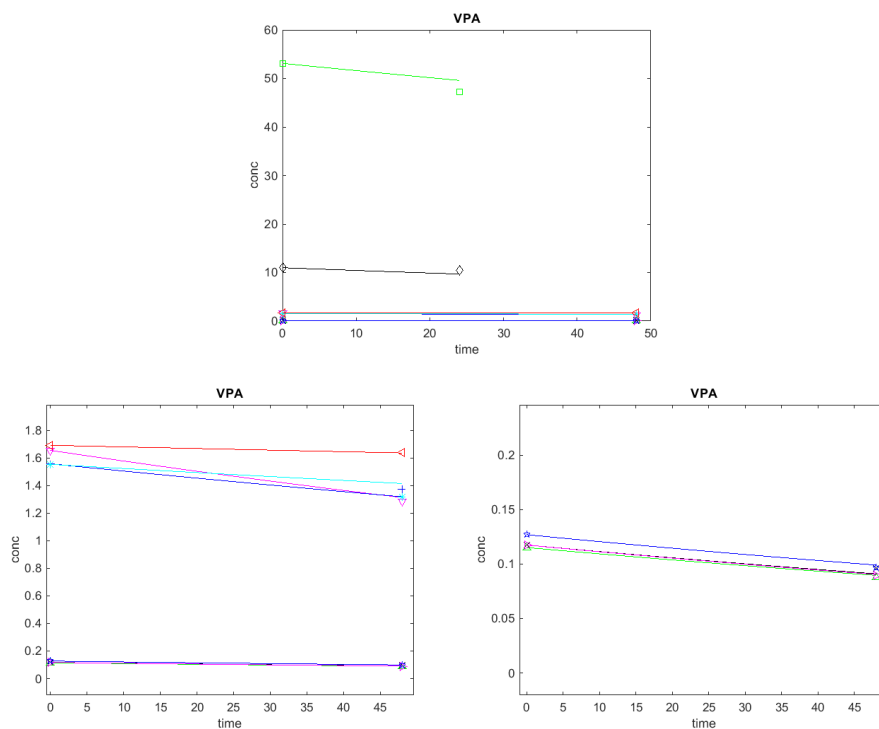


Figure SM4 VPA removal by HepaRG cells. The lower parts show data at a magnified concentration scale.

Cell size determination for upscaling HepaRG to PHH

For the determination of the cell volumes of HepaRG cells and primary human hepatocytes, both cell types were brought in suspension using cryopreserved HepaRG cells and primary human hepatocytes. 20 μ L of each suspension were mixed with an equal volume of trypan blue (Invitrogen Life Technologies, Darmstadt, Germany) and pipetted onto a Countess™ cell counting chamber slide (Invitrogen Life Technologies, Darmstadt, Germany). A Countess™ Automated Cell Counter (Invitrogen Life Technologies, Darmstadt, Germany) was used to determine the average size of living cells including the distribution of the cell size (figure S5.4). Cells with a diameter below 5 μ m and above 23 μ m were excluded from the calculation of the average cell size to avoid including cell debris and cell clusters into the calculation. Average cell sizes were used to calculate the volume of HepaRG cells and primary human hepatocytes under the assumption of a spherical cell shape.

Average cell size in HepaRG cells was 11.8 μ m and 13.5 μ m for primary human hepatocytes. Volumes calculated from the diameters were 0.86 and 1.29 pL, respectively, resulting in a volume ratio R_v of 1.5.

Supplementary discussion

Characterization of the test system

There was no significant change in the viability of the culture upon 28-day cultivation. The CYP450 activities (CYP2D6, CYP1A2, CYP2B6, CYP3A4 and CYP2E1) in the present study remained stable over the 28-day cultivation period. Additionally, we previously reported high CYP2C9 activity in serum-free HepaRG culture (Klein et al., 2014).

HepaRG cultures have been reported to show mRNA levels and activity of various transporters; namely uptake transporters such as Na⁺-taurocholate cotransporting polypeptide (NTCP) and organic anion transporting polypeptide (OATP); efflux transporters such as bile salt export pump (BSEP), multidrug resistance associated proteins (MRP), multidrug resistance proteins (MDR) and breast cancer resistance protein (BCRP) (Anthérieu et al., 2012a; Bachour-El Azzi et al., 2015; Kanebratt and Andersson, 2008; Kotani et al., 2012; Le Vee et al., 2013; Pernelle et al., 2011; Sharanek et al., 2014; Ulvestad et al., 2012). In the present study, HepaRG cells with and without serum show comparable MRP2 activity (drug efflux). Investigation of all transporters was beyond the scope of this study. However, the presence of metabolites in culture supernatants especially the glucuronide conjugates proves functional uptake of parent compounds and efflux of drug metabolites in our system. Bosentan is taken up by OATP transporters (Treiber et al., 2007), whereas uptake mechanisms of VPA are discussed controversially. Various hypotheses include passive diffusion and transporter-mediated uptake by OATP, monocarboxylate transporters and solute carrier 4A11 (Booth et al., 1996; Fischer et al., 2008; Terbach et al., 2011; Thwaites and Anderson, 2007). The glucuronide conjugates of both compounds are secreted *via* the MRP2 transporters (Fahrmayr et al., 2013; Jedlitschky et al., 1996).

We detected glucuronide conjugates of both bosentan and VPA in our experiments. In addition, all major metabolites of bosentan described in literature (Ro 48-5033, Ro 47-8634, Ro 47-8634-OH) and primary metabolites of VPA (OH-VPA and ene-VPA) were detected. Keto-VPA, 2,4-diene-VPA and VPA-CoA could not be detected probably due to the instability of these metabolites and/or generally low abundance. Additionally, we found that the metabolism of bosentan was significantly changed upon induction with rifampicin and resulted in more oxidation products in the supernatant. Bosentan is a substrate for CYP3A4 (Treiber et al., 2007) and therefore induction of these enzymes led to an increase in the oxidative metabolism of bosentan in HepaRG cultures. In case of VPA, changes in

drug metabolism upon induction were minor. VPA is not a substrate of CYP3A4, hence effects of CYP3A4 induction on metabolism of VPA were lower as compared to bosentan (figure S5.8). Summarizing, we found that HepaRG cells in our setup, not only exhibit stable metabolism similar to *in vivo* but also respond to induction of CYP450 leading to changes in drug metabolism.

Investigating the binding of the tested drugs in our *in vitro* system, we show that phenomena inherent to *in vitro* systems such as compound degradation or plastic binding are negligible for the investigated drugs in our experimental setup.

Supplementary material of chapter 6

Supplementary figures

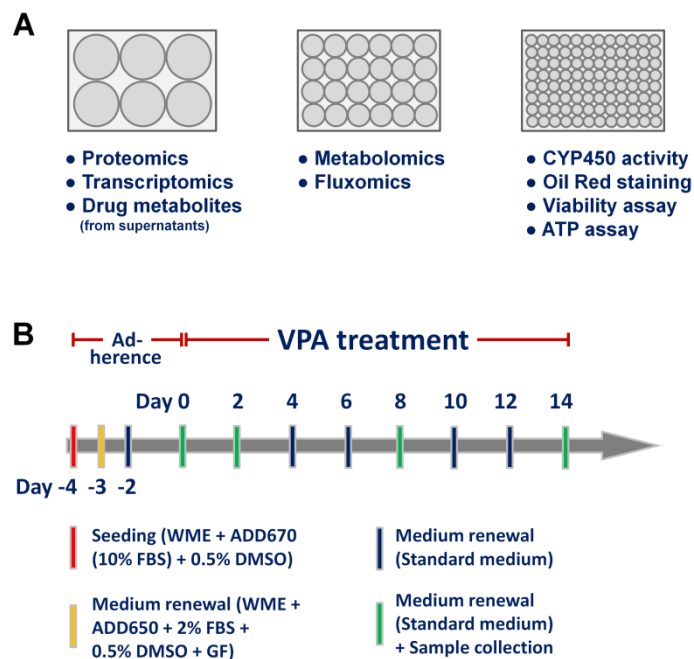


Figure S6.1 Experimental design. Summary of the plate setups (6-, 24- or 96-well) used for the different analyses (A) and the cultivation scheme highlighting the time points for medium renewal and sampling (B). In case of fluxomics data, sampling was additionally performed on day 4 and 12. Standard medium refers to Williams Medium E (WME) with 0.5% dimethyl sulfoxide (DMSO), additive 650 (ADD650) obtained from Biopredic International and epidermal and hepatocyte growth factor (GF). VPA, valproic acid; FBS, fetal bovine serum.

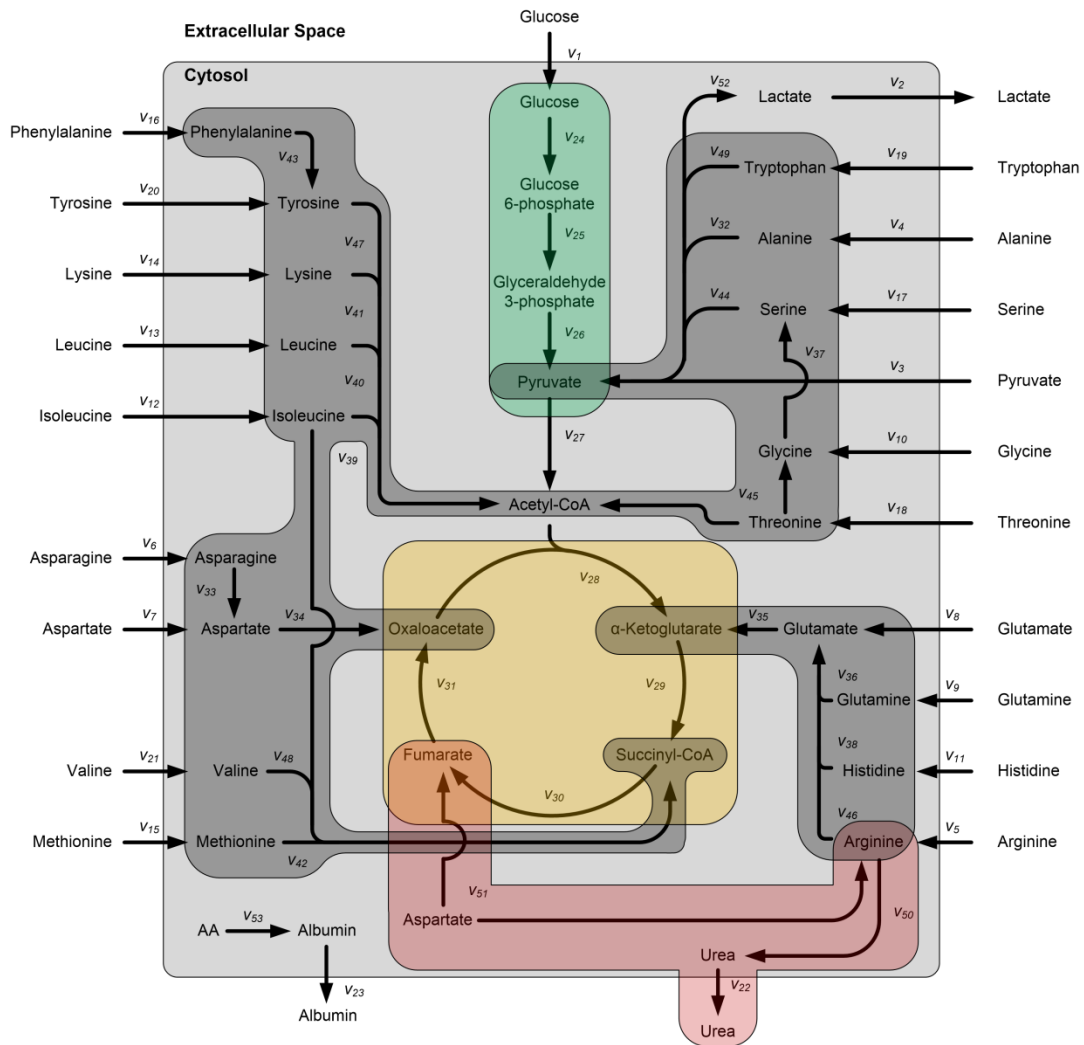


Figure S6.2 Metabolic network for flux analysis. In the metabolic network, all 53 reactions that were applied in the metabolic flux analysis are depicted. The glycolytic pathway, tricarboxylic acid and urea cycle, and the amino acid metabolism are highlighted in green, yellow, red and grey respectively. AA, amino acids.

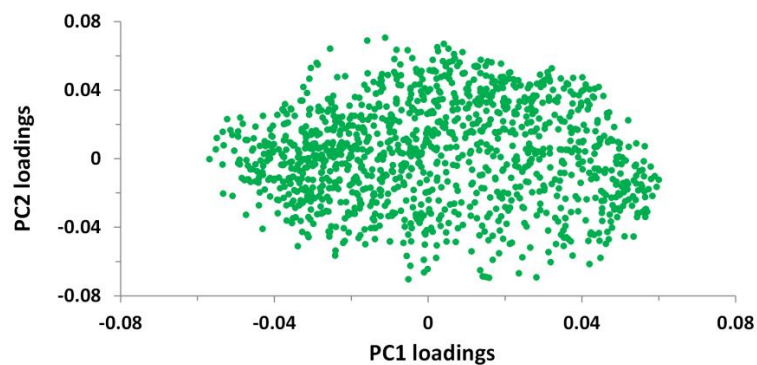


Figure S6.3 Loading coefficients of intracellular metabolome data for the first two principal components (PC), shown in figure 6.7.

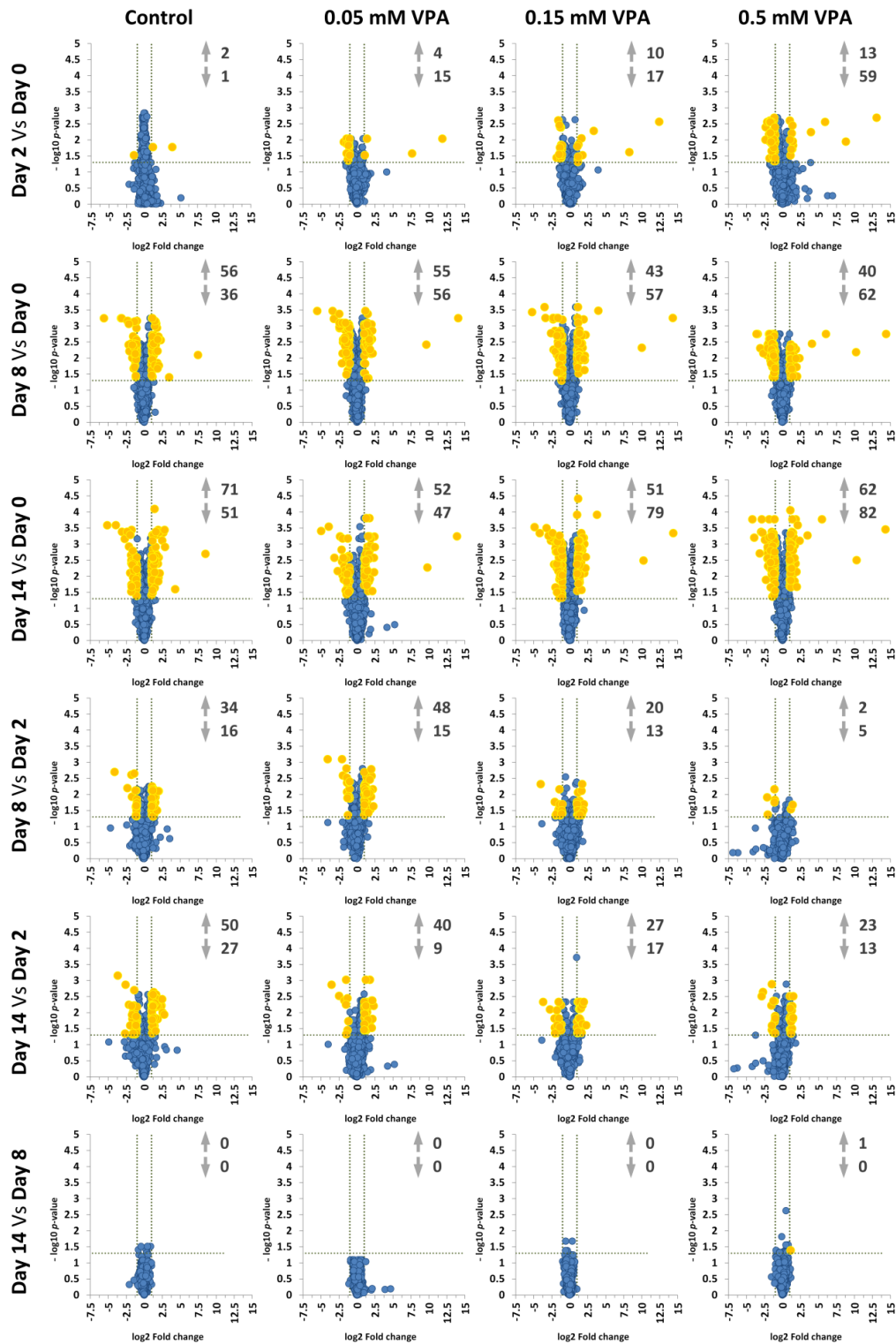


Figure S6.4 Volcano plot comparing the intracellular metabolome in HepaRG cells upon exposure to valproic acid (VPA) at different time points. A p -value of 0.05 and an absolute \log_2 fold change of 1 were selected as thresholds which are indicated by dotted lines. Metabolites exceeding both thresholds are highlighted as yellow circles, while all other metabolites are depicted as blue circles. For the former, metabolites are further distinguished according to whether levels are decreasing or increasing, with corresponding numbers indicated. The p -values are based on a t -test with subsequent Benjamini-Hochberg correction for multiple testing. Measurement of the underlying data has been performed by Nicola Zamboni at ETH Zurich, Switzerland.

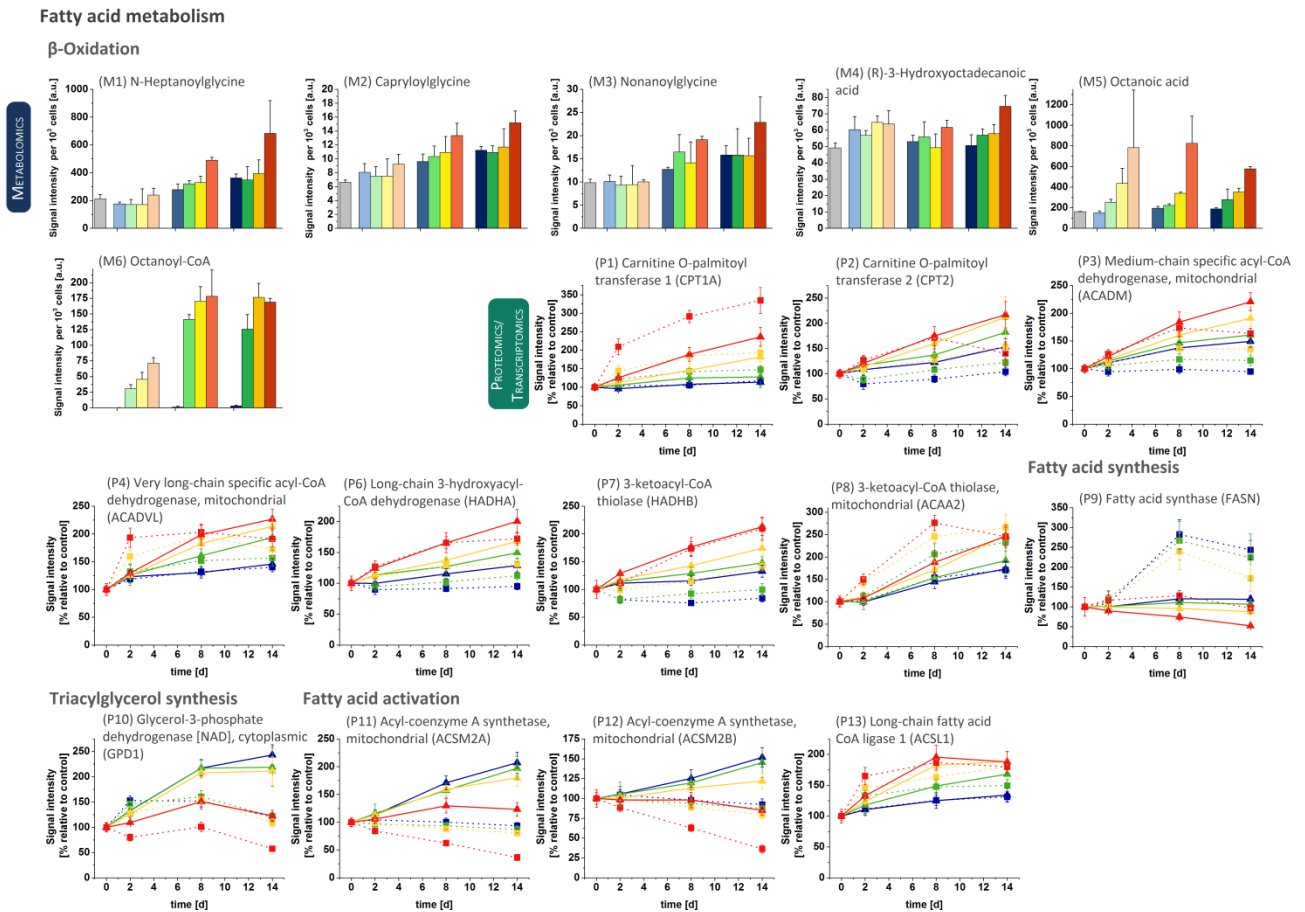


Figure S6.5 Time courses of metabolites, proteins and transcripts in fatty acid metabolism for HepaRG cells treated with valproic acid (VPA) for two weeks. Profiles of selected molecules within fatty acid metabolism that were shown to be particularly affected by 2-week treatment with VPA are depicted. Further, selected enzymes within the top 250 significantly altered proteins based on ANOVA were added. Furthermore, the subset was completed by the key enzymes of the corresponding pathways. The graph complements figure 6.9 in the main body of the chapter and metabolite (M) and protein (P) numbers match. Proteome and transcriptome data were normalized to day 0 and plotted in the same graph. The gene name is given in brackets. Proteome data is represented by triangles and full lines, whereas transcriptome data is represented as squares with dashed lines. VPA concentrations are color coded. Blue, green, yellow and red represent the control and 0.05 mM, 0.15 mM and 0.5 mM VPA respectively. For the metabolome data, the time points day 2, 8 and 14 are represented by increasingly dark colors, while the common control on day 0 is presented in grey. Error bars indicate standard deviation with $n = 3$.

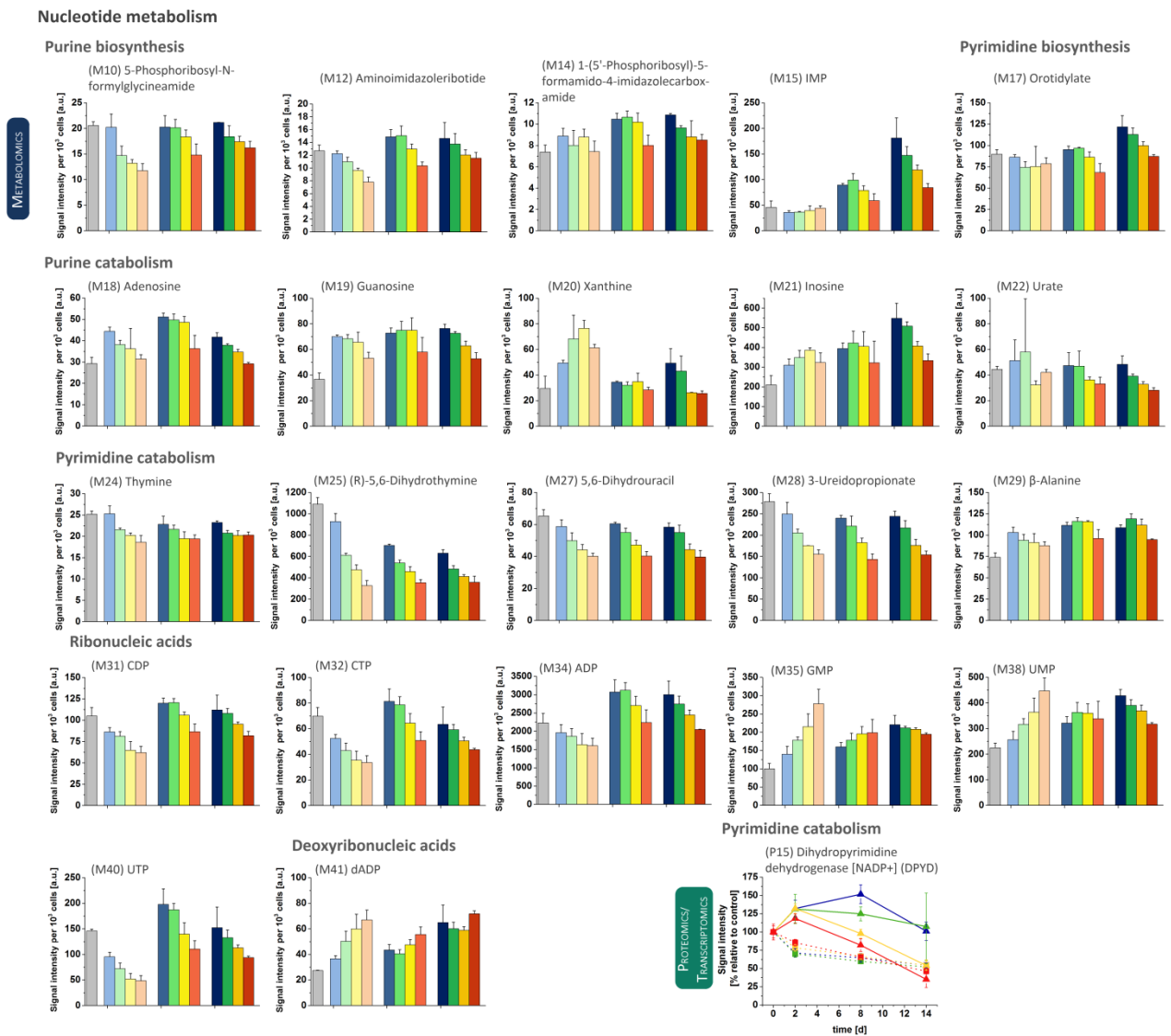


Figure S6.6 Time courses of metabolites, proteins and transcripts in nucleotide metabolism for HepaRG cells treated with valproic acid (VPA) for two weeks. Profiles of selected molecules within nucleotide metabolism that were shown to be particularly affected by 2-week treatment with VPA are depicted. Further, selected enzymes within the top 250 significantly altered proteins based on ANOVA were added. Furthermore, the subset was completed by the key enzymes of the corresponding pathways. The graph complements figure 6.9 in the main body of the chapter and metabolite (M) and protein (P) numbers match. Proteome and transcriptome data were normalized to day 0 and plotted in the same graph. The gene name is given in brackets. Proteome data is represented by triangles and full lines, whereas transcriptome data is represented as squares with dashed lines. VPA concentrations are color coded. Blue, green, yellow and red represent the control and 0.05 mM, 0.15 mM and 0.5 mM VPA respectively. For the metabolome data, the time points day 2, 8 and 14 are represented by increasingly dark colors, while the common control on day 0 is presented in grey. Error bars indicate standard deviation with $n = 3$.

Amino acid metabolism

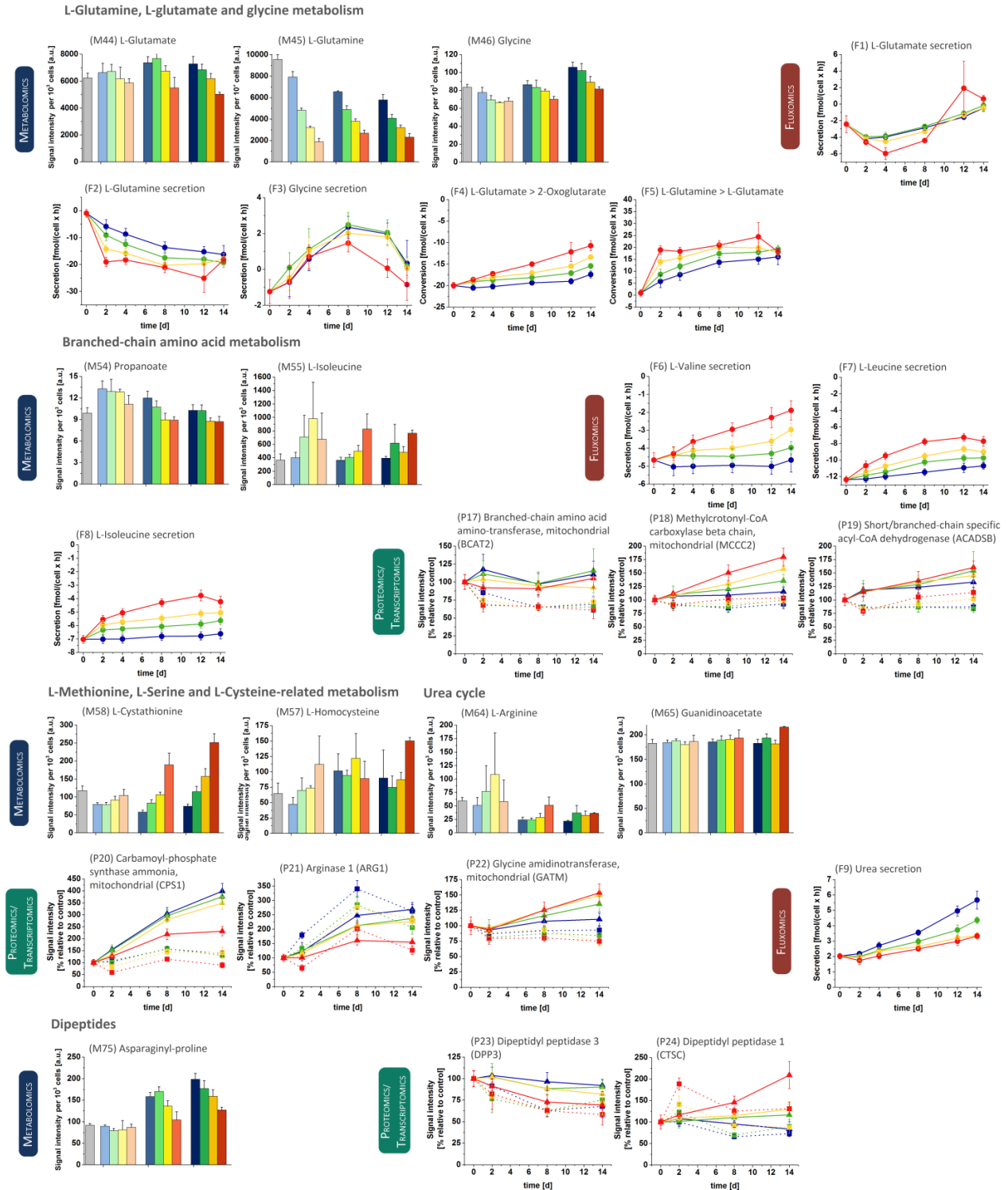


Figure S6.7 Time courses of metabolites, proteins, transcripts and fluxes in amino acid metabolism for HepaRG cells treated with valproic acid (VPA) for two weeks. Profiles of selected molecules within amino acid metabolism that were shown to be particularly affected by 2-week treatment with VPA are depicted. Further, selected enzymes within the top 250 significantly altered proteins based on ANOVA were added. Furthermore, the subset was completed by the key enzymes of the corresponding pathways. The graph complements figure 6.9 in the main body of the chapter and metabolite (M) and protein (P) numbers match. Proteome and transcriptome data were normalized to day 0 and plotted in the same graph. The gene name is given in brackets. Proteome data is represented by triangles and full lines, whereas transcriptome data is represented as squares with dashed lines. VPA concentrations are color coded. Blue, green, yellow and red

represent the control and 0.05 mM, 0.15 mM and 0.5 mM VPA respectively. For the metabolome data, the time points day 2, 8 and 14 are represented by increasingly dark colors, while the common control on day 0 is presented in grey. Error bars indicate standard deviation with $n = 3$.

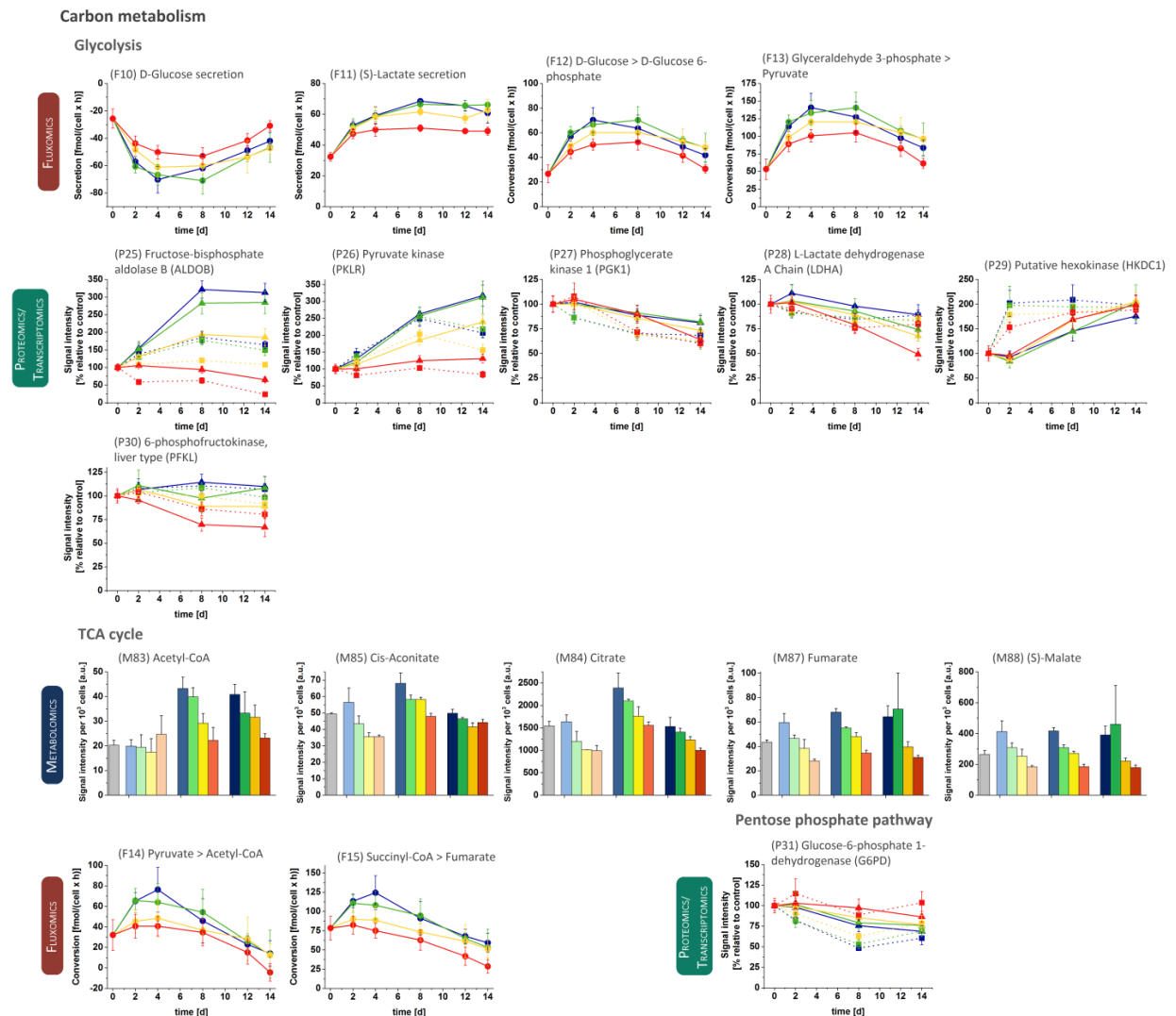


Figure S6.8 Time courses of metabolites, proteins and transcripts in carbon metabolism for HepaRG cells treated with valproic acid (VPA) for two weeks. Profiles of selected molecules within carbon metabolism that were shown to be particularly affected by 2-week treatment with VPA are depicted. Further, selected enzymes within the top 250 significantly altered proteins based on ANOVA were added. Furthermore, the subset was completed by the key enzymes of the corresponding pathways. The graph complements figure 6.9 in the main body of the chapter and metabolite (M) and protein (P) numbers match. Proteome and transcriptome data were normalized to day 0 and plotted in the same graph. The gene name is given in brackets. Proteome data is represented by triangles and full lines, whereas transcriptome data is represented as squares with dashed lines. VPA concentrations are color coded. Blue, green, yellow and red represent the control and 0.05 mM, 0.15 mM and 0.5 mM VPA respectively. For the metabolome data, the time points day 2, 8 and 14 are represented by increasingly dark colors, while the common control on day 0 is presented in grey. Error bars indicate standard deviation with $n = 3$.

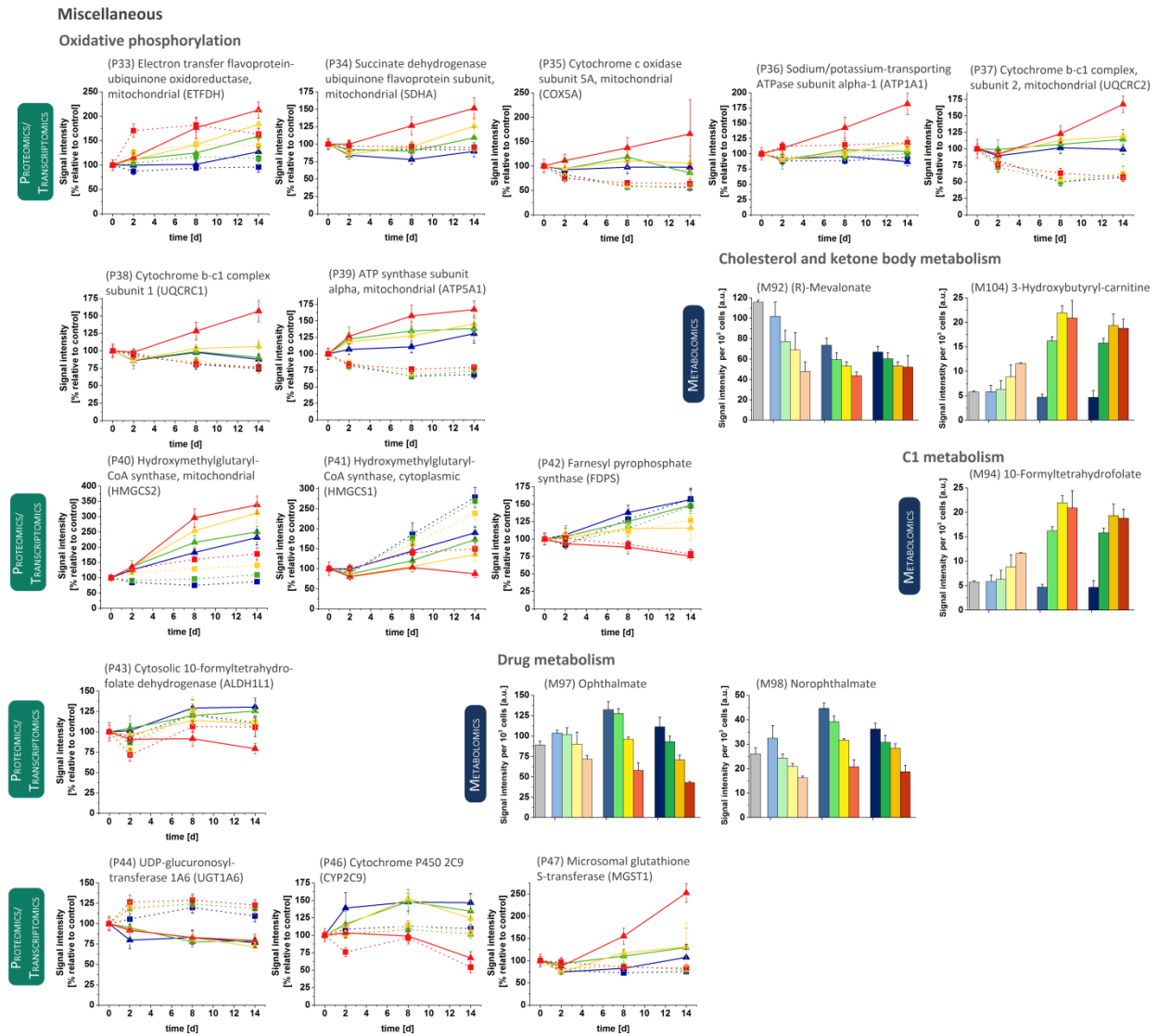


Figure S6.9 Time courses of metabolites, proteins and transcripts in miscellaneous pathways for HepaRG cells treated with valproic acid (VPA) for two weeks. Profiles of selected molecules within miscellaneous pathways that were shown to be particularly affected by 2-week treatment with VPA are depicted. Further, selected enzymes within the top 250 significantly altered proteins based on ANOVA were added. Furthermore, the subset was completed by the key enzymes of the corresponding pathways. The graph complements figure 6.9 in the main body of the chapter and metabolite (M) and protein (P) numbers match. Proteome and transcriptome data were normalized to day 0 and plotted in the same graph. The gene name is given in brackets. Proteome data is represented by triangles and full lines, whereas transcriptome data is represented as squares with dashed lines. VPA concentrations are color coded. Blue, green, yellow and red represent the control and 0.05 mM, 0.15 mM and 0.5 mM VPA respectively. For the metabolome data, the time points day 2, 8 and 14 are represented by increasingly dark colors, while the common control on day 0 is presented in grey. Error bars indicate standard deviation with $n = 3$.

Supplementary tables

Table S6.1 LC-MS/MS parameters used for valproic acid and its metabolites. Transitions used for quantification are highlighted in bold.

Compound	Molecular ion (m/z)	Transition ion (m/z)	Declustering potential (V)	Focusing potential (V)	Collision energy (eV)
VPA	143	143	-40	-140	-15
VPA-d6	149	149	-20	-120	-5
VPA-beta-D-glucuronide	319	175	-40	-180	-15
	319	113	-40	-180	-20
3-OH-VPA	159	101	-40	-120	-15
	159	97	-40	-120	-7
4-OH-VPA	159	141	-60	-90	-18
	159	113	-60	-90	-20
	159	99	-60	-90	-25
3-keto-VPA	157	113	-30	-60	-5
	157	95	-30	-60	-15

Table S6.2 Reactions used for metabolite balancing. EC, extracellular; IC, intracellular.

Reaction Number	Substrate	Product	Reaction Number	Substrate	Product
v1	Glucose _{EC}	Glucose _{IC}	v2	Lactate _{EC}	Lactate _{IC}
v3	Pyruvate _{EC}	Pyruvate _{IC}	v4	Alanine _{EC}	Alanine _{IC}
v5	Arginine _{EC}	Arginine _{IC}	v6	Asparagine _{EC}	Asparagine _{IC}
v7	Aspartate _{EC}	Aspartate _{IC}	v8	Glutamate _{EC}	Glutamate _{IC}
v9	Glutamine _{EC}	Glutamine _{IC}	v10	Glycine _{EC}	Glycine _{IC}
v11	Histidine _{EC}	Histidine _{IC}	v12	Isoleucine _{EC}	Isoleucine _{IC}
v13	Leucine _{EC}	Leucine _{IC}	v14	Lysine _{EC}	Lysine _{IC}
v15	Methionine _{EC}	Methionine _{IC}	v16	Phenylalanine _{EC}	Phenylalanine _{IC}
v17	Serine _{EC}	Serine _{IC}	v18	Threonine _{EC}	Threonine _{IC}
v19	Tryptophan _{EC}	Tryptophan _{IC}	v20	Tyrosine _{EC}	Tyrosine _{IC}
v21	Valine _{EC}	Valine _{IC}	v22	Urea _{EC}	Urea _{IC}
v23	Albumin _{EC}	Albumin _{IC}	v24	Glucose _{EC}	Glucose-6-phosphate
v25	Glucose-6-phosphate	2 × Glyceroldehyde-3-phosphate	v26	Glyceroldehyde-3-phosphate	Pyruvate _{IC}
v27	Pyruvate _{IC}	Acetyl-CoA	v28	Oxaloacetate + Acetyl-CoA	α-Ketoglutarate
v29	α-Ketoglutarate	Succinyl-CoA	v30	Succinyl-CoA	Fumarate
v31	Fumarate	Oxaloacetate	v32	Alanine _{IC}	Pyruvate _{IC}
v33	Asparagine _{IC}	Aspartate _{IC}	v34	Aspartate _{IC}	Oxaloacetate
v35	Glutamate _{IC}	α-Ketoglutarate	v36	Glutamine _{IC}	Glutamate _{IC}
v37	Glycine _{IC}	Serine _{IC}	v38	Histidine _{IC}	Glutamate _{IC}
v39	Isoleucine _{IC}	Succinyl-CoA + Acetyl-CoA	v40	Leucine _{IC}	3 × Acetyl-CoA
v41	Lysine _{IC}	2 × Acetyl-CoA	v42	Methionine _{IC}	Succinyl-CoA
v43	Phenylalanine _{IC}	Tyrosine _{IC}	v44	Serine _{IC}	Pyruvate _{IC}
v45	Arginine _{IC}	Acetyl-CoA + Glycine _{IC}	v46	Threonine _{IC}	Glutamate _{IC}
v47	Tyrosine _{IC}	Acetyl-CoA	v48	Valine _{IC}	Succinyl-CoA
v49	Tryptophan _{IC}	Pyruvate _{IC}	v50	Arginine _{IC}	Urea _{IC}
v51	Aspartate _{IC}	Fumarate + Arginine _{IC}	v52	Pyruvate _{IC}	Lactate _{IC}
v53	62 × Alanine _{IC} + 24 × Arginine _{IC} + 17 × Asparagine _{IC} + 36 × Aspartate _{IC} + 62 × Glutamate _{IC} + 20 × Glutamine _{IC} + 12 × Glycine _{IC} + 16 × Histidine _{IC} + 8 × Isoleucine _{IC} + 61 × Leucine _{IC} + 59 × Lysine _{IC} + 6 × Methionine _{IC} + 31 × Phenylalanine _{IC} + 24 × Serine _{IC} + 28 × Serine _{IC} + 1 × Tryptophan _{IC} + 18 × Tyrosine _{IC} + 41 × Valine _{IC}				

Table S6.3 Dynamic formation of CYP450 products in the course of 14-day valproic acid (VPA) treatment with different concentrations. Absolute values are given in amol/(cell × h), determined via LC-MS. SD, standard deviation.

Product formation [amol/(cell × h)]	Day 0		Day 2		Day 8		Day 14		
	Mean	SD	Mean	SD	Mean	SD	Mean	SD	
CYP2D6	Untreated		29.3	1.2	57.5	2.4	49.4	3.2	
	0.05 mM VPA	16.4	1.0	27.8	2.6	47.7	4.0	37.6	4.8
	0.15 mM VPA			26.9	2.0	41.4	2.6	31.1	3.7
	0.5 mM VPA			22.7	1.8	27.5	0.4	15.6	0.9
CYP1A2	Untreated		71.2	3.2	85.6	12.9	112.3	9.2	
	0.05 mM VPA	0	0	68.9	1.0	110.5	11.9	69.4	9.7
	0.15 mM VPA			75.0	2.7	77.4	6.5	43.0	38.7
	0.5 mM VPA			49.0	44.3	89.7	54.2	75.0	2.9
CYP2B6	Untreated		46.6	4.4	59.6	7.5	45.9	8.4	
	0.05 mM VPA	16.6	3.8	47.1	5.9	62.5	4.4	34.6	5.0
	0.15 mM VPA			53.8	3.1	76.8	21.3	36.8	1.6
	0.5 mM VPA			52.6	14.3	85.0	7.3	36.6	2.5
CYP3A4	Untreated		166.7	21.4	379.4	31.7	323.5	29.2	
	0.05 mM VPA	108.9	1.7	151.8	7.2	322.0	39.6	245.9	22.3
	0.15 mM VPA			142.2	8.7	283.9	30.0	202.0	9.6
	0.5 mM VPA			130.7	19.3	163.3	10.6	114.4	23.1

Table S6.4 List of altered metabolites during 14-day valproic acid (VPA) exposure. Metabolites correspond to highlighted metabolites in figure 6.8, i.e. those with a *p*-value of 0.05 or lower and an absolute log₂ fold change of at least 1.

Metabolite	0.05 mM		0.15 mM		0.5 mM		0.05 mM		0.15 mM		0.5 mM		0.05 mM		0.15 mM		0.5 mM	
	Day 2						Day 8						Day 14					
	Ctrl		0.05 mM		0.05 mM		Ctrl		0.05 mM		Ctrl		0.05 mM		Ctrl		0.05 mM	
10-Formyltetrahydrofolate							X	X	X					X	X			
1-(sn-Glycero-3-phospho)-1D-myo-inositol															X			X
2-O-α-L-Fucopyranosyl-galactose															X			X
5-Tetradecenoic acid														X	X			X
Caprylic acid									X		X				X			
Demethylphyloquinone			X															
Dihydrothymine			X															
Fumaric acid			X												X			
Glutamyl-Methionine															X			
Glycerol 3-phosphate									X		X				X			
Hypogecic acid															X			
Imidazole-4-acetaldehyde			X												X			
Indoleacetyl glutamine																		X
Inosinic acid															X			
L-Cystathionine									X		X			X	X			X
L-Glutamine	X	X							X					X	X			
L-Histidine															X			
L-Malic acid			X						X						X			
LysoSM(d18:1)									X		X	X			X			X
N-Acetylglutamine			X						X						X			
NADH									X		X				X			
Norophtalmic acid									X						X			
Octanoyl-CoA								X	X					X	X			
Ophthalmic acid									X		X				X			X
Pantothenic acid															X			
Succinyladenosine			X						X						X			
Taurine									X		X				X			X
Tetrahydroaldosterone-3-glucuronide															X			
Unknown139		X																
Unknown152															X			
Unknown17		X							X						X			
Unknown183		X							X						X			
Unknown191															X			
Unknown192		X						X	X		X			X	X	X	X	X
Unknown193		X																
Unknown201	X	X																
Unknown210		X							X						X			
Unknown222									X		X				X			X
Unknown24															X			X
Unknown242									X		X			X	X			X
Unknown254									X		X				X			
Unknown260															X			
Unknown276										X					X			X
Unknown317															X			X
Unknown321							X	X	X					X	X			
Unknown345		X																
Unknown355									X		X				X			X
Unknown356		X							X						X			
Unknown376										X				X	X			X
Unknown387																	X	X
Unknown39		X							X						X			
Unknown428																	X	
Unknown44																	X	
Unknown443		X							X									
Unknown475									X									
Unknown511		X																
Unknown513															X			
Unknown532									X						X			X
Unknown555															X			
Unknown574															X			
Unknown589									X						X			
Unknown6									X		X				X			X
Unknown616									X						X			
Unknown649									X									
Unknown661		X																
Unknown726									X		X			X	X			X
Unknown734									X									
Unknown751							X	X	X				X	X	X			
Valproic acid glucuronide	X	X						X	X	X		X		X	X	X	X	X

References

- Abdel-Misih, S.R.Z., Bloomston, M., 2010. Liver Anatomy. *Surg. Clin. North Am.* 90, 643–653. doi:10.1016/j.suc.2010.04.017
- Acharjee, A., Kloosterman, B., Visser, R.G.F., Maliopaard, C., 2016. Integration of multi-omics data for prediction of phenotypic traits using random forest. *BMC Bioinformatics* 17, 180. doi:10.1186/s12859-016-1043-4
- Adler, P., Bolten, C.J., Dohnt, K., Hansen, C.E., Wittmann, C., 2013. Core Fluxome and Metafluxome of Lactic Acid Bacteria under Simulated Cocoa Pulp Fermentation Conditions. *Appl. Environ. Microbiol.* 79, 5670–5681. doi:10.1128/AEM.01483-13
- Adler, P., Frey, L.J., Berger, A., Bolten, C.J., Hansen, C.E., Wittmann, C., 2014. The Key to Acetate: Metabolic Fluxes of Acetic Acid Bacteria under Cocoa Pulp Fermentation-Simulating Conditions. *Appl. Environ. Microbiol.* 80, 4702–4716. doi:10.1128/AEM.01048-14
- Aires, C.C.P., IJlst, L., Stet, F., Prip-Buus, C., de Almeida, I.T., Duran, M., Wanders, R.J.A., Silva, M.F.B., 2010. Inhibition of hepatic carnitine palmitoyl-transferase I (CPT IA) by valproyl-CoA as a possible mechanism of valproate-induced steatosis. *Biochem. Pharmacol.* 79, 792–799. doi:10.1016/j.bcp.2009.10.011
- Aires, C.C.P., Soveral, G., Luís, P.B.M., ten Brink, H.J., de Almeida, I.T., Duran, M., Wanders, R.J. a, Silva, M.F.B., 2008. Pyruvate uptake is inhibited by valproic acid and metabolites in mitochondrial membranes. *FEBS Lett.* 582, 3359–66. doi:10.1016/j.febslet.2008.08.028
- Aires, C.C.P., van Cruchten, A., IJlst, L., de Almeida, I.T., Duran, M., Wanders, R.J. a, Silva, M.F.B., 2011. New insights on the mechanisms of valproate-induced hyperammonemia: inhibition of hepatic N-acetylglutamate synthase activity by valproyl-CoA. *J. Hepatol.* 55, 426–34. doi:10.1016/j.jhep.2010.11.031
- Alexopoulou, A., Dourakis, S.P., Mantzoukis, D., Pitsariotis, T., Kandyli, A., Deutsch, M., Archimandritis, A.J., 2008. Adverse drug reactions as a cause of hospital admissions: A 6-month experience in a single center in Greece. *Eur. J. Intern. Med.* 19, 505–510. doi:10.1016/j.ejim.2007.06.030
- Andrae, U., Singh, J., Ziegler-Skylakakis, K., 1985. Pyruvate and related alpha-ketoacids protect mammalian cells in culture against hydrogen peroxide-induced cytotoxicity. *Toxicol. Lett.* 28, 93–98. doi:10.1016/0378-4274(85)90015-3
- Aninat, C., Piton, A., Glaise, D., Le Charpentier, T., Langouët, S., Morel, F., Guguen-Guillouzo, C., Guillouzo, A., 2006. Expression of cytochromes P450, conjugating enzymes and nuclear receptors in human hepatoma HepaRG cells. *Drug Metab. Dispos.* 34, 75–83. doi:10.1124/dmd.105.006759.other
- Anthérieu, S., Bachour-El Azzi, P., Dumont, J., Abdel-Razzak, Z., Guguen-Guillouzo, C., Fromenty, B., Robin, M.-A., Guillouzo, A., Azzi, P.B., Abdel-, Z., 2012a. Oxidative stress plays a major role in chlorpromazine-induced cholestasis in human heparg cells. *Hepatology* 57, 1518–29. doi:10.1002/hep.26160
- Anthérieu, S., Chesné, C., Li, R., Guguen-Guillouzo, C., Guillouzo, A., 2012b. Optimization of the HepaRG cell model for drug metabolism and toxicity studies. *Toxicol Vitro.* 26, 1278–85. doi:10.1016/j.tiv.2012.05.008
- Anthérieu, S., Rogue, A., Fromenty, B., Guillouzo, A., Robin, M.-A., 2011. Induction of vesicular steatosis by amiodarone and tetracycline is associated with up-regulation of lipogenic genes in HepaRG cells. *Hepatology* 53, 1895–1905. doi:10.1002/hep.24290
- Aritomi, K., Ishitsuka, Y., Tomishima, Y., Shimizu, D., Abe, N., Shuto, T., Irikura, M., Kai, H., Irie, T., 2014. Evaluation of Three-Dimensional Cultured HepG2 Cells in a Nano Culture Plate System: an In Vitro Human Model of Acetaminophen Hepatotoxicity. *J. Pharmacol. Sci.* 124, 218–229. doi:10.1254/jphs.13135FP
- Bachour-El Azzi, P., Sharanek, A., Burban, A., Li, R., Guevel, R., Abdel-Razzak, Z., Stieger, B., Guguen-Guillouzo, C., Guillouzo, A., 2015. Comparative Localization and Functional Activity of the Main Hepatobiliary Transporters in HepaRG Cells and Primary Human Hepatocytes. *Toxicol Sci* 145, 157–168. doi:10.1093/toxsci/kfv041
- Baillie, T.A., Rettie, A.E., 2011. Role of biotransformation in drug-induced toxicity: influence of intra- and inter-species differences in drug metabolism. *Drug Metab. Pharmacokinet.* 26, 15–29.

doi:10.2133/dmpk.DMPK-10-RV-089

- Baker, B.M., Chen, C.S., 2012. Deconstructing the third dimension: how 3D culture microenvironments alter cellular cues. *J. Cell Sci.* 125, 3015–24. doi:10.1242/jcs.079509
- Barrera, G., 2012. Oxidative Stress and Lipid Peroxidation Products in Cancer Progression and Therapy. *ISRN Oncol.* 2012, 1–21. doi:10.5402/2012/137289
- Bataller, R., Brenner, D.A., 2005. Liver fibrosis. *J. Clin. Invest.* 115, 209–18. doi:10.1172/JCI24282
- Bates, D.W., Spell, N., Cullen, D.J., Burdick, E., Laird, N., Petersen, L.A., Small, S.D., Sweitzer, B.J., Leape, L.L., 1997. The costs of adverse drug events in hospitalized patients. Adverse Drug Events Prevention Study Group. *JAMA* 277, 307–11.
- Baxter, M.A., Rowe, C., Alder, J., Harrison, S., Hanley, K.P., Park, B.K., Kitteringham, N.R., Goldring, C.E., Hanley, N.A., 2010. Generating hepatic cell lineages from pluripotent stem cells for drug toxicity screening. *Stem Cell Res.* 5, 4–22. doi:10.1016/j.scr.2010.02.002
- Begriche, K., Massart, J., Robin, M.-A., Borgne-Sanchez, A., Fromenty, B., 2011. Drug-induced toxicity on mitochondria and lipid metabolism: Mechanistic diversity and deleterious consequences for the liver. *J. Hepatol.* 54, 773–794. doi:10.1016/j.jhep.2010.11.006
- Begue, J.-M., Guguen-Guillouzo, C., Pasdoloup, N., Guillouzo, A., 1984. Prolonged Maintenance of Active Cytochrome P-450 in Adult Rat Hepatocytes Co-Cultured with Another Liver Cell Type. *Hepatology* 4, 839–842. doi:10.1002/hep.1840040507
- Benga, G., Ferdinand, W., 1995. Amino acid composition of rat and human liver microsomes in normal and pathological conditions. *Biosci. Rep.* 15, 111–116.
- Berezhkovskiy, L.M., 2011. The corrected traditional equations for calculation of hepatic clearance that account for the difference in drug ionization in extracellular and intracellular tissue water and the corresponding corrected PBPK equation. *J. Pharm. Sci.* 100, 1167–1183. doi:10.1002/jps.22324
- Berezhkovskiy, L.M., Khojasteh, S.C., Halladay, J.S., Hop, C.E.C.A., 2009. On the prediction of hepatic clearance using the diluted plasma in metabolic stability assay. *J. Pharm. Sci.* doi:10.1002/jps.21582
- Bersanelli, M., Mosca, E., Remondini, D., Giampieri, E., Sala, C., Castellani, G., Milanese, L., 2016. Methods for the integration of multi-omics data: mathematical aspects. *BMC Bioinformatics* 17, S15. doi:10.1186/s12859-015-0857-9
- Betteridge, D.J., 2000. What is oxidative stress? *Metabolism.* 49, 3–8.
- Bhatia, S.N., Balis, U.J., Yarmush, M.L., Toner, M., 1999. Effect of cell-cell interactions in preservation of cellular phenotype: cocultivation of hepatocytes and nonparenchymal cells. *FASEB J.* 13, 1883–1900.
- Bhattacharya, M., Malinen, M.M., Lauren, P., Lou, Y.R., Kuisma, S.W., Kanninen, L., Lille, M., Corlu, A., Guguen-Guillouzo, C., Ikkala, O., Laukkanen, A., Urtti, A., Yliperttula, M., 2012. Nanofibrillar cellulose hydrogel promotes three-dimensional liver cell culture, in: *Journal of Controlled Release.* pp. 291–298. doi:10.1016/j.jconrel.2012.06.039
- Blaauboer, B.J., Andersen, M.E., 2007. The need for a new toxicity testing and risk analysis paradigm to implement REACH or any other large scale testing initiative [2]. *Arch. Toxicol.* 81, 385–387. doi:10.1007/s00204-006-0175-0
- Blanchard, N., Hewitt, N.J., Silber, P., Jones, H., Coassolo, P., Lavé, T., 2006. Prediction of hepatic clearance using cryopreserved human hepatocytes: a comparison of serum and serum-free incubations. *J. Pharm. Pharmacol.* 58, 633–641. doi:10.1211/jpp.58.5.0008
- Blanchard, N., Richert, L., Notter, B., Delobel, F., David, P., Coassolo, P., Lavé, T., 2004. Impact of serum on clearance predictions obtained from suspensions and primary cultures of rat hepatocytes. *Eur. J. Pharm. Sci.* 23, 189–199. doi:10.1016/j.ejps.2004.07.007
- Boelsterli, U.A., 2003. Diclofenac-induced liver injury: A paradigm of idiosyncratic drug toxicity. *Toxicol. Appl. Pharmacol.* doi:10.1016/S0041-008X(03)00368-5
- Bois, F.Y., Jamei, M., Clewell, H.J., 2010. PBPK modelling of inter-individual variability in the pharmacokinetics of environmental chemicals 278, 256–267. doi:10.1016/j.tox.2010.06.007
- Booth, C.L., Pollack, G.M., Brouwer, K.L.R., 1996. Hepatobiliary disposition of valproic acid and valproate glucuronide: Use of a pharmacokinetic model to examine the rate-limiting steps and potential sites of drug interactions. *Hepatology* 23, 771–780. doi:10.1053/jhep.1996.v23.pm0008666331
- Borst, P., Evers, R., Kool, M., Wijnholds, J., 2000. A Family of Drug Transporters: the Multidrug

- Resistance-Associated Proteins. *JNCI J. Natl. Cancer Inst.* 92, 1295–1302. doi:10.1093/jnci/92.16.1295
- Bort, R., MacÉ, K., Boobis, A., Gómez-Lechón, M.J., Pfeifer, A., Castell, J., 1999. Hepatic metabolism of diclofenac: Role of human CYP in the minor oxidative pathways. *Biochem. Pharmacol.* 58, 787–796. doi:10.1016/S0006-2952(99)00167-7
- Bort, R., Ponsoda, X., Jover, R., Gómez-Lechón, M.J., Castell, J. V., 1998. Diclofenac toxicity to hepatocytes: a role for drug metabolism in cell toxicity. *J. Pharmacol. Exp. Ther.* 288, 65–72.
- Borzelleca, J.F., 2000. Paracelsus: Herald of Modern Toxicology. *Toxicol. Sci.* 53, 2–4. doi:10.1093/toxsci/53.1.2
- Brandon, E.F., Raap, C.D., Meijerman, I., Beijnen, J.H., Schellens, J.H., 2003. An update on in vitro test methods in human hepatic drug biotransformation research: pros and cons. *Toxicol. Appl. Pharmacol.* 189, 233–246. doi:10.1016/S0041-008X(03)00128-5
- Broeders, J.J.W., Blaauboer, B.J., Hermens, J.L.M., 2013. In vitro biokinetics of chlorpromazine and the influence of different dose metrics on effect concentrations for cytotoxicity in Balb/c 3T3, Caco-2 and HepaRG cell cultures. *Toxicol. In Vitro* 27, 1057–64. doi:10.1016/j.tiv.2013.01.010
- Brosnan, J.T., Brosnan, M.E., 2006. Branched-chain amino acids: enzyme and substrate regulation. *J Nutr* 136, 207S–11S. doi:136/1/207S [pii]
- Browning, J.D., Szczepaniak, L.S., Dobbins, R., Nuremberg, P., Horton, J.D., Cohen, J.C., Grundy, S.M., Hobbs, H.H., 2004. Prevalence of hepatic steatosis in an urban population in the United States: Impact of ethnicity. *Hepatology* 40, 1387–1395. doi:10.1002/hep.20466
- Brvar, M., Fokter, N., Bunc, M., Mozina, M., 2009. The frequency of adverse drug reaction related admissions according to method of detection, admission urgency and medical department specialty. *BMC Clin. Pharmacol.* 9, 8. doi:10.1186/1472-6904-9-8
- Buendia, M.A., 2002. Genetic alterations in hepatoblastoma and hepatocellular carcinoma: Common and distinctive aspects, in: *Medical and Pediatric Oncology*. pp. 530–535. doi:10.1002/mpo.10180
- Burcham, P.C., Harman, A.W., 1990. Mitochondrial dysfunction in paracetamol hepatotoxicity: In vitro studies in isolated mouse hepatocytes. *Toxicol. Lett.* 50, 37–48. doi:10.1016/0378-4274(90)90250-P
- Burkard, A., Dähn, C., Heinz, S., Zutavern, A., Sonntag-Buck, V., Maltman, D., Przyborski, S., Hewitt, N.J., Braspenning, J., 2012. Generation of proliferating human hepatocytes using upcyte® technology: characterisation and applications in induction and cytotoxicity assays. *Xenobiotica* 42, 939–956. doi:10.3109/00498254.2012.675093
- Camp, J.P., Capitano, A.T., 2007. Induction of zone-like liver function gradients in HepG2 cells by varying culture medium height. *Biotechnol. Prog.* 23, 1485–91. doi:10.1021/bp070308v
- Carapito, C., Burel, A., Guterl, P., Walter, A., Varrier, F., Bertile, F., Van Dorsselaer, A., 2014. MSDA, a proteomics software suite for in-depth Mass Spectrometry Data Analysis using grid computing. *Proteomics* 14, 1014–1019. doi:10.1002/pmic.201300415
- Castell, J. V., Jover, R., Martínez-Jiménez, C.P., Gómez-Lechón, M.J., 2006. Hepatocyte cell lines: their use, scope and limitations in drug metabolism studies. *Expert Opin. Drug Metab. Toxicol.* 2, 183–212. doi:10.1517/17425255.2.2.183
- Castro, S.V., Carvalho, A.A., Silva, C.M.G., Faustino, L.R., Campello, C.C., Lucci, C.M., Báó, S.N., Figueiredo, J.R., Rodrigues, A.P.R., 2011. Freezing solution containing dimethylsulfoxide and fetal calf serum maintains survival and ultrastructure of goat preantral follicles after cryopreservation and in vitro culture of ovarian tissue. *Cell Tissue Res.* 346, 283–292. doi:10.1007/s00441-011-1257-8
- Cerec, V., Glaise, D., Garnier, D., Morosan, S., Turlin, B., Drenou, B., Gripon, P., Kremsdorf, D., Guguen-Guillouzo, C., Corlu, A., 2007. Transdifferentiation of hepatocyte-like cells from the human hepatoma HepaRG cell line through bipotent progenitor. *Hepatology* 45, 957–967. doi:10.1002/hep.21536
- Cervený, L., Svecova, L., Anzenbacherova, E., Vrzal, R., Staud, F., Dvorak, Z., Ulrichova, J., Anzenbacher, P., Pavek, P., 2007. Valproic Acid Induces CYP3A4 and MDR1 Gene Expression by Activation of Constitutive Androstane Receptor and Pregnane X Receptor Pathways. *Drug Metab. Dispos.* 35, 1032–1041. doi:10.1124/dmd.106.014456
- Chang, X., Kleinstreuer, N., Ceger, P., Hsieh, J., Allen, D., Casey, W., 2015. Application of Reverse Dosimetry to Compare In Vitro and In Vivo Estrogen Receptor Activity. *Appl. Vitro. Toxicol.* 1,

- 33–44. doi:10.1089/aivt.2014.0005
- Chatterjee, S., Richert, L., Augustijns, P., Annaert, P., 2013. Hepatocyte-based in vitro model for assessment of drug-induced cholestasis. *Toxicol. Appl. Pharmacol.* 274, 124–36. doi:10.1016/j.taap.2013.10.032
- Chawade, A., Alexandersson, E., Levander, F., 2014. Normalyzer: A tool for rapid evaluation of normalization methods for omics data sets. *J. Proteome Res.* 13, 3114–3120. doi:10.1021/pr401264n
- Chen, M., Yi, L., Zhang, Y., Zhou, X., Ran, L., Yang, J., Zhu, J., Zhang, Q., Mi, M., 2016. Resveratrol Attenuates Trimethylamine- N -Oxide (TMAO)-Induced Atherosclerosis by Regulating TMAO Synthesis and Bile Acid Metabolism via Remodeling of the Gut Microbiota. *MBio* 7, e02210-15. doi:10.1128/mBio.02210-15
- Chen, S.-F., Chang, Y.-C., Nieh, S., Liu, C.-L., Yang, C.-Y., Lin, Y.-S., 2012. Nonadhesive Culture System as a Model of Rapid Sphere Formation with Cancer Stem Cell Properties. *PLoS One* 7, e31864. doi:10.1371/journal.pone.0031864
- Chiarugi, A., Dölle, C., Felici, R., Ziegler, M., 2012. The NAD metabolome--a key determinant of cancer cell biology. *Nat. Rev. Cancer* 12, 741–52. doi:10.1038/nrc3340
- Choi, J.M., Oh, S.J., Lee, J., Jeon, J.S., Ryu, C.S., Kim, Y., Lee, K., Kim, S.K., 2015. Prediction of Drug-Induced Liver Injury in HepG2 Cells Cultured with Human Liver Microsomes. *Chem. Res. Toxicol.* doi:10.1021/tx500504n
- Clark, S., Francis, P.S., Conlan, X. a, Barnett, N.W., 2007. Determination of urea using high-performance liquid chromatography with fluorescence detection after automated derivatisation with xanthidol. *J. Chromatogr. A* 1161, 207–213. doi:10.1016/j.chroma.2007.05.085
- Classen, D.C., 1997. Adverse drug events in hospitalized patients. Excess length of stay, extra costs, and attributable mortality. *JAMA J. Am. Med. Assoc.* 277, 301–306. doi:10.1001/jama.277.4.301
- Coecke, S., Pelkonen, O., Leite, S.B., Bernauer, U., Bessems, J.G., Bois, F.Y., Gundert-Remy, U., Loizou, G., Testai, E., Zaldívar, J.-M., 2013. Toxicokinetics as a key to the integrated toxicity risk assessment based primarily on non-animal approaches. *Toxicol. Vitro* 27, 1570–1577. doi:10.1016/j.tiv.2012.06.012
- Cohen, S.D., Pumford, N.R., Khairallah, E.A., Boekelheide, K., Pohl, L.R., Amouzadeh, H.R., Hinson, J.A., 1997. Selective protein covalent binding and target organ toxicity. *Toxicol. Appl. Pharmacol.* 143, 1–12. doi:10.1006/taap.1996.8074
- Collins, F.S., 2011. Reengineering translational science: the time is right. *Sci. Transl. Med.* 3, 90cm17. doi:10.1126/scitranslmed.3002747
- Cover, C., Mansouri, A., Knight, T.R., Bajt, M.L., Lemasters, J.J., Pessayre, D., Jaeschke, H., 2005. Peroxynitrite-induced mitochondrial and endonuclease-mediated nuclear DNA damage in acetaminophen hepatotoxicity. *J. Pharmacol. Exp. Ther.* 315, 879–887. doi:10.1124/jpet.105.088898
- Cui, Y., Paules, R.S., 2010. Use of transcriptomics in understanding mechanisms of drug-induced toxicity. *Pharmacogenomics* 11, 573–585. doi:10.2217/pgs.10.37
- Cuperlović-Culf, M., Barnett, D. a, Culf, A.S., Chute, I., 2010. Cell culture metabolomics: applications and future directions. *Drug Discov. Today* 15, 610–21. doi:10.1016/j.drudis.2010.06.012
- Dahlin, D.C., Miwa, G.T., Lu, A.Y., Nelson, S.D., 1984. N-acetyl-p-benzoquinone imine: a cytochrome P-450-mediated oxidation product of acetaminophen. *Proc. Natl. Acad. Sci.* 81, 1327–1331. doi:10.1073/pnas.81.5.1327
- Darnell, M., Ulvestad, M., Ellis, E., Weidolf, L., Andersson, T.B., 2012. In vitro evaluation of major in vivo drug metabolic pathways using primary human hepatocytes and HepaRG cells in suspension and a dynamic three-dimensional bioreactor system. *J. Pharmacol. Exp. Ther.* 343, 134–44. doi:10.1124/jpet.112.195834
- Dash, A., Inman, W., Hoffmaster, K., Sevidal, S., Kelly, J., Obach, R.S., Griffith, L.G., Tannenbaum, S.R., 2009. Liver tissue engineering in the evaluation of drug safety. *Expert Opin. Drug Metab. Toxicol.* 5, 1159–1174. doi:10.1517/17425250903160664
- Dearfield, K.L., Jacobson-Kram, D., Brown, N.A., Williams, J.R., 1983. Evaluation of a human hepatoma cell line as a target cell in genetic toxicology. *Mutat. Res.* 108, 437–449.
- DeBerardinis, R.J., Cheng, T., 2010. The diverse functions of glutamine in metabolism, cell biology

- and cancer. *Oncogene* 29, 313–324. doi:10.1038/onc.2009.358.Q
- Denko, N.C., 2008. Hypoxia, HIF1 and glucose metabolism in the solid tumour. *Nat. Rev. Cancer* 8, 705–713. doi:10.1038/nrc2468
- Derks, T.G.J., Touw, C.M.L., Ribas, G.S., Biancini, G.B., Vanzin, C.S., Negretto, G., Mescka, C.P., Reijngoud, D.J., Smit, G.P.A., Wajner, M., Vargas, C.R., 2014. Experimental evidence for protein oxidative damage and altered antioxidant defense in patients with medium-chain acyl-CoA dehydrogenase deficiency. *J. Inherit. Metab. Dis.* 37, 783–789. doi:10.1007/s10545-014-9700-0
- Diener, B., Utesch, D., Beer, N., Durk, H., Oesch, F., 1993. A method for the cryopreservation of liver parenchymal cells for studies of xenobiotics. *Cryobiology* 30, 116–127. doi:S0011-2240(83)71011-4 [pii]r10.1006/cryo.1993.1011
- Dingemans, J., Van Giersbergen, P.L.M., 2004. Clinical pharmacology of bosentan, a dual endothelin receptor antagonist. *Clin. Pharmacokinet.* doi:10.2165/00003088-200443150-00003
- Donato, M.T., Goethals, F., Gómez-Lechón, M.J., Deboyser, D., De Coster, I., Roberfroid, M., Castell, J.V., 1992. Toxicity of the antitumoral drug datelliptium in hepatic cells: Use of models in vitro for the prediction of toxicity in vivo. *Toxicol. Vitro.* 6, 295–302. doi:10.1016/0887-2333(92)90019-N
- Donato, M.T., Jover, R., Gómez-lechón, M.J., 2013. Hepatic Cell Lines for Drug Hepatotoxicity Testing : Limitations and Strategies to Upgrade their Metabolic Competence by Gene Engineering 946–968.
- Dong, J., Mandenius, C.-F., Lübberstedt, M., Urbaniak, T., Nüssler, A.K.N., Knobloch, D., Gerlach, J.C., Zeilinger, K., 2008. Evaluation and optimization of hepatocyte culture media factors by design of experiments (DoE) methodology. *Cytotechnology* 57, 251–261. doi:10.1007/s10616-008-9168-6
- Dreifuss, F.E., Santilli, N., Langer, D.H., Sweeney, K.P., Moline, K.A., Menander, K.B., 1987. Valproic acid hepatic fatalities: a retrospective review. *Neurology* 37, 379–85.
- Du, Y., Han, R., Wen, F., Ng San San, S., Xia, L., Wohland, T., Leo, H.L., Yu, H., 2008. Synthetic sandwich culture of 3D hepatocyte monolayer. *Biomaterials* 29, 290–301. doi:10.1016/j.biomaterials.2007.09.016
- Dunn, J.C., Yarmush, M.L., Koebe, H.G., Tompkins, R.G., 1989. Hepatocyte function and extracellular matrix geometry: long-term culture in a sandwich configuration. *FASEB J.* 3, 174–7. doi:10.1093/nar/gks1337
- Dunn, W.B., Bailey, N.J.C., Johnson, H.E., 2005. Measuring the metabolome: current analytical technologies. *Analyst* 130, 606–625. doi:10.1039/b418288j
- Dunne, S., Shannon, B., Dunne, C., Cullen, W., 2013. A review of the differences and similarities between generic drugs and their originator counterparts, including economic benefits associated with usage of generic medicines, using Ireland as a case study. *BMC Pharmacol. Toxicol.* 14, 1. doi:10.1186/2050-6511-14-1
- Eadie, M., Hooper, W., Dickinson, R., 1988. Valproate-associated hepatotoxicity and its biochemical mechanisms. *Med Toxicol Advers. Drug Exp* 3, 85–106.
- Edgerton, D.S., 2006. Insulin's direct effects on the liver dominate the control of hepatic glucose production. *J. Clin. Invest.* 116, 521–527. doi:10.1172/JCI27073
- EFSA, 2014. Modern methodologies and tools for human hazard assessment of chemicals 1 12, 1–87. doi:10.2903/j.efsa.2014.3638
- Eriksson, C., Gustavsson, A., Kronvall, T., Tysk, C., 2011. Hepatotoxicity by bosentan in a patient with portopulmonary hypertension: a case-report and review of the literature. *J. Gastrointest. Liver Dis.* 20, 77–80.
- Fahrmayr, C., König, J., Auge, D., Mieth, M., Fromm, M.F., 2012. Identification of drugs and drug metabolites as substrates of multidrug resistance protein 2 (MRP2) using triple-transfected MDCK-OATP1B1-UGT1A1-MRP2 cells. *Br. J. Pharmacol.* 165, 1836–1847. doi:10.1111/j.1476-5381.2011.01672.x
- Fahrmayr, C., König, J., Auge, D., Mieth, M., Münch, K., Segrestaa, J., Pfeifer, T., Treiber, a, Fromm, M., 2013. Phase I and II metabolism and MRP2-mediated export of bosentan in a MDCKII-OATP1B1-CYP3A4-UGT1A1-MRP2 quadruple-transfected cell line. *Br. J. Pharmacol.* 169, 21–33. doi:10.1111/bph.12126
- Farrell, G.C., Larter, C.Z., 2005. Nonalcoholic Fatty Liver Disease : From Steatosis to Cirrhosis

- Introduction : Early Insights and 99–112. doi:10.1002/hep.20973
- Fasinu, P., J. Bouic, P., Rosenkranz, B., 2012. Liver-Based In Vitro Technologies for Drug Biotransformation Studies - A Review. *Curr. Drug Metab.* 13, 215–224. doi:10.2174/138920012798918426
- Fattinger, K., Funk, C., Pantze, M., Weber, C., Reichen, J., Stieger, B., Meier, P.J., 2001. The endothelin antagonist bosentan inhibits the canalicular bile salt export pump: A potential mechanism for hepatic adverse reactions. *Clin. Pharmacol. Ther.* 69, 223–231. doi:10.1067/mcp.2001.114667
- Felter, S., Lane, R.W., Latulippe, M.E., Craig Llewellyn, G., Olin, S.S., Scimeca, J.A., Trautman, T.D., 2009. Refining the threshold of toxicological concern (TTC) for risk prioritization of trace chemicals in food. *Food Chem. Toxicol.* 47, 2236–2245. doi:10.1016/j.fct.2009.06.018
- Ferreira, L.M.R., 2010. Cancer metabolism: The Warburg effect today. *Exp. Mol. Pathol.* doi:10.1016/j.yexmp.2010.08.006
- Ferreira, R.J., dos Santos, D.J., Ferreira, M.-J.U., 2015. P-glycoprotein and membrane roles in multidrug resistance. *Future Med. Chem.* 7, 929–946. doi:10.4155/fmc.15.36
- Filhoulaud, G., Guilmeau, S., Dentin, R., Girard, J., Postic, C., 2013. Novel insights into ChREBP regulation and function. *Trends Endocrinol. Metab.* 24, 257–268. doi:10.1016/j.tem.2013.01.003
- Finck, B.N., Bernal-Mizrachi, C., Han, D.H., Coleman, T., Sambandam, N., LaRiviere, L.L., Holloszy, J.O., Semenkovich, C.F., Kelly, D.P., 2005. A potential link between muscle peroxisome proliferator-activated receptor- α signaling and obesity-related diabetes. *Cell Metab.* 1, 133–144. doi:10.1016/j.cmet.2005.01.006
- Fischer, W., Praetor, K., Metzner, L., Neubert, R.H.H., Brandsch, M., 2008. Transport of valproate at intestinal epithelial (Caco-2) and brain endothelial (RBE4) cells: mechanism and substrate specificity. *Eur. J. Pharm. Biopharm.* 70, 486–92. doi:10.1016/j.ejpb.2008.05.022
- Fisher, C., Broderick, W., 2003. Sodium valproate or valproate semisodium: is there a difference in the treatment of bipolar disorder? *Psychiatr. Bull.* 27, 446 LP-448. doi:10.1192/pb.02-068
- Forte, G., Minieri, M., Cossa, P., Antenucci, D., Sala, M., Gnocchi, V., Fiaccavento, R., Carotenuto, F., De Vito, P., Baldini, P.M., Prat, M., Di Nardo, P., 2006. Hepatocyte growth factor effects on mesenchymal stem cells: proliferation, migration, and differentiation. *Stem Cells* 24, 23–33. doi:10.1634/stemcells.2004-0176
- Foufelle, F., Fromenty, B., 2016. Role of endoplasmic reticulum stress in drug-induced toxicity. *Pharmacol. Res. Perspect.* 4, e00211. doi:10.1002/prp2.211
- Frey, O., Misun, P.M., Fluri, D.A., Hengstler, J.G., Hierlemann, A., 2014. Reconfigurable microfluidic hanging drop network for multi-tissue interaction and analysis. *Nat. Commun.* 5, 1–11. doi:10.1038/ncomms5250
- Fromenty, B., Pessayre, D., 1995. Inhibition of mitochondrial beta-oxidation as a mechanism of hepatotoxicity. *Pharmacol. Ther.* doi:10.1016/0163-7258(95)00012-6
- Fuhrer, T., Heer, D., Begemann, B., Zamboni, N., 2011. High-throughput, accurate mass metabolome profiling of cellular extracts by flow injection-time-of-flight mass spectrometry. *Anal. Chem.* 83, 7074–7080. doi:10.1021/ac201267k
- Fuhrer, T., Zamboni, N., 2015. High-throughput discovery metabolomics. *Curr. Opin. Biotechnol.* 31, 73–78. doi:10.1016/j.copbio.2014.08.006
- Gabbay, E., Fraser, J., McNeil, K., 2007. Review of bosentan in the management of pulmonary arterial hypertension. *Vasc. Heal. Risk Manag.* 3, 887–900.
- García-Cañaveras, J.C., Castell, J. V., Donato, M.T., Lahoz, A., 2016. A metabolomics cell-based approach for anticipating and investigating drug-induced liver injury. *Sci. Rep.* 6, 27239. doi:10.1038/srep27239
- García-Cañaveras, J.C., Jiménez, N., Gómez-Lechón, M.J., Castell, J. V., Donato, M.T., Lahoz, A., 2015. LC-MS untargeted metabolomic analysis of drug-induced hepatotoxicity in HepG2 cells. *Electrophoresis* 36, 2294–2302. doi:10.1002/elps.201500095
- Gerets, H.H.J., Tilmant, K., Gerin, B., Chanteux, H., Depelchin, B.O., Dhalluin, S., Atienzar, F. a., 2012. Characterization of primary human hepatocytes, HepG2 cells, and HepaRG cells at the mRNA level and CYP activity in response to inducers and their predictivity for the detection of human hepatotoxins. *Cell Biol. Toxicol.* 28, 69–87. doi:10.1007/s10565-011-9208-4
- Giugliano, D., Ceriello, A., Esposito, K., 2008. Glucose metabolism and hyperglycemia, in: *American Journal of Clinical Nutrition.* doi:87/1/217S [pii]

- Godoy, P., Hengstler, J.G., Ilkavets, I., Meyer, C., Bachmann, A., Müller, A., Tuschl, G., Mueller, S.O., Dooley, S., 2009. Extracellular matrix modulates sensitivity of hepatocytes to fibroblastoid dedifferentiation and transforming growth factor β -induced apoptosis. *Hepatology* 49, 2031–2043. doi:10.1002/hep.22880
- Gómez-Lechón, M.J., Ponsoda, X., O'Connor, E., Donato, T., Castell, J. V., Jover, R., 2003. Diclofenac induces apoptosis in hepatocytes by alteration of mitochondrial function and generation of ROS. *Biochem. Pharmacol.* 66, 2155–2167. doi:10.1016/j.bcp.2003.08.003
- Gómez-Lechón, M.J., Tolosa, L., Donato, M.T., 2015. Metabolic activation and drug-induced liver injury: *in vitro* approaches for the safety risk assessment of new drugs. *J. Appl. Toxicol.* n/a-n/a. doi:10.1002/jat.3277
- Gottfried, E., Lang, S.A., Renner, K., Bosserhoff, A., Gronwald, W., Rehli, M., Einhell, S., Gedig, I., Singer, K., Seilbeck, A., Mackensen, A., Grauer, O., Hau, P., Dettmer, K., Andreesen, R., Oefner, P.J., Kreutz, M., 2013. New Aspects of an Old Drug – Diclofenac Targets MYC and Glucose Metabolism in Tumor Cells. *PLoS One* 8, e66987. doi:10.1371/journal.pone.0066987
- Göttlicher, M., Minucci, S., Zhu, P., Krämer, O.H., Schimpf, A., Giavara, S., Sleeman, J.P., Lo Coco, F., Nervi, C., Pelicci, P.G., Heinzl, T., 2001. Valproic acid defines a novel class of HDAC inhibitors inducing differentiation of transformed cells. *EMBO J.* 20, 6969–6978. doi:10.1093/emboj/20.24.6969
- Grant, D.M., 1991. Detoxification pathways in the liver. *J. Inherit. Metab. Dis.* 14, 421–30. doi:10.1007/BF01797915
- Greaves, P., Williams, A., Eve, M., 2004. First dose of potential new medicines to humans: how animals help. *Nat. Rev. Drug Discov.* 3, 226–236. doi:10.1038/nrd1329
- Gregory, J.C., Buffa, J.A., Org, E., Wang, Z., Levison, B.S., Zhu, W., Wagner, M.A., Bennett, B.J., Li, L., DiDonato, J.A., Lusic, A.J., Hazen, S.L., 2015. Transmission of Atherosclerosis Susceptibility with Gut Microbial Transplantation. *J. Biol. Chem.* 290, 5647–5660. doi:10.1074/jbc.M114.618249
- Griffith, L.G., Swartz, M.A., 2006. Capturing complex 3D tissue physiology in vitro. *Nat. Rev. Mol. Cell Biol.* 7, 211–224. doi:10.1038/nrm1858
- Gripon, P., Rumin, S., Urban, S., Le Seyec, J., Glaise, D., Cannie, I., Guyomard, C., Lucas, J., Trepo, C., Guguen-Guillouzo, C., 2002. Infection of a human hepatoma cell line by hepatitis B virus. *Pnas* 99, 15655–60.
- Groothuis, F.A., Heringa, M.B., Nicol, B., Hermens, J.L.M., Blaauboer, B.J., Kramer, N.I., 2015. Dose metric considerations in *in vitro* assays to improve quantitative *in vitro*–*in vivo* dose extrapolations. *Toxicology* 332, 30–40. doi:10.1016/j.tox.2013.08.012
- Guengerich, F.P., 2011. Mechanisms of drug toxicity and relevance to pharmaceutical development. *Drug Metab. Pharmacokinet.* 26, 3–14. doi:10.2133/dmpk.DMPK-10-RV-062
- Gugler, R., Schell, A., Eichelbaum, M., Fröscher, W., Schulz, H.U., 1977. Disposition of valproic acid in man. *Eur. J. Clin. Pharmacol.* 12, 125–132. doi:10.1007/BF00645133
- Guguen-Guillouzo, C., Clement, B., Baffet, G., Beaumont, C., Morelchany, E., Glaise, D., Guillouzo, A., 1983. Maintenance and reversibility of active albumin secretion by adult rat hepatocytes co-cultured with another liver epithelial cell type. *Exp. Cell Res.* 143, 47–54. doi:10.1016/0014-4827(83)90107-6
- Guguen-Guillouzo, C., 2002. Isolation and Culture of Animal and Human Hepatocytes, in: *Culture of Epithelial Cells*. John Wiley & Sons, Inc., New York, USA, pp. 337–379. doi:10.1002/0471221201.ch11
- Guillouzo, A., 1998. Liver cell models in *in vitro* toxicology, in: *Environmental Health Perspectives*. pp. 511–532. doi:10.1289/ehp.98106511
- Guillouzo, A., Beaune, P., Gascoin, M.N., Begue, J.M., Campion, J.P., Guengerich, F.P., Guguen-Guillouzo, C., 1985. Maintenance of cytochrome P-450 in cultured adult human hepatocytes. *Biochem. Pharmacol.* 34, 2991–5.
- Guillouzo, A., Corlu, A., Aninat, C., Glaise, D., Morel, F., Guguen-Guillouzo, C., 2007. The human hepatoma HepaRG cells: a highly differentiated model for studies of liver metabolism and toxicity of xenobiotics. *Chem. Biol. Interact.* 168, 66–73. doi:10.1016/j.cbi.2006.12.003
- Guillouzo, A., Morel, F., Ratanasavanh, D., Chesne, C., Guguen-Guillouzo, C., 1990. Long-term culture of functional hepatocytes. *Toxicol. Vitro.* 4, 415–427. doi:10.1016/0887-2333(90)90092-8
- Gujral, J.S., Knight, T.R., Farhood, A., Bajt, M.L., Jaeschke, H., 2002. Mode of cell death after

- acetaminophen overdose in mice: Apoptosis or oncotic necrosis? *Toxicol. Sci.* 67, 322–328. doi:10.1093/toxsci/67.2.322
- Gunes, A., Bilir, E., Zengil, H., Babaoglu, M.O., Bozkurt, A., Yasar, U., 2007. Inhibitory Effect of Valproic Acid on Cytochrome P450 2C9 Activity in Epilepsy Patients. *Basic Clin. Pharmacol. Toxicol.* 100, 383–386. doi:10.1111/j.1742-7843.2007.00061.x
- Gunness, P., Mueller, D., Shevchenko, V., Heinzle, E., Ingelman-Sundberg, M., Noor, F., 2013. 3D organotypic cultures of human HepaRG cells: a tool for in vitro toxicity studies. *Toxicol. Sci.* 133, 67–78. doi:10.1093/toxsci/kft021
- Guo, J., Luo, Y., Fan, D., Yang, B., Gao, P., Ma, X., Zhu, C., 2010. Medium optimization based on the metabolic-flux spectrum of recombinant *Escherichia coli* for high expression of human-like collagen II. *Biotechnol. Appl. Biochem.* 57, 55–62. doi:10.1042/BA20100081
- Guo, Y., Hu, C., He, X., Qiu, F., Zhao, L., 2012. Effects of UGT1A6, UGT2B7, and CYP2C9 Genotypes on Plasma Concentrations of Valproic Acid in Chinese Children with Epilepsy. *Drug Metab. Pharmacokinet.* doi:10.2133/dmpk.DMPK-11-NT-144
- Gutting, B.W., Updyke, L.W., Amacher, D.E., 2002. Diclofenac activates T cells in the direct popliteal lymph node assay and selectively induces IgG1 and IgE against co-injected TNP-OVA. *Toxicol. Lett.* 131, 167–180. doi:10.1016/S0378-4274(02)00029-2
- Hahne, M., Reichl, S., 2011. Development of a serum-free human cornea construct for in vitro drug absorption studies: The influence of varying cultivation parameters on barrier characteristics. *Int. J. Pharm.* 416, 268–279. doi:10.1016/j.ijpharm.2011.07.004
- Hamon, J., Renner, M., Jamei, M., Lukas, A., Kopp-Schneider, A., Bois, F.Y., 2015. Quantitative in vitro to in vivo extrapolation of tissues toxicity. *Toxicol. Vitr.* In press. doi:10.1016/j.tiv.2015.01.011
- Hans, M.A., Heinzle, E., Wittmann, C., 2003. Free intracellular amino acid pools during autonomous oscillations in *saccharomyces cerevisiae*. *Biotechnol. Bioeng.* 82, 143–151. doi:10.1002/bit.10553
- Hart, S.N., Li, Y., Nakamoto, K., Subileau, E., Steen, D., Zhong, X., 2010. A comparison of whole genome gene expression profiles of HepaRG cells and HepG2 cells to primary human hepatocytes and human liver tissues. *Drug Metab. Dispos.* 38, 988–994. doi:10.1124/dmd.109.031831
- Haynes, C.M., Titus, E.A., Cooper, A.A., 2004. Degradation of Misfolded Proteins Prevents ER-Derived Oxidative Stress and Cell Death. *Mol. Cell* 15, 767–776. doi:10.1016/j.molcel.2004.08.025
- Higuchi, Y., Kawai, K., Yamazaki, H., Nakamura, M., Bree, F., Guguen-Guillouzo, C., Suemizu, H., 2014. The human hepatic cell line HepaRG as a possible cell source for the generation of humanized liver TK-NOG mice. *Xenobiotica.* 44, 146–53. doi:10.3109/00498254.2013.836257
- Hinz, B., Chevts, J., Renner, B., Wuttke, H., Rau, T., Schmidt, A., Szelenyi, I., Brune, K., Werner, U., 2005. Bioavailability of diclofenac potassium at low doses. *Br. J. Clin. Pharmacol.* 59, 80–84. doi:10.1111/j.1365-2125.2005.02226.x
- Hoekstra, R., Nibourg, G. a a, van der Hoeven, T. V, Ackermans, M.T., Hakvoort, T.B.M., van Gulik, T.M., Lamers, W.H., Elferink, R.P.O., Chamuleau, R. a F.M., 2011. The HepaRG cell line is suitable for bioartificial liver application. *Int. J. Biochem. Cell Biol.* 43, 1483–1489. doi:10.1016/j.biocel.2011.06.011
- Howard, R.B., Christensen, A.K., Gibbs, F.A., Pesch, L.A., 1967. The enzymatic preparation of isolated intact parenchymal cells from rat liver. *J. Cell Biol.* 35, 675–684. doi:10.1083/jcb.35.3.675
- Hrach, J., Mueller, S.O., Hewitt, P., 2011. Development of an in vitro liver toxicity prediction model based on longer term primary rat hepatocyte culture. *Toxicol. Lett.* 206, 189–196. doi:10.1016/j.toxlet.2011.07.012
- Humbert, M., Segal, E.S., Kiely, D.G., Carlsen, J., Schwierin, B., Hoepfer, M.M., 2007. Results of European post-marketing surveillance of bosentan in pulmonary hypertension. *Eur. Respir. J.* 30, 338–344. doi:10.1183/09031936.00138706
- ICRP, 2002. ICRP Publication 89: Basic anatomical and physiological data for use in radiological protection: Reference values. *Ann. ICRP* 3–4., 265. doi:10.1016/S0146-6453(03)00002-2
- Iizuka, K., 2013. Recent progress on the role of ChREBP in glucose and lipid metabolism. *Endocr. J.* 60, 543–55.

- Isom, H.C., Secott, T., Georgoff, I., Woodworth, C., Mummaw, J., 1985. Maintenance of differentiated rat hepatocytes in primary culture. *Proc. Natl. Acad. Sci. U. S. A.* 82, 3252–6. doi:10.1073/pnas.82.10.3252
- Iyer, V. V., Yang, H., Ierapetritou, M.G., Roth, C.M., 2010. Effects of glucose and insulin on HepG2-C3A cell metabolism. *Biotechnol Bioeng* 107, 347–356. doi:10.1002/bit.22799
- Jaenisch, R., Bird, A., 2003. Epigenetic regulation of gene expression: how the genome integrates intrinsic and environmental signals. *Nat. Genet.* 33, 245–254. doi:10.1038/ng1089
- Jaeschke, H., 1990. Glutathione disulfide formation and oxidant stress during acetaminophen-induced hepatotoxicity in mice in vivo: the protective effect of allopurinol. *J. Pharmacol. Exp. Ther.* 255, 935–941.
- Jedlitschky, G., Leier, I., Buchholz, U., Barnouin, K., Kurz, G., Keppler, D., 1996. Transport of glutathione, glucuronate, and sulfate conjugates by the MRP gene-encoded conjugate export pump. *Cancer Res.* 56, 988–994.
- Jennen, D.G.J., Magkoufopoulou, C., Ketelslegers, H.B., van Herwijnen, M.H.M., Kleinjans, J.C.S., van Delft, J.H.M., 2010. Comparison of HepG2 and HepaRG by whole-genome gene expression analysis for the purpose of chemical hazard identification. *Toxicol. Sci.* 115, 66–79. doi:10.1093/toxsci/kfq026
- Jetten, M.J. a, Kleinjans, J.C.S., Claessen, S.M., Chesné, C., van Delft, J.H.M., 2013. Baseline and genotoxic compound induced gene expression profiles in HepG2 and HepaRG compared to primary human hepatocytes. *Toxicol. In Vitro* 27, 2031–40. doi:10.1016/j.tiv.2013.07.010
- Jeyapaul, J., Jaiswal, A.K., 2000. Nrf2 and c-Jun regulation of antioxidant response element (ARE)-mediated expression and induction of γ -glutamylcysteine synthetase heavy subunit gene. *Biochem. Pharmacol.* 59, 1433–1439. doi:10.1016/S0006-2952(00)00256-2
- Jin, Y.S., Jeffries, T.W., 2004. Stoichiometric network constraints on xylose metabolism by recombinant *Saccharomyces cerevisiae*. *Metab. Eng.* 6, 229–238. doi:10.1016/j.ymben.2003.11.006
- Joseph, S.B., Laffitte, B.A., Patel, P.H., Watson, M.A., Matsukuma, K.E., Walczak, R., Collins, J.L., Osborne, T.F., Tontonoz, P., 2002. Direct and Indirect Mechanisms for Regulation of Fatty Acid Synthase Gene Expression by Liver X Receptors. *J. Biol. Chem.* 277, 11019–11025. doi:10.1074/jbc.M111041200
- Josse, R., Aninat, C., Glaize, D., Dumont, J., Fessard, V., Morel, F., Poul, J.-M., Guguen-Guillouzo, C., Guillouzo, A., 2008. Long-Term Functional Stability of Human HepaRG Hepatocytes and Use for Chronic Toxicity and Genotoxicity Studies. *Drug Metab. Dispos.* 36, 1111–1118. doi:10.1124/dmd.107.019901
- Josse, R., Rogue, A., Lorge, E., Guillouzo, A., 2012. An adaptation of the human HepaRG cells to the in vitro micronucleus assay. *Mutagenesis* 27, 295–304. doi:10.1093/mutage/ger076
- Jover, R., Ponsoda, X., Castell, J.V., Gómez-Lechón, M.J., 1992. Evaluation of the cytotoxicity of ten chemicals on human cultured hepatocytes: Predictability of human toxicity and comparison with rodent cell culture systems. *Toxicol. Vitro* 6, 47–52. doi:10.1016/0887-2333(92)90084-5
- Jover, R., Roque, B., Gomez-Lechon, M., Castell, J., 2001. Cytochrome P450 regulation by hepatocyte nuclear factor 4 in human hepatocytes: A study using adenovirus-mediated antisense targeting. *Hepatology* 33, 668–675. doi:10.1053/jhep.2001.22176
- Jung, S.-N., Yang, W.K., Kim, J., Kim, H.S., Kim, E.J., Yun, H., Park, H., Kim, S.S., Choe, W., Kang, I., Ha, J., 2008. Reactive oxygen species stabilize hypoxia-inducible factor-1 α protein and stimulate transcriptional activity via AMP-activated protein kinase in DU145 human prostate cancer cells. *Carcinogenesis* 29, 713–721. doi:10.1093/carcin/bgn032
- Jürgensen, J., Seltsam, A., Jörres, A., 2001. Fatal acute diclofenac-induced immune hemolytic anemia. *Ann. Hematol.* 80, 440–442. doi:10.1007/s002770100316
- Kanebratt, K.P., Andersson, T.B., 2008. Evaluation of HepaRG cells as an in vitro model for human drug metabolism studies. *Drug Metab. Dispos.* 36, 1444–1452. doi:10.1124/dmd.107.020016
- Kaplowitz, N., 2004. Drug-Induced Liver Injury. *Clin Infect Dis.* 38, 44–48. doi:10.1086/381446
- Kaplowitz, N., 2005. Idiosyncratic drug hepatotoxicity. *Nat. Rev. Drug Discov.* 4, 489–499. doi:10.1038/nrd1750
- Kelley, D., Mokan, M., Veneman, T., 1994. Impaired postprandial glucose utilization in non-insulin-dependent diabetes mellitus. *Metabolism* 43, 1549–1557. doi:10.1016/0026-0495(94)90015-9
- Kelm, J.M., Fussenegger, M., 2004. Microscale tissue engineering using gravity-enforced cell

- assembly. *Trends Biotechnol.* 22, 195–202. doi:10.1016/j.tibtech.2004.02.002
- Kelts, J.L., Cali, J.J., Duellman, S.J., Shultz, J., 2015. Altered cytotoxicity of ROS-inducing compounds by sodium pyruvate in cell culture medium depends on the location of ROS generation. *Springerplus* 4, 269. doi:10.1186/s40064-015-1063-y
- Kenna, J.G., Stahl, S.H., Eakins, J.A., Foster, A.J., Andersson, L.C., Bergare, J., Billger, M., Elebring, M., Elmore, C.S., Thompson, R.A., 2014. Multiple Compound-Related Adverse Properties Contribute to Liver Injury Caused by Endothelin Receptor Antagonists. *J. Pharmacol. Exp. Ther.* 352, 281–290. doi:10.1124/jpet.114.220491
- Kiang, T.K.L., Ho, P.C., Anari, M.R., Tong, V., Abbott, F.S., Chang, T.K.H., 2006. Contribution of CYP2C9, CYP2A6, and CYP2B6 to valproic acid metabolism in hepatic microsomes from individuals with the CYP2C9*1/*1 genotype. *Toxicol. Sci.* 94, 261–271. doi:10.1093/toxsci/kfl096
- Kiang, T.K.L., Teng, X.W., Surendradoss, J., Karagiozov, S., Abbott, F.S., Chang, T.K.H., 2011. Glutathione depletion by valproic acid in sandwich-cultured rat hepatocytes: Role of biotransformation and temporal relationship with onset of toxicity. *Toxicol. Appl. Pharmacol.* 252, 318–324. doi:10.1016/j.taap.2011.03.004
- Kietzmann, T., 2017. Metabolic zonation of the liver: The oxygen gradient revisited. *Redox Biol.* 11, 622–630. doi:10.1016/j.redox.2017.01.012
- Kim, J.W., Tchernyshyov, I., Semenza, G.L., Dang, C. V., 2006. HIF-1-mediated expression of pyruvate dehydrogenase kinase: A metabolic switch required for cellular adaptation to hypoxia. *Cell Metab.* 3, 177–185. doi:10.1016/j.cmet.2006.02.002
- Kim, M., Lee, J.Y., Jones, C.N., Revzin, A., Tae, G., 2010. Heparin-based hydrogel as a matrix for encapsulation and cultivation of primary hepatocytes. *Biomaterials* 31, 3596–3603. doi:10.1016/j.biomaterials.2010.01.068
- Kim, M., Rai, N., Zorraquino, V., Tagkopoulos, I., 2016. Multi-omics integration accurately predicts cellular state in unexplored conditions for *Escherichia coli*. *Nat. Commun.* 7, 13090. doi:10.1038/ncomms13090
- Klassen, L.W., Thiele, G.M., Duryee, M.J., Schaffert, C.S., DeVeney, A.L., Hunter, C.D., Olinga, P., Tuma, D.J., 2008. An in vitro method of alcoholic liver injury using precision-cut liver slices from rats. *Biochem. Pharmacol.* 76, 426–436. doi:10.1016/j.bcp.2008.05.012
- Klein, S., Heinzle, E., 2012. Isotope labeling experiments in metabolomics and fluxomics. *Wiley Interdiscip. Rev. Syst. Biol. Med.* 4, 261–72. doi:10.1002/wsbm.1167
- Klein, S., Maggioni, S., Bucher, J., Mueller, D., Niklas, J., Shevchenko, V., Mauch, K., Heinzle, E., Noor, F., 2016. In Silico Modeling for the Prediction of Dose and Pathway-Related Adverse Effects in Humans From In Vitro Repeated-Dose Studies. *Toxicol. Sci.* 149, 55–66. doi:10.1093/toxsci/kfv218
- Klein, S., Mueller, D., Schevchenko, V., Noor, F., 2014. Long-term maintenance of HepaRG cells in serum-free conditions and application in a repeated dose study. *J. Appl. Toxicol.* 34, 1078–1086. doi:10.1002/jat.2929
- Kleiner, D.E., 2014. Liver histology in the diagnosis and prognosis of drug-induced liver injury. *Clin. Liver Dis.* 4, 12–16. doi:10.1002/cld.371
- Kleiner, D.E., Chalasani, N.P., Lee, W.M., Fontana, R.J., Bonkovsky, H.L., Watkins, P.B., Hayashi, P.H., Davern, T.J., Navarro, V., Reddy, R., Talwalkar, J.A., Stolz, A., Gu, J., Barnhart, H., Hoofnagle, J.H., 2014. Hepatic histological findings in suspected drug-induced liver injury: Systematic evaluation and clinical associations. *Hepatology* 59, 661–670. doi:10.1002/hep.26709
- Kleinjans, J.C.S., 2003. Principles in toxicological risk analysis. *Toxicol. Lett.* 140–141, 311–315. doi:10.1016/S0378-4274(03)00027-4
- Knudsen, T.B., Keller, D. a., Sander, M., Carney, E.W., Doerrer, N.G., Eaton, D.L., Fitzpatrick, S.C., Hastings, K.L., Mendrick, D.L., Tice, R.R., Watkins, P.B., Whelan, M., 2015. FutureTox II: In vitro Data and In Silico Models for Predictive Toxicology. *Toxicol. Sci.* 143, 256–267. doi:10.1093/toxsci/kfu234
- Ko, H.C., Gelb, B.D., 2014. Concise Review: Drug Discovery in the Age of the Induced Pluripotent Stem Cell. *Stem Cells Transl. Med.* 3, 500–509. doi:10.5966/sctm.2013-0162
- Kopf, T., Peer, M., Schmitz, G., 2012. Genetic and Metabolic Determinants of Fatty Acid Chain Length and Desaturation, Their Incorporation into Lipid Classes and Their Effects on Risk of Vascular and Metabolic Disease, in: *Genetics Meets Metabolomics*. Springer New York, New

- York, NY, pp. 191–231. doi:10.1007/978-1-4614-1689-0_13
- Kostadinova, R., Boess, F., Applegate, D., Suter, L., Weiser, T., Singer, T., Naughton, B., Roth, A., 2013. A long-term three dimensional liver co-culture system for improved prediction of clinically relevant drug-induced hepatotoxicity. *Toxicol. Appl. Pharmacol.* 268, 1–16. doi:10.1016/j.taap.2013.01.012
- Kota, B.P., Huang, T.H.W., Roufogalis, B.D., 2005. An overview on biological mechanisms of PPARs. *Pharmacol. Res.* doi:10.1016/j.phrs.2004.07.012
- Kotani, N., Maeda, K., Debori, Y., Camus, S., Li, R., Chesne, C., Sugiyama, Y., 2012. Expression and transport function of drug uptake transporters in differentiated HepaRG cells. *Mol. Pharm.* 9, 3434–3441. doi:10.1021/mp300171p
- Krähenbühl, S., Brandner, S., Kleinle, S., Liechti, S., Straumann, D., 2000. Mitochondrial diseases represent a risk factor for valproate-induced fulminant liver failure. *Liver* 20, 346–8.
- Krause, P., Saghatolislam, F., Koenig, S., Unthan-Fechner, K., Probst, I., 2009. Maintaining hepatocyte differentiation in vitro through co-Culture with hepatic stellate cells. *Vitr. Cell. Dev. Biol. - Anim.* 45, 205–212. doi:10.1007/s11626-008-9166-1
- Kretzrommel, A., Boelsterli, U.A., 1993. Diclofenac Covalent Protein Binding Is Dependent on Acyl Glucuronide Formation and Is Inversely Related to P450-Mediated Acute Cell Injury in Cultured Rat Hepatocytes. *Toxicol. Appl. Pharmacol.* 120, 155–161. doi:10.1006/taap.1993.1097
- Kroes, R., Renwick, A., Cheeseman, M., Kleiner, J., Mangelsdorf, I., Piersma, A., Schilter, B., Schlatter, J., van Schothorst, F., Vos, J., Würtzen, G., 2004. Structure-based thresholds of toxicological concern (TTC): guidance for application to substances present at low levels in the diet. *Food Chem. Toxicol.* 42, 65–83. doi:10.1016/j.fct.2003.08.006
- Krömer, J.O., Fritz, M., Heinzele, E., Wittmann, C., 2005. In vivo quantification of intracellular amino acids and intermediates of the methionine pathway in *Corynebacterium glutamicum*. *Anal. Biochem.* 340, 171–3. doi:10.1016/j.ab.2005.01.027
- Kubinyi, H., 2003. Opinion: Drug research: myths, hype and reality. *Nat. Rev. Drug Discov.* 2, 665–668. doi:10.1038/nrd1156
- Kunz-Schughart, L. a, Freyer, J.P., Hofstaedter, F., Ebner, R., 2004. The use of 3-D cultures for high-throughput screening: the multicellular spheroid model. *J. Biomol. Screen.* 9, 273–85. doi:10.1177/1087057104265040
- Laine, J.E., Auriola, S., Pasanen, M., Juvonen, R.O., 2009. Acetaminophen bioactivation by human cytochrome P450 enzymes and animal microsomes. *Xenobiotica.* 39, 11–21. doi:10.1080/00498250802512830
- Lammert, C., Bjornsson, E., Niklasson, A., Chalasani, N., 2010. Oral medications with significant hepatic metabolism at higher risk for hepatic adverse events. *Hepatology* 51, 615–620. doi:10.1002/hep.23317
- Lane, A.N., Fan, T.W.-M., 2015. Regulation of mammalian nucleotide metabolism and biosynthesis. *Nucleic Acids Res.* 43, 2466–2485. doi:10.1093/nar/gkv047
- Larson, A.M., Polson, J., Fontana, R.J., Davern, T.J., Lalani, E., Hynan, L.S., Reisch, J.S., Schi??dt, F. V., Ostapowicz, G., Shakil, A.O., Lee, W.M., 2005. Acetaminophen-induced acute liver failure: Results of a United States multicenter, prospective study. *Hepatology* 42, 1364–1372. doi:10.1002/hep.20948
- Le Vee, M., Noel, G., Jouan, E., Stieger, B., Fardel, O., 2013. Polarized expression of drug transporters in differentiated human hepatoma HepaRG cells. *Toxicol. Vitr.* 27, 1979–1986. doi:10.1016/j.tiv.2013.07.003
- Lee, J.-W., Bae, S.-H., Jeong, J.-W., Kim, S.-H., Kim, K.-W., 2004. Hypoxia-inducible factor (HIF-1)alpha: its protein stability and biological functions. *Exp. Mol. Med.* 36, 1–12. doi:10.1038/emm.2004.1
- Leeuwen, C., Vermeire, T., 2007. Risk Assessment of Chemicals. Springer Netherlands, Dordrecht. doi:10.1007/978-1-4020-6102-8
- Lefebvre, P., Cariou, B., Lien, F., Kuipers, F., Staels, B., 2009. Role of bile acids and bile acid receptors in metabolic regulation. *Physiol. Rev.* 89, 147–191. doi:10.1152/physrev.00010.2008
- Leite, S.B., Wilk-Zasadna, I., Zaldivar, J.M., Airola, E., Reis-Fernandes, M. a, Mennecozzi, M., Guguen-Guillouzo, C., Chesne, C., Guillou, C., Alves, P.M., Coecke, S., 2012. Three-dimensional HepaRG model as an attractive tool for toxicity testing. *Toxicol. Sci.* 130, 106–16. doi:10.1093/toxsci/kfs232

- Leung, L., Kalgutkar, A.S., Obach, R.S., 2012. Metabolic activation in drug-induced liver injury. *Drug Metab. Rev.* 44, 18–33. doi:10.3109/03602532.2011.605791
- Liebler, D.C., Guengerich, F.P., 2005. Elucidating mechanisms of drug-induced toxicity. *Nat. Rev. Drug Discov.* 4, 410–420. doi:10.1038/nrd1720
- Lim, J., Lee, H., Hojung, M., Song, J., 2009. Coupling mitochondrial dysfunction to endoplasmic reticulum stress response: A molecular mechanism leading to hepatic insulin resistance. *Cell. Signal.* 21, 169–177. doi:10.1016/j.cellsig.2008.10.004
- Limonciel, A., Aschauer, L., Wilmes, A., Prajczek, S., Leonard, M.O., Pfaller, W., Jennings, P., 2011. Lactate is an ideal non-invasive marker for evaluating temporal alterations in cell stress and toxicity in repeat dose testing regimes. *Toxicol. Vitro.* 25, 1855–1862. doi:10.1016/j.tiv.2011.05.018
- Listenberger, L.L., Han, X., Lewis, S.E., Cases, S., Farese, R. V., Ory, D.S., Schaffer, J.E., 2003. Triglyceride accumulation protects against fatty acid-induced lipotoxicity. *Proc. Natl. Acad. Sci.* 100, 3077–3082. doi:10.1073/pnas.0630588100
- Liu, X., LeCluyse, E., Brouwer, K., Gan, L., Lemasters, J., Stieger, B., Meier, P., Brouwer, K., 1999. Biliary excretion in primary rat hepatocytes cultured in a collagen-sandwich configuration. *Am J Physiol.* 277, G12-21.
- Lluis, J.M., Morales, A., Blasco, C., Colell, A., Mari, M., Garcia-Ruiz, C., Fernandez-Checa, J.C., 2005. Critical role of mitochondrial glutathione in the survival of hepatocytes during hypoxia. *J. Biol. Chem.* 280, 3224–3232. doi:10.1074/jbc.M408244200
- López-Terrada, D., Cheung, S.W., Finegold, M.J., Knowles, B.B., 2009. Hep G2 is a hepatoblastoma-derived cell line. *Hum. Pathol.* 40, 1512–1515. doi:10.1016/j.humpath.2009.07.003
- Low, Y., Sedykh, A., Fourches, D., Golbraikh, A., Whelan, M., Rusyn, I., Tropsha, A., 2013. Integrative Chemical–Biological Read-Across Approach for Chemical Hazard Classification. *Chem. Res. Toxicol.* 26, 1199–1208. doi:10.1021/tx400110f
- Lu, F., Kacew, S., 2002. *Lu's basic toxicology*, 4th ed. Taylor & Francis.
- Lübberstedt, M., Müller-Vieira, U., Mayer, M., Biemel, K.M., Knöspel, F., Knobloch, D., Nüssler, A.K., Gerlach, J.C., Zeilinger, K., 2011. HepaRG human hepatic cell line utility as a surrogate for primary human hepatocytes in drug metabolism assessment in vitro. *J. Pharmacol. Toxicol. Methods* 63, 59–68. doi:10.1016/j.vascn.2010.04.013
- Luís, P.B.M., Ruiten, J.P.N., Aires, C.C.P., Soveral, G., de Almeida, I.T., Duran, M., Wanders, R.J. a, Silva, M.F.B., 2007. Valproic acid metabolites inhibit dihydrolipoyl dehydrogenase activity leading to impaired 2-oxoglutarate-driven oxidative phosphorylation. *Biochim. Biophys. Acta* 1767, 1126–33. doi:10.1016/j.bbabi.2007.06.007
- Luís, P.B.M., Ruiten, J.P.N., Ijlst, L., Tavares de Almeida, I., Duran, M., Mohsen, A.-W., Vockley, J., Wanders, R.J. a, Silva, M.F.B., 2011. Role of isovaleryl-CoA dehydrogenase and short branched-chain acyl-CoA dehydrogenase in the metabolism of valproic acid: implications for the branched-chain amino acid oxidation pathway. *Drug Metab. Dispos.* 39, 1155–1160. doi:10.1124/dmd.110.037606.sant
- MacAllister, S.L., Young, C., Guzdek, A., Zhidkov, N., O'Brien, P.J., 2013. Molecular cytotoxic mechanisms of chlorpromazine in isolated rat hepatocytes. *Can. J. Physiol. Pharmacol.* 91, 56–63. doi:10.1139/cjpp-2012-0223
- Makishima, M., Okamoto, a Y., Repa, J.J., Tu, H., Learned, R.M., Luk, a, Hull, M. V, Lustig, K.D., Mangelsdorf, D.J., Shan, B., 1999. Identification of a nuclear receptor for bile acids. *Science* 284, 1362–1365. doi:10.1126/science.284.5418.1362
- Malinen, M.M., Kanninen, L.K., Corlu, A., Isoniemi, H.M., Lou, Y.R., Yliperttula, M.L., Urtti, A.O., 2014. Differentiation of liver progenitor cell line to functional organotypic cultures in 3D nanofibrillar cellulose and hyaluronan-gelatin hydrogels. *Biomaterials.* doi:10.1016/j.biomaterials.2014.03.020
- Manov, I., Hirsh, M., Iancu, T.C., 2004. N-acetylcysteine does not protect HepG2 cells against acetaminophen-induced apoptosis. *Basic Clin. Pharmacol. Toxicol.* 94, 213–225. doi:10.1111/j.1742-7843.2004.pto940504.x
- Marroquin, L.D., Hynes, J., Dykens, J.A., Jamieson, J.D., Will, Y., 2007. Circumventing the Crabtree Effect: Replacing Media Glucose with Galactose Increases Susceptibility of HepG2 Cells to Mitochondrial Toxicants. *Toxicol. Sci.* 97, 539–547. doi:10.1093/toxsci/kfm052
- Martignoni, M., Groothuis, G.M.M., de Kanter, R., 2006. Species differences between mouse, rat, dog,

- monkey and human CYP-mediated drug metabolism, inhibition and induction. *Expert Opin. Drug Metab. Toxicol.* 2, 875–894. doi:10.1517/17425255.2.6.875
- Maschmeyer, I., Lorenz, A.K., Schimek, K., Hasenberg, T., Ramme, A.P., Hübner, J., Lindner, M., Drewell, C., Bauer, S., Thomas, A., Sambo, N.S., Sonntag, F., Lauster, R., Marx, U., 2015. A four-organ-chip for interconnected long-term co-culture of human intestine, liver, skin and kidney equivalents. *Lab Chip* 15, 2688–2699. doi:10.1039/C5LC00392J
- Matsuo, M., Terai, K., Kameda, N., Matsumoto, A., Kurokawa, Y., Funase, Y., Nishikawa, K., Sugaya, N., Hiruta, N., Kishimoto, T., 2012. Designation of enzyme activity of glycine-N-acyltransferase family genes and depression of glycine-N-acyltransferase in human hepatocellular carcinoma. *Biochem. Biophys. Res. Commun.* 420, 901–906. doi:10.1016/j.bbrc.2012.03.099
- Mavri-Damelin, D., Damelin, L.H., Eaton, S., Rees, M., Selden, C., Hodgson, H.J.F., 2008. Cells for bioartificial liver devices: the human hepatoma-derived cell line C3A produces urea but does not detoxify ammonia. *Biotechnol. Bioeng.* 99, 644–651. doi:10.1002/bit
- Mavri-Damelin, D., Eaton, S., Damelin, L.H., Rees, M., Hodgson, H.J.F., Selden, C., 2007. Ornithine transcarbamylase and arginase I deficiency are responsible for diminished urea cycle function in the human hepatoblastoma cell line HepG2. *Int. J. Biochem. Cell Biol.* 39, 555–564. doi:10.1016/j.biocel.2006.10.007
- McGill, M.R., Li, F., Sharpe, M.R., Williams, C.D., Curry, S.C., Ma, X., Jaeschke, H., 2014. Circulating acylcarnitines as biomarkers of mitochondrial dysfunction after acetaminophen overdose in mice and humans. *Arch. Toxicol.* 88, 391–401. doi:10.1007/s00204-013-1118-1
- McGill, M.R., Sharpe, M.R., Williams, C.D., Taha, M., Curry, S.C., Jaeschke, H., 2012. The mechanism underlying acetaminophen-induced hepatotoxicity in humans and mice involves mitochondrial damage and nuclear DNA fragmentation. *J. Clin. Invest.* 122, 1574–83. doi:10.1172/JCI59755
- McGill, M.R., Yan, H.M., Ramachandran, a, Murray, G.J., Rollins, D.E., Jaeschke, H., 2011. HepaRG cells: a human model to study mechanisms of acetaminophen hepatotoxicity. *Hepatology* 53, 974–982. doi:10.1002/hep.24132
- Meng, Q., 2010. Three-dimensional culture of hepatocytes for prediction of drug-induced hepatotoxicity. *Expert Opin. Drug Metab. Toxicol.* 6, 733–746. doi:10.1517/17425251003674356
- Metallo, C.M., Gameiro, P.A., Bell, E.L., Mattaini, K.R., Yang, J., Hiller, K., Jewell, C.M., Johnson, Z.R., Irvine, D.J., Guarente, L., Kelleher, J.K., Vander Heiden, M.G., Iliopoulos, O., Stephanopoulos, G., 2011. Reductive glutamine metabolism by IDH1 mediates lipogenesis under hypoxia. *Nature*. doi:10.1038/nature10602
- Meyers, L.L., Beierschmitt, W.P., Khairallah, E.A., Cohen, S.D., 1988. Acetaminophen-induced inhibition of hepatic mitochondrial respiration in mice. *Toxicol. Appl. Pharmacol.* 93, 378–387.
- Misu, H., Takamura, T., Matsuzawa, N., Shimizu, A., Ota, T., Sakurai, M., Ando, H., Arai, K., Yamashita, T., Honda, M., Yamashita, T., Kaneko, S., 2007. Genes involved in oxidative phosphorylation are coordinately upregulated with fasting hyperglycaemia in livers of patients with type 2 diabetes. *Diabetologia* 50, 268–277. doi:10.1007/s00125-006-0489-8
- Mitchell, J.R., Jollow, D.J., Potter, W.Z., Davis, D.C., Gillette, J.R., Brodie, B.B., 1973. Acetaminophen-Induced Hepatic Necrosis. I. Role of Drug Metabolism. *J. Pharmacol. Exp. Ther.* 187, 185–194.
- Moore, M.C., Coate, K.C., Winnick, J.J., An, Z., Cherrington, A.D., 2012. Regulation of Hepatic Glucose Uptake and Storage In Vivo. *Adv. Nutr. An Int. Rev. J.* 3, 286–294. doi:10.3945/an.112.002089
- Moura, C., Acurcio, F., Belo, N., 2009. Drug-drug interactions associated with length of stay and cost of hospitalization. *J. Pharm. Pharm. Sci.* 12, 266–272. doi:10.18433/J35C7Z
- Mueller, D., Heinzle, E., 2013. Stable isotope-assisted metabolomics to detect metabolic flux changes in mammalian cell cultures. *Curr. Opin. Biotechnol.* 24, 54–59. doi:10.1016/j.copbio.2012.10.015
- Mueller, D., Heinzle, E., Noor, F., 2013. 3D Hepatic In Vitro Models as Tools for Toxicity Studies. *Curr. Tissue Eng.* 2, 12. doi:10.2174/2211542011302010007
- Mueller, D., Krämer, L., Hoffmann, E., Klein, S., Noor, F., 2014. 3D organotypic HepaRG cultures as in vitro model for acute and repeated dose toxicity studies. *Toxicol. Vitr.* 28, 104–112.

- doi:10.1016/j.tiv.2013.06.024
- Mueller, D., Müller-Vieira, U., Biemel, K.M., Tascher, G., Nüssler, A.K., Noor, F., 2012. Biotransformation of diclofenac and effects on the metabolome of primary human hepatocytes upon repeated dose exposure. *Eur. J. Pharm. Sci.* 45, 716–724. doi:10.1016/j.ejps.2012.01.014
- Mueller, D., Tascher, G., Müller-Vieira, U., Knobloch, D., Nuessler, A.K., Zeilinger, K., Heinzle, E., Noor, F., 2011. In-depth physiological characterization of primary human hepatocytes in a 3D hollow-fiber bioreactor. *J. Tissue Eng. Regen. Med.* 5, e207–e218. doi:10.1002/term
- Mulchey, K., Bshouty, Z., 2009. An atypical presentation of liver enzyme elevation resulting from bosentan use. *Can. Respir. J.* 16, e54–e56.
- Nagy, G., Kardon, T., Wunderlich, L., Szarka, A., Kiss, A., Schaff, Z., Bánhegyi, G., Mandl, J., 2007. Acetaminophen induces ER dependent signaling in mouse liver. *Arch. Biochem. Biophys.* 459, 273–279. doi:10.1016/j.abb.2006.11.021
- Nanau, R.M., Neuman, M.G., 2013. Adverse drug reactions induced by valproic acid. *Clin. Biochem.* doi:10.1016/j.clinbiochem.2013.06.012
- National Research Council, 2007. *Toxicity Testing in the 21st Century: A vision and a strategy.* National Academy Press; Washington, DC, Washington, D.C. doi:10.17226/11970
- Nelson, D.L., Cox, M.M., 2008. *Lehninger Principles of Biochemistry* 5th ed. Book. doi:10.2307/1309148
- Nelson, S.D., 1990. Molecular Mechanisms of the Hepatotoxicity Caused by Acetaminophen. *Semin Liver Dis* 10, 267–278. doi:10.1055/s-2008-1040482
- Neuman, M.G., Shear, N.H., Jacobson-Brown, P.M., Katz, G.G., Neilson, H.K., Malkiewicz, I.M., Cameron, R.G., Abbott, F., 2001. CYP2E1-mediated modulation of valproic acid-induced hepatocytotoxicity. *Clin. Biochem.* 34, 211–218. doi:10.1016/S0009-9120(01)00217-X
- NIH, n.d. Livertox [WWW Document]. URL www.livertox.nih.gov (accessed 3.26.16).
- Niklas, J., Heinzle, E., 2011. Metabolic Flux Analysis in Systems Biology of Mammalian Cells, in: *Genomics and Systems Biology of Mammalian Cell Culture.* Springer Berlin Heidelberg, Berlin, Heidelberg, pp. 109–132. doi:10.1007/10_2011_99
- Niklas, J., Noor, F., Heinzle, E., 2009. Effects of drugs in subtoxic concentrations on the metabolic fluxes in human hepatoma cell line Hep G2. *Toxicol. Appl. Pharmacol.* 240, 327–36. doi:10.1016/j.taap.2009.07.005
- Nishimura, T., Hu, Y., Wu, M., Pham, E., Suemizu, H., Elazar, M., Liu, M., Idilman, R., Yurdaydin, C., Angus, P., Stedman, C., Murphy, B., Glenn, J., Nakamura, M., Nomura, T., Chen, Y., Zheng, M., Fitch, W.L., Peltz, G., 2013. Using Chimeric Mice with Humanized Livers to Predict Human Drug Metabolism and a Drug-Drug Interaction. *J. Pharmacol. Exp. Ther.* 344, 388–396. doi:10.1124/jpet.112.198697
- Obach, R.S., Baxter, J.G., Liston, T.E., Silber, B.M., Jones, B.C., MacIntyre, F., Rance, D.J., Wastall, P., 1997. The prediction of human pharmacokinetic parameters from preclinical and in vitro metabolism data. *J. Pharmacol. Exp. Ther.* 283, 46–58.
- Oda, E., Ohki, R., Murasawa, H., Nemoto, J., Shibue, T., Yamashita, T., Tokino, T., Taniguchi, T., Tanaka, N., 2000. Noxa, a BH3-only member of the Bcl-2 family and candidate mediator of p53-induced apoptosis. *Science* 288, 1053–8.
- Okita, K., Nakagawa, M., Hyenjong, H., Ichisaka, T., Yamanaka, S., 2008. Generation of Mouse Induced Pluripotent Stem Cells Without Viral Vectors. *Science* (80-.). 322, 949–953. doi:10.1126/science.1164270
- Olson, H., Betton, G., Robinson, D., Thomas, K., Monro, a, Kolaja, G., Lilly, P., Sanders, J., Sipes, G., Bracken, W., Dorato, M., Van Deun, K., Smith, P., Berger, B., Heller, a, 2000. Concordance of the toxicity of pharmaceuticals in humans and in animals. *Regul. Toxicol. Pharmacol.* 32, 56–67. doi:10.1006/rtph.2000.1399
- Ong, R.C.Y., Lei, J., Lee, R.K.Y., Cheung, J.Y.N., Fung, K.P., Lin, C., Ho, H.P., Yu, B., Li, M., Kong, S.K., 2008. Polyphyllin D induces mitochondrial fragmentation and acts directly on the mitochondria to induce apoptosis in drug-resistant HepG2 cells. *Cancer Lett.* 261, 158–164. doi:10.1016/j.canlet.2007.11.005
- Organ, C.L., Otsuka, H., Bhushan, S., Wang, Z., Bradley, J., Trivedi, R., Polhemus, D.J., Tang, W.H.W., Wu, Y., Hazen, S.L., Lefer, D.J., 2016. Choline Diet and Its Gut Microbe-Derived Metabolite, Trimethylamine N-Oxide, Exacerbate Pressure Overload-Induced Heart Failure. *Circ. Hear. Fail.* 9, e002314. doi:10.1161/CIRCHEARTFAILURE.115.002314

- Orman, M. a, Ierapetritou, M.G., Androulakis, I.P., Berthiaume, F., 2011. Metabolic response of perfused livers to various oxygenation conditions. *Biotechnol. Bioeng.* 108, 2947–57. doi:10.1002/bit.23261
- Padda, M.S., Sanchez, M., Akhtar, A.J., Boyer, J.L., 2011. Drug-induced cholestasis. *Hepatology* 53, 1377–1387. doi:10.1002/hep.24229
- Parkinson, A., Mudra, D., Johnson, C., Dwyer, A., Carroll, K., 2004. The effects of gender, age, ethnicity, and liver cirrhosis on cytochrome P450 enzyme activity in human liver microsomes and inducibility in cultured human hepatocytes. *Toxicol. Appl. Pharmacol.* 199, 193–209. doi:10.1016/j.taap.2004.01.010
- Parks, D.J., Blanchard, S.G., Bledsoe, R.K., Chandra, G., Consler, T.G., Kliewer, S. a, Stimmel, J.B., Willson, T.M., Zavacki, a M., Moore, D.D., Lehmann, J.M., 1999. Bile acids: natural ligands for an orphan nuclear receptor. *Science* 284, 1365–1368. doi:10.1126/science.284.5418.1365
- Perestrelo, A.R., Águas, A.C.P., Rainer, A., Forte, G., 2015. Microfluidic Organ / Body-on-a-Chip Devices at the Convergence of Biology and Microengineering 31142–31170. doi:10.3390/s151229848
- Pernelle, K., Le Guevel, R., Glaise, D., Stasio, C.G.-D., Le Charpentier, T., Bouaita, B., Corlu, a, Guguen-Guillouzo, C., 2011. Automated detection of hepatotoxic compounds in human hepatocytes using HepaRG cells and image-based analysis of mitochondrial dysfunction with JC-1 dye. *Toxicol. Appl. Pharmacol.* 254, 256–266. doi:10.1016/j.taap.2011.04.018
- Perucca, E., Gatti, G., Frigo, G.M., Crema, A., 1978. Pharmacokinetics of valproic acid after oral and intravenous administration. *Br J Clin Pharmacol.* 5, 313–318.
- Perucca, E., Grimaldi, R., Gatti, G., Pirracchio, S., Crema, F., Frigo, G.M., 1984. Pharmacokinetics of valproic acid in the elderly. *Br. J. Clin. Pharmacol.* 17, 665–669.
- Pfaller, W., Balls, M., Clothier, R., Coecke, S., Ekwall, B., Hanley, B.A., Hartung, T., Michael, P., Schmuck, G., Śladowski, D., Vericat, J., Wendel, A., Wolf, A., 2001. Novel Advanced In Vitro Methods for Long- term Toxicity Testing. *Altern Lab Anim.* 4, 393–426.
- Pirmohamed, M., James, S., Meakin, S., Green, C., Scott, A.K., Walley, T.J., Farrar, K., Park, B.K., Breckenridge, A.M., 2004. Adverse drug reactions as cause of admission to hospital: prospective analysis of 18 820 patients. *BMJ* 329, 15–19. doi:10.1136/bmj.329.7456.15
- Pond, S.M., Tozer, T.N., 1984. First-Pass Elimination. *Clin. Pharmacokinet.* 9, 1–25. doi:10.2165/00003088-198409010-00001
- Poulin, P., 2013. Prediction of total hepatic clearance by combining metabolism, transport, and permeability data in the in vitro - in vivo extrapolation methods: Emphasis on an apparent fraction unbound in liver for drugs. *J. Pharm. Sci.* 102, 2085–2095. doi:10.1002/jps.23562
- Poulin, P., Kenny, J.R., Hop, C.E.C.A., Haddad, S., 2012. In vitro-in vivo extrapolation of clearance: Modeling hepatic metabolic clearance of highly bound drugs and comparative assessment with existing calculation methods. *J. Pharm. Sci.* 101, 838–851. doi:10.1002/jps.22792
- Powell-Jackson, P., Tredger, J., Williams, R., 1984. Hepatotoxicity to sodium valproate: a review. *Gut* 6, 673–681.
- Prieto, P., Baird, A.W., Blauboer, B.J., Ripoll, J.V.C., Corvi, R., Dekant, W., Dietl, P., Gennari, A., Gribaldo, L., Griffin, J.L., Hartung, T., Heindel, J.J., Hoet, P., Jennings, P., Marocchio, L., Noraberg, J., Pazos, P., Westmorland, C., Wolf, A., Wright, J., Pfaller, W., 2006. The assessment of repeated dose toxicity in vitro: A proposed approach, in: *ATLA Alternatives to Laboratory Animals*. pp. 315–341.
- Puchades-Carrasco, L., Pineda-Lucena, A., 2015. Metabolomics in pharmaceutical research and development. *Curr. Opin. Biotechnol.* 35, 73–77. doi:10.1016/j.copbio.2015.04.004
- Quinn, M., McMillin, M., Galindo, C., Frampton, G., Pae, H.Y., DeMorrow, S., 2014. Bile acids permeabilize the blood brain barrier after bile duct ligation in rats via Rac1-dependent mechanisms. *Dig. Liver Dis.* 46, 527–534. doi:10.1016/j.dld.2014.01.159
- Rabinowich, L., Shibolet, O., 2015. Drug Induced Steatohepatitis : An Uncommon Culprit of a Common Disease 2015.
- Rakhshandehroo, M., Knoch, B., Müller, M., Kersten, S., 2010. Peroxisome Proliferator-Activated Receptor Alpha Target Genes. *PPAR Res.* 2010, 1–20. doi:10.1155/2010/612089
- Ramaiahgari, S.C., Den Braver, M.W., Herpers, B., Terpstra, V., Commandeur, J.N.M., Van De Water, B., Price, L.S., 2014. A 3D in vitro model of differentiated HepG2 cell spheroids with improved liver-like properties for repeated dose high-throughput toxicity studies. *Arch. Toxicol.*

- 88, 1083–1095. doi:10.1007/s00204-014-1215-9
- Ramalho, R.M., Viana, R.J.S., Low, W.C., Steer, C.J., Rodrigues, C.M.P., 2008. Bile acids and apoptosis modulation: an emerging role in experimental Alzheimer's disease. *Trends Mol. Med.* 14, 54–62. doi:10.1016/j.molmed.2007.12.001
- Rebello, S.P., Costa, R., Estrada, M., Shevchenko, V., Brito, C., Alves, P.M., 2014. HepaRG microencapsulated spheroids in DMSO-free culture: novel culturing approaches for enhanced xenobiotic and biosynthetic metabolism. *Arch. Toxicol.* doi:10.1007/s00204-014-1320-9
- Richert, L., Liguori, M.J., Abadie, C., Heyd, B., Mantion, G., Halkic, N., Waring, J.F., 2006. Gene expression in human hepatocytes in suspension after isolation is similar to the liver of origin, is not affected by hepatocyte cold storage and cryopreservation, but is strongly changed after hepatocyte plating. *Drug Metab. Dispos.* 34, 870–879. doi:10.1124/dmd.105.007708
- Roberts, L.D., Souza, A.L., Gerszten, R.E., Clish, C.B., 2012. Targeted Metabolomics, in: *Current Protocols in Molecular Biology*. John Wiley & Sons, Inc., Hoboken, NJ, USA. doi:10.1002/0471142727.mb3002s98
- Rodriguez-Antona, C., Donato, M.T., Boobis, A., Edwards, R.J., Watts, P.S., Castell, J. V, Gomez-Lechon, M.J., 2002. Cytochrome P450 expression in human hepatocytes and hepatoma cell lines: molecular mechanisms that determine lower expression in cultured cells. *Xenobiotica* 32, 505–520. doi:10.1080/00498250210128675
- Ron, D., Walter, P., 2007. Signal integration in the endoplasmic reticulum unfolded protein response. *Nat. Rev. Mol. Cell Biol.* 8, 519–529. doi:10.1038/nrm2199
- Rotroff, D.M., Wetmore, B. a, Dix, D.J., Ferguson, S.S., Clewell, H.J., Houck, K. a, Lecluyse, E.L., Andersen, M.E., Judson, R.S., Smith, C.M., Sochaski, M. a, Kavlock, R.J., Boellmann, F., Martin, M.T., Reif, D.M., Wambaugh, J.F., Thomas, R.S., 2010. Incorporating human dosimetry and exposure into high-throughput in vitro toxicity screening. *Toxicol. Sci.* 117, 348–358. doi:10.1093/toxsci/kfq220
- Rowland, M., Balant, L., Peck, C., 2004. Physiologically based pharmacokinetics in Drug Development and Regulatory Science: a workshop report (Georgetown University, Washington, DC, May 29–30, 2002). *AAPS J.* 6, 56–67. doi:10.1208/ps060106
- Sae-Lee, C., Moolsuwan, K., Chan, L., Pongvarin, N., 2016. ChREBP Regulates Itself and Metabolic Genes Implicated in Lipid Accumulation in β -Cell Line. *PLoS One* 11, e0147411. doi:10.1371/journal.pone.0147411
- Said, S.A., Ammar, E.S.M., Suddek, G.M., 2005. Effect of bosentan (ETA/ETB receptor antagonist) on metabolic changes during stress and diabetes. *Pharmacol. Res.* 51, 107–115. doi:10.1016/j.phrs.2004.05.009
- Sandanger, T.M., Huber, S., Moe, M.K., Braathen, T., Leknes, H., Lund, E., 2011. Plasma concentrations of parabens in postmenopausal women and self-reported use of personal care products: the NOWAC postgenome study. *J. Expo. Sci. Environ. Epidemiol.* 21, 595–600. doi:10.1038/jes.2011.22
- Sano, R., Reed, J.C., 2013. ER stress-induced cell death mechanisms. *Biochim. Biophys. Acta - Mol. Cell Res.* 1833, 3460–3470. doi:10.1016/j.bbamcr.2013.06.028
- Schilling, B., Rardin, M.J., MacLean, B.X., Zawadzka, a. M., Frewen, B.E., Cusack, M.P., Sorensen, D.J., Bereman, M.S., Jing, E., Wu, C.C., Verdin, E., Kahn, C.R., MacCoss, M.J., Gibson, B.W., 2012. Platform-independent and Label-free Quantitation of Proteomic Data Using MS1 Extracted Ion Chromatograms in Skyline: APPLICATION TO PROTEIN ACETYLATION AND PHOSPHORYLATION. *Mol. Cell. Proteomics* 11, 202–214. doi:10.1074/mcp.M112.017707
- Schumacher, A., Rujan, T., Hoefkens, J., 2014. A collaborative approach to develop a multi-omics data analytics platform for translational research. *Appl. Transl. Genomics* 3, 105–108. doi:10.1016/j.atg.2014.09.010
- Schutte, M., Fox, B., Baradez, M.-O., Devonshire, A., Minguez, J., Bokhari, M., Przyborski, S., Marshall, D., 2011. Rat Primary Hepatocytes Show Enhanced Performance and Sensitivity to Acetaminophen During Three-Dimensional Culture on a Polystyrene Scaffold Designed for Routine Use. *Assay Drug Dev. Technol.* doi:10.1089/adt.2011.0371
- Setchell, K.D., Rodrigues, C.M., Clerici, C., Solinas, A., Morelli, A., Gartung, C., Boyer, J., 1997. Bile acid concentrations in human and rat liver tissue and in hepatocyte nuclei. *Gastroenterology* 112, 226–235.

- Sevilla-Tirado, F.J., González-Vallejo, E.B., Leary, A.C., Breedt, H.J., Hyde, V.J., Fernández-Hernando, N., 2003. Bioavailability of two new formulations of paracetamol, compared with three marketed formulations, in healthy volunteers., *Methods and findings in experimental and clinical pharmacology*. doi:10.1358/mf.2003.25.7.778092
- Sévin, D.C., Kuehne, A., Zamboni, N., Sauer, U., 2015. Biological insights through nontargeted metabolomics. *Curr. Opin. Biotechnol.* 34, 1–8. doi:10.1016/j.copbio.2014.10.001
- Seyfarth, H., Favreau, N., Tennert, C., Ruffert, C., Halank, M., Wirtz, H., Mössner, J., Rosendahl, J., Kovacs, P., Wittenburg, H., 2014. Genetic susceptibility to hepatotoxicity due to bosentan treatment in pulmonary hypertension. *Ann. Hepatol.* 13, 803–809.
- Sharaneq, A., Bachour-El Azzi, P., Al-Attrache, H., Savary, C.C., Humbert, L., Rainteau, D., Guguen-Guillouzo, C., Guillouzo, A., 2014. Different Dose-Dependent Mechanisms are Involved in Early Cyclosporine A-Induced Cholestatic Effects in HepaRG Cells. *Toxicol. Sci.* 5, 1–16. doi:10.1093/toxsci/kfu122
- Sharma, V., McNeill, J.H., 2009. To scale or not to scale: the principles of dose extrapolation. *Br. J. Pharmacol.* 157, 907–921. doi:10.1111/j.1476-5381.2009.00267.x
- Shaulian, E., Karin, M., 2002. AP-1 as a regulator of cell life and death. *Nat. Cell Biol.* 4, E131–E136. doi:10.1038/ncb0502-e131
- Sheldon, L.S., Cohen Hubal, E.A., 2009. Exposure as part of a systems approach for assessing risk. *Environ. Health Perspect.* 117, 119–1194. doi:10.1289/ehp.0800407
- Shi, D., Xie, F., Zhai, C., Stern, J.S., Liu, Y., Liu, S., 2009. The role of cellular oxidative stress in regulating glycolysis energy metabolism in hepatoma cells. *Mol. Cancer* 8, 32. doi:10.1186/1476-4598-8-32
- Shimada, M., Yamashita, Y.I., Tanaka, S., Shirabe, K., Nakazawa, K., Ijima, H., Sakiyama, R., Fukuda, J., Funatsu, K., Sugimachi, K., 2007. Characteristic gene expression induced by polyurethane foam/spheroid culture of hepatoma cell line, Hep G2 as a promising cell source for bioartificial liver. *Hepatogastroenterology.* 54, 814–820.
- Shirkey, R.J., Jellett, L.B., Kappatos, D.C., Maling, T.J., Macdonald, A., 1985. Distribution of sodium valproate in normal whole blood and in blood from patients with renal or hepatic disease. *Eur. J. Clin. Pharmacol.* 28, 447–452.
- Shu, L., Zhao, Y., Kurt, Z., Byars, S.G., Tukiainen, T., Kettunen, J., Orozco, L.D., Pellegrini, M., Lusi, A.J., Ripatti, S., Zhang, B., Inouye, M., Mäkinen, V.-P., Yang, X., 2016. Mergeomics: multidimensional data integration to identify pathogenic perturbations to biological systems. *BMC Genomics* 17, 874. doi:10.1186/s12864-016-3198-9
- Shukla, S.J., Huang, R., Austin, C.P., Xia, M., 2010. The future of toxicity testing: A focus on in vitro methods using a quantitative high-throughput screening platform. *Drug Discov. Today* 15, 997–1007. doi:10.1016/j.drudis.2010.07.007
- Silva, M.F.B., Aires, C.C.P., Luis, P.B.M., Ruiter, J.P.N., IJst, L., Duran, M., Wanders, R.J. a., Tavares de Almeida, I., 2008. Valproic acid metabolism and its effects on mitochondrial fatty acid oxidation: A review. *J. Inherit. Metab. Dis.* 31, 205–216. doi:10.1007/s10545-008-0841-x
- Skehan, P., Storeng, R., Scudiero, D., Monks, A., McMahon, J., Vistica, D., Warren, J.T., Bokesch, H., Kenney, S., Boyd, M.R., 1990. New colorimetric cytotoxicity assay for anticancer-drug screening. *J. Natl. Cancer Inst.* 82, 1107–1112. doi:10.1093/jnci/82.13.1107
- Sleiman, S.F., Henry, J., Al-Haddad, R., El Hayek, L., Abou Haidar, E., Stringer, T., Ulja, D., Karuppagounder, S.S., Holson, E.B., Ratan, R.R., Ninan, I., Chao, M. V., 2016. Exercise promotes the expression of brain derived neurotrophic factor (BDNF) through the action of the ketone body β -hydroxybutyrate. *Elife* 5. doi:10.7554/eLife.15092
- Snawder, J.E., Roe, A.L., Benson, R.W., Roberts, D.W., 1994. Loss of CYP2E1 and CYP1A2 activity as a function of acetaminophen dose: relation to toxicity. *Biochem. Biophys. Res. Commun.* 203, 532–539. doi:10.1006/bbrc.1994.2215
- Soga, T., Baran, R., Suematsu, M., Ueno, Y., Ikeda, S., Sakurakawa, T., Kakazu, Y., Ishikawa, T., Robert, M., Nishioka, T., Tomita, M., 2006. Differential Metabolomics Reveals Ophthalmic Acid as an Oxidative Stress Biomarker Indicating Hepatic Glutathione Consumption. *J. Biol. Chem.* 281, 16768–16776. doi:10.1074/jbc.M601876200
- Sohlenius-Sternbeck, A.-K., 2006. Determination of the hepatocellularity number for human, dog, rabbit, rat and mouse livers from protein concentration measurements. *Toxicol. In Vitro* 20, 1582–6. doi:10.1016/j.tiv.2006.06.003

- Soldatow, V., LeCluyse, E., Griffith, L., Rusyn, I., 2013. In vitro models for liver toxicity testing. *Toxicol. Res. (Camb)*. 2, 23–39. doi:10.1039/C2TX20051A.
- Staels, B., Fonseca, V.A., 2009. Bile Acids and Metabolic Regulation: Mechanisms and clinical responses to bile acid sequestration. *Diabetes Care* 32, S237–S245. doi:10.2337/dc09-S355
- Stefan, H., Fraunberger, B., 2005. [Valproate sustained release in the treatment of epilepsy]. *Fortschr. Neurol. Psychiatr.* 73, 681–6. doi:10.1055/s-2004-830299
- Stevens, J.L., Baker, T.K., 2009. The future of drug safety testing: expanding the view and narrowing the focus. *Drug Discov. Today* 14, 162–167. doi:10.1016/j.drudis.2008.11.009
- Strigun, A., Noor, F., Pironti, A., Niklas, J., Yang, T.H., Heinzle, E., 2011a. Metabolic flux analysis gives an insight on verapamil induced changes in central metabolism of HL-1 cells. *J. Biotechnol.* 155, 299–307. doi:10.1016/j.jbiotec.2011.07.028
- Strigun, A., Wahrheit, J., Beckers, S., Heinzle, E., Noor, F., 2011b. Metabolic profiling using HPLC allows classification of drugs according to their mechanisms of action in HL-1 cardiomyocytes. *Toxicol. Appl. Pharmacol.* 252, 183–191. doi:10.1016/j.taap.2011.02.008
- Sturla, S.J., Boobis, A.R., FitzGerald, R.E., Hoeng, J., Kavlock, R.J., Schirmer, K., Whelan, M., Wilks, M.F., Peitsch, M.C., 2014. Systems Toxicology: From Basic Research to Risk Assessment. *Chem. Res. Toxicol.* 27, 314–329. doi:10.1021/tx400410s
- Subathra Devi, C., Saini, A., Rastogi, S., Jemimah Naine, S., Mohanasrinivasan, V., 2015. Strain improvement and optimization studies for enhanced production of erythromycin in bagasse based medium using *Saccharopolyspora erythraea* MTCC 1103. *3 Biotech* 5, 23–31. doi:10.1007/s13205-013-0186-5
- Sugano, K., Kansy, M., Artursson, P., Avdeef, A., Bendels, S., Di, L., Ecker, G.F., Faller, B., Fischer, H., Gerebtzoff, G., Lennernaes, H., Senner, F., 2010. Coexistence of passive and carrier-mediated processes in drug transport. *Nat. Rev. Drug Discov.* 9, 597–614. doi:10.1038/nrd3187
- Sumida, A., Fukuen, S., Yamamoto, I., Matsuda, H., Naohara, M., Azuma, J., 2000. Quantitative analysis of constitutive and inducible CYPs mRNA expression in the HepG2 cell line using reverse transcription-competitive PCR. *Biochem. Biophys. Res. Commun.* 267, 756–760. doi:10.1006/bbrc.1999.2029
- Sumida, K., Igarashi, Y., Toritsuka, N., Matsushita, T., Abe-Tomizawa, K., Aoki, M., Urushidani, T., Yamada, H., Ohno, Y., 2011. Effects of DMSO on gene expression in human and rat hepatocytes. *Hum. Exp. Toxicol.* 30, 1701–1709. doi:10.1177/09603271111399325
- Sutherland, R.M., Inch, W.R., McCredie, J.A., Kruuv, J., 1970. A Multi-component Radiation Survival Curve Using an in Vitro Tumour Model. *Int. J. Radiat. Biol. Relat. Stud. Physics, Chem. Med.* 18, 491–495. doi:10.1080/09553007014551401
- Suzuki, Y., Cox, S., Hayes, J., Walson, P.D., 1991. Valproic acid dosages necessary to maintain therapeutic concentrations in children. *Ther. Drug Monit.* 13, 314–317. doi:10.1097/00007691-199107000-00006
- Takahashi, K., Tanabe, K., Ohnuki, M., Narita, M., Ichisaka, T., Tomoda, K., Yamanaka, S., 2007. Induction of pluripotent stem cells from adult human fibroblasts by defined factors. *Cell* 131, 861–872. doi:10.1016/j.cell.2007.11.019
- Takahashi, K., Yamanaka, S., 2006. Induction of Pluripotent Stem Cells from Mouse Embryonic and Adult Fibroblast Cultures by Defined Factors. *Cell* 126, 663–676. doi:10.1016/j.cell.2006.07.024
- Takekawa, M., Saito, H., 1998. A Family of Stress-Inducible GADD45-like Proteins Mediate Activation of the Stress-Responsive MTK1/MEKK4 MAPKKK. *Cell* 95, 521–530. doi:10.1016/S0092-8674(00)81619-0
- Tan, Y., Xiao, E., Xiao, L., Yuan, Y., Ma, C., Shang, Q., Bian, D., Li, Y., Chen, Z., Chang, Q., 2012. VEGF165 expressing bone marrow mesenchymal stem cells differentiate into hepatocytes under HGF and EGF induction in vitro. *Cytotechnology* 64, 635–647. doi:10.1007/s10616-012-9439-0
- Tandra, S., Yeh, M.M., Brunt, E.M., Vuppalanchi, R., Cummings, O.W., Ünalp-Arida, A., Wilson, L.A., Chalasani, N., 2011. Presence and significance of microvesicular steatosis in nonalcoholic fatty liver disease. *J. Hepatol.* 55, 654–659. doi:10.1016/j.jhep.2010.11.021
- Tang, W., Borel, A.G., Fujimiya, T., Abbott, F.S., 1995. Fluorinated analogues as mechanistic probes in valproic acid hepatotoxicity: hepatic microvesicular steatosis and glutathione status. *Chem. Res. Toxicol.* 8, 671–82.
- Teng, S., Barcellini-Couget, S., Beaudouin, R., Brochot, C., Desousa, G., Rahmani, R., Pery, A.R.R., 2015. BK/TD models for analyzing in vitro impedance data on cytotoxicity. *Toxicol. Lett.* 235,

- 96–106. doi:10.1016/j.toxlet.2015.03.011
- Terbach, N., Shah, R., Kelemen, R., Klein, P.S., Gordienko, D., Brown, N.A., Wilkinson, C.J., Williams, R.S.B., 2011. Identifying an uptake mechanism for the antiepileptic and bipolar disorder treatment valproic acid using the simple biomedical model *Dictyostelium*. *J. Cell Sci.* 124, 2267–2276. doi:10.1242/jcs.084285
- Thomas, C., Pellicciari, R., Pruzanski, M., Auwerx, J., Schoonjans, K., 2008. Targeting bile-acid signalling for metabolic diseases. *Nat. Rev. Drug Discov.* 7, 678–693. doi:10.1038/nrd2619
- Thomas, M., Bayha, C., Vetter, S., Hofmann, U., Schwarz, M., Zanger, U.M., Braeuning, A., 2015. Activating and Inhibitory Functions of WNT/b-Catenin in the Induction of Cytochromes P450 by Nuclear Receptors in HepaRG Cells. *Mol Pharmacol* 87, 1–8. doi:http://dx.doi.org/10.1124/mol.114097402
- Thomas, M., Burk, O., Klumpp, B., Kandel, B.A., Damm, G., Weiss, T.S., Klein, K., Schwab, M., Zanger, U.M., 2013. Direct transcriptional regulation of human hepatic cytochrome P450 3A4 (CYP3A4) by peroxisome proliferator-activated receptor alpha (PPARalpha). *Mol Pharmacol* 83, 709–718.
- Thomson, J.A., Itskovitz-Eldor, J., Shapiro, S.S., Waknitz, M.A., Swiergiel, J.J., Marshall, V.S., Jones, J.M., 1998. Embryonic stem cell lines derived from human blastocysts. *Science* (80-.). 282, 1145–1147. doi:10.1126/science.282.5391.1145
- Thwaites, D.T., Anderson, C.M.H., 2007. H⁺-coupled nutrient, micronutrient and drug transporters in the mammalian small intestine. *Exp. Physiol.* 92, 603–619. doi:10.1113/expphysiol.2005.029959
- Tolosa, L., Gómez-Lechón, M.J., López, S., Guzmán, C., Castell, J. V., Donato, M.T., Jover, R., 2016. Human Upcyte Hepatocytes: Characterization of the Hepatic Phenotype and Evaluation for Acute and Long-Term Hepatotoxicity Routine Testing. *Toxicol. Sci.* kfw078. doi:10.1093/toxsci/kfw078
- Tomita, Y., Yuasa, C., Ni, R., Ishimura, K., Ichihara, A., 1995. Long-term maintenance of function rat hepatocytes in primary culture by additions of pyruvate and various hormones. *Biochim. Biophys. Acta* 1243, 329–335. doi:10.1016/0304-4165(94)00155-Q
- Treiber, A., Schneider, R., Häusler, S., Stieger, B., 2007. Bosentan is a substrate of human OATP1B1 and OATP1B3: Inhibition of hepatic uptake as the common mechanism of its interactions with cyclosporin A, rifampicin, and sildenafil. *Drug Metab. Dispos.* 35, 1400–1407. doi:10.1124/dmd.106.013615
- Tse, G., Yan, B.P., Chan, Y.W.F., Tian, X.Y., Huang, Y., 2016. Reactive Oxygen Species, Endoplasmic Reticulum Stress and Mitochondrial Dysfunction: The Link with Cardiac Arrhythmogenesis. *Front. Physiol.* 7. doi:10.3389/fphys.2016.00313
- Tsutsumi, S., Gotoh, T., Tomisato, W., Mima, S., Hoshino, T., Hwang, H.-J., Takenaka, H., Tsuchiya, T., Mori, M., Mizushima, T., 2004. Endoplasmic reticulum stress response is involved in nonsteroidal anti-inflammatory drug-induced apoptosis. *Cell Death Differ.* 11, 1009–1016. doi:10.1038/sj.cdd.4401436
- Ubeaud, G., Schmitt, C., Jaeck, D., Lave, T., Coassolo, P., 1995. Bosentan, a new endothelin receptor antagonist: prediction of the systemic plasma clearance in man from combined in vivo and in vitro data. *Xenobiotica.* 25, 1381–1390. doi:10.3109/00498259509061925
- Ulvestad, M., Darnell, M., Molden, E., Ellis, E., Åsberg, A., Andersson, T.B., 2012. Evaluation of organic anion-transporting polypeptide 1B1 and CYP3A4 activities in primary human hepatocytes and HepaRG cells cultured in a dynamic three-dimensional bioreactor system. *J. Pharmacol. Exp. Ther.* 343, 145–56. doi:10.1124/jpet.112.195750
- Uzi, D., Barda, L., Scaiewicz, V., Mills, M., Mueller, T., Gonzalez-Rodriguez, A., Valverde, A.M., Iwawaki, T., Nahmias, Y., Xavier, R., Chung, R.T., Tirosh, B., Shibolet, O., 2013. CHOP is a critical regulator of acetaminophen-induced hepatotoxicity. *J. Hepatol.* 59, 495–503. doi:10.1016/j.jhep.2013.04.024
- Vanhaecke, T., Foriers, a, Geerts, a, Shephard, E., Vercruyssen, a, Rogiers, V., 2001. Pyruvate-induced long-term maintenance of glutathione S-transferase in rat hepatocyte cultures 335–346.
- Varma, a, Palsson, B.O., 1994a. Stoichiometric flux balance models quantitatively predict growth and metabolic by-product secretion in wild-type *Escherichia coli* W3110. *Appl. Environ. Microbiol.* 60, 3724–3731.
- Varma, a, Palsson, B.O., 1994b. Predictions for oxygen supply control to enhance population stability of engineered production strains. *Biotechnol. Bioeng.* 43, 275–285. doi:10.1002/bit.260430403

- Vinken, M., 2015. Adverse Outcome Pathways and Drug-Induced Liver Injury Testing. *Chem. Res. Toxicol.* 28, 1391–1397. doi:10.1021/acs.chemrestox.5b00208
- Vodovotz, Y., Prelich, J., Lagoa, C., Barclay, D., Zamora, R., Murase, N., Gandhi, C.R., 2012. Augmenter of liver regeneration (ALR) is a novel biomarker of hepatocellular stress/inflammation: in vitro, in vivo and in silico studies. *Mol. Med.* 18, 1421–9. doi:10.2119/molmed.2012.00183
- Vuppala, P., Janagam, D., Balabathula, P., 2013. Importance of ADME and Bioanalysis in the Drug Discovery. *J. Bioequiv. Availab.* 5, 4–5. doi:10.4172/jbb.10000e31
- Wajner, M., Amaral, A.U., 2016. Mitochondrial dysfunction in fatty acid oxidation disorders: insights from human and animal studies. *Biosci. Rep.* 36, e00281–e00281. doi:10.1042/BSR20150240
- Walsky, R.L., Boldt, S.E., 2008. In vitro cytochrome P450 inhibition and induction. *Curr. Drug Metab.* 9, 928–939. doi:10.2174/138920008786485128
- Wang, W., Lin, R., Zhang, J., Mao, Y., Bu, X., Ji, Q., Zhai, X., Lin, Q., Yang, L., Zhang, K., 2012. Involvement of fatty acid metabolism in the hepatotoxicity induced by divalproex sodium. *Hum. Exp. Toxicol.* 31, 1092–101. doi:10.1177/0960327112444477
- Wang, Z., Klipfell, E., Bennett, B.J., Koeth, R., Levison, B.S., DuGar, B., Feldstein, A.E., Britt, E.B., Fu, X., Chung, Y.-M., Wu, Y., Schauer, P., Smith, J.D., Allayee, H., Tang, W.H.W., DiDonato, J.A., Lusis, A.J., Hazen, S.L., 2011. Gut flora metabolism of phosphatidylcholine promotes cardiovascular disease. *Nature* 472, 57–63. doi:10.1038/nature09922
- Wang, Z., Roberts, A.B., Buffa, J.A., Levison, B.S., Zhu, W., Org, E., Gu, X., Huang, Y., Zamanian-Daryoush, M., Culley, M.K., DiDonato, A.J., Fu, X., Hazen, J.E., Krajcik, D., DiDonato, J.A., Lusis, A.J., Hazen, S.L., 2015. Non-lethal Inhibition of Gut Microbial Trimethylamine Production for the Treatment of Atherosclerosis. *Cell* 163, 1585–1595. doi:10.1016/j.cell.2015.11.055
- Warrier, M., Shih, D.M., Burrows, A.C., Ferguson, D., Gromovsky, A.D., Brown, A.L., Marshall, S., McDaniel, A., Schugar, R.C., Wang, Z., Sacks, J., Rong, X., Vallim, T. de A., Chou, J., Ivanova, P.T., Myers, D.S., Brown, H.A., Lee, R.G., Crooke, R.M., Graham, M.J., Liu, X., Parini, P., Tontonoz, P., Lusis, A.J., Hazen, S.L., Temel, R.E., Brown, J.M., 2015. The TMAO-Generating Enzyme Flavin Monooxygenase 3 Is a Central Regulator of Cholesterol Balance. *Cell Rep.* 10, 326–338. doi:10.1016/j.celrep.2014.12.036
- Waxman, D.J., Holloway, M.G., 2009. Sex Differences in the Expression of Hepatic Drug Metabolizing Enzymes. *Mol. Pharmacol.* 76, 215–228. doi:10.1124/mol.109.056705
- Weber, C., Gasser, R., Hopfgartner, G., 1999. Absorption, excretion, and metabolism of the endothelin receptor antagonist bosentan in healthy male subjects. *Drug Metab Dispos* 27, 810–815.
- Weber, C., Schmitt, R., Birnboeck, H., Hopfgartner, G., Van Marie, S.P., Peeters, P.A.M., Jonkman, J.H.G., Jones, C.R., 1996. Pharmacokinetics and pharmacodynamics of the endothelin-receptor antagonist bosentan in healthy human subjects. *Clin. Pharmacol. Ther.* 60, 124–137. doi:10.1016/S0009-9236(96)90127-7
- Wen, X., Wang, J.-S., Kivistö, K.T., Neuvonen, P.J., Backman, J.T., 2001. In vitro evaluation of valproic acid as an inhibitor of human cytochrome P450 isoforms: preferential inhibition of cytochrome P450 2C9 (CYP2C9). *Br. J. Clin. Pharmacol.* 52, 547–553. doi:10.1046/j.0306-5251.2001.01474.x
- Westmoreland, C., Carmichael, P., Dent, M., Fentem, J., MacKay, C., Maxwell, G., Pease, C., Reynolds, F., 2010. Assuring safety without animal testing: Unilever’s ongoing research programme to deliver novel ways to assure consumer safety. *ALTEX* 27, 61–5.
- Wetmore, B. a, Wambaugh, J.F., Ferguson, S.S., Sochaski, M. a, Rotroff, D.M., Freeman, K., Clewell, H.J., Dix, D.J., Andersen, M.E., Houck, K. a, Allen, B., Judson, R.S., Singh, R., Kavlock, R.J., Richard, A.M., Thomas, R.S., 2012. Integration of dosimetry, exposure, and high-throughput screening data in chemical toxicity assessment. *Toxicol. Sci.* 125, 157–74. doi:10.1093/toxsci/kfr254
- Wilkening, S., Stahl, F., Bader, A., 2003. Comparison of primary human hepatocytes and hepatoma cell line HepG2 with regard to their biotransformation properties. *Drug Metab. Dispos.* 31, 1035–1042. doi:10.1124/dmd.31.8.1035
- Wilmes, A., Limonciel, A., Aschauer, L., Moenks, K., Bielow, C., Leonard, M.O., Hamon, J., Carpi, D., Ruzek, S., Handler, A., Schmal, O., Herrgen, K., Bellwon, P., Burek, C., Truisi, G.L., Hewitt, P., Di Consiglio, E., Testai, E., Blaauboer, B.J., Guillou, C., Huber, C.G., Lukas, A., Pfaller, W.,

- Mueller, S.O., Bois, F.Y., Dekant, W., Jennings, P., 2013. Application of integrated transcriptomic, proteomic and metabolomic profiling for the delineation of mechanisms of drug induced cell stress. *J. Proteomics* 79, 180–194. doi:10.1016/j.jprot.2012.11.022
- Winnike, J.H., Peditakis, P., Wolak, J.E., McClelland, R.E., Watkins, P.B., Macdonald, J.M., 2012. Stable isotope resolved metabolomics of primary human hepatocytes reveals a stressed phenotype. *Metabolomics* 8, 34–49. doi:10.1007/s11306-011-0284-5
- Wise, D.R., Thompson, C.B., 2010. Glutamine addiction: a new therapeutic target in cancer. *Trends Biochem Sci* 35, 427–433. doi:S0968-0004(10)00091-5 [pii]10.1016/j.tibs.2010.05.003
- Wishart, D.S., 2008. Quantitative metabolomics using NMR. *TrAC Trends Anal. Chem.* 27, 228–237. doi:10.1016/j.trac.2007.12.001
- Wishart, D.S., 2016. Emerging applications of metabolomics in drug discovery and precision medicine. *Nat. Rev. Drug Discov.* 15, 473–484. doi:10.1038/nrd.2016.32
- Wittwehr, C., Aladjov, H., Ankley, G., Byrne, H.J., de Knecht, J., Heinzle, E., Klambauer, G., Landesmann, B., Luijten, M., MacKay, C., Maxwell, G., Meek, M.E. (Bette), Paini, A., Perkins, E., Sobanski, T., Villeneuve, D., Waters, K.M., Whelan, M., 2017. How Adverse Outcome Pathways Can Aid the Development and Use of Computational Prediction Models for Regulatory Toxicology. *Toxicol. Sci.* 155, 326–336. doi:10.1093/toxsci/kfw207
- Worth, A., Fuart-Gatnik, M., Lapenna, S., Lo Piparo, E., Mostrag-Szlichtyng, A., Serafimova, R., 2011. The use of computational methods in the toxicological assessment of chemicals in food: current status and future prospects. Publications Office of the European Union. doi:10.2788/6234
- Xia, J., Sinelnikov, I. V., Han, B., Wishart, D.S., 2015. MetaboAnalyst 3.0-making metabolomics more meaningful. *Nucleic Acids Res.* 43, W251–W257. doi:10.1093/nar/gkv380
- Xia, M., Huang, R., Witt, K.L., Southall, N., Fostel, J., Cho, M.H., Jadhav, A., Smith, C.S., Inglese, J., Portier, C.J., Tice, R.R., Austin, C.P., 2008. Compound cytotoxicity profiling using quantitative high-throughput screening. *Environ. Health Perspect.* 116, 284–291. doi:10.1289/ehp.10727
- Xie, Y., McGill, M.R., Dorko, K., Kumer, S.C., Schmitt, T.M., Forster, J., Jaeschke, H., 2014. Mechanisms of acetaminophen-induced cell death in primary human hepatocytes. *Toxicol. Appl. Pharmacol.* doi:10.1016/j.taap.2014.05.010
- Yan, Z., Li, J., Huebert, N., Caldwell, G.W., Du, Y., Zhong, H., 2005. Detection of a Novel Reactive Metabolite of Diclofenac : Evidence for Cyp2C9-Mediated Bioactivation Via Arene Oxides 33, 706–713. doi:10.1124/dmd.104.003095.1994a
- Yang, L., Moss, T., Mangala, L.S., Marini, J., Zhao, H., Wahlig, S., Armaiz-Pena, G., Jiang, D., Achreja, A., Win, J., Roopaimoole, R., Rodriguez-Aguayo, C., Mercado-Uribe, I., Lopez-Berestein, G., Liu, J., Tsukamoto, T., Sood, A.K., Ram, P.T., Nagrath, D., 2014. Metabolic shifts toward glutamine regulate tumor growth, invasion and bioenergetics in ovarian cancer. *Mol. Syst. Biol.* 10. doi:10.1002/msb.20134892
- Yang, T.H., Bolten, C.J., Coppi, M. V., Sun, J., Heinzle, E., 2009. Numerical bias estimation for mass spectrometric mass isotopomer analysis. *Anal. Biochem.* 388, 192–203. doi:10.1016/j.ab.2009.03.005
- Yilmaz, Y., 2012. Alimentary Pharmacology and Therapeutics Review article : is non-alcoholic fatty liver disease a spectrum , or are steatosis and non-alcoholic steatohepatitis distinct conditions ? doi:10.1111/apt.12046
- Yoon, E., Babar, A., Choudhary, M., Kutner, M., Pysopoulos, N., 2016. Acetaminophen-Induced Hepatotoxicity: a Comprehensive Update. *J. Clin. Transl. Hepatol.* 4. doi:10.14218/JCTH.2015.00052
- Yoon, M., Efremenko, A., Blauboer, B.J., Clewell, H.J., 2014. Evaluation of simple in vitro to in vivo extrapolation approaches for environmental compounds. *Toxicol. Vitro.* 28, 164–170. doi:10.1016/j.tiv.2013.10.023
- Yoshida, H., Hirozane, K., Kimoto, H., Hayashi, T., Akiyama, T., Katayama, H., Watanabe, M., Yoshitomi, H., Kamiya, A., 1999. Valproic acid elimination rate and urinary excretion of its glucuronide conjugate in patients with epilepsy. *Biol. Pharm. Bull.* 22, 716–720. doi:10.1248/bpb.22.716
- Zhang, D., Luo, G., Ding, X., Lu, C., 2012. Preclinical experimental models of drug metabolism and disposition in drug discovery and development. *Acta Pharm. Sin. B* 2, 549–561. doi:10.1016/j.apsb.2012.10.004
- Zhou, S.-F., Liu, J.-P., Chowbay, B., 2009. Polymorphism of human cytochrome P450 enzymes and

its clinical impact. *Drug Metab. Rev.* 41, 89–295. doi:10.1080/03602530902843483

Zhou, W., Capello, M., Fredolini, C., Piemonti, L., Liotta, L.A., Novelli, F., Petricoin, E.F., 2011. Proteomic analysis of pancreatic ductal adenocarcinoma cells reveals metabolic alterations. *J. Proteome Res.* 10, 1944–1952. doi:10.1021/pr101179t

Zhou, W., Liotta, L.A., Petricoin, E.F., 2012. Cancer metabolism: What we can learn from proteomic analysis by mass spectrometry. *Cancer Genomics and Proteomics.*

Danksagung

Ich bedanke mich ganz herzlich bei Herrn Professor Elmar Heinzle und Frau Doktor Fozia Noor, die es mir ermöglichten meine Doktorarbeit am Institut der Technischen Biochemie anzufertigen, und die mir darüber hinaus mit hilfreichen Diskussionen beiseite standen.

Bei Herrn Professor Gert-Wieland Kohring möchte ich mich zudem sehr herzlich für die Zeit und Mühe zur Zweitbegutachtung meiner Arbeit bedanken.

Weiterer Dank für die angenehme Zeit in der Arbeitsgruppe gilt meinen ehemaligen Kollegen. Darunter Christian Priesnitz, Christian Weyler, Saskia Sperber, Esther Hoffmann, Lisa Katharina Blaß, Malina Orsini, Judith Wahrheit, Yannic Nonnenmacher, Averina Nicolae und Yeda Rumi Kaminski. Christian Priesnitz möchte ich dabei ganz besonders dafür danken, dass er meine Begeisterung für Sport wiedererweckt hat und auch Christian Weyler für die regelmäßige Gesellschaft beim Training. Judith Wahrheit möchte ich zusätzlich für fachliche Diskussionen und ihre Meinung zu meinen Ideen danken. Separat sei an dieser Stelle auch noch meine Nachfolgerin Yeda Rumi Kaminski erwähnt, der ich für ihre Freundschaft und Unterstützung ganz besonders herzlich danken möchte und der ich auf diesem Wege noch alles erdenklich Gute für ihre Doktorarbeit wünsche. Daniel Müller danke ich für zahlreiche Diskussionen und Hilfestellungen in der Anfangszeit meiner Doktorarbeit. Für Hilfe bei der Betreuung der Übungen zur Bioreaktionstechnik möchte ich Averina Nicolae danken. Nicht zuletzt gilt mein Dank auch Michel Fritz für die Unterstützung bei den unzähligen technischen Problemen an unseren Instrumenten. Frau Doktor Susanne Kohring sei recht herzlich gedankt für die zuweilen nicht immer einfachen organisatorischen Angelegenheiten und für die Unterstützung der gesamten Arbeitsgruppe.

Des Weiteren gilt mein Dank meinen zwei ehemaligen Master-Studenten Ghamdan Beshr und Suellen Almeida Dragon, sowie meinem ehemaligen Bachelor-Studenten Michael Wolf, für die Zeit und Mühe die sie in ihre Arbeit gesteckt haben und für die Möglichkeit voneinander zu lernen.

Für die im Rahmen der Doktorarbeit entstandenen Kollaborationen möchte ich mich ganz besonders bei Doktor Silvia Maggioni und Valery Shevchenko für die hervorragende Metabolitenquantifizierung, und bei Doktor Joachim Bucher für Unterstützung bei der einen oder anderen Berechnung bedanken. Nicht zuletzt bedanke ich mich bei Georg Tascher für die stets angenehme Gesellschaft auf Konferenzen, sowie für seinen Einsatz innerhalb des NOTOX Projektes. Auch allen anderen Partnern des NOTOX Projektes, die rege zum Erfolg des Projektes beigetragen haben, sei sehr herzlich gedankt.

Bei Lara Schmielau bedanke ich mich für die Motivation und gelegentliche Abwechslung gegen Ende der Arbeit.

Für die Finanzierung des Projektes und dieser Doktorarbeit danke ich der Europäischen Kommission, die diese im Rahmen des 7. Forschungsrahmenprogramms zusammen mit Cosmetics Europe zur Verfügung stellte.

Contributions

Chapter 2

The experiment was designed by Sebastian Klein together with Ghamdan Beshr, Daniel Mueller, Fozia Noor and Elmar Heinzle. The experiments and all measurements were conducted by Ghamdan Beshr, with exception of analysis of samples for CYP450 activity. CYP450 activity measurements were performed by Valery Shevchenko at Biopredic International. Data evaluation and writing of the publication draft was done by Sebastian Klein and involved discussions with Fozia Noor and Elmar Heinzle.

Chapter 3

Sebastian Klein designed the experiment together with Fozia Noor. All experiments were conducted by Sebastian Klein, except for the quantification of valproic acid and its metabolite. The latter was conducted by Silvia Maggioni at Mario Negri Institute in Milan. Evaluation of the data and writing of the publication draft was done by Sebastian Klein, involving discussions with Fozia Noor and Elmar Heinzle. Elmar Heinzle provided the method for the calculation of oxygen diffusion and consumption, which was revised by Sebastian Klein.

Chapter 4

The experimental design was set up by Sebastian Klein in collaboration with Daniel Mueller and Fozia Noor. Experiments including analysis and data evaluation were conducted by Sebastian Klein. The publication was written by Sebastian Klein, and Fozia Noor revised the manuscript.

Chapter 5

Sebastian Klein designed the experiments together with Fozia Noor and Daniel Mueller. Experiments and analysis were conducted by Sebastian Klein. Drug concentrations were determined by Silvia Maggioni at Mario Negri Institute in Milan. Pharmacelsus GmbH contributed with the quantification of drug metabolites. CYP450 products were quantified by Valery Shevchenko from Biopredic International. Evaluation of the data was performed by Sebastian Klein, and insilico biotechnology AG assisted in the extrapolation of *in vitro* data. Elmar Heinzle performed the estimation of drug kinetics. The manuscript was written by Sebastian Klein. Fozia Noor and Elmar Heinzle helped with discussions, and Daniel Mueller and Joachim Bucher assisted with their feedback.

Chapter 6

The experimental design was worked out in close collaboration with several partners within the NOTOX project. These include partners from Saarland University (Institute for Biochemical Engineering and Epigenetics), Insilico Biotechnology AG, Biopredic International, Karolinska Institutet, CNRS Strasbourg and Cambridge Cell Networks. Sebastian Klein, Daniel Mueller and Yeda Kaminski took care of the cultivation of HepaRG cells. Daniel Mueller performed the Oil Red O staining. Sebastian Klein took microscopic pictures and determined viability, ATP content, extracellular metabolite concentrations and collected samples for CYP450 activity, intracellular metabolite and drug concentration measurements. Measurements for CYP450 activity were conducted by Valery Shevchenko, Biopredic International. Transcriptome data originates from Karolinska Institutet (Inger Johansson, Magnus Ingelman-Sundberg), while proteome data was measured at CNRS Strasbourg (Georg Tascher, Fabrice Bertile, Alain van Dorsselaer). The intracellular metabolome data was measured at ETH Zurich (Tobias Fuhrer, Nicola Zamboni) and drug

quantification was performed at Mario Negri Institute, Milan (Silvia Maggioni). Evaluation of data and writing of the chapter were done by Sebastian Klein. Elmar Heinzle supported the writing with discussion and feedback.

Curriculum vitae

Persönliche Daten

Name	Sebastian Klein
Geburtsdatum	16.12.1984
Geburtsort	Stuttgart
Staatsangehörigkeit	Deutsch

Ausbildung und Berufserfahrung

September 2015 – Oktober 2016	Knowledge Manager bei der Biocrates Life Sciences AG in Innsbruck, Österreich
Juni 2011 – Juli 2017	Promotion am Institut der Technischen Biochemie an der Universität des Saarlandes zum Thema „Towards the assessment of human-relevant repeated dose toxicity using an <i>in vitro</i> systems toxicological approach“ im Rahmen des EU-Projektes „NOTOX“
März 2010 – Januar 2011	Diplomarbeit am Institut für Medizinische Mikrobiologie und Hygiene der Eberhard Karls Universität Tübingen über die „Deletion des Anbu Operons in <i>Yersinia enterocolitica</i> und Untersuchung des resultierenden Phänotyps“
August 2008 – Januar 2011	Studium der Biologie (Diplom) an der Eberhard Karls Universität Tübingen im Hauptstudium mit Schwerpunkten Mikrobiologie, Biochemie und Immunologie
Oktober 2006 – September 2008	Studium der Biologie (Diplom) an der Universität Hohenheim im Grundstudium

Publikationen

- 2012 1) **Klein, S.**, & Heinzle, E. (2012), Isotope labeling experiments in metabolomics and fluxomics. *Wiley Interdisciplinary Reviews. Systems Biology and Medicine*, 4(3), 261–72. doi:10.1002/wsbm.1167
- 2013 2) **Klein, S.**, Mueller, D., Schevchenko, V., & Noor, F. (2013), Long-term maintenance of HepaRG cells in serum-free conditions and application in a repeated dose study. *Journal of Applied Toxicology : JAT*, (August). doi:10.1002/jat.2929
- 2014 3) Mueller, D., Krämer, L., Hoffmann, E., **Klein, S.**, & Noor, F. (2014), 3D organotypic HepaRG cultures as *in vitro* model for acute and repeated dose toxicity studies. *Toxicology in Vitro*, 28(1), 104–12. doi:10.1016/j.tiv.2013.06.024
- 4) Towards the Replacement of *in vivo* Repeated Dose Systemic Toxicity Testing, Volume 4, 2014 ISBN: 978-2-9539634-3-4, Beitrag
- 2015 5) Towards the Replacement of *in vivo* Repeated Dose Systemic Toxicity Testing, Volume 5, 2015 ISBN: 978-2-9539634-4-1, Beitrag
- 2016 6) Towards the Replacement of *in vivo* Repeated Dose Systemic Toxicity Testing, Volume 6, 2016 ISBN: 978-2-9539634-5-8, Beitrag
- 7) **Klein, S.**, Maggioni, S., Bucher, J., Niklas, J., Mueller, D., Shevchenko, V., Mauch, K., Heinzle, E., Noor, F. (2016), *In silico* modeling for the prediction of dose and pathway related adverse effects in humans from *in vitro* repeated-dose studies. *Toxicological Sciences*, 149(1), 55-66. doi: 10.1093/toxsci/kfv218.

Posterbeiträge

- 2012 1) Bucher *et al.*, Large multi-scale modeling of long term toxic effects in organotypic cultures. SEURAT meeting, Lissabon (Portugal)
- 2) Klein *et al.*, Serum-free long-term repeated dose and acute toxicity studies using the HepaRG cell line. EUSAAT, Linz (Österreich)
- 2013 3) Klein *et al.*, Analysis of metabolic fluxes and metabolic competence during serum-free long-term cultivation of HepaRG cells. EASL, Luxemburg (Luxemburg)
- 4) Mueller *et al.*, Systems toxicology approach to assess the effects of acetaminophen on HepaRG *in vitro* cultures. EASL, Luxemburg (Luxemburg)
- 5) Beshr *et al.*, Effect of diclofenac and acetaminophen on the metabolic fluxes in liver cells. EASL, Luxemburg (Luxemburg)
- 6) Almeida *et al.*, The effects of different cultivation techniques on the metabolome of human liver cells. EASL, Luxemburg (Luxemburg)
- 7) Klein *et al.*, Systems toxicology approach to assess acute effects of acetaminophen on HepaRG *in vitro* cultures. SEURAT meeting, Lissabon (Portugal)

-
- 2014
- 8) Klein *et al.*, Biokinetics and metabolome analysis on HepaRG cells upon bosentan exposure for the assessment of repeated dose toxicity. SEURAT meeting, Barcelona (Spanien)
 - 9) Klein *et al.*, Case study: Multi-omics study on long term repeated dose toxicity of valproic acid with steatosis as mechanism of action. SEURAT meeting, Barcelona (Spanien)
 - 10) Puigvert *et al.*, Toxicity of valproic acid as revealed from experiments in 2D and 3D HepaRG systems. SEURAT meeting, Barcelona (Spanien)
 - 11) Cellière *et al.*, Modeling spheroid formation and *in vitro* toxicity aiming at toxicity simulations *in vivo*. SEURAT meeting, Barcelona (Spanien)
 - 12) Klein *et al.*, Comparison of viability assays in 2D HepaRG cultures. ESTIV, Egmond aan Zee (Niederlande)
 - 13) Klein *et al.*, Biokinetics and metabolic flux analysis on HepaRG cells upon valproic acid exposure for the assessment of acute and repeated dose toxicity. ESTIV, Egmond aan Zee (Niederlande)
- 2015
- 14) Klein *et al.*, Effects of repeated dose bosentan exposure on the carbon metabolism of 2D and 3D HepaRG cultures in a two-week study, SEURAT meeting, Barcelona (Spanien)
 - 15) Kaminski *et al.*, Evaluation of regulation and delayed toxicity response of HepaRG cells upon acetaminophen exposure. SEURAT meeting, Barcelona (Spanien)
 - 16) Puigvert *et al.*, Repeated dose toxicity of valproic acid (VPA) in a 3D HepaRG system. SEURAT meeting, Barcelona (Spanien)
 - 17) Weltin *et al.*, Continuous lactate monitoring by microsensors in spheroid 3D tumor cell cultures. TRANSDUCERS, Anchorage (USA)

Voträge

- 2015
- 1) “Serum-free long term maintenance of differentiated HepaRG cells and their application in repeated-dose toxicity assessment”, SEURAT meeting, Barcelona (Spanien)
- 2016
- 2) “Targeted Metabolomics in Oncology”, Workshop zum Thema Metabolomics in Biomedical Research, Tübingen (Deutschland)